Technische Universität München

Wissenschaftszentrum Weihenstephan für Ernährung, Landnutzung und Umwelt

Fachgebiet für Biostatistik

Statistical modeling of risk and trends in the life sciences with applications to forestry, plant breeding, phenology, and cancer

Andreas Böck

Vollständiger Abdruck der von der Fakultät Wissenschaftszentrum Weihenstephan für Ernährung, Landnutzung und Umwelt der Technischen Universität München zur Erlangung des akademischen Grades eines

Doktors der Naturwissenschaften

genehmigten Dissertation.

Vorsitzende: Univ.-Prof. Dr. Ch.-C. Schön

Prüfer der Dissertation:

1. Univ.-Prof. D. Pauler Ankerst, Ph.D.
2. Univ.-Prof. Dr. A. Menzel

Die Dissertation wurde am 18.11.2013 bei der Technischen Universität München eingereicht und durch die Fakultät Wissenschaftszentrum Weihenstephan für Ernährung, Landnutzung und Umwelt am 17.04.2014 angenommen.

Statistical modeling of risk and trends in the life sciences with applications to forestry, plant breeding, phenology, and cancer

Andreas Böck

Danksagung

Danke sagen möchte ich . . .

. . . Donna Ankerst für die äußerst engagierte Betreuung und fachliche Unterstützung.

. . . Chris-Carolin Schön und Yongle Li (Leo) für die Einblicke in die Welt der Pflanzenzucht und die Interaktion mit ihrem Lehrstuhl.

. . . Annette Menzel und Chiara Ziello für das angenehme Zusammenspiel im Anwendungsbeispiel der Phänologie.

. . . Peter Biber und Jochen Dieler für die begeisterte Aufklärung über den Lebens- und Leidensweg der Bäume.

. . . Hannes Petermeier für fachlichen und freundschaftlichen Rat, gepaart mit tatkräftiger Unterstützung bei allen Problemen des Büro- und Campuslebens.

. . . Josef und Ulf für ihre Hilfsbereitschaft und den kurzweiligen Büroalltag der letzten Jahre.

. . . Esther und Martina für die Anmerkungen und Verbesserungsvorschläge zu dieser Arbeit.

. . . meiner Familie.

Zusammenfassung

Empirische Belastbarkeit ist eine allgegenwärtige Anforderung an die Forschung – auch oder vor allem in den Lebenswissenschaften. In dieser Arbeit wird für vier typische Themengebiete gezeigt, wie statistische Methodik eingesetzt wird um diesem Ziel gerecht zu werden. Augenmerk liegt auf verschiedenen Stufen der statistischen Modellierung und dem Verweis auf Überschneidungen der eingesetzten Methodik zwischen den unterschiedlichen thematischen Bereichen. Die Ergebnisse der statistischen Auswertungen werden anschaulich präsentiert und in Bezug auf die inhaltliche Problemstellung interpretiert.

Im ersten Teil der Arbeit steht die Neuentwicklung eines Risikomodells für die Forstwissenschaften im Fokus. Ziel ist es die Sterblichkeit einzelner Bäume in Abhängigkeit ihrer lokalen Konkurrenzsituation gegenüber anderen Bäumen vorherzusagen. Die Modellentwicklung beginnt mit einer Bestandsaufnahme der vorhandenen Information, die sich in Form der Stichprobe und der Literatur zu diesem Thema ausdrückt, und dem Definieren des genauen Einsatzszenarios des zu erstellenden Modells. Mithilfe von Ergebnissen der deskriptiven Auswertung im Bezug auf die beobachtete Sterblichkeit und den am Baum gemessenen Größen, leiten wir daraus die Konsequenzen für die statistische Modellbildung ab. Eine geeignete Modellklasse wird vom zeitstetigen Coxmodell ausgehend unter Ausnutzung der Gemeinsamkeit zum binären Regressionsmodell hergeleitet. Zur Sterblichkeitsvorhersage dient die Verallgemeinerung des logistischen Regressionsmodells zur Klasse der generalisierten additiven gemischten Modelle, die dem Stichprobendesign gerecht wird und eine flexible Kombination von Kovariableneffekten ermöglicht. Für die Variablenselektion innerhalb dieser Klasse werden Maße zur Quantifizierung der Modellvorhersagegüte eingeführt und in einem Kreuzvalidierungsschema ausgewertet. Eine abschließende Vereinfachung der Parametrisierung des Modells erlaubt eine unkomplizierte Anwendung und Implementierung.

Die im zweiten Teil dieser Arbeit betrachteten Versuchsreihen der Pflanzenzucht wurden zum Zwecke einer Assoziationsstudie durchgeführt, von der Rückschlüsse für die Züchtung robuster Roggenarten gezogen werden sollen. Aus statistischer Sicht stellen die Versuche sehr gute Ausgangsbedingungen bereit, da es sich um geplante Experimente handelt, die mit Hilfe von Randomisierung und Blockbildung die Einflüsse von nicht beobachteten Bedingungen quantifizierbar bzw. kontrollierbar machen. Ausgewertet werden die Beobachtungen mittels eines gemischten linearen Modelles, das mehrere Ebenen des Verwandtschaftsgrades der unterschiedlichen Arten zueinander berücksichtigt und den longitudinalen Aspekt der Ver-

suchsreihen aufgreift. Die dafür eingesetzten Komponenten des Regressionsmodells werden detailliert beschrieben. Zuletzt werden die genetischen Merkmale mit statistisch signifikantem Zusammenhang zur Frosttoleranz präsentiert und eingeordnet.

Im Abschnitt aus dem Themengebiet der Phänologie wird untersucht wie sich die Blütezeit verschiedener Arten im Laufe der letzten 30 Jahre geändert hat. Mit Techniken der Meta-Analyse wird eine Vielzahl von lokal beobachteten Trends in ein statistisches Modell zusammengeführt, und somit eine übergreifende Betrachtung ermöglicht. Bei der Herangehensweise wird die unterschiedliche Unsicherheit die den einzelnen Trends anhaftet berücksichtigt und untersucht inwiefern der geographische Standort der Messstationen die Ergebnisse beeinflusst. Unter anderem ließ sich beobachten, dass bei Arten, die ihre Pollen mithilfe des Windes zu anderen Pflanzen übertragen, der langjährige Trend hin zu einem früherem Blütebeginn stärker ausgeprägt ist als bei Arten, die durch Insekten bestäubt werden. Nicht zuletzt sind derartige Resultate für die Allergologie relevant. Ob sich insgesamt auf eine länger werdende Pollensaison schließen lässt, kann von den Ergebnissen der Studie nur indirekt angedeutet werden. Es werden jedoch Ansätze aufgezeigt, wie sich diese Fragestellung mit ähnlichen Daten empirisch untersuchen lässt.

Der Aspekt der Modellvalidierung wird im medizinischen Abschnitt erneut aufgegriffen. Bestehende Risikomodelle für Prostatakrebs werden auf ihren Nutzen hin bewertet. Sie beruhen hauptsächlich auf dem prostataspezifischen Antigen und wurden entwickelt, um Patienten und Ärzten eine Hilfestellung zu geben, wann der mit Risiken verbundene Eingriff einer Biopsie gerechtfertigt ist. Neben bereits eingeführter Maße zur Modellbewertung wird ein weitere Größe, welche die persönlichen Umstände des Patienten mit einbezieht, zur Beurteilung des Risikomodells herangezogen. Die Validierung findet an zehn externen Kohorten statt, und gibt an ob das Risiko von Betroffenen, bei denen die Biopsie nachträglich tatsächlich einen Krebsbefund feststellen ließ, zuverlässig höher bewertet wird als bei Männern ohne Prostatakrebsbefund. Wie auch das absolute Niveau der Risikovorhersage, das nur für einen Teil der untersuchten Personen gut vorhersehbar ist, fallen die Resultate gemischt aus, und hängen unter anderem von der unterschiedlichen Prävalenz/Inzidenz in den Kohorten und den studienspezifischen Abläufen ab.

Abstract

Empirical capacity is a ubiquitous claim for the research—even or especially in the life sciences. In this work the use of statistical models to achieve this objective is presented in four important areas of life science. The focus is on different stages of statistical modeling and discussion of overlapping methodology in the diverse thematic areas. The results of statistical analysis are presented vividly and interpreted in relation to the substantive problem.

The first part of this thesis focuses on the development of a risk model for the forest sciences aiming to predict the mortality of individual trees as a function of their local competition from other trees. The model development starts with an inventory of existing information, which is expressed in the form of the sample and literature on this topic, and the definition of the exact deployment scenario of the model to be created. Together with the results of descriptive analyses in relation to the observed mortality and measured tree quantities the consequences for statistical modeling are derived. A suitable model meeting the requirements is deduced from the continuous-time Cox model by exploiting the equivalence to binary regression models when transitioning to the discrete case. For prediction of mortality, the generalization of standard logistic regression models to the class of generalized additive mixed models is used allowing to map the sampling design and to include a flexible combination of covariate effects. For purpose of variable selection within this class metrics quantifying different aspects of the predictive quality of the model are presented and evaluated in a cross-validation scheme. A parametrical simplification of the chosen model ensures ease of use and implementation. The estimation of the proposed model is based on over 14,000 individual observations in the experimental plots and a combination of four competition indices.

The growing trials of plant breeding considered in this work were conducted for an association study aiming to draw conclusions for breeding robust species of rye. From a statistical point of view, these planned experiments are advantageous to quantify and control unobserved conditions by means of randomization and blocking building. The trials are analyzed using linear mixed models taking multiple levels of relationship between different varieties of rye and longitudinal data structures into account. A detailed description of the individual components of the regression models is made and the genetic characteristics with significant association to frost tolerance are discussed.

The phenology section examines whether the flowering dates of different species have

changed over the last 30 years. With techniques of meta-analysis, a variety of locally observed trends is merged in a statistical model allowing for a powerful overarching assessment. In this approach, the uncertainty that adheres to the individual trends is taken into account and it is examined how the spatial variation has to be considered in the analysis of the developments. Among other things, significant indications exist that for species relying on the wind to carry their pollen to other plants, the long-term trend to flower earlier in the year is more pronounced than for species pollinated by insects. Not least, such findings are relevant for the field of allergology. Whether longer pollen seasons are to be expected in the future may only be indirectly indicated by the results of the study. However, possible modeling approaches on how to investigate this issue empirically on similar kinds of data are given.

The focal point in the medical section is model validation. The usefulness of existing risk models for prostate cancer is investigated; these models are mainly based on the prostate specific antigen and designed to help patients and physicians to determine whether a biopsy with its inherent risks is warranted. Besides established measures of model performance another metric is introduced, which includes the personal circumstances of the patient in the assessment of the risk model. The validation is implemented by means of ten external cohorts, and indicates whether the risk of persons where the subsequently performed biopsy actually detects cancer is predicted reliably higher than in men without prostate cancer diagnosis. It is shown that the absolute level of risk predictions is calibrated only for a part of the investigated persons and that the results vary depending on the cohort-specific prevalence/incidence and study-specific procedures.

Publications

This thesis contains parts which have already appeared or will appear in publications where discussed statistical methodology has been used. Those publications and the associated author contributions are:

(1) A. Böck, J. Dieler, P. Biber, H. Pretzsch, and D. P. Ankerst (2013). Predicting tree mortality for European Beech in Southern Germany using spatially explicit competition indices. *Forest Science*. To appear.

> A.B. derived the statistical concept, performed all data handling and statistical analysis and wrote the paper. H.P. provided the data and P.B. and J.D. advice on the data. D.A. provided supervision and helped with the paper editing.

(2) Y. Li, A. Böck, G. Haseneyer, V. Korzun, P. Wilde, C.-C. Schön, D. P. Ankerst, and E. Bauer (2011). Association analysis of frost tolerance in rye using candidate genes and phenotypic data from controlled, semi-controlled, and field phenotyping platforms. *BMC Plant Biology 11*, 146.

> Y.L. and A.B. share first authorship; Y.L. carried out the candidate gene and population structure analysis and drafted the manuscript, while A.B. conceived the statistical models, performed the statistical analyses, including relevant graphics, and drafted the methods and results sections concerning statistics. G.H. participated in the molecular analyses and interpretation of the results. D.A. reviewed all statistics. V.K. provided SSR marker data. P.W. developed the plant material. E.B. and C.S. designed and coordinated the study and interpreted the results. All authors edited the final manuscript.

(3) C. Ziello, A. Böck, N. Estrella, D. P. Ankerst, and A. Menzel (2012). First flowering of wind-pollinated species with the greatest phenological advances in Europe. *Ecography 35*(11), 1017–1023.

> C.Z. and A.M. conceived the analysis. Specifically, A.B. developed the idea of applying weighted linear mixed models for the meta analysis of the COST data, selected statistical methods and wrote R scripts. C.Z. performed the analyses and wrote the paper. N.E., D.A. and A.M. edited the final paper.

(4) D. P. Ankerst, A. Böck, S. J. Freedland, I. M. Thompson, A. M. Cronin, M. J. Roobol, J. Hugosson, J. Stephen Jones, M. W. Kattan, E. A. Klein, F. Hamdy, D. Neal, J. Donovan, D. J. Parekh, H. Klocker, W. Horninger, A. Benchikh, G. Salama, A. Villers, D. M. Moreira, F. H. Schröder, H. Lilja, and A. J. Vickers (2012). Evaluating the PCPT risk calculator in ten international biopsy cohorts: results from the prostate biopsy collaborative group. *World Journal of Urology 30*(2), 181–187, and

(5) D. P. Ankerst, A. Böck, S. J. Freedland, J. Stephen Jones, A. M. Cronin, M. J. Roobol, J. Hugosson, M. W. Kattan, E. A. Klein, F. Hamdy, D. Neal, J. Donovan, D. J. Parekh, H. Klocker, W. Horninger, A. Benchikh, G. Salama, A. Villers, D. M. Moreira, F. H. Schröder, H. Lilja, A. J. Vickers, and I. M. Thompson (2012). Evaluating the prostate cancer prevention trial high grade prostate cancer risk calculator in 10 international biopsy cohorts: results from the prostate biopsy collaborative group. *World Journal of Urology*. To appear.

A.B. conceived the statistical plan and performed all statistical analysis. Due to membership in the consortium D.A. was required to be first author and wrote the manuscript. All other authors contributed data.

Contents

List of Figures

List of Tables

Introduction

Empirical evidence forms the basis for inference in the life sciences. Accordingly, much effort and cost are invested in performing trials, recording, collecting, and storing data. Statistical methodology deals with finding optimal approaches in terms of planning, ascertainment, and analysis. Therefore it is imperative to additionally involve the capabilities of modern statistical methods to enhance subject matter understanding. The aim of this thesis is to quantify the risk of certain threats in different fields of the life sciences in order to more accurately predict the occurrence of these threats in the future. Therefore, risk models for application in forestry, plant breeding, phenology, and oncology are developed and validated using modern state-of-the-art statistical methodology.

One of the most basic statistical association models is linear regression and it is the fundament for the analyses of the plant breeding experiments of Chapter 2 and the phenological observations in Chapter 3. Through linear regression the impact of one or more exploratory variables x on a metric quantity y can be statistically examined presuming the additive relationship

$$y = \beta_0 + \beta_1 x_1 + \ldots + \beta_p x_p.$$

Although called the linear model, nonlinear relationships can be accommodated by transforming either the outcome or explanatory variables. As it is not realistic to assume a strictly deterministic relationship between y and x and measurements do not have infinite accuracy, the above equation is extended by a probabilistic term, here in an additive manner, leading to a proposed model for a sample of n observations:

$$y_i = \beta_0 + \beta_{1i} x_{1i} + \ldots + \beta_p x_{pi} + \varepsilon_i = \boldsymbol{x}_i' \boldsymbol{\beta} + \varepsilon_i, \quad i = 1, \ldots, n.$$

For the distribution of ε an assumption is made, which should reflect the sample design and accurately describe the distribution of the observed data, which can be checked in a subsequent residual analysis. A standard choice is to assume independent and identically distributed (iid) normal errors $\varepsilon_i \overset{\text{iid}}{\sim} \mathrm{N}(0, \sigma^2)$. This implies that the data y are randomly collected, are independent, and are normally distributed given x, with equal variance (homogeneity of variance). No distributional assumption is made for the parameter vector $\boldsymbol{\beta}$ in this model. Alternative assumptions for the error term allow to formulate advanced ap-

proaches, with t-distributed errors yielding robust regression for the mean, and asymmetric Laplace distributed errors yielding quantile regression for quantiles of the distribution, in particular the median.

Whenever possible and meaningful the design of an experiment or data collection should provide a metric outcome, since continuous metric data provide richer information than categorical or grouped data. Coarsening by grouping into classes, such as by dichotomizing size into small/medium/large, results in a loss of information in likelihood-based inference. However, truly categorical outcomes, such as mortality (alive versus dead) must be modeled on the categorical scale. Relating a dichotomous variable such as mortality to covariates can be achieved by a statistical model that effectively inserts a metric variable in between. An unobservable (latent) variable is postulated as being the driving force behind mortality. The latent variable exists on a continuum (such as severity of bad health) and when it reaches a threshold, the outcome of mortality is experienced. This is in fact the statistical definition of the commonly used logistic regression model for binary events. Specifically, the observed variable y assumes either value 0 or 1, such as corresponding to alive versus dead, respectively. It connects to a latent variable $\tilde{y}$ with threshold τ by the mechanism

$$y = \begin{cases} 1 \text{ (dead)} & \text{if } \tilde{y} > \tau \\ 0 \text{ (alive)} & \text{if } \tilde{y} \leq \tau. \end{cases}$$

A probabilistic model is assumed for the latent variable conditional on observed covariates:

$$\tilde{y}_i = \beta_0 + \beta_{1i}\, x_{1i} + \ldots + \beta_p\, x_{pi} + \varepsilon_i, \quad i = 1, \ldots, n.$$

From this relationship, the probability of death for the ith individual, π, is

$$\pi_i = \mathbf{P}(y_i = 1) = \mathbf{P}(\boldsymbol{x}_i'\boldsymbol{\beta} + \varepsilon_i > \tau) = 1 - h(-\boldsymbol{x}_i'\boldsymbol{\beta}),$$

where $h(.)$ is the cumulative density function assumed for ε. Specifying $h(.)$ as the standard logistic distribution

$$h(\eta) = \frac{\exp(\eta)}{1 + \exp(\eta)}$$

results in the logistic regression model for y on $\boldsymbol{x}$:

$$\mathbf{P}(y_i = 1|\boldsymbol{x}_i) = \frac{\exp(\boldsymbol{x}_i'\boldsymbol{\beta})}{1 + \exp(\boldsymbol{x}_i'\boldsymbol{\beta})} \quad i = 1, \ldots, n.$$

In contrast to linear regression for metric outcomes, there is no free variance parameter in the logistic error distribution. Its fixed value is needed for unique estimation of $\beta_1, \ldots, \beta_p$. Otherwise only the ratio of two β coefficients would be unambiguous. Another restriction is made by specifying $\tau = 0$ to obtain an identifiable intercept β_0. Loosely speaking, these

restrictions pay tribute to the fact that the scale of $\tilde{y}$ is unknown and the sample of binary y observations does not allow to extract information concerning dispersion in the underlying vector of probabilities π_i. Impacts which can be attributed to theses scale issues in comparison to linear models are discussed in Mood (2010).

Logistic regression has become the most commonly used model for binary outcomes and risk prediction in medical statistics (it is used in this context in Chapter 4). This can be attributed to the fact that it provides meaningful interpretable effect estimates in retrospective case control designs as well as in prospective cohort studies. A commonly encountered example provides an illustration, which also introduces some basic metrics in risk modeling. Of key interest in epidemiological studies is the quantification of the relative risk (RR) of exposed individuals E (for example, smokers) compared to non-exposed $\bar{E}$ (non-smokers) for developing a certain disease (lung cancer). This can be achieved by setting up a cohort of healthy persons comprising both exposed and non-exposed individuals who are followed over a time period of, say, 20 years. The data obtained from this kind of study results in the following 2 by 2 table, where the letters a, b, c, d represent the observed counts:

	Developed disease	
Exposed	D (yes)	$\bar{D}$ (no)
E (yes)	a	b
$\bar{E}$ (no)	c	d

The risk of the disease for exposed individuals, π_E, is estimated by $a/(a+b)$, and for non-exposed individuals, $\pi_{\bar{E}}$, by $c/(c+d)$. The relative risk of the disease associated with the exposure thus is

$$RR(D) = \frac{\pi_E}{\pi_{\bar{E}}}.$$

Another metric quantifying the impact of the exposure is the odds ratio (OR) (Szumilas, 2010). It begins with the odds ($odds$) in favor of an event, which is the ratio of the probability that the event happens to the probability that the event does not happen:

$$\begin{aligned} odds(D|E) &= \frac{\pi_E}{1-\pi_E} \quad \text{(odds in exposed)}, \\ odds(D|\bar{E}) &= \frac{\pi_{\bar{E}}}{1-\pi_{\bar{E}}} \quad \text{(odds in non-exposed)}, \\ OR(D) &= \frac{odds(D|E)}{odds(D|\bar{E})}, \end{aligned}$$

which is estimated by

$$\widehat{OR}(D) = \frac{a \cdot d}{b \cdot c}.$$

For a rare disease, when probabilities π_E and $\pi_{\bar{E}}$ to develop the disease are small for both

exposed and non-exposed, respectively, the relative risk can be approximated by the odds ratio, $RR(D) \approx OR(D)$. However, for rare diseases the prospective design of a cohort study is not efficient. Hundreds of thousands of individuals must be followed for long periods of time in order to capture sufficient numbers of diseased cases, incurring a prohibitive cost burden. An alternative concept to circumvent this problem is to perform a case-control study (Breslow et al., 1980). Here, individuals are not followed until outbreak of the disease, but individuals suffering from the disease (cases) are selected from a population retrospectively, such as through the scanning of hospital records. Suitable controls without the disease are matched according to individual factors, such as being in similar age. The exposure status is established afterwards. The case-control design is a leading competitor for modeling the rare event of tree mortality in forests covered in Chapter 1. The limitation of the case-control design is that it is not possible to infer the risk of disease as the counts of cases and controls are artificially fixed. The advantage is that the odds ratio can still be used to approximate the relative risk because odds ratios behave symmetrically in terms of switching disease and exposure,

$$OR(E) = \frac{odds(E|D)}{odds(E|\bar{D})} = \frac{odds(D|E)}{odds(D|\bar{E})} = OR(D).$$

For the relative risk this is not valid in general: $RR(D) \neq RR(E)$.

The parameters $\beta_1, \ldots, \beta_p$ of the logistic regression model parametrize the log odds ratio with respect to a unit change in the according covariates $x_1, \ldots, x_p$. Thus, logistic regression can be used to estimate the odds ratio in the case-control design. If we set $y = 1$ for all cases, $y = 0$ for all controls, $x = 1$ for all exposed individuals, $x = 0$ for the non-exposed, and estimate the model

$$\mathbf{P}(y = 1|x) = \frac{\exp(\beta_0 + \beta_1 x)}{1 + \exp(\beta_0 + \beta_1 x)}.$$

then the odds ratio of disease with respect to exposure is

$$\frac{\mathbf{P}(y = 1|x = 1)}{1 - \mathbf{P}(y = 1|x = 1)} \Big/ \frac{\mathbf{P}(y = 1|x = 0)}{1 - \mathbf{P}(y = 1|x = 0)} = \exp(\beta_1).$$

One is able to retrieve useful effect estimates regardless of the base level of mortality. The strength of using a model-based approach, such as logistic regression, over traditional epidemiological tabular methods, is the easy expandability to account for multiple risk factors and confounders by including additional parameters. The ubiquitous use of logistic regression is not confined to the medical context. It can be used whenever the objective is to quantify the probability of occurrence of specific events or the presence of certain characteristics or states. In forestry, it is the dominant model for the prediction of tree mortality (cf. Table 1.5). A peculiarity to be minded in this context is that the proportion of trees where mortality was actually observed is very low (rare events). Consequences for the performance of logistic regression are discussed in King and Zeng (2001).

Alternatively, event data may be more finely modeled in terms of the time until the event occurs. Time to event data are addressed by survival models. In practice, there is often the situation that the time spans of observations are recorded only coarsely, leading to discrete time survival models. Discrete survival time models may be approximated by logistic regression models, as we will perform in our analyses of mortality of beech trees in a German network that inspected trees only approximately every 5 years (Chapter 1).

If rich time-to-event data are available in metric form, Cox regression is a common choice, since it accommodates censoring of observations, which occurs when individuals are known to survive only up to a specific time point but not what happens afterwards, allows the incorporation of covariates in terms of a linear predictor affecting a hazard ratio, and makes no parametric assumptions on the baseline hazard (Cox, 1972). This model is not described in more detail here since none of the outcomes in this thesis were of the continuous time-to-event type, but issues and potential future directions would apply analogously as for the other statistical models used here. Approaches towards survival models which make more explicit use of the actually observed time spans than the Cox model, which only employs the chronological order of the events, are dealt with in Kneib and Fahrmeir (2004) and Carstensen (2005).

A central issue to all the statistical models that incorporate explanatory variables to explain variation is how to incorporate random effects to account for residual heterogeneity due to less tangible effects, such as by differences in geographic locations or by machine. The term mixed models reflects the fact that the model comprises further random effects with a distributional assumption in addition to fixed effects which are understood as unknown but existent true (hence fixed) quantities (McCulloch and Searle, 2001). Mixed models have made it into routine practice in virtually all fields of the life sciences including ecology (Zuur, 2009), medicine (Brown and Prescott, 2006), veterinary research (Duchateau et al., 1998), agricultural sciences (Gbur et al., 2012), and animal breeding (Mrode and Thompson, 2005). However, the application of mixed models is less motivated by the philosophy about interpreting quantities as random or fixed but more motivated by the pragmatism to flexibly incorporate subjective understandings in the model. Furthermore, mixed models have their frequentist counterpart in penalized estimation approaches. The connection of ridge regression with the normality assumption of random effects is the one example. The purposes of random effects in mixed models range from accounting for the hierarchical structure of the sample (trees organized in plots, measurements originating from phenological stations, block building in growing trials), incorporating secondary information about the sample (relatedness of genotypes, geographic coordinates), and achieving a data-driven selection of model complexity (penalized splines, baseline mortality over time). The strength of generalized mixed models is to allow rather any combinations of such building blocks in the systematic part of the model independently from the outcome-specific distribution. By replacing a series of repeated analyses (say over different trials) into a single analysis using random effects,

multiple testing is more controllable, the power (effective sample size) of the experiment is increased, and inference concerning global versus site-specific trends is permitted. For this reason, mixed models are used in most of the applications in this thesis (Chapters 1–3). Whatever the type of statistical model, external validation on a completely independent data set is the proof of principle that the model can be used in practice. State-of-the art approaches in the application and validation of statistical modeling for a variety of outcome types and experimental settings are demonstrated in the remaining chapters of this thesis.

In Chapter 1 (Forestry) we examine the steps of model development, which involve descriptive analyses, a literature review of similar studies, and the presentation of imposed consequences. The final risk model is derived from a discrete approximation to the Cox model and is refined to the class of generalized additive mixed models. The statistical tools applied include nonparametric tests, function approximation using splines and the specification of random effects reflecting spatial and temporal structures of dependency. Model selection is based on performance measures which were calculated in a cross validation scheme. Accompanying graphs illustrate a way of communicating the results.

In Chapter 2 (Plant breeding), we present an association study with the objective of deducting new breeding programs on robust kinds of rye. For this study growing trials on several genotypes in three different platforms were designed and conducted employing techniques of randomization and block-building. The results are related to the occurring variations of genetic markers in the plant genome. These markers were selected in advance to cover regions linked to frost tolerance as indicated by previous studies (candidate gene approach). The statistical association model includes the genetic similarity of different genotypes explicitly and accounts for the particular sampling design. By application of this model several genetic markers are identified, which are most promising across all three platforms in terms of breeding purposes.

Chapter 3 (Phenology) covers a meta analysis on phenological data. The aim of the analysis was to infer the developments in long-term trends for different species from the records of flowering dates available in aggregated form in the COST (European Cooperation in Science and Technology) network. In detail, we investigate potential evidence that flowering dates of wind pollinated species have advanced more than insect pollinated plants and whether the length of the flowering season within a calendar year has become longer in the past decades, as pollen in the air are a major trigger for allergies. We demonstrate how to treat observations which do not arise from a simple random sample and how to handle the multiple testing problem arising when several hypotheses are examined on the same data. Further, we show how a spatial correlation structure can be embedded in the model and use bootstrap combined with spline methods for diagnostic purposes.

In Chapter 4 (Cancer) we assess the quality and benefit of model-based prostate cancer predictions. Prostate cancer is one of the leading causes of cancer death in men in Western Europe and the United States; more than 670,000 men are diagnosed with prostate cancer

every year (European Randomized study of Screening for Prostate Cancer, 2013). Two existing prostate cancer risk calculators are validated using new external data not involved in the preceding development stage. We introduce measures that evaluate the prediction performance in terms of calibration and discrimination abilities. Further, we discuss whether usage of these calculators can provide a clinical benefit for the considered validation cohorts.

Finally we conclude with a discussion on future research needed for the modeling of outcomes of the type that have arisen in the four applications of this thesis.

Chapter 1

Forestry

Parts of the following chapter will be published in "Predicting tree mortality for European beech in southern Germany using spatially explicit competition indices" by A. Böck, J. Dieler, P. Biber, H. Pretzsch, and D. P. Ankerst (accepted in Forest Science 2013). Figure 1.2 was provided by Jochen Dieler, Figure 1.3 by Peter Biber. Figures which are equivalent to those of the article are indicated with "reproduced", those which are similar but basing on different data with "in style of".

1.1 Introduction

Tree mortality prediction is an essential component of single tree-based forest growth models, including the growth simulator SILVA (Pretzsch et al., 2002). The SILVA simulation software was developed in 1989 and is since maintained by the Chair for Forest Growth and Yield at the Technische Universität München (SILVA website, 2013). It allows the simulation of forest growth for complex structured pure and mixed stands following an individualized tree approach. A stand is seen as a system of single trees having different characteristics, that mutually influence each other. Inter-tree relationships are derived from positions and sizes of trees relative to each other, and used to calculate competition indices (CI), which in turn enter the simulation model. The user can specify various scenarios for thinning concepts and intensity up to a maximum simulation length of 145 years. The program updates the forest profile at 5-year intervals. The results can be assessed in terms of timber production, and economical and structural characteristics, which are useful for decision-making in forest as well as landscape management, for educational purposes, and as leads to further scientific enquiries. The general simulation procedure takes place in three steps: 1.) Set up the management and site conditions, and, if needed, complete missing information via the stand structure generator; 2.) Calculate the competition measures and apply the model for mortality, thinning, and increment; 3.) Generate the various outputs.

Our work was focused on developing a new statistical model for the mortality component, highlighted in Figure 1.1. Toward that goal, we present the development process of a

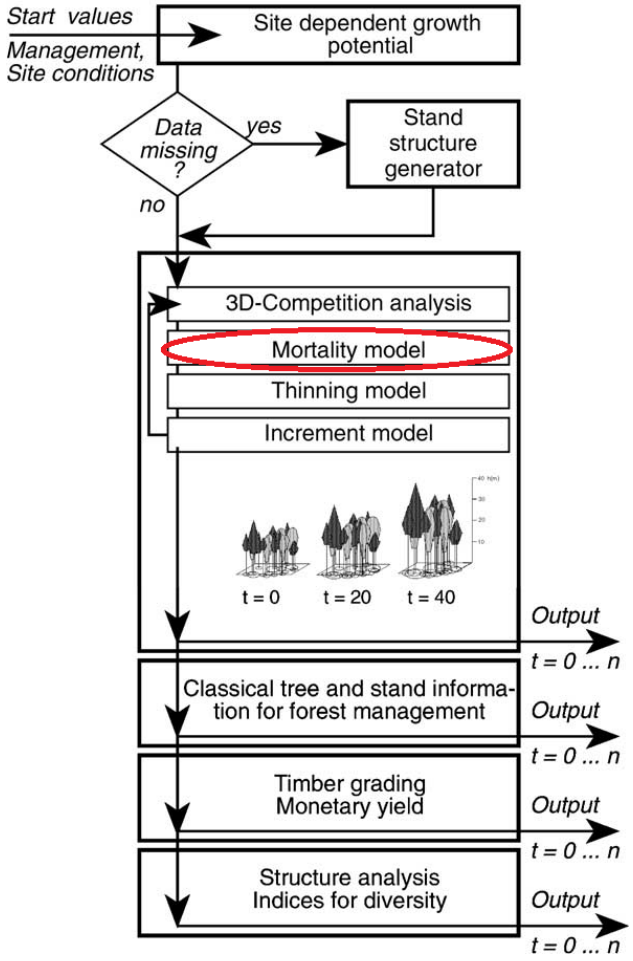

Figure 1.1: Flowchart for the SILVA simulator. This study focuses on the mortality model component, marked in red. Figure reproduced from Pretzsch et al. (2002), Figure 1.

mortality prediction model applied to approximately 6,000 beech trees. The procedures have wider applicability to five-year mortality prediction for long term forest research plot, as well as any interval prediction where relevant data are available across many scientific fields. We describe the design of the survey, how the data are collected and outline the statistical challenges and needs in such modeling scenarios. These include the treatment of dependencies between multiple observations on the same tree or plot and the implications of tree mortality as a rare event. We provide an overview of the literature for predicting tree mortality and motivate the chosen model, starting with the Cox proportional hazards model (Cox, 1972). We then show how model selection was performed, including measures of model performance and the validation schemes. We also provide full model details allowing others to use the model for their own purposes, by implementing it in online calculators or in spreadsheet calculators such as Excel, whenever a mortality risk prediction is required.

1.2 Data and exploratory methods

1.2.1 Data source and mortality

Data were collected from beech trees taken from multiple plots at eight test sites in Bavaria, Germany that were undergoing surveillance from 1985 until 2007 (Figure 1.2). Individual trees were observed between one to four observation periods during these years, with observation periods ranging from three to ten years (most five years). Individual tree-periods where the tree experienced mortality through man-made thinning or natural disasters such as storms were excluded. Generally, the terms mortality and mortality rate are used interchangeably, denoting the number of deaths by a certain cause occurring in a given population at risk during a specified time period (World Health Organization, 2013). As the observed mortality rates were based on time periods of different lengths, they only have limited interpretability. Therefore we also calculated standardized 5-year mortality rates. The inclusion criteria resulted in 6,189 beech trees and 14,239 tree-periods from 29 plots. The data are summarized in Table 1.1.

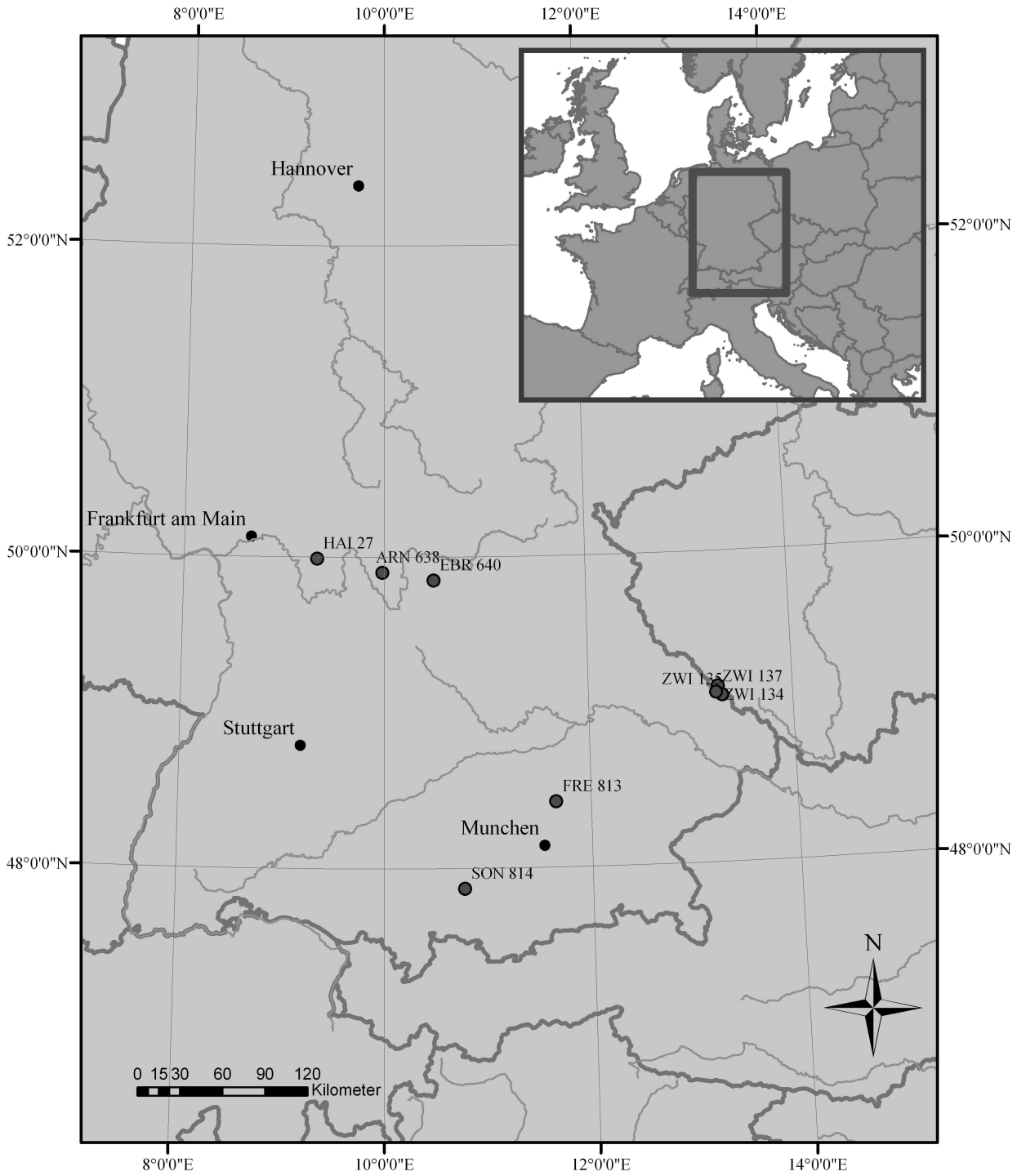

Figure 1.2: Location of test sites in Bavaria, Germany. Figure reproduced from Böck et al. (2013)

1.2.2 Variables and risk factors

We included only plots that had a minimal mortality of 1% for all observation periods. Within the included plots, we included only individual tree-periods that had information on all risk factors at the beginning of an observation period and mortality (yes versus no) at the end of the same observation period. Results based on a more liberal inclusion of survey

		Number of			Mortality in % per	
Plot	Test site	trees	periods	dead trees	period	5-year period
1	814	98	182	27	14.84	11.27
2	813	172	320	47	14.69	13.44
3	640	307	507	58	11.44	13.02
4	640	348	589	48	8.15	9.24
5	640	973	1,742	112	6.43	6.04
6	135	307	970	51	5.26	5.61
7	814	193	472	23	4.87	5.30
8	638	398	831	34	4.09	4.41
9	137	366	629	22	3.50	1.75
10	135	291	1,109	35	3.16	3.33
11	640	164	317	10	3.15	2.64
12	134	104	353	11	3.12	3.31
13	640	184	359	11	3.06	2.56
14	638	238	548	16	2.92	3.23
15	137	199	322	7	2.17	1.09
16	640	285	285	6	2.11	2.11
17	134	107	345	7	2.03	2.16
18	134	68	254	5	1.97	2.08
19	134	55	203	4	1.97	2.08
20	813	81	161	3	1.86	1.69
21	134	46	167	3	1.80	1.90
22	814	62	167	3	1.80	2.01
23	640	58	116	2	1.72	1.72
24	814	154	440	6	1.36	1.56
25	813	44	74	1	1.35	1.25
26	135	295	967	13	1.34	1.43
27	135	269	942	11	1.17	1.24
28	135	226	771	8	1.04	1.10
29	27	97	97	1	1.03	0.52
Overall		6,189	14,239	585	4.11	3.92

Table 1.1: Summary of beech trees included in the analysis. Test sites refer to Figure 1.2.

plots can be found in Böck et al. (2013).

Risk factors considered in the prediction models comprised measures of the size of individual trees, indices covering different aspects of competition, site quality information, calendar year, and period length, Table 1.2 contains a detailed description. Tree size was measured by the diameter at breast height (*DBH*) and by *Height*, but as *Height* was only measured for a sample of trees and estimated for the others, it was not preferred over *DBH*. Both were treated as potential candidate variables for mortality prediction in the model selection stage of analysis. The age of the trees has not been considered as a risk factor, since often the age of trees is unknown and since the model must be applicable to both even- and uneven-aged stands. However, age inevitably correlates with tree size. To quantify

the competition of a tree, its size and location relative to other trees in the neighborhood are used to construct competition indices (CI), which partly build upon one another. The CIs are derived from local vertical profiles, as outlined in Figure 1.3, and sum over defined upright ranges with overlapping regions, called integrals. *CICUM60* measures the vertical competition profile from top stand height down to 60% of the tree of interest's height. Similar to *KKL*, a simple geometric competition index (see Pretzsch et al., 2002), it is designed to measure overall momentary competition and in our approach is split into two parts: *CIIntra* is the component of *CICUM60* attributable to trees that belong to the same species as the tree of interest, so that it quantifies intraspecific competition, and *CIConifer* represents the portion of *CICUM60* which originates from conifer species.

In order to divide competition into the ecologically different aspects of overshading and lateral constriction (Assmann, 1961; Pretzsch, 1992), the integral value at the tree's top is assigned to the measure *CIOvershade* originating from other crowns above the tree, which cause overshading. The difference $CILateral = CICUM60 - CIOvershade$ is used as a measure for lateral competition, where high values indicate competition not caused by overshading.

From a temporal point of view, all CIs mentioned above measure momentary competition,

Characteristic	Definition	Range of observations
PeriodOnset	First year of survey period.	[1985, 2000]
PeriodOffset	Last year of survey period.	[1989, 2007]
PeriodLength	Length of the observation period in years.	[3, 10]
DBH	Diameter at breast height (1.3 m) in cm.	[0.8, 90.9]
Height	Tree height in m.	[1.4, 43.6]
KKL	Quantifies light competition by neighboring trees.	[0.0, 90.9]
CIIntra	Competition from trees of the same species as the tree of interest.	[5.9, 517.6]
CIConifer	Competition from conifer trees.	[0.0, 204]
CIOvershade	Extension of over-shading by other trees.	[0.0, 505.9]
CILateral	Lateral competition of a tree.	[0.0, 436.9]
DBHdom	Estimation of the DBH (in cm) a tree would have at its current height if pre-dominant for its whole life.	[1.34, 116.6]
RelDBHdom	Ratio of DBHdom to DBH that measures long-term competition.	[0.2, 1]
SiteIndex	Plot- and species-wise site index, expressed as stand height at age 40 (derived from standard yield tables).	[5.5, 22.5]

Table 1.2: Definitions of variables and risk factors used in the analysis. For all competition indices, higher values indicate more competition; for *SiteIndex*, higher values indicate better growth conditions.

which can be strongly influenced by ad-hoc thinnings, for example. A different aspect is the long term-competition, which expresses the typical competition a tree has undergone during its life, and is meant to accumulate the competition from the past. To quantify the long-term competition without knowing the entire history of a tree and its neighbors, a different concept that compares actual tree size to a reference tree size is needed. If a given tree size is

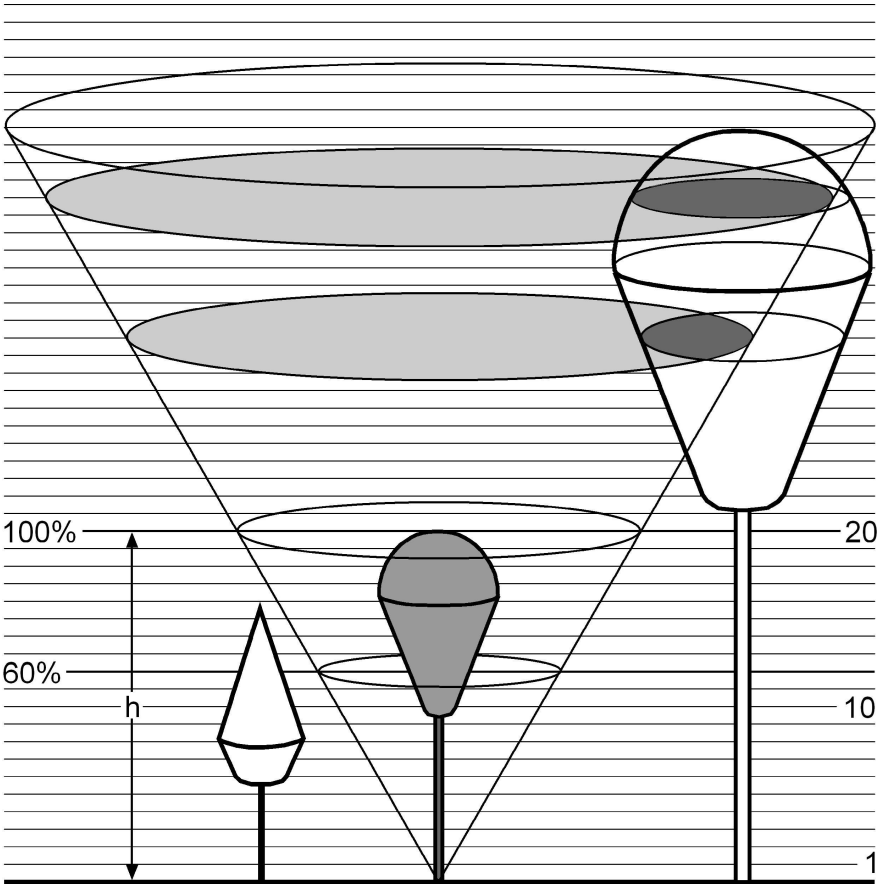

Figure 1.3: Principle for determining vertical competition profiles. The space around a tree of interest (shaded in gray) is stacked with horizontal planes spaced at distances 1/20th of the tree of interest's height. An upturned cone with an opening angle of 60 degrees is placed with its tip in the tree's footpoint. The intersection areas of the cone and the horizontal planes form a series of circles that become larger with increasing distance from the forest floor. Any neighbor tree that touches that cone is considered a competitor. Thus, the left tree is not a competitor while the right tree is. The three-dimensional crown models of Pretzsch (2001) are applied to measure the overlapped area (shown in dark gray) of each competitor's crown with the respective cone-intersection-circle (shown in light gray). The relative proportions of the overlapped areas to the cone-intersection-circles are summed up plane-wise, and then the profiles are stepwise integrated from their topmost point down to the forest floor. The resulting integrals are multiplied by 1/20 (one step width relative to the tree of interest's height). The integral value obtained at 60% of the tree of interest's height is the competition index *CICUM60*, a general measure of competition. *CIIntra* is the component of *CICUM60* that comes from trees that belong to the same species as the tree of interest, whereas *CIConifer* is the component resulting from coniferous competitors, such as Norway spruce and Scots pine. Figure reproduced from Böck et al. (2013)

small compared to a reference tree size, the tree must have experienced strong competition in the past and vice versa. As trees under competition suffer a reduction in diameter increment more than in height increment, the *DBHdom* measure is used as a reference. This measure is defined as the DBH a pre-dominant tree has at a given height and is estimated as follows. From a subsample of the data the allometric relationship, $DBHdom = 0.6553 \cdot Height^{1.327}$, is estimated (assuming the units m for *Height* and cm for *DHB*) and used to estimate the DBH a tree could have achieved at its current height under very low competition during its life up until the present. Dividing the tree's current *DBH* by the estimated *DBHdom* yields the measure *RelDBHdom*. Low values of *RelDBHdom* indicate the tree has undergone stronger long-term competition, while larger values near or even exceeding 1 indicate the tree has not suffered much competition throughout its life. Finally, site quality (*SiteIndex*) is expressed through the expected mean stand height in m at age 40 years based on the yield table for European beech by Schober (1967).

In addition to the tree-related characteristics, variables originating from the sampling design were included in the analysis. The calendar years at the beginning and end of each observation period are denoted as *periodOnset* and *periodOffset*, the time between those, as *periodLength*. A description of all variables acting as candidates to be included in the prediction model are summarized in Table 1.2.

To report mortality as a function of time we restructured the observations and calculated the mortality rate on a calendar year basis. The mortality rate within a calendar year was calculated by the ratio

$$\frac{\text{Number of mortalities during calendar year}}{\text{Number of observed trees at risk during the calendar year}},$$

where number of trees at risk are those that were alive and in the study at the beginning of the calendar year. The exact year of mortality of a specific tree is not known within its period of observation and was therefore distributed uniformly during the respective period. For example, a tree observed as dead at the end of the survey period from 1995 to 1998, contributes 1/3 to the numerator, and 1 to the denominator for each of the three years. Finally, the annual mortality rates were translated to 5-year rates by multiplying by 5 (van Belle and Fisher, 2004, chap. 15). We present the 5-year mortality for each year, along with 95% confidence intervals obtained from a normal approximation to the binomial distribution, as well as the number of deaths and exposure time. The course of mortality over the years, which is smoothed owing to the calculation method, is also displayed as graph.

1.2.3 Contrasting risk factors in mortality versus non-mortality periods

In a primary stage towards the prediction model we evaluated each risk variable separately. The object of investigation was whether and how values of the risk factors differed

between tree-observation periods that resulted in mortality versus non-mortality. We preferred this by-period approach to an analysis at tree level, as the latter would require a longitudinal analysis of the trees or a reduction of multiple observations of the same tree to a single one. For this in turn, further assumptions are needed, it does not reflect the aspired by-period prediction and moreover does not make use of the entire data set. Indeed, the statistical tests in the following paragraph rely on the assumption of independent observations and we will discuss to what extent this assumption is justified in the model development section.

By means of numerical statistical measures and tests we compared risk factors and observational characteristics between tree-observation periods with and without mortality using means, standard deviations (SD), and ranges. As a measure of association between a continuous variable (risk factor) and a dichotomous variable (mortality) we report the area underneath the receiver operating characteristic (ROC) curve (AUC)(Tom, 2006). Technically, the ROC curve is a graph of the false positive fraction (FPF) against the true positive fraction (TPF) for all possible thresholds of a the risk factor. The FPF is the proportion of alive subjects with a risk factor higher than the threshold, that means erroneously classified as dead and TPF is the proportion of dead subjects with a risk factor higher than the threshold. Let $x \in \mathbb{R}$ be the risk factor, $y \in \{0; 1\}$ the observed mortality being 1 for a dead tree, 0 for a live tree, and *cut* the threshold, then the FPF and TPF are calculated as

$$FPF_{cut} = \frac{\sum I(x_i > cut) I(y_i = 0)}{\sum I(y_i = 0)}$$

and

$$TPF_{cut} = \frac{\sum I(x_i > cut) I(y_i = 1)}{\sum I(y_i = 1)},$$

respectively, where the sum includes all observations $i = 1, \ldots, n$ and the indicator function $I()$ evaluates to 1 if the statement in its argument holds and 0 otherwise. The AUC quantifies the ability of a risk factor to distinguish between mortality and non-mortality periods. It equals the probability that for a randomly chosen pair of single tree observation periods, where one observation period of the pair resulted in mortality and the other not, the risk factor is higher for the period with mortality (if high values of the risk factor are associated with mortality, lower otherwise). An AUC close to 100% indicates good discrimination of the risk factor for mortality, while an AUC close to 50% indicates that the risk factor exhibits no better discriminating ability between observation periods with mortality versus non-mortality than flipping a coin. So, in its standard form AUC is reported as a number between 0.5 and 1 and does not provide information about the direction in which a risk factor acts, that is whether high values of the risk factor indicate mortality. We provide this additional information when needed. As a rank-based measure the AUC is invariant to

monotone transformations, which means it leads to the same conclusion whether or not a monotone transformation is applied to the risk factor. It can be shown that the Wilcoxon

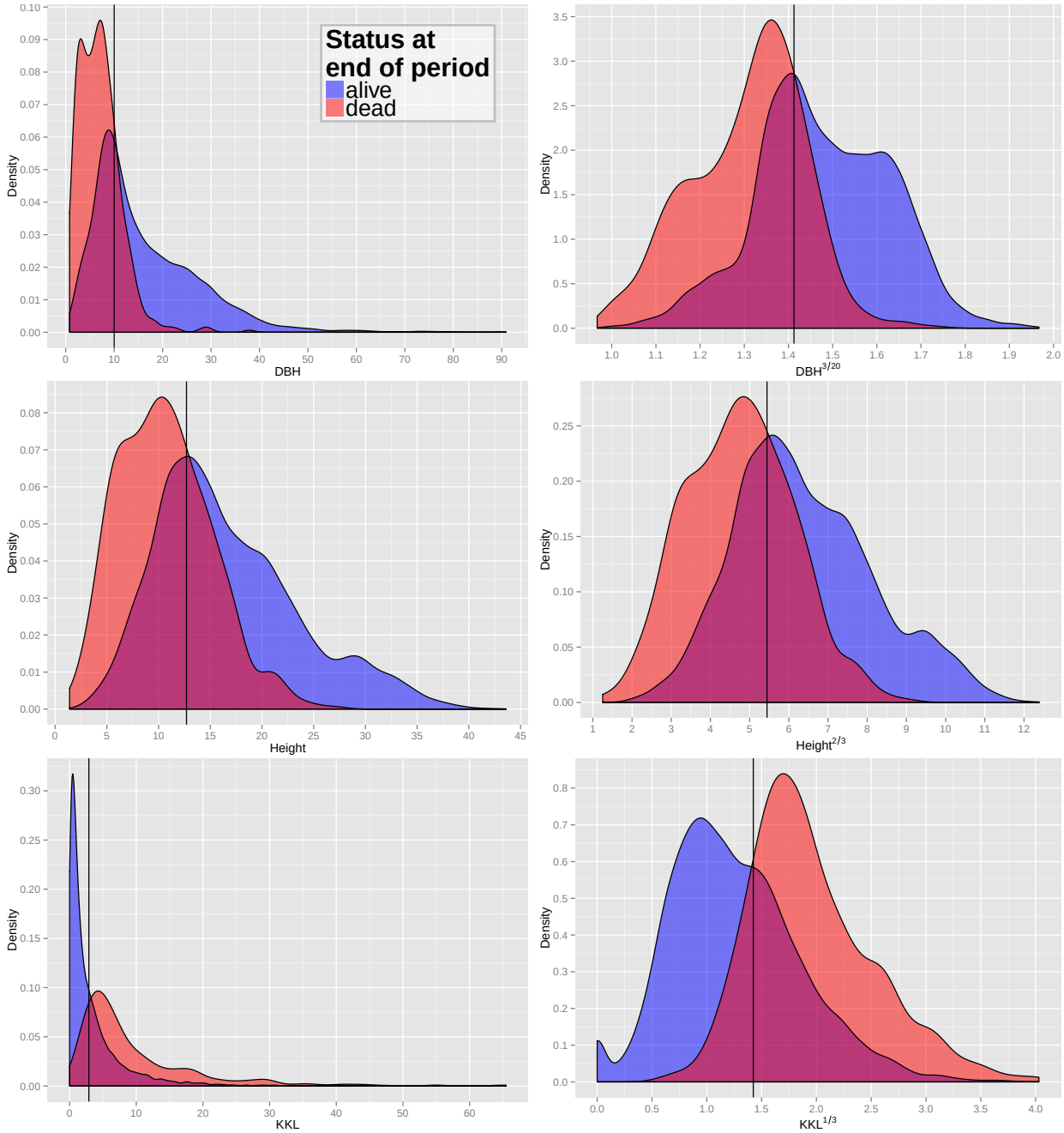

Figure 1.4: Plot of kernel density estimates of the distributions of risk factors on the original scale (left) and after applying a transformation to achieve a more compact and symmetric shape (right). The black vertical lines indicate optimal separation thresholds given in Table 1.4.

test statistic is equivalent to the AUC, allowing interpretation of the result of the Wilcoxon test as a test with null hypothesis that AUC=0.5. The null hypothesis of the two sample Wilcoxon test is "equal medians in both groups", but also makes the implicit assumption that the shapes of the distributions of the risk factors, and hence their variances, are the

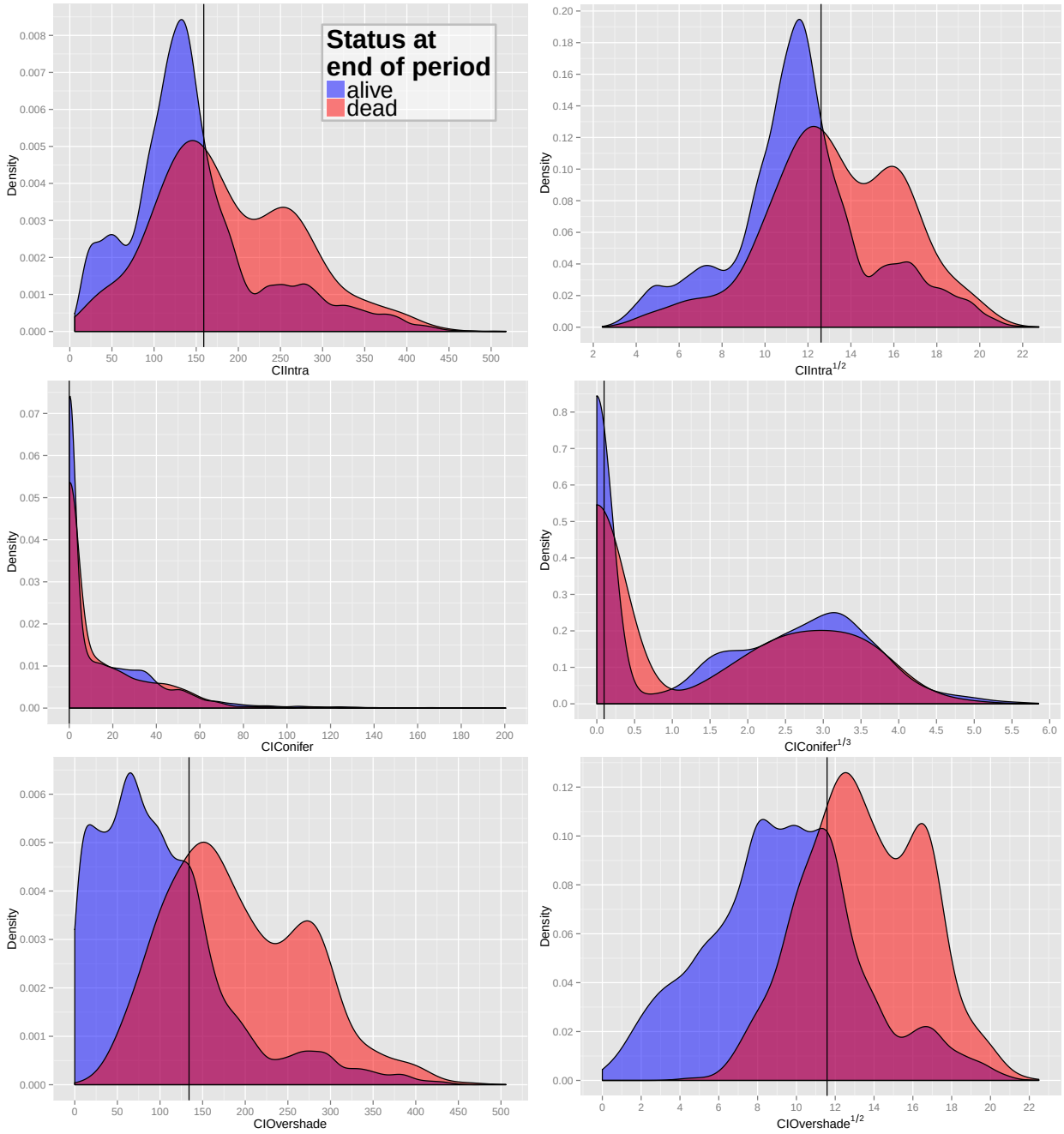

Figure 1.4 continued.

same (Fahrmeir et al., 2003, p. 457). We compared the results to an alternative test relaxing this assumption suggested in Brunner and Munzel (2000).

Besides the AUC, we report an optimal threshold based on the maximization of the Youden index, TPF + FPF - 1 (Youden, 1950), which provides a specific cutoff, cut_{Youden}, for distinguishing mortality versus non-mortality periods,

$$cut_{Youden} = \arg\max_{cut}\{TPF_{cut} + FPF_{cut} - 1\}.$$

The Youden index assumes that the error made by assigning non-mortality to a period which

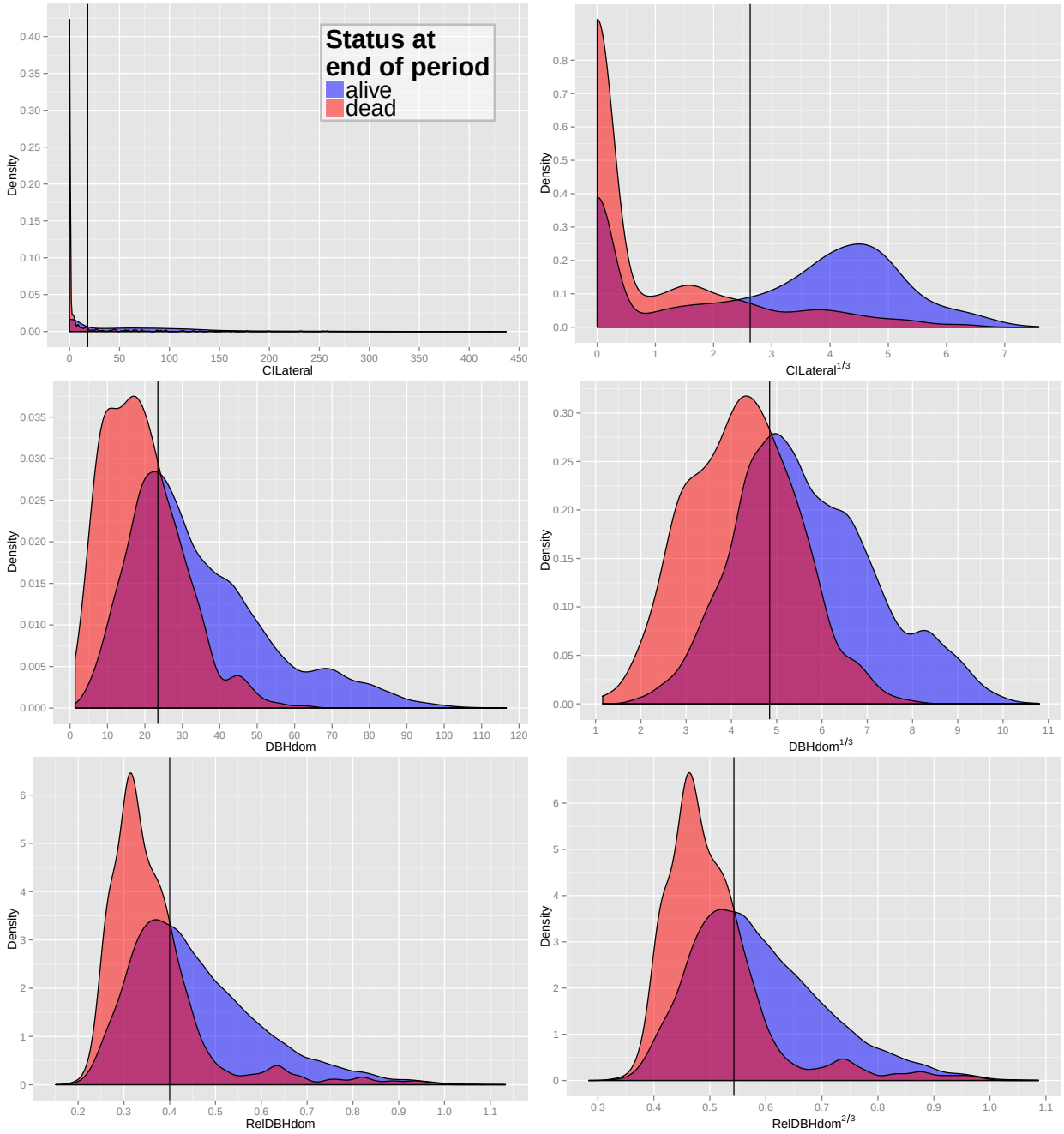

Figure 1.4 continued.

actually ends in mortality is treated equally to the reverse error arising when mortality is assigned to a period not ending in mortality. We provide the optimal threshold to enhance the understanding of "what is high" and "what is low", as the scales of the CIs hardly have an intuitive meaning.

We show graphs of kernel-density estimators (Venables and Ripley, 1999, sec. 5.6) of the continuous risk factors, which allow one to capture different aspects of the distributions visually. Well separated distributions will correspond to high AUCs. They were estimated separately for periods with and without observed mortality, the individual densities therefore integrate to one. Due to this characteristic the frequency relation of the two groups to each

other is not evident, but the overlaid densities allow the following interpretation. For a specific measurement of a risk factor, say $DBH = 20$ (see Figure 1.4 top left for an example) the overlaid densities imply that there was a higher proportion of live rather than dead trees. However, this interpretation assumes that mortality and non-mortality periods are equally likely a priori and one has to keep in mind that the marginal density estimates of risk the factors are aggregated over all plots, years, and other factors that might influence mortality. Graphs with little overlap of the mortality- and non-mortality curves indicate good discrimination in terms of the range of the risk factors. Vertical black lines indicate the optimal thresholds of separation based on the Youden index, cut_{Youden}.

Concerning the growth of a tree it is obvious that variables such as *DBH* and *Height* are strongly connected with each other, as both variables quantify the abstract concept of tree size. It is very likely that this connection can be seen in terms of empirical correlations in the data set as well. Similarly, the way that CIs partly build upon one another likely leads to strong inter-dependencies. We looked at rank correlations between pairs of risk factors, which allowed us to empirically assess to what extent different CIs measure different aspects of competition. Having the planned regression model for mortality in mind, where the risk factors would act as independent variables, it was important to know which variables contributed additional information not already present in others. Rank correlation as a measure of association is limited by the fact that it only captures monotone relationships. Inspection of scatter plots in addition to raw correlation values helps to overcome this shortcoming. Non parametric loess smoothers (Cleveland et al., 1992) are overlaid in the graphs, which indicate the shape of possible non-monotone dependence. Like for the AUC, rank correlations are invariant against strictly monotone transformations, providing maximum generalizability at this stage of model development.

In the descriptive methods presented so far we ignored the hierarchical structure of the data. The statistical measures and graphs were calculated over all plots (stands), which could either weaken or amplify the true effects of the risk factors. Assuming homogeneous conditions across different plots we expect little variation on quantities such as the AUC, correlations, and thresholds obtained within single plots compared to the aggregated calculation. We conducted a stratified analysis of the risk factors and compare results with the aggregated analysis, allowing to investigate the potential impact of a hierarchical approach. Plot specific rank correlations between risk factors, optimal thresholds, and AUCs are presented. We do not show the variables *periodLength* and *periodOnset* since they hardly vary within a single plot, as well as the variable *SiteIndex*, which is a characteristic of the whole plot and therefore cannot be explored at the plot level.

We present the results of the descriptive analysis in the following section, along with the implications for the mortality model.

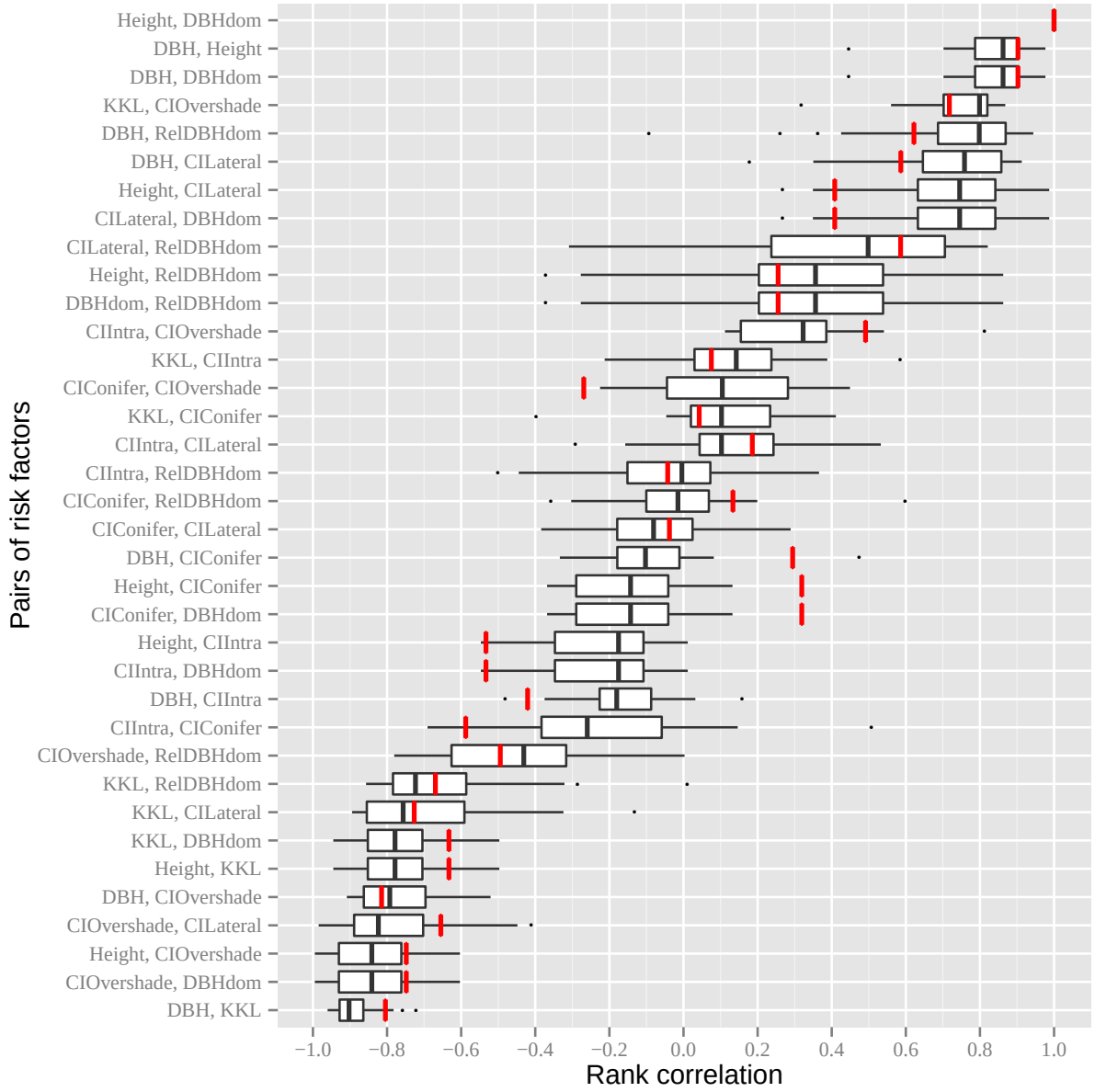

Figure 1.5: Boxplot of rank correlations calculated for each pair of risk factors. The red marks indicate the correlation coefficient aggregated over all plots.

1.3 Model development

1.3.1 Exploratory results and implications for modeling

In total 14,239 single tree observation periods comprising 6,189 beech trees from 29 plots were used for analysis. Six single observations were removed as outliers since they were clearly isolated, falling out of the range of the other observations, and could not be seen as representative of the entire data set. One of the outliers had $KKL = 120.13$, and five outliers had *RelDBHdom* values of 1.27, 1.33, 1.40, 1.44, and 2.11, respectively. At the end of 585 observation periods the tree was recorded as dead, resulting in an overall 5-year mortality

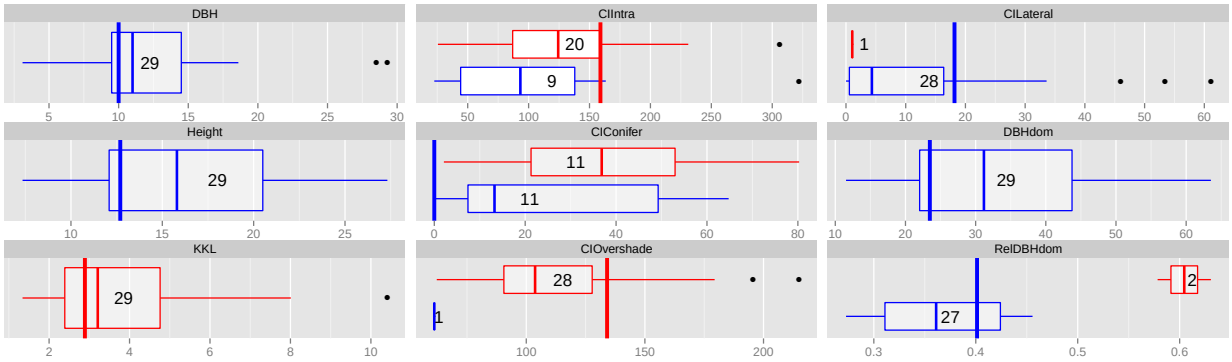

Figure 1.6: Boxplots of thresholds obtained by maximization of the Youden index in each plot. The color indicates the direction: Red indicates values greater as the threshold are associated with mortality, blue indicates smaller values as the threshold are associated with mortality. Thick vertical lines show the threshold calculated over all plots. The numbers next to/within the boxplots count the plots where the risk factor acts in the particular direction. Counts do not add up to 29 within one risk factor if there are plots having the same value of the risk factor for all periods.

rate of 3.9% (Table 1.3).

5-year mortality rates varied substantially between plots, with the highest at 13.44% (Table 1.1). The lowest rate was observed in Plot 29 where each of the 97 trees contributed a observation period of ten years (in sum 970 years of exposure time) and only one died, resulting in a 5-year mortality rate of 0.52%. In Table 1.1 the plots are arranged decreasingly by mortality per period which is not consistent with the order of the 5-year mortality. The biggest difference is visible in Plot 9, having a mortality per period twice as high as standardized to a 5-year period. The reason is because Plot 9 was surveyed strictly in ten year intervals. The big divergence indicates that we need to consider the exposure time, namely the length of the observation period, as part of the observed mortality rate instead of as a risk factor, and use an approach which harmonizes the data. We addressed this issue via an offset term in the mortality model.

Between 1986 and 2007 the mortality rate ranged between 3% and 5.5% except for the years 1990 to 1994 where the rate dropped below 1% (Table 1.3, Figure 1.7). Due to the way that data were collected and restructured to calculate yearly mortality rates, it is hard to assess the actual distribution of yearly test statistics with null hypotheses of equal mortality rates. Nevertheless, the pointwise confidence intervals visualized in Figure 1.7, which ignore these issues, support the impression that the low mortality rates between 1990 and 1994 did not only occur by chance. The foresters could not give any explanations for the 4% dip during these years; neither explanations of natural kind, such as a change in the weather nor of technical kind, such as a change in recording. Thus we left these years in the analysis but addressed the temporal heterogeneity by a random effect for calendar year.

For each of the observation periods included in the analysis, measurements of 13 potential risk factors for mortality listed in Table 1.2 were available at the beginning of the observation

	5-year mortality (%)			number	exposure
	rate	lower	upper	of deaths	time (years)
1986	4.45	2.64	7.31	15.75	1,768
1987	4.45	2.64	7.31	15.75	1,768
1988	3.62	2.14	5.96	15.75	2,177
1989	3.62	2.14	5.96	15.75	2,177
1990	0.10	0.00	1.38	0.40	1,977
1991	0.10	0.00	1.38	0.40	1,977
1992	0.48	0.11	1.66	2.51	2,634
1993	0.48	0.11	1.66	2.51	2,634
1994	0.48	0.11	1.66	2.51	2,634
1995	3.21	2.06	4.93	21.31	3,318
1996	3.21	2.11	4.82	23.91	3,724
1997	5.11	3.90	6.65	54.66	5,352
1998	5.25	4.04	6.78	57.56	5,485
1999	5.25	4.04	6.78	57.56	5,485
2000	5.36	4.11	6.94	56.29	5,256
2001	4.65	3.48	6.18	47.33	5,085
2002	4.65	3.48	6.18	47.33	5,085
2003	4.65	3.48	6.18	47.33	5,085
2004	4.65	3.48	6.18	47.33	5,085
2005	4.66	3.10	6.90	24.98	2,681
2006	4.28	2.46	7.24	14.04	1,639
2007	4.28	2.46	7.24	14.04	1,639
Overall	3.92	3.61	4.24	585.00	74,665

Table 1.3: 5-year mortality rates on annual basis with 95% confidence intervals (lower, upper). Periods with observed mortality are distributed among the involved years, leading to non-integer numbers of deaths.

period. Of these, nine were individual tree characteristics: *DBH*, *Height*, *KKL*, *CIIntra*, *CIConifer*, *CIOvershade*, *CILateral*, and *RelDBHdom*. Table 1.4 contrasts the risk factors and characteristics across periods associated with mortality versus non-mortality. There was a statistically significant difference in risk factors between mortality and non-mortality observation periods for all of the nine individual tree characteristics (all AUC p-values < 0.003). However, the p-values might be biased downwards because the independence assumption is violated for multiple observations of the same tree. The Brunner-Munzel test created pratically the same results (not shown). The average DBH of trees that experienced a mortality at the end of an observation period was 7 ± 4.4 cm (mean $\pm$ standard deviation), less than half of the average DBH of observation periods that did not result in mortality (16.3 ± 11.0 cm). This yielded high discriminatory power of DBH alone for the prediction of tree mortality, with an overall AUC of 80.5% (Figure 1.8). Small values of *DBH* were associated with mortality among all plots. Similarly, *Height* was also lower among mortality compared

	Non-mortality periods			Mortality periods					
	mean	SD	range	mean	SD	range	AUC in %	p-value[1]	threshold[2]
DBH	16.34	11.03	[0.80, 90.90]	7.04	4.36	[0.90, 37.90]	80.51	<0.001	10.00
Height	16.68	6.92	[1.40, 43.60]	10.63	4.46	[1.40, 27.07]	76.55	<0.001	12.70
KKL	3.44	4.96	[0.00, 60.54]	9.56	9.22	[0.27, 65.47]	81.15	<0.001	2.89
CIIntra	147.51	80.95	[5.87, 517.65]	187.58	84.82	[14.59, 444.42]	64.86	<0.001	158.97
CIConifer	15.98	23.85	[0.00, 200.44]	13.59	20.33	[0.00, 120.22]	53.62	0.002	0.00
CIOvershade	101.29	78.44	[0.00, 505.85]	191.60	81.22	[21.93, 461.42]	80.75	<0.001	134.07
CILateral	59.84	68.50	[0.00, 436.91]	10.85	32.05	[0.00, 257.63]	75.83	<0.001	18.17
DBHdom	34.53	18.62	[1.34, 116.62]	19.26	10.33	[1.34, 62.77]	76.55	<0.001	23.47
RelDBHdom	0.46	0.14	[0.15, 1.13]	0.37	0.11	[0.20, 0.97]	73.16	<0.001	0.40
SiteIndex	15.48	3.86	[5.54, 22.50]	16.42	4.60	[5.54, 22.50]	58.47	<0.001	18.10
periodLength	5.24	1.64	[3.00, 10.00]	5.26	1.58	[3.00, 10.00]	50.64	0.570	6.00
periodOnset	1994.02	5.02	[1985, 2000]	1995.83	4.47	[1985, 2000]	60.98	0.572	1994

[1] P-value of Wilcoxon test, applicable for testing H_0: AUC=0.5. [2] Threshold obtained from maximization of Youden index.

Table 1.4: Characteristics of trees in observation periods associated with mortality versus no mortality.

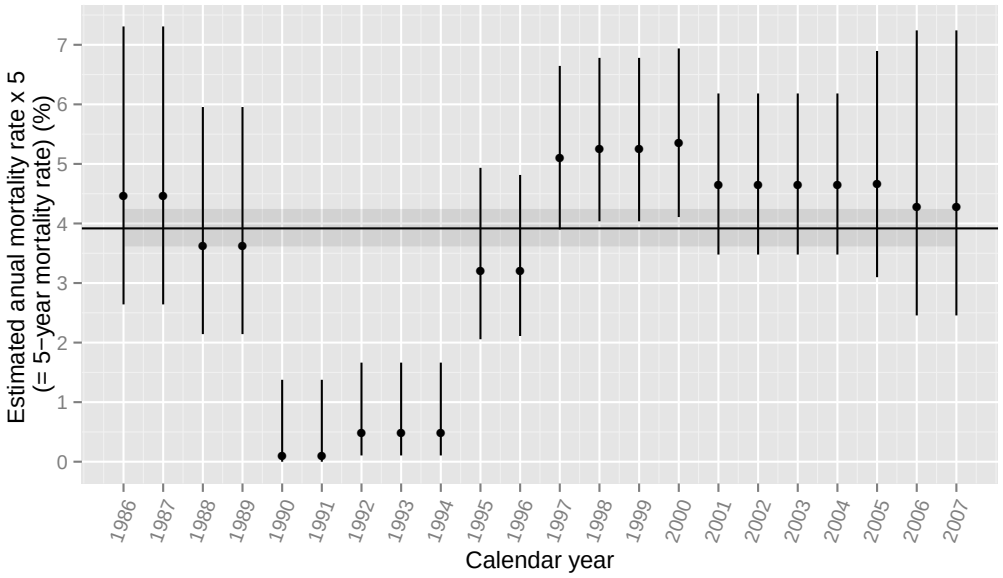

Figure 1.7: Estimated 5-year mortalities evolving over time, with 95% pointwise confidence intervals (vertical lines). Horizontal line and gray-shaded area show mortality averaged over all years with 95% confidence interval.

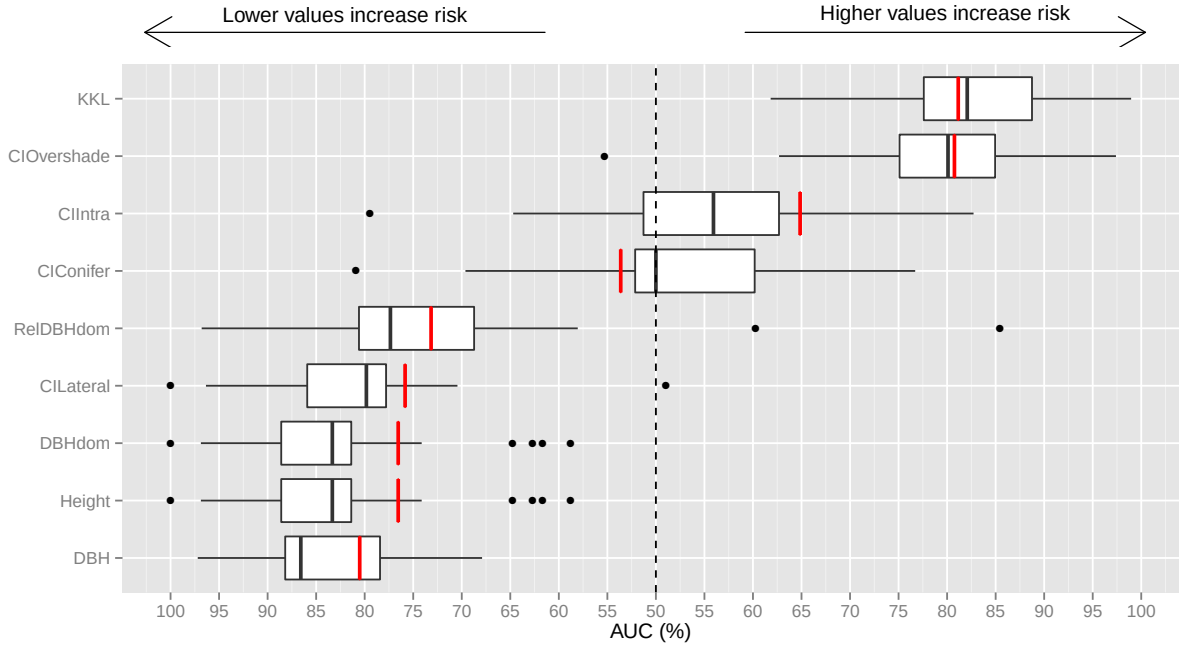

Figure 1.8: Boxplots of AUCs of risk factors calculated in each plot separately. Red lines indicate the AUCs calculated over all plots (cf. Table 1.4). AUCs to the left of the middle line imply that low values of the risk factor are associated with mortality, on the right high values are associated with mortality.

to non-mortality observation periods (10.6 ± 4.5 m versus 16.7 ± 6.9 m) but it had lower discriminatory ability than *DBH* (76.5% versus 80.5%). *DBHdom* gave exactly the same results in terms of AUC as *Height*, being a strictly monotone transformation of it. The similarity of these three variables is also seen in the high correlation coefficients of 1.0 and 0.9,

respectively (Figure 1.9).

Similarly, small values of the variables *CILateral*, *RelDBHdom*, and *CIConifer* were observed more often in mortality observation periods. This behavior was not expected for the long term CI *RelDBHdom*, which by its calculation method (Table 1.2) assigns large values for trees who had experienced competition in the past. *CIConifer* alone had low discrimination power (AUC = 53.6%). Accordingly, in half of the plots, mortality was associated with high values, half with small values (Figure 1.8). Similarly for *CIIntra* (AUC = 64.9%), in about 25% of the plots small values were related to mortality, in 75% high values. The

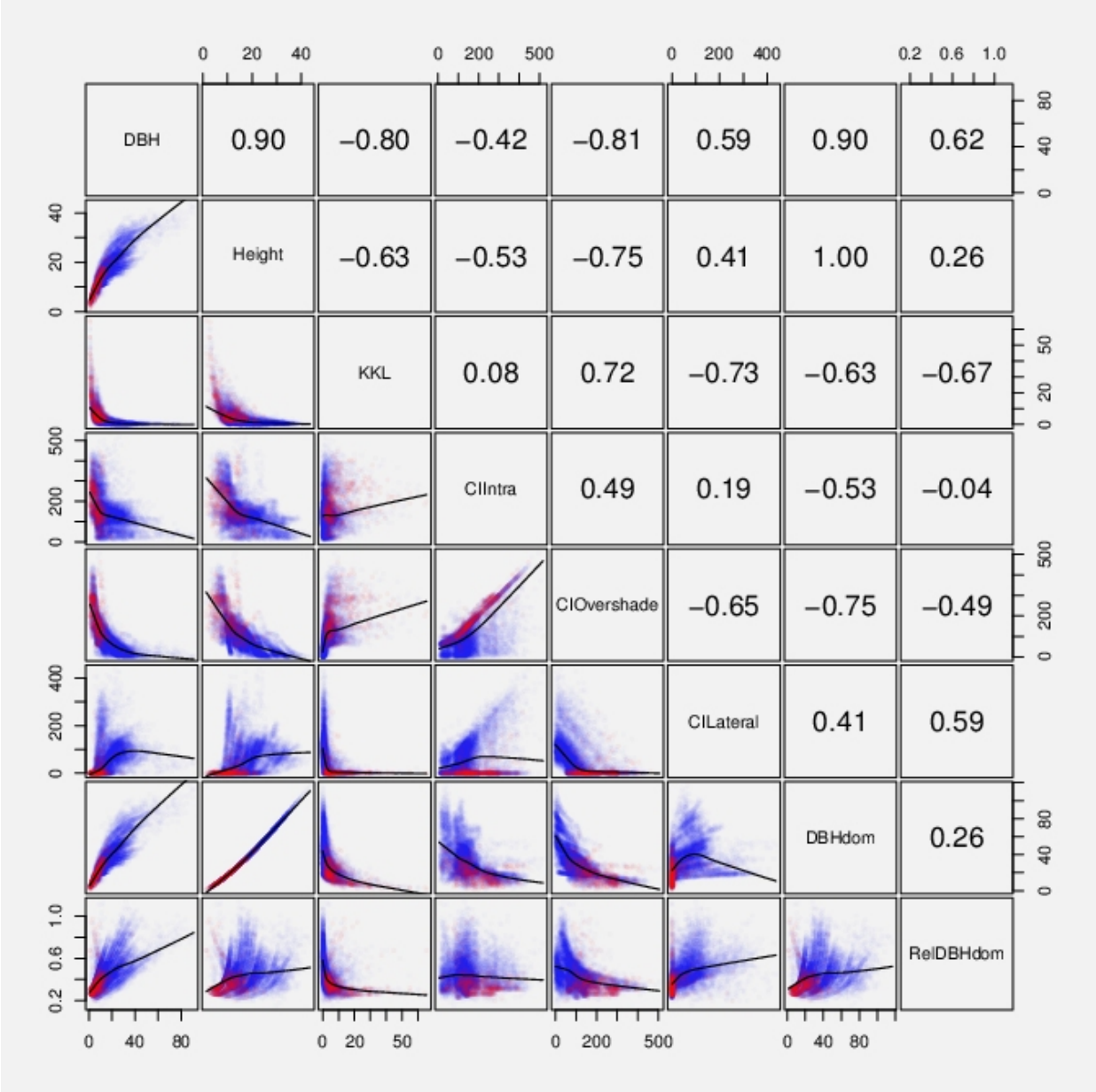

Figure 1.9: Empirical rank correlation between pairs of continuous risk factors. The coefficients are given in the upper triangle, the lower triangle shows the scatter plots. Periods resulting in mortality are colored in red, otherwise in blue. The black line shows a nonparametric loess curve.

two risk factors *CIConifer* and *CIIntra* alone were of limited use for predicting mortality, at least in a monotone fashion. However, relaxing that restriction and accounting for other CI in parallel, they might still contribute valuable information in a mortality model. *KKL* and *CIOvershade* were the CIs with highest AUCs (81.1% and 80.8%, respectively) and acted in the expected direction, with high values associated with smortality. The plot-specific variable *SiteIndex* was lower among non-mortality compared to mortality periods (AUC 58.46%), which indicated better growth conditions in non-mortality periods at a first glance, but the validity of that on single tree-period is not given due to the plot-specific character of the variable, resulting in the same constant value of *SiteIndex* for all tree periods within a plot at all observed calendar years. Finally, there was no statistical difference in the length of observation periods between those associated with mortality and non-mortality (Table 1.4), though this observation does not affect the importance of *periodLength* in the definition of mortality rates. We observed that risk factors with good overall discriminatory capabilities are available and that they might be further enhanced when we account for the hierarchical structure (plot-specific AUCs often better than overall AUC, Figure 1.8).

Figure 1.4 shows the empirical distributions of risk factors in mortality and non-mortality periods. Besides the quantities of location (mean) and variability (SD) already provided in Table 1.4, the skewness and potential multimodel shape can be assessed by this figure. The distributions of *Height* and *RelDBHdom* were unimodal with slight skewness towards larger trees. The majority of tree heights were near 12 m, but a smaller group of trees had larger heights near 30 m. The distribution of *DBH* indicated slight bimodality within mortality periods, with a minority fraction of larger trees. For *CIIntra* and *CIOvershade* most of threes within non-mortality periods had small values. The majority of trees were observed in periods without light competition from neighboring trees ($KKL = 0$), competition from conifer trees ($CIConifer = 0$), or lateral competition ($CILateral = 0$). We will refer to these accumulations on a single value (here zero) as point masses in the next section. In particular the extreme skewness of *CILateral* and *KKL* suggested that transformations are needed to zoom into areas of interest, figuratively speaking.

The single threshold obtained by maximization of the Youden index (shown by a vertical line in Figure 1.4) illustrates where the density of the risk factor in non-mortality periods was significantly shifted from the density in mortality periods. For risk factors where the densities overlap extensively, we cannot achieve good separation with a single threshold, as seen in the case of *CIConifer*. The thresholds calculated in each plot are given in Figure 1.6. As for the AUC, orientation of the thresholds, that is, whether values above or below thresholds are associated with mortality are indicated. For *DBH* all 29 plots had the same orientation, meaning that values below the threshold were higher associated with mortality. The same applied for *Height* and *DBHdom*, whereas for *KKL*, all plots consistently showed association of mortality with values above the threshold. Again, *CIConifer* behaves most extreme, in eleven plots values higher than the threshold indicate mortality, and in 11 plots,

values lower than the threshold. A threshold for the remaining 7 plots could not be calculated as in these plots *CIConifer* was zero for all trees.

The empirical correlations, summarized in Figure 1.9, were strongly and statistically significantly negative for the risk factor pairs *DBH* & *KKL* (-0.80), *CIOvershade* & *DBHdom* (-0.75), *Height* & *CIOvershade* (-0.75), *DBH* & *CIOvershade* (-0.81), and *KKL* & *CILateral* (-0.73). High correlations were observed for *DBH* & *Height* (0.90), *DBH* & *DBHdom* (0.90), and *KKL* & *CIOvershade* (0.72). *Height* & *DBHdom* were in perfect rank correlation, being a monotone transformation of each other. We found no relevant correlation of *CIConifer* & *CILateral* (-0.04), *RelDBHdom* & *CIIntra* (-0.04), and *KKL* & *CIConifer* (0.04). Only the relationship between *CILateral* and *DBHdom* (0.41) looked severely non-monotone according to the loess smoother, but the variation was too large for inferring a meaningful functional dependency (Figure 1.9). Comparison of correlation coefficients within single plots with aggregated estimates painted a mixed picture. For strong correlations the overall estimates were lower (in absolute value) except for the variables *DBH* and *Height* (or *DBHdom*), for medium correlations the differences were bigger, but no general trend was obvious. The sign of the correlation coefficient changed in 20 out of 36 pairs in at least one plot compared to the aggregated coefficient.

In summary we list several implications to be considered in building a mortality model.

- Mortality is a rare event, present in only 4.11% of the observations in this data set.
- Mortality varies considerably over time.
- Mortality varies considerably between plots.
- Mortality is measured over different sized intervals and needs to be standardized.
- Risk factors differ in distribution between mortality and non-mortality periods.
- Multiple observation periods of the same tree are not necessarily independent.
- Multiple observations within one plot cannot be assumed to be independent, i.e. there is spatial correlation.
- Risk factors have partly functional dependencies by definition and/or strong empirical correlation between each other.

1.3.2 Literature review for individual tree mortality models

Before presenting our own individual tree mortality model we review modeling approaches suggested and applied in the literature.

There have been various individual tree mortality models developed for many different species of trees; Table 1.5 contains a list. All mortality models in the literature that we have consulted included DBH or some measure of basal area, and logistic regression was by

Reference	Tree species	Method	Outcome
Buchman et al. (1983)	Jack pine, Red pine, Balsam fir, Quaking aspen, Sugar maple	Extended logistic regression involving powers of parameters and variables	1-year survival[1]
Hamilton (1986)	Western white pine, Douglas/grand fir, Western red cedar, Western hemlock	Logistic regression	1-year mortality
Burgman et al. (1994)	Mountain ash, Alpine ash	Cox model	Instantaneous hazard rate
Dobbertin and Biging (1998)	Ponderosa pine, White fir	CART[2]	5-year mortality
Monserud and Sterba (1999)	Norway spruce, White fir, European larch, Scots pine, European beech, Oak	Logistic regression	5-year mortality
Eid and Tuhus (2001)	Norway spruce, Scots pine Birch, other broadleaved	Generalized logistic regression	Mortality (arbitrary base)
Hasenauer et al. (2001)	Norway spruce	Neural networks, logistic regression	5-year mortality
Fridman and Stahl (2001)	Pine spruce	Logistic regression	5-year mortality
Yao et al. (2001)	Trembling aspen, White spruce, Lodgepole pine	Generalized logistic regression	2- to 25-year mortality
Pretzsch et al. (2002)	Norway spruce, Silver fir, Scots pine, Common beech, Sessile oak	Logistic regression	5-year mortality
Palahi et al. (2003)	Scots pine	Logistic regression	5-year mortality
Bigler and Bugmann (2003)	Norway spruce	Logistic regression	Mortality (arbitrary base)
Yang et al. (2003)	White spruce	Generalized logistic regression	Mortality (arbitrary base)
Zhao et al. (2004)	30 different species, categorized in 6 groups	Logistic regression	5-year mortality
Rose et al. (2006)	Pine	Multilevel grouped Cox model[3]	Mortality (arbitrary base)
Fan et al. (2006)	Oak dominated mixed stands	CART[2]	3-year mortality
Bravo-Oviedo et al. (2006)	Maritime pine, Scots pine	Logistic regression	5-year mortality
Das et al. (2007)	White fir, Sugar pine	Logistic regression	1-year mortality
Wunder et al. (2007)	Deciduous trees, Conifer	Logistic regression	Mortality (arbitrary base)
Fortin et al. (2008)	American beech, Yellow birch, Red maple, Sugar maple, Balsam fir	binomial GLMM[4] with complementary log-log link	5-year mortality
Rathbun et al. (2010)	Western hemlock, Douglas fir, Western red cedar	Generalized logistic regression	Mortality (arbitrary base)
Das et al. (2008)	White fir, Red fir, Incense cedar, Sugar pine	Logistic regression	1-year mortality
Kiernan et al. (2009)	Sugar maple, American beech, White ash, Bellow birch, Striped maple, Mixed conifers	Logistic regression, GEE[5] modeling intra-tree correlation	Different period lengths, length used as factor variable
Adame et al. (2010)	Pyrenean oak	Logistic mixed model (random intercept)	10-year mortality

[1]Survival: 1-mortality, [2]CART: Classfication and Regression Trees, [3] Corresponds to binomial regression with complementary log-log link and random effects, [4]GLMM: Generalized Linear Mixed Model, [5]GEE: Generalized Estimating Equation.

Table 1.5: Previously published individual tree mortality models.

far the most commonly used statistical model. The initial mortality model in SILVA was presented by Pretzsch et al. (2002) and was based on a subset of the same data as for our application. They also used logistic regression, but instead of using all observation periods, they selected an equal-sized series of observation periods from trees that had survived to observation periods where trees had died, mimicking the efficient case control designs used for rare diseases in medicine. Their mortality model indicated an increased risk of mortality for trees with smaller DBH, with lower ratios of heights to DBH, with larger values of a site index (estimated stand top height at age 50 years), and with larger ratios of estimated tree basal area growth over the next 5 years to DBH. Our findings for DBH and *SiteIndex* in the exploratory univariate analyses were significant in the same direction. However, the ratio *Height*/*DBH* was found to act in the opposite direction in the univariate analysis (AUC = 78.4%, p-value < 0.001, not shown in previous tables).

Monserud and Sterba (1999) used logistic regression to develop individual tree mortality models for the six major forest species of Austria, one being European beech, using a single 5-year remeasurement period of a permanent plot network of the Austrian National Forest Inventory. In addition for use in an individual tree stand growth simulator, their aim was to provide a general mortality model to replace outdated yield tables that were still being used at the time. Their inventory recorded an overall 5-year mortality rate for European beech of 4.3%, which is very close to what was observed in our study (4.1%), and they elucidated the obstacles present for accurately modeling rare events. In order to make their model generally applicable in Austria, where they argued that most stands failed to meet the definition of even-aged, they intentionally excluded site index and age of individual trees from consideration in their model, arguing that tree size is already an integrated response to these factors. In their introduction they outlined that the most popular statistical method for modeling individual tree mortality is logistic regression, but that Weibull and Gamma regression have also been applied. Further they stated that in their data, the nonparametric approaches recursive partitioning and neural networks did not lead to significant improvement in the ability to predict mortality compared to classical statistical methods, but were applied successfully elsewhere (Monserud and Sterba, 1999).

Using permanent plot data from a mountainous region in Switzerland, Wunder et al. (2007) focused on prediction models for European beech that distinguished between growth-dependent and growth-independent mortality. The growth-dependent models used as a risk factor the relative basal area increment between two measurement periods divided by the basal area at the second measurement period. Location site and DBH were included as growth-independent risk factors. Their data showed that trees that died experienced lower relative growths in the period before death than comparable time periods among trees that survived. A spline fit for the relationship of relative growth to survival revealed a nonlinear relationship. The impact of growth on survival was stronger among trees with smaller relative growths than among trees with higher relative growths. Among the two sites in their study,

trees with larger DBH had a higher chance of survival. Their prediction model obtained an AUC of 89.6% using bootstrapping.

The above prediction models did not incorporate random effects to account for results varying among plots. In their prediction models for northern hardwood stands, which included American beech, in Quebec Canada, Fortin et al. (2008) stressed the importance of accounting for risk differences among plots that could not be explained by measured individual tree risk factors, such as soil and weather conditions, as well as for different intervals of measurement to account for changing conditions. They used a binomial regression model with complementary log-log link, that included a fixed offset term to account for variable lengths of observation periods. In addition to significant contributions of the random effects, they additionally found that tree vigor, DBH and basal area had an impact on survival, with the effects of DBH and basal area nonlinear in nature. In their model, some common distance-independent competition indices, including the sum of basal area for all trees with DBH greater than the tree of interest, the relative position of the tree in the cumulative basal area distribution, and the ratio between DBH and plot mean quadratic diameter, did not have a significant impact on mortality.

In their modeling of tree mortality following selection in upstate New York for a multitude of species, including American beech, Kiernan et al. (2009) contrasted ordinary logistic regression with a Generalized Estimating Equation (GEE) approach that accounts for dependencies between observation periods on the same tree. Both models found that mortality increased with the ratio of basal area to DBH, with time of observation, and with number of trees in the plot, and gave similar predictions. The GEE approach had slightly lower prediction error, in particular for smaller trees with DBH less than 15 cm. By accounting for the dependence between observation intervals rather than treating multiple observation periods from the same tree as independent, the standard errors of parameters estimated by the GEE approach were larger, which the authors suggested to yield in more honest statistical significance results.

Another regression model frequently applied to deal with observation periods of unequal length is generalized logistic regression (Eid and Tuhus, 2001; Yao et al., 2001; Yang et al., 2003; Rathbun et al., 2010) (Table 1.5). The standard logistic regression model does not include a time component and relates the probability of death to the covariate vector $\boldsymbol{x}$ in the form

$$\mathbf{P}(y=1) = \frac{e^{\boldsymbol{x}\boldsymbol{\beta}}}{1+e^{\boldsymbol{x}\boldsymbol{\beta}}} = \frac{1}{1+e^{-\boldsymbol{x}\boldsymbol{\beta}}},$$

where $y = 1$ denotes mortality versus $y = 0$ non-mortality, and $\boldsymbol{\beta}$ is the parameter vector. For the generalized logistic regression as proposed by Monserud (1976), the model is stated for the probability of survival,

$$\mathbf{P}(y=0) = 1 - \frac{1}{1+e^{-\boldsymbol{x}\boldsymbol{\beta}}},$$

and extended by the parameter L,

$$\mathbf{P}(y=0) = \left(1 - \frac{1}{1+e^{-\boldsymbol{x}\boldsymbol{\beta}}}\right)^{L}.$$

L is the length of the observation period (for example in years) and by exponentiating the probability of survival is ensured to be one for the next moment and to decrease with increasing time L,

$$\lim_{L\to 0} \mathbf{P}(y=0) = 1, \quad \lim_{L\to\infty} \mathbf{P}(y=0) = 0.$$

Incorporating the sampling design of the survey explicitly into the mortality model has gained popularity during the last decade. The importance of considering multiple sources of heterogeneity was successfully demonstrated in recent multilevel models (Rose et al., 2006). We think there are at least two reasons for the trend towards more complex models. First, the current data basis has become larger and more complex which allows the fitting of these advanced models. Second, software and their interfaces have advanced, allowing more convenient calculation. Nevertheless, with increasing complexity of a model, the interpretation of the results becomes more complex as well, and cannot be communicated as easily. Most often standard theory for statistical testing does not apply and measures such as goodness of fit have to be adapted.

1.3.3 From Cox to GAMM

In this section we describe the use of a generalized linear model (GLM) as a prediction tool for tree mortality and its expansions, leading to a generalized additive mixed model (GAMM). The regression model is motivated by assumptions with regard to the distribution of the dependent variable, the outcome. In our case we assume that the individual mortality of a tree is a random variable which depends, among other things, on the set of risk factors available in this study. If the moment of death is not known for every tree in the study, like in the present situation where most of the trees remain alive, mortality, or more precisely, the mortality rate, needs two components to be well defined: a dichotomous indicator for the status (dead/alive) and a component measuring the corresponding time. If the exact time point of death for an individual tree is not known, it is said to be censored. Statistical methods suitable for this type of data are referred to as survival/failure time analyses, with the Cox model (Cox, 1972) being the most prominent. In its original form it relates the hazard or instantaneous rate of mortality λ at any time t to covariates $\boldsymbol{x}$,

$$\lambda(t) = \lambda_0(t)\exp(\boldsymbol{\beta}'\boldsymbol{x})$$

and it requires survival times to be measured continuously over time. The baseline hazard, $\lambda_0(t)$, describes the behavior of the risk over time at baseline levels of covariates and does not have to be further specified. The individual covariate vector $\boldsymbol{x}$ and the parameters $\boldsymbol{\beta}$ act

multiplicatively on the baseline hazard, resulting in the proportional hazard property. Extensions are available to allow for discrete or interval censored survival times and inclusion of covariates varying in time (Kalbfleisch and Prentice, 2002). Both generalizations are required for the data set at hand. Treating the time as discrete avoids having to deal explicitly with computationally demanding interval censoring. Simulation studies showed similar results for both approaches (Kneib, 2006). The discrete version of the Cox model is a binary regression model with complementary log-log link, but the better known logit-link or others can be used as well. All those discrete models converge to the continuous time Cox model (Kalbfleisch and Prentice, 2002, p. 136). This relationship allows the use of standard GLM software after some data augmentation. The observations have to be split at every unique period onset or offset date (see Figure 1.10 for an illustration). Choosing the logit link, $g(\pi) = \log \frac{\pi}{1-\pi}$, results in the logistic regression model for the discrete hazard rate λ,

$$\pi_{it} = \mathbf{P}(y_{it} = 1 \,|\, \boldsymbol{x}_{it}) = \frac{\exp(\eta_{it})}{1 + \exp(\eta_{it})} \equiv \lambda(t \,|\, \boldsymbol{x}_{it}), \tag{1.1}$$

where y_{it} is the status of tree i at the end of interval t, with covariates $\boldsymbol{x}_{it}$ measured at the beginning of each interval, which is the end of the previous interval. The linear predictor η_{it} consists of two parts, a parameterization of the baseline hazard, which is the same for all trees, and the covariate effects:

$$\eta_{it} = \beta_{0t} + \boldsymbol{x}'_{it}\boldsymbol{\beta}.$$

That means the discrete baseline hazard is estimated by a distinct intercept variable for each interval, as shown in Figure 1.10c. In other words this variable does the bookkeeping, ensuring that at any time point the appropriate risk set (denominator) is used.

This approach is perfectly suitable when all observation periods are synchronized meaning that trees were visited at time points common for all trees. For our observation scheme it is an oversimplification and cannot be adopted directly. For an illustration of the difficulty of asynchronous observation intervals, consider tree 3 in Figure 1.10 in year 1995. We need to assign a value for y but only know that the tree died somewhen between 1992 and 1997. The pooling of repeated observations discussed in Cupples et al. (1988) overcomes this problem by assuming a constant baseline hazard over time. In doing so, the observations are used the way they naturally arise in the survey: the information about beginning, end, and length of the single periods is not further regarded. Technically, the parameters β_{0t} are simplified to a single coefficient β_0, representing the constant hazard. The implicit assumption made by this parsimonious parameterization is to consider the time at which information is recorded as not relevant to mortality, the underlying risk is assumed to be the same in each interval. Further one assumes that the mechanism by which the covariates effect the outcome is independent of time, reflected by time-constant parameters $\boldsymbol{\beta}$. Thus, the relationship between DBH and mortality in the time period 1985 to 1990 is the same as that relationship between 2000

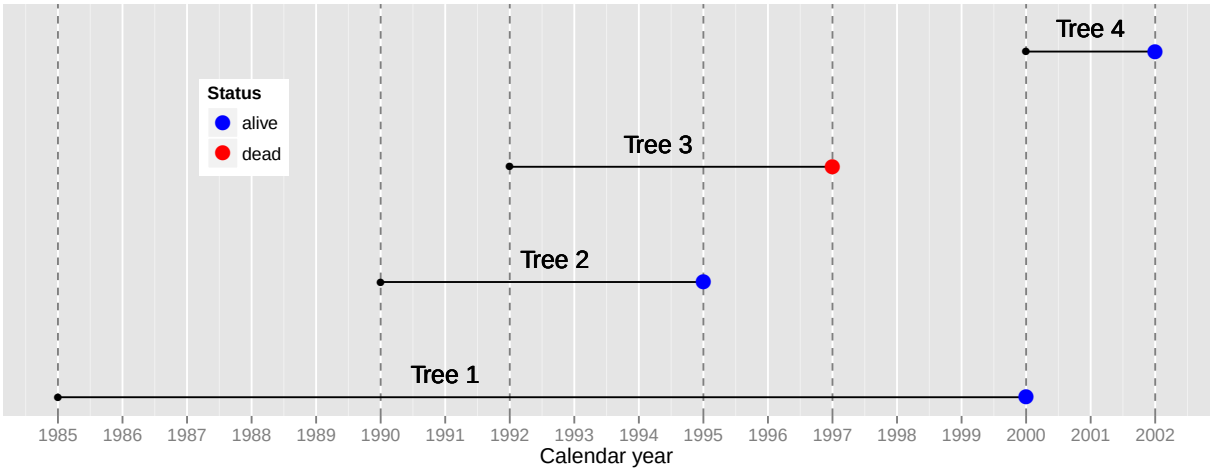

(a) Visualization of four tree-period observations with their status (dead/alive) at the end of the period. Vertical lines indicate where to split to achieve a data set suitable for binary regression.

Tree	Onset	Offset	Status
1	1985	2000	alive
2	1990	1995	alive
3	1992	1997	dead
4	2000	2002	alive

(b) Organization of four example trees before data augmentation.

Tree	Interval number	Onset	Offset	y
1	1	1985	1990	0
1	2	1990	1992	0
1	3	1992	1995	0
1	4	1995	1997	0
1	5	1997	2000	0
2	2	1990	1992	0
2	3	1992	1995	0
3	3	1992	1995	?
3	4	1995	1997	1
4	5	2000	2002	0

(c) Organization after data augmentation. Problem: Unknown status of tree 3 in year 1995.

Figure 1.10: Data augmentation for the discrete time Cox model. Variable y to be used as outcome in a binary regression model, whith $y = 1$ denoting mortality and $y = 0$ otherwise.

and 2002, say. A third assumption is that the current risk relies only on the information of the previous interval. This Markov assumption states the long term history of a tree to be unimportant for mortality prediction. Abbott (1985) and D'Agostino et al. (1990) demonstrated the asymptotic equivalence of the grouped Cox proportional hazards survival model to pooled logistic regression for short intervals.

The approach we chose follows the parsimonious approach of Cupples et al.'s (1988) pooling method but integrates some modifications to relax the limiting assumptions. It was not possible to estimate the baseline hazard on such a fine grid as postulated by the discrete Cox model, but we wanted nonetheless to allow for a non constant baseline hazard

over time. Instead of splitting the observations at every onset and offset date we used only the individual onsets (variable *periodOnset*) to define the grouping structure to estimate the baseline hazard. This involves a coarsening compared to the discrete Cox model and the approach can therefore be interpreted as a sort of temporal smoothing. However, the strict assumption of time-constant risk profiles is attenuated allowing the baseline hazard to vary within the total observation time to pick up environmental changes in course. Further, modeling *periodOnset* as a random effect has the advantage that it implies a correlation between observations sharing the same onset year, quantifies the variability in time, and allows an easier generalization of the results, while avoiding a reference category.

We included the length of the observation period as an offset term in the model which additionally reduced the differences to the discrete Cox model. An offset term means to include a covariate to the right hand side of the regression equation while the corresponding parameter is not estimated but set a constant value (usually 1). Using the length of the observation period as such an offset term mirrors the intuitive understanding that a risk for mortality within a ten-year period should be twice as high as within a five-year period. More precisely, within a logistic model the offset acts on the log-odds scale in contrast to the log-scale in Poisson risk(-rate) regression where the offset approach is routinely applied. The same arguments as in Abbott (1985) and D'Agostino et al. (1990) hold that for small risks x, the logit function, $f(x) = \log(x/(1-x))$, and the logarithmic function are good approximations of each other.

The analysis involved multiple observations of the same tree, which raises the question how the dependency was treated. We argue that since pooled logistic regression with rare events is asymptotically equivalent to grouped Cox regression, which handles this dependence alternatively through the Cox regression likelihood, one does not need to additionally adjust for it. However, we are aware of the fact that the pure dimension of the augmented dataset does not necessarily correspond to the number of independent observations as needed for asymptotic considerations of statistical testing or the calculation of Akaike's Information Criterions (AIC) and Bayesian Information Criterion (BIC) (Akaike, 1974; Schwarz, 1978).

The literature consistently reports that transformations of risk factors improved prediction models. Fortin et al. (2008) used DBH and DBH^2 in their models, Monserud and Sterba (1999) found $1/DBH$ to suit best. However, there is no way to know which particular transformation is most appropriate for each of our risk factors, because the functional form is dependent on other risk factors in the model, and no previous model used the same set of variables (and model structure) to ours. Trying only few combinations of common transformations on a single risk factor x, such as $x^2, x^3, \log(x), \sqrt{x}, \exp(x)$ leads to a high number of candidate models when applied simultaneously to a set of risk factors. Allowing terms like $x + x^2$ even amplifies the problem.

Still, high-order polynomials act global on the whole domain of a risk factor and are not suited to capture local characteristics of the data (Fahrmeir et al., 2007, p. 294). We

chose spline functions in order to flexibly, and simultaneously model smooth functional relationships for multiple covariates in a data driven way, which has been successfully applied in many fields. Nevertheless we used transformations on the risk factors as a first step to achieve symmetric and compact empirical distributions. That might not be absolutely necessary, but in our opinion helped to stabilize the procedure and reduced the impact of the knot locations of the spline. Three of the risk factors, *KKL*, *CILateral*, and *CIConifer* had a disproportionately large number of zeros (point masses), these were removed for seeking the optimal transform. The considered transformations were power transformations where power could range from 0.01 to 1. The Kolmogorov-Smirnov (KS) test for normality was used to find an optimal power transform with the transform corresponding to the smallest value of the KS test statistic declared as optimal. The optimal power was rounded to the next even fraction and the variable was transformed by this power for all further analyses, including the spline construction. The resulting transformations along with their effect on the shape of the empirical distributions are shown in Figure 1.4. The spline approach applied to transformed risk factors x allows a more flexible modeling than a global polynomial. It is intended to approximate the unknown functional relationship $g(x)$ of a covariate to the outcome y, by the spline $s(x)$,

$$g(x) \approx s(x).$$

The spline function $s(x)$ is defined as follows: The domain of x is divided in intervals by selecting a set of m knots. Within each interval the spline is parameterized as a polynomial of degree l, $p_l(x)$,

$$p_l(x) = \gamma_0 + \gamma_1 x + \gamma_2 x^2 + \ldots + \gamma_l x^l.$$

Further, to ensure global smoothness, $s(x)$ must be $l-1$ times continuously differentiable not only within the intervals, but also at the connection points between the intervals. For estimation within a regression framework a constructive representation, which fulfills these requirements, is needed. Basis functions, B, are utilized to parameterize the spline function,

$$s(x) = \sum_{j=1}^{d} \delta_j B_j(x),$$

where $d = m+l-1$ linear combinations of basis functions are needed when a l-degree B-spline basis (Eilers and Marx, 1996) with m knots is used. The basis functions are recursively defined, following (Fahrmeir et al., 2007, p. 304 ff.),

$$B_j^0(x) = I_{[\kappa_j, \kappa_{j+1})}(x) = \begin{cases} 1 & \kappa_j \leq x < \kappa_{j+1}, \\ 0 & \text{otherwise}, \end{cases} \qquad j = 1, \ldots, d-1,$$

$$B_j^1(x) = \frac{x - \kappa_j}{\kappa_{j+1} - \kappa_j} I_{[\kappa_j, \kappa_{j+1})}(x) + \frac{\kappa_{j+2} - x}{\kappa_{j+2} - \kappa_{j+1}} I_{[\kappa_{j+1}, \kappa_{j+2})}(x),$$

$$B_j^l(x) = \frac{x - \kappa_j}{\kappa_{j+l} - \kappa_j} B_j^{l-1}(x) + \frac{\kappa_{j+l+1} - x}{\kappa_{j+l+1} - \kappa_{j+1}} B_{j+1}^{l-1}(x),$$

with κ_j being the knots/interval limits, and the range of j depending on the degree of the polynomial within an interval and the number of knots used. We used a cubic (degree $l = 3$) B-spline with 5 inner knots resulting in $d = 5 + 3 - 1 = 7$ parameters δ_j to be estimated per risk factor (thus $B_j(x) \equiv B_j^3(x), j = 1, \ldots, 7$). Additionally, we specified a normality prior to the second-order differences of spline coefficients δ_j, leading to penalized splines. The penalization reduces the sensitivity of the number of knots to the model fit and stabilizes parameter estimation in areas with little information in the data. For risk factors with point masses (KKL, CILateral, CIConifer), we added an extra term to the regression equation allowing for a jump discontinuity at the point mass. The term is an indicator variable set to one for values of the risk factor at the point mass and zero otherwise. Figure 1.11 illustrates the concept in a simulated example.

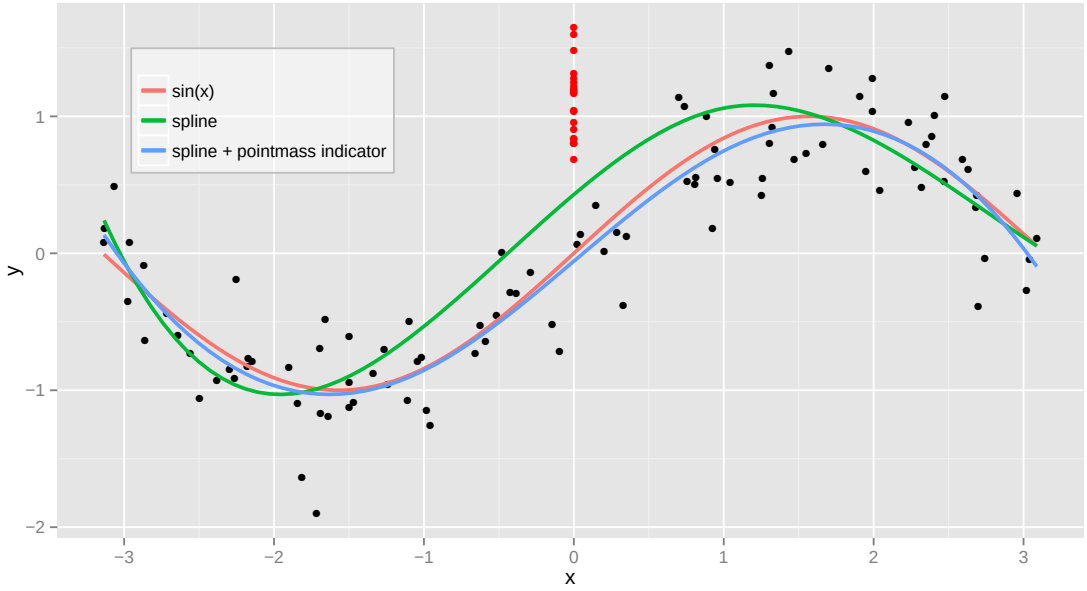

Figure 1.11: Illustration of a point mass effect on splines. 100 samples from an uniform distribution on $-\pi$ to π serve as covariates: $x_i \overset{iid}{\sim} U(-\pi, \pi)$. The samples y_i are drawn conditionally on the value of x_i, with $y_i \sim \mathrm{N}(\mu = \sin(x_i), \sigma = 0.3)$, $i = 1, \ldots, 100$ (black color). In addition, 20 points with $x_i = 0, i = 101, \ldots, 120$ were sampled from $y_i \overset{iid}{\sim} N(\mu = 1, \sigma = 0.3), i = 101, \ldots, 120$ (red color). The 'true' sinus curve of the expectation is shown in red, two models including a spline were fitted on the 120 pairs of (y_i, x_i): the green curve is the expectation without an additional point mass indicator in the regression formula, the blue curve shows the expectation of the model with an indicator term $I(x_i = 0)$.

A regression model involving a sum of smooth functions of covariates is often called Additive Model (AM), according to Hastie and Tibshirani (1990), and accents the generalization compared to a linear model. We therefore denote the model described above, with all its components, as GAMM (Wood, 2006, chap. 6) but also GLMM (Generalized Linear Mixed Model)

is appropriate as the spline representation is still linear in its coefficients.

1.3.4 Final model structure

In sum, the steps above resulted in a GAMM with multiple risk factors, relating the probability of death π of an individual tree within the observation period to risk factors measured at the beginning of the observation period, the calendar year, the tree's plot and the length of the observation period as follows:

$$\begin{aligned}\log\left(\frac{\pi_{ijk}}{1-\pi_{ijk}}\right) = \beta_0 + \text{offset}_{ijk} + \gamma_i + \gamma_j + s_1(DBH_{ijk}^{3/20}) + \\ s_2(Height_{ijk}^{2/3}) + s_3(KKL_{ijk}^{1/3}) + s_4(CIIntra_{ijk}^{1/2}) \\ s_5(CIConifer_{ijk}^{1/3}) + s_6(CIOvershade_{ijk}^{1/2}) + s_7(CILateral_{ijk}^{1/3}) + \\ s_8(DBHdom_{ijk}^{1/3}) + s_9(RelDBHdom_{ijk}^{2/3}) + s_{10}(SiteIndex_{ijk}) + \\ \beta_1 I(KKL_{ijk}=0) + \beta_2 I(CILateral_{ijk}=0) + \beta_3 I(CIConifer_{ijk}=0).\end{aligned} \tag{1.2}$$

The single components are:

π_{ijk}: Probability of death for tree k from plot j at the end of period i ($\pi_{ijk} = \mathbf{P}(y_{ijk} = 1 \mid \text{covariates})$).

β_0: Global intercept of model.

offset_{ijk}: $\left(\log\left(\frac{periodLength}{5}\right)\right)_{ijk}$.

γ_i: Random effect for *periodOnset* i, i =1985, 1987, 1989, 1991, 1994, 1995, 1996, 1997, 1999, 2000; with $\gamma_i \sim \text{N}(0, \sigma_{periodOnset})$.

γ_j: Random effect for plot j, $j = 1, \ldots, 29$; with $\gamma_j \sim \text{N}(0, \sigma_{plot})$.

$s(x)$: Evaluation of spline function for covariate x; $\text{s}(x) = \sum_{l=1}^{d} \delta_l B_l(x)$, where δ_l are the coefficients of the penalized spline and B_l the spline basis functions. The penalization of coefficients is expressed by a regularization prior, $\delta_l \sim \text{N}(0, \sigma_s)$. The splines were set up separately for each risk factor. We used a spline of degree 3 with 5 inner knots resulting in $d = 5 + 3 - 1 = 7$ parameters δ_l to be estimated per risk factor (Fahrmeir et al., 2007, p.303).

$\beta_1, \beta_2, \beta_3$: Coefficients according to the point mass effects, where $I(KKL_{ijk} = 0)$ is meant to evaluate to 1 if $KKL_{ijk} = 0$, and 0 otherwise. Similarly for *CILateral* and *CIConifer*.

The model expression above implies that all of the risk factors (Table 1.2) appeared in the final model, but we used model selection to pare down the model to an optimal parsimonious model that is more likely to be accurate on external validation. This process is described next.

1.3.5 Selection of risk factors

We followed the recommendations in Harrell et al. (1996) that no more than $p = m/10$ predictor degrees of freedom should be examined for fitting a model aiming for good prediction, where degrees of freedom is understood as the number of coefficients in model fitting in this context. In the case of a logistic regression model for mortality, or equivalently a survival model, m is determined as the number of non-censored event times. In our data that is the number of dead trees, $m = 585$, resulting in $p \approx 58$ free parameters as the upper limit to use in the prediction model. The model structure as stated in Model 1.2 involves 102 coefficients, but most of them are subject to restrictions due to normality assumptions (plot and period effects) and penalization (smooth spline effects), leading to an effective number considerably lower than that. However, we regarded Model 1.2 as the upper bound in terms of complexity, and did not consider further effects such as interactions between risk factors.

For the actual selection of an optimal set of risk factors to include in the mortality prediction model, we performed an internal cross-validation. The particular cross-validation scheme reflected the hierarchical structure of the observations and the ultimate purpose of the model, which would be to predict 5-year mortality for a tree in a new plot. For median (or conditional) prediction the *periodOnset* and *plot* random effects would all be set to zero (Skrondal and Rabe-Hesketh, 2009). We used k-fold cross validation with $k = 29$ to correspond to the 29 plots represented in the data. Each of the 29 plots served in turn as a single test data set with the remaining 28 plots combined as a training set, resulting in 29 internal cross-validations. For each training set, a set of candidate models were fit and parameter estimates were used to predict the mortality for trees in the corresponding validation set. To reduce the influence of multi-collinearity among the risk factors on stability of the model selection process, the Spearman correlations among the transformed risk factors (Figure 1.5 and 1.9) were assessed and models containing two risk factors with correlations exceeding 0.75 in absolute value were dropped from further consideration.

Basically, we constructed the set of candidate models by building all subsets of smooth terms $(s_1, \ldots, s_9)$ in Model 1.2, excluding those with pairs of high correlation as mentioned above. Point mass effects were always included along with the according smoothed effect. The global intercept, offset term, and the random effects for *plot* and *periodOnset* were included in all of the candidate models at this stage. We investigated the performance of the resulting 67 models and used the best ones as a basis for further investigation. For example, if the functional form of a smooth effect looked linear, the term was replaced by a simple linear term, and the modified model was again assessed by cross-validation. In stepwise modifying, dropping and adding terms, we tried to further improve the performance and where appropriate, simplify the model, basing all actions on cross-validation. At the end we ran 142 models through this machinery and ultimately picked a final model among those

performing best. We will describe the measures of model performance in the following section.

1.3.6 Measures of model performance

Assessment of the predictive abilities of candidate models was an essential part in model development. Considering the purpose of the tree mortality model, we based all calculations on the predicted values $\hat{y} = \hat{\pi}$ $(0 \leq \hat{y} \leq 1)$, corresponding to the predicted mortality from the logistic regression model, and its relationship to the true outcome $y \in \{0; 1\}$ in the test data. Measures of model performance all deal with the distance of $\hat{y}$ to y but highlight different aspects of performance. Our focus was on *discrimination*, which measures how strong the predictions differ in n observations with $y = 1$ and $y = 0$, and *calibration*, which measures the agreement between observed outcomes and predictions from a frequentist point of view. If we predict a 20% risk of mortality for a tree, we should observe approximately 20 of 100 trees with such a prediction to experience mortality. Quantities combining different aspects are said to measure *overall performance* (Steyerberg et al., 2010). An extensive list of performance measures, along with their calculation rule and interpretation can be found in the Appendix. For model selection we focused on the AUC (discrimination), the calibration slope (calibration), and for overall model performance on R^2 and Brier score (Steyerberg, 2009, p. 257). The AUC for a covariate x, as described in Section 1.2.3, also applies for the case where x is a predicted probability of mortality, instead of a risk factor. Thus, $\hat{y}$, such as that arriving from a model fit to a training set of trees has same interpretation with the difference that we assess the separation ability of the whole model, a combination of several risk factors. The calibration slope (CS), is the estimated slope coefficient, $\hat{\beta}$, of a logistic regression model of true outcome y on the predicted risks $\hat{y}$,

$$\log\left(\frac{\mathbf{P}(y=1)}{1-\mathbf{P}(y=1)}\right) = \alpha + \beta \log\left(\frac{\hat{y}}{1-\hat{y}}\right),$$

$$CS \equiv \hat{\beta},$$

that is the model predictions $\hat{y}$ are transformed and used as the regressor variable in the logistic model. A calibration slope for a perfectly calibrated model is 1, while coefficients lower than 1 indicate that the predictions are too extreme. Too extreme means that the observed mortality is higher than predicted for low-risk trees and lower than predicted for high-risk trees (Steyerberg et al., 2001). The R^2 is based on the binomial likelihood, and can be interpreted in analogy to a linear regression model, as the proportion of variance explained by the model. For logistic regression, Nagelkerke (1991) standardized the binomial likelihood-based R^2_{Lik} with the theoretically maximal reachable R^2, which depends on the proportion of success ($y_i = 1$) in the data set to ensure the value of 1 for a perfect fit, analogous to linear regression. Log likelihoods of intercept-only and risk factor-based prediction models

	AUC (%)	Brier score (%)	R^2 (%)	Calibration slope
Model 1 with smooth terms[1]	84.41	3.87	18.95	0.694
Model 2 with parametric terms[2]	84.64	3.81	20.04	0.681
Model 3 with parametric terms[3]	85.04	3.80	20.67	0.689

[1] including $\hat{s}_1(KKL^{2/3})$, $\hat{s}_4(CIIntra^{1/2})$, $\hat{s}_5(CIConifer^{2/3})$, $\hat{s}_6(CIOvershade^{1/2})$, $\hat{\beta}_3(CIConifer = 0)$

[2] including $\hat{b}_1 KKL^{1/3}$, $\hat{b}_2 KKL^{2/3}$, $\hat{b}_3 CIOvershade$, $\hat{b}_4 CIOvershade^{1/2}$, $\hat{b}_5 CIIntra^{1/2}$, $\hat{b}_6 CIconifer^{1/3}$ $\hat{b}_7 CIconifer^{2/3}$, $\hat{b}_8(CIConifer = 0)$

[3] including terms from Model 2 and $\hat{b}_9 RelDBHdom^{2/3}$, $\hat{b}_{10} RelDBHdom^{4/3}$

Table 1.6: Performance in cross validation for three exemplary candidate models.

are given by

$$l_0 = \sum_i y_i \log \bar{y} + (y_i - 1) \log(1 - \bar{y}),$$

$$l_{pred} = \sum_i y_i \log \hat{y}_i + (y_i - 1) \log(1 - \hat{y}_i),$$

respectively, yielding

$$R^2_{Lik} = 1 - \exp\{(l_0 - l_{pred})(2/n)\},$$

$$R^2_{Nag} = \frac{R^2_{Lik}}{1 - \exp\{l_0(2/n))\}}.$$

In our case of a logistic regression model, the Brier score reports the mean squared prediction error, a measure routinely used to assess the goodness of fit in linear models,

$$Brier = \frac{1}{n} \sum_{i=1}^{n} (y_i - \hat{y}_i)^2.$$

1.4 Mortality prediction model

1.4.1 Model equation

The cross-validation process produced a set of models having practically the same optimal performance, although these models were based on different risk factors. At the end model choice was also based on subjective decisions, where we replaced smooth effect terms by simpler parametric expressions to facilitate interpretation without sacrificing model performance. As an example, Table 1.6 lists the performance measures for three models, with smooth and strictly parametric terms. Model 3 is slightly better in all criteria, but we argue that the more parsimonious Model 2 is more likely to reach the same high performance applied to external data. We fitted our chosen model to the entire data set, which led to the effects shown in Table 1.7. Only the four competition indices *KKL*, *CIOvershade*, *CIIntra*, and *CIConifer* appeared in the final model. These CIs are derived measures that utilize the

geometric relationship of neighboring trees in addition to tree size. Together they outweighed the crude predictor *DBH*. Multiple entries of the same predictor, such as $KKL^{1/3}$ and $KKL^{2/3}$, reflect the optimal transformations of the predictor. We arrived at these polynomial terms by visually assessing the smooth spline effects on the transformed risk factors. As the smooth effects showed simple functional forms we were able to replace them by polynomial terms without sacrificing performance in cross validation. To illustrate, we recap the stages to get the final form for the risk factor *KKL*. The KS-test suggested the transformation $KKL^{1/3}$ to get a well shaped empirical distribution, without severe skewness. The smooth spline effect of $KKL^{1/3}$ looked quadratic in a model with good performance. Replacing the smooth effect by a polynomial of degree 2, $KKL^{1/3} + (KKL^{1/3})^2$, showed the same performance as the model with the smooth term. In sum this can be expressed as $KKL^{1/3} + KKL^{2/3}$ in the final model. Risk of mortality increased slowly with increasing *KKL*, and flattened out for high values of *KKL* past 27, where there were not many observations in the data set. Interpretation of the effects of the three other predictors on risk can be more easily visualized in Figures 1.12, 1.13, 1.14, and 1.15, which show the combined effect of each predictor on risk after adjusting for the effects of the other predictors on risk. Similar behavior of increasing risk for small values turning into decreasing risk at some point was observed for *CIOvershade* and *CIConifer*, though the rates of increase were lower. In contrast, after adjusting for the other components in the model, risk steadily decreased as *CIIntra* increased. Finally, variation due to calendar year of the observation period (random effect standard deviation (SD)=1.72) was twice as

	Log odds ratio (SD)	Odds ratio (95% CI)	p-value
Intercept	-15.83 (1.52)	0.00 (0.00, 0.00)	< 0.001
KKL			
$KKL^{1/3}$	2.78 (0.54)	16.11 (5.62, 46.19)	0.003
$KKL^{2/3}$	-0.39 (0.12)	0.68 (0.54, 0.86)	0.098
CIOvershade			
$CIOvershade^{1/2}$	1.28 (0.16)	3.59 (2.61, 4.94)	< 0.001
CIOvershade	-0.03 (0.006)	0.97 (0.96, 0.98)	< 0.001
CIIntra			
$CIIntra^{1/2}$	-0.21 (0.05)	0.81 (0.74, 0.89)	< 0.001
CIConifer			
$CIConifer^{1/3}$	1.70 (0.53)	5.48 (1.94, 15.48)	0.004
$CIConifer^{2/3}$	-0.36 (0.09)	0.70 (0.58, 0.83)	< 0.001
I($CIConifer = 0$)	0.56 (0.81)	1.75 (0.36, 8.63)	0.82
Random effects	SD	95% CI	
plot	0.69	(0.17, 2.81)	
periodOnset	1.72	(0.18 16.7)	

SD=Standard deviation; CI=confidence interval; I(X)=effect for X versus not X

Table 1.7: Estimates and significance results from the chosen prediction model.

large as the variation due to plot (SD = 0.69) (Table 1.7). The large confidence intervals for the standard deviations of the random effects indicate that these estimates are rather vague and the intervals overlap widely.

To predict the mortality risk for a new tree during the next 5 years, we suggest to apply

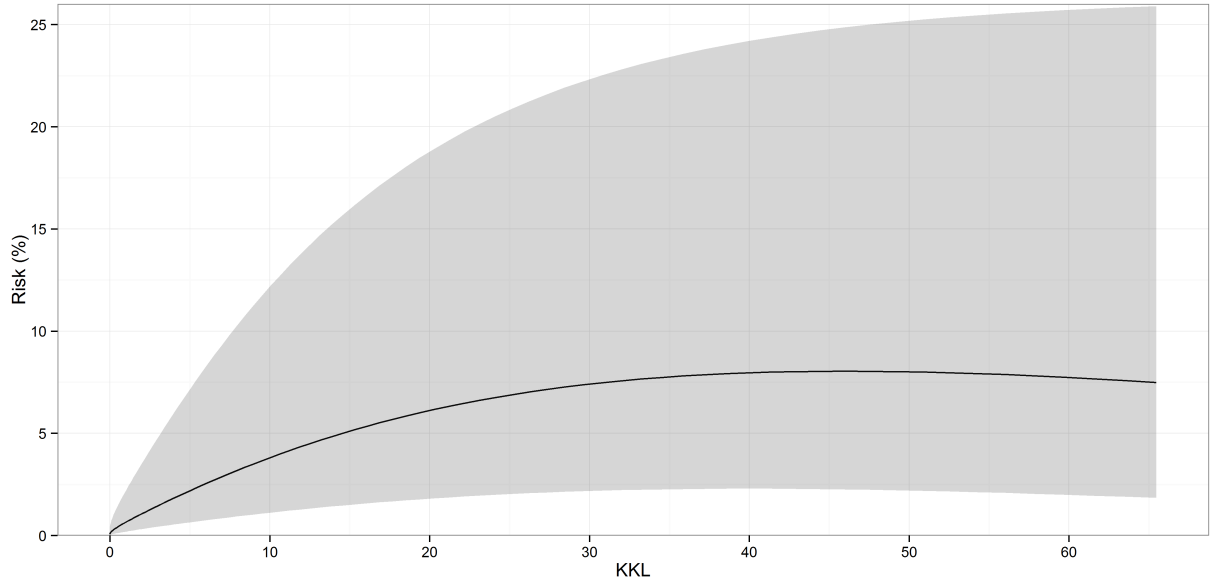

Figure 1.12: Risk of mortality in the next 5 years (solid line) according to *KKL* (x-axis) with pointwise 95% confidence intervals (shaded region). Values for the other risk factors were set at their median values and random effects to zero. Figure in style of Böck et al. (2013)

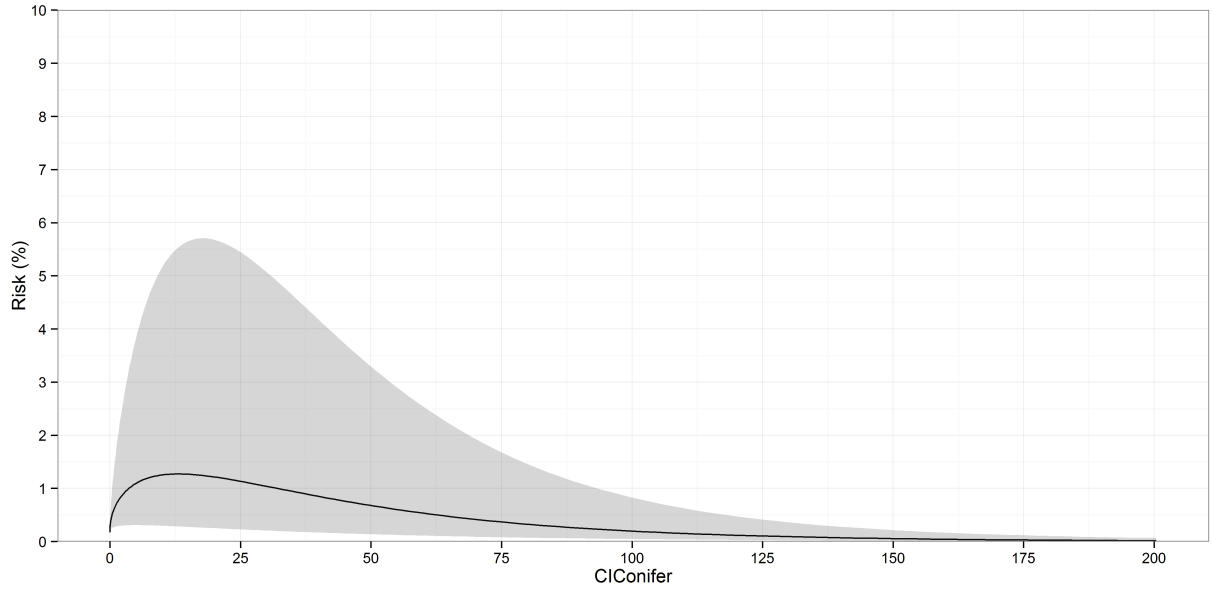

Figure 1.13: Risk of mortality in the next 5 years (solid line) according to *CIConifer* (x-axis) with pointwise 95% confidence intervals (shaded region). Values for the other risk factors were set at their median values and random effects to zero. Figure in style of Böck et al. (2013)

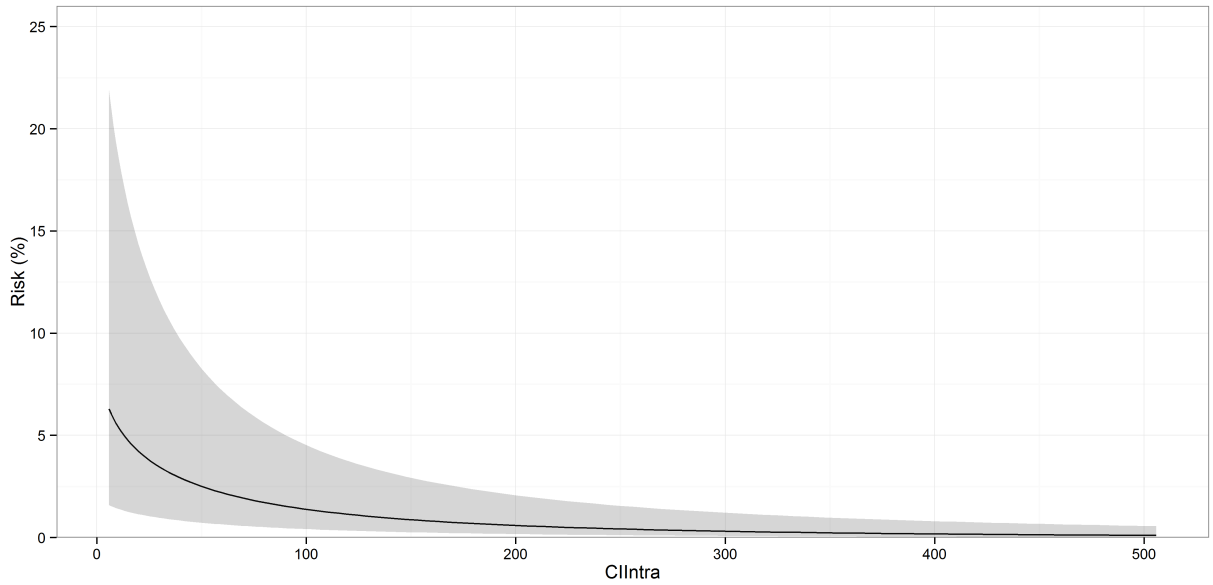

Figure 1.14: Risk of mortality in the next 5 years (solid line) according to *CIIntra* (x-axis) with pointwise 95% confidence intervals (shaded region). Values for the other risk factors were set at their median values and random effects to zero. Figure in style of Böck et al. (2013)

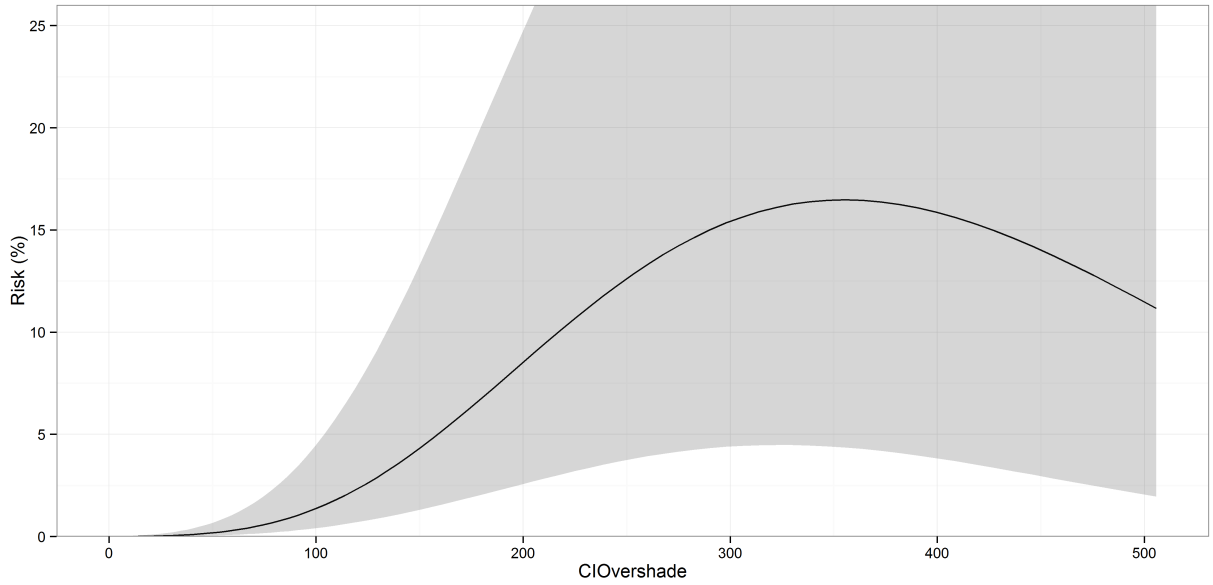

Figure 1.15: Risk of mortality in the next 5 years (solid line) according to *CIOvershade* (x-axis) with pointwise 95% confidence intervals (shaded region). Values for the other risk factors were set at their median values and random effects to zero. Figure in style of Böck et al. (2013)

the following equation,

$$\begin{aligned}\log\frac{\hat{\pi}}{1-\hat{\pi}} = &-15.83 + 2.78\,KKL^{1/3} - 0.39\,KKL^{2/3} + \\ &1.28\,CIOvershade^{1/2} - 0.03\,CIOvershade - 0.21\,CIIntra^{1/2} + \\ &1.70\,CIConifer^{1/3} - 0.36\,CIConifer^{2/3} + 0.56\,I(CIConifer = 0) \\ &= \hat{\eta},\end{aligned} \tag{1.3}$$

	AUC (%)	Brier score (%)	R^2 (%)	Calibration slope
Cross validation	84.64	3.81	20.04	0.681
Internal validation	88.93	3.35	31.62	1.048

Table 1.8: Contrasting performance according to different validation schemes. Cross validation: Leave-one-plot-out cross validation of final model. Internal validation: Final model fitted on entire data (leading to Equation 1.3) is validated on the same data using all information of the fitted model, including random effect estimates.

where $I(CIConifer = 0)$ equals 1 if *CIConifer* has the value 0 and equals 0 otherwise, and the result $\hat{\eta}$ is transformed to the probability scale by $\hat{\pi} = \exp(\hat{\eta})/(1 + \exp(\hat{\eta}))$.

1.4.2 Contrasting performance

Finally, we want to contrast the performance measures according to internal and cross validation using a model with the same set of covariates. Table 1.8 lists the AUC, Brier score, pseudo R^2, and calibration slope. The cross validation results are based on the model structure which led to the final model, that is, included terms were the covariates from Equation1.3, the random effects for plot and period and the offset term. To recall, in that leave-one-plot-out cross validation the coefficients differed from those in the aforementioned equation in each of the models fitted on the 29 training datasets. The actual coefficients we suggest for use to obtain risk predictions are those from the model fitted to the entire dataset. For this we show the internal validation: Model fitting and model assessment were based on the same data, all information were used to obtain prediction, including random effects coefficients.

Internal validation clearly had the best performance, mainly because internal predictions are always well-calibrated. As our approach of cross validation is somewhere in between of internal and external validation, it is reasonable to expect an AUC around 80%, a fairly good separation ability, for similar but new data. The calibration slope was below unity, which indicates some overfitting. That means we are not able to quantify the mortality risk very accurately on average. A general shrinkage of the coefficients might overcome this. On the other hand we observed an calibration slope above unity for the per definition well-calibrated internal predictions. This effect was induced by the random effects in the model, as fixed effects only models show perfect calibration in terms of average measures such as *calibration slope* or *calibration in the large*, which contrast mean predictions against mean outcomes (a fixed effects only model would obtain a calibration slope equal to unity). The fact that random effects with normality assumption are somewhat lower in magnitude than their fixed effects counterparts would be, finally leads to an underrating of actually high risks and the overestimation of small risks. In other words, the shrinkage effect, which is desirable to correct for overfitting, is seen in an underfitting tendency in the internal prediction performance. Measures of goodness-of-fit, which represent a distance between the observed outcomes and

the predictions, showed a drop down of 12% (Brier score) and 35% (R^2). We attribute this discrepancy to the over-optimism of internal validation and the fact that, on principle, the results of binomial regression models can hardly be generalized to different settings (Mood, 2010). However, the good separation ability seen on the AUC showed only a moderate decline of 4.8%, giving occasion to believe that predictions on external data will also deliver valuable information to identify trees which are particularly at risk.

1.5 Summary and outlook

The review of the literature combined with the results of this study show that a variety of statistical methods have effectively been used for modeling the rare event of forest mortality. Forest mortality models are designed with specific objectives in mind, these objectives determine the risk factors used in the model. In contrast to other models, mortality models in this study were specifically designed to capitalize on the many geometrical and distance-based competition indices that are calculated with detailed forest inventory data through the SILVA simulator. As such, competition indices outweighed the effect of the crude predictor *DBH* or other predictors of tree size. The mortality model presented here was developed for European Beech, one of the largest of two species currently under observation as part of the Bavarian forest network. A next step would be to move on to another common species, the Douglas fir and to assess whether a similar risk profile for mortality holds.

In this study we focused on modeling the functional dependency of mortality on risk factors, accounting for the peculiarities of the sampling design. A probabilistic model was fitted using the maximum likelihood approach. McIntosh and Pepe (2002) show the optimality of such models in terms of AUC. However, it might be worth trying to directly optimize measures of model performance which were used for now only for model assessment. This would result in different loss functions than the one presently applied, the negative binomial likelihood, and the discussion of proper scoring rules (Gneiting and Raftery, 2007).

Investigations concerning to relax the normality assumption of the random effects via Dirichlet process priors (Kleinman and Ibrahim, 1998b; Wang, 2010) did not show enhancements in terms of model performance. On the contrary, based on our examinations we found the normality constraint to be rather helpful in rare-events logistic regression, having a stabilizing effect. Further, the methods suggested in Pregibon (1981) and Landwehr et al. (1984) for the detection of outliers were not expedient as they mainly sorted out the few trees where mortality was observed. The computationally demanding model selection based on the cross validation of a large set of candidate models was not contradictory to AIC/BIC procedures, which could be obtained faster, but had two advantages: The dependency of the results on the specification of the effective sample size (Zou and Normand, 2001) which is a quantity needed in both criteria could be avoided. In our setting with longitudinal observations and possibly multiple levels of random effects, it is somewhat unclear how to derive a suitable

quantity of effective sample size. Further, both AIC and BIC provide no support on the decision about which type of risk predictions from a random effects model (conditional versus marginal) should be used.

Chapter 2

Plant breeding

This chapter emphasizes the statistical methods used in the article "Association analysis of frost tolerance in rye using candidate genes and phenotypic data from controlled, semi-controlled, and field phenotyping platforms" (Y. Li, A. Böck, G. Haseneyer, V. Korzun, P. Wilde, C.-C. Schön, D. P. Ankerst, and E. Bauer, 2011b), while shortening the biological background and subject matter considerations. For those we refer to the original article and its supplementary material, which provide more details. Figures in the original article were produced by Li and partly recreated on the underlying data by the author of this thesis to match the style of this dissertation (referenced with "recreated").

2.1 Introduction

Frost stress, one of the important abiotic stresses, not only limits the geographic distribution of crop production but also adversely affects crop development and yield through cold-induced desiccation, cellular damage and inhibition of metabolic reactions (Gusta et al., 1997; Chinnusamy et al., 2007). Thus, crop varieties with improved tolerance to frost are of enormous value for countries with severe winters. Frost tolerance (FT) is one of the most critical traits that determine winter survival of winter cereals (Saulescu and Braun, 2001). Among small grain cereals, rye (Secale cereale L.) is the most frost tolerant species and thus can be used as a cereal model for studying and improving FT (Fowler and Limin, 1987; Hommo, 1994). After cold acclimation where plants are exposed to a period of low, but non-freezing temperature, the most frost-tolerant rye cultivar can survive under severe frost stress down to approximately -30 °C (Thomashow, 1999). Tests for evaluating FT can be generally separated into direct and indirect approaches. For direct approaches, where plants are exposed to both cold acclimation and freezing tests, plant survival rate, leaf damage, regeneration of the plant crown, electrolyte leakage, and chlorophyll fluorescence are often used as phenotypic endpoints (Saulescu and Braun, 2001). For indirect approaches, where plants are only exposed to cold acclimation, the endpoints of water content (Fowler et al., 1981), proline (Dorffling et al., 1990), and cold-induced proteins (Houde et al., 1992) are

often used. The evaluation of FT can be conducted either naturally under field conditions or artificially in growth chambers, with both methods associated with advantages and disadvantages. Under field conditions, plant damage during winter is not only affected by low temperature stress per se, but also by the interaction of a range of factors such as snow coverage, water supply, and wind. Therefore, measured phenotypes are the result of the full range of factors affecting winter survival. Opportunities for assessing FT are highly dependent upon temperature and weather conditions during the experiment. In contrast, frost tests in growth chambers allow for a better control of environmental variation and are not limited to one trial per year. However, they are limited in capacity and may not correlate well with field performance. Therefore, it has been recommended to test FT under both natural and controlled conditions whenever possible (Saulescu and Braun, 2001).

Identification of genes underlying traits of agronomic interest is pivotal for genome-based breeding. Due to methodological advances in molecular biology, plant breeders can now select varieties with favorable alleles through molecular markers, including single nucleotide polymorphisms (SNPs), identified in genes linked to desirable traits (Rafalski, 2002; Tester and Langridge, 2010). Whole genome- and candidate gene-based association studies have identified large numbers of genomic regions and individual genes related to a range of traits (Harjes et al., 2008; Malosetti et al., 2007; Thornsberry et al., 2001; Zhao et al., 2007). However, underlying population structure and/or familial relatedness (kinship) between genotypes under study have proven to be a big challenge, leading to false positive associations between molecular markers and traits in plants due to the heavily admixed nature of plant populations (Aranzana et al., 2005). In response, several advanced statistical approaches have been developed for genotype-phenotype association studies, including genomic control (Devlin and Roeder, 1999), structured association (Pritchard et al., 2000), and linear mixed model-based methodologies (Stich et al., 2008; Yu et al., 2006).

The main objective of this study was to identify SNP alleles and haplotypes conferring superior FT through candidate gene-based association studies performed in three phenotyping platforms: controlled, semi-controlled, and field.

2.2 Methods

2.2.1 Plant material and DNA extraction

Plant material was derived from four Eastern and one Middle European cross-pollinated winter rye breeding populations: 44 plants from EKOAGRO (Poland), 68 plants from Petkus (Germany), 33 plants from PR 2733 (Belarus), 41 plants from ROM103 (Poland), and 15 plants from SMH2502 (Poland). To determine the haplotype phase, a gamete capturing process was performed by crossing between 15 and 68 plants of each source population to the same self-fertile inbred line, Lo152. Each resulting heterozygous S_0 plant represented one gamete of the respective source population. S_0 plants were selfed to obtain S_1 families

and these were subsequently selfed to produce $S_{1:2}$ families, which were used in phenotyping experiments. For molecular analyses, genomic DNA of S_0 plants was extracted from leaves according to a procedure described previously in Rogowsky et al. (1991).

2.2.2 Phenotypic data assessment

Controlled platform In the controlled platform, experiments were performed in climate chambers at −19 °C and −21 °C in 2008 and 2009, respectively. The trials were run at ARI Martonvásár (MAR), Hungary, using established protocols (Vagujfalvi et al., 2003). Briefly, seedlings were cold-acclimated in a six week hardening program with gradually decreasing temperatures from 15 °C to −2 °C. After that, the plants were exposed to freezing temperatures within six days by decreasing the temperature from −2 °C to −19 °C or −21 °C and then held at the lowest temperature for eight hours. After the freezing step, temperature was gradually increased to 17 °C for regeneration. The ability of plants to re-grow was measured after two weeks using a recovery score, which ranged on a scale from 0: completely dead, 1: little sign of life, 2: intensive damage, 3: moderate damage, 4: small damage, to 5: no damage. The light intensity was 260 μmol/m^2s during the seedling growth and the hardening process, whereas the freezing cycle was carried out in a dark environment. The experiment in 2008 contained 139 S_1 families. The experiment in 2009 contained 201 $S_{1:2}$ families, augmenting the same 139 S_1 families from the experiment in 2008 with an additional 62 $S_{1:2}$ families. Five plants of each S_1 or $S_{1:2}$ family were grown as one respective test unit with five replicates per temperature and year. Due to the limited capacity of climate chambers, genotypes were randomly assigned into three and four chambers in 2008 and 2009, respectively.

Semi-controlled platform In the semi-controlled platform, experiments during the years 2008 and 2009 were performed with three replicates per year at Oberer Lindenhof (OLI), Germany, using the same 139 S_1 families and 201 $S_{1:2}$ families. From each family a test unit of 25 plants was grown outdoors in wooden boxes one meter above the ground in a randomized complete block design (RCBD) (Montgomery, 2001, chap 4). The RCBD was complete in the sense that the complete entity of genotypes was replicated three times. In case of snowfall, plants were protected from snow coverage to avoid damage by snow molds. Two weeks after a frost period of 2-4 weeks with average daily temperatures around or below 0 °C, usually frost at least during the night, and with minimum temperatures as indicated in Additional File 1 of Li et al. (2011), % leaf damage was assessed among the 25 plants of each family by recording the percentage of plant that had dry and yellow leaves,

$$\frac{\text{Number of plants with at least one dry or yellow leaf}}{25}.$$

In order to keep the same sign/direction as with the measurements in the controlled and field platforms, % leaf damage was replaced by % plants with undamaged leaves, calculated as 100% - % leaf damage. Outcomes were recorded in January, February, and April of 2008

for the 139 S_1 families, and in February and March of 2009 for the 201 $S_{1:2}$ families.

Field platform In the field platform, experiments were performed with the same 201 $S_{1:2}$ families in five different environments in 2009: Kasan, Russia (KAS); Lipezk, Russia (LIP1); Minsk, Belarus (MIN); Saskatoon, Canada, two different fields (SAS1 and SAS2); and in one environment in 2010: Lipezk, Russia (LIP2). Depending on the environment, test units comprised 50-100 plants. The outcome, % survival, was calculated as the number of intact plants after winter divided by the total number of germinated plants before winter. RCBDs with two replicates were used for the SAS1 and SAS2 environments, while all other environments used the lattice design with three replicates each. In the lattice design the field is divided into cells, characterized by row and column numbers to be incorporated into the statistical analysis. The climate data of the semi-controlled and field platforms are provided as supplementary material of Li et al. (2011).

2.2.3 Obtaining genetic components for association model

In order to correct for confounding effects in the association studies, population structure and kinship were estimated. Therefore, from the DNA material of each genotype 37 simple sequence repeat (SSR) markers were extracted, which were chosen based on their experimental quality and map location as providing good coverage of the rye genome; details are found in (Li et al., 2011). Primers and PCR conditions were described in detail by Khlestkina et al. (2004) for rye microsatellite site (RMS) markers and by Hackauf and Wehling (2002) for Secale cereale microsatellite (SCM) markers. Fragments were separated with an ABI 3130xl Genetic Analyzer (Applied Biosystems Inc., Foster City, CA, USA) and allele sizes were assigned using the program GENEMAPPER (Applied Biosystems Inc., Foster City, CA, USA).

Population structure Population structure was inferred from the 37 SSR markers using the `STRUCTURE` software v2.2, which is based on a Bayesian model-based clustering algorithm that incorporates admixture and allele correlation models to account for genetic material exchange in populations resulting in shared ancestry (Pritchard et al., 2000). Prior distributions were specified for the model parameters and inference was based on the posterior distribution, which was explored via a Markov Chain Monte Carlo (MCMC) sampling scheme. Essentially, the method assigned each individual to a predetermined number of groups (k), characterized by a set of allele frequencies at each locus, assuming that the loci are in Hardy-Weinberg equilibrium and linkage equilibrium. In other words, the clustering aims to find population groupings that are in the least possible disequilibrium. For each genotype g_i, a vector $\boldsymbol{q}_i$ of length k is estimated, providing probabilities (or membership fractions) for each group Z_j:

$$\mathbf{P}(g_i \text{ originates from } Z_j) = q_{i,j},$$

with $i = 1, \ldots, 201$, $j = 1, \ldots, k$, and the restriction $\sum_{j=1}^{k} q_{i,j} = 1$. The population structure matrix $\boldsymbol{Q}_{STRUCTURE}$ with dimension $201 \times k$ contains the estimates for all genotypes used in the association model with individual elements given by

$$\boldsymbol{Q}_{STRUCTURE}(i, j) = q_{i,j}.$$

Ten runs for values of k ranging from two to eleven were performed using a burn-in period of 50,000 MCMC samples followed by 50,000 MCMC iterations used for inference. Inference for k is not possible in the same manner as for $\boldsymbol{Q}_{STRUCTURE}$ because k is not part of the MCMC sampling scheme. However, posterior probabilities of each k were approximated using those ten runs, and the maximum posteriori k was determined. Details for that approximation are found in the Appendix of Pritchard et al. (2000).

Kinship A kinship matrix $\boldsymbol{K}$ was estimated from the same SSR markers using the allele-similarity method (Hayes and Goddard, 2008), which guarantees a positive semi-definite relationship matrix among the 201 genotypes. This was stored to be used for the covariance structure of the random genotype effects in the linear mixed model for the association analysis. For a given locus, the similarity index S_{xy} between two genotypes x and y was 1 when they had an identical number of repeats in the SSR marker and were 0 otherwise. S_{xy} was averaged over the 37 loci, and transformed and standardized as $\tilde{S}_{xy} = (S_{xy} - S_{min})/(1 - S_{min})$, where S_{min} was the minimum S_{xy} over all genotypes. The entries of the kinship matrix $\boldsymbol{K}$ stored the relationship indices $\tilde{S}_{xy}$ for every pair of genotypes. An example is given in Section 2.2.6.

2.2.4 SNP-FT association model

Twelve candidate genes – *ScCbf2*, *ScCbf6*, *ScCbf9b*, *ScCbf11*, *ScCbf12*, *ScCbf14*, *ScCbf15*, *ScDhn1*, *ScDhn3*, *ScDreb2*, *ScIce2*, and *ScVrn1* – were selected for analysis due to their previously proven putative role in the FT network (Badawi et al., 2008; Campoli et al., 2009; Choi et al., 1999; Francia et al., 2007; Galiba et al., 1995). Details on candidate gene sequencing, SNP and insertion-deletion (Indel) detection, haplotype structure and linkage disequilibrium (LD) were described earlier (Li et al., 2011), except for *ScDreb2*, which is described in Supplementary file 2 of (Li et al., 2011). Indels were treated as single polymorphic sites, and, to be more convenient, polymorphic sites along the sequence in each gene were numbered starting with "SNP1" and are referred to in the text as SNPs instead of differentiating between SNPs and Indels.

SNP-FT associations in all platforms were performed using linear mixed models that evaluated the effects of 170 SNPs with minor allele frequencies (MAF) $> 5\%$ individually, adjusting for population structure, kinship and platform-specific effects. A one stage approach was chosen for analysis which directly models the phenotypic data as the response.

The general form of the linear mixed model for the three platforms was

$$\begin{aligned} \boldsymbol{y} = \mathbf{1}\beta_0 + \boldsymbol{x}_{SNP}\beta_{SNP} \; + \; & \boldsymbol{Q}_{STRUCTURE}\boldsymbol{\beta}_{STRUCTURE} + \\ & \boldsymbol{X}_{PLATFORM}\boldsymbol{\beta}_{PLATFORM} \; + \; \boldsymbol{Z}_{PLATFORM}\boldsymbol{\gamma}_{PLATFORM} + \\ & \boldsymbol{Z}_{GENOTYPE}\boldsymbol{\gamma}_{GENOTYPE} + \boldsymbol{\varepsilon}. \end{aligned} \tag{2.1}$$

More precise descriptions are given below, where for better readability the subscripts were dropped if the context allowed. (platform-specific details are regarded afterwards):

$\boldsymbol{y}$ Vector of platform-specific phenotypes with dimension $n\times 1$.

$\mathbf{1}\beta_0$ Design vector with solely 1 entries $\mathbf{1}$ ($n\times 1$) and scalar intercept coefficient β_0.

$\boldsymbol{x}_{SNP}\beta_{SNP}$

Design vector $\boldsymbol{x}_{SNP}$ ($n\times 1$) for bi-allelic SNP containing entries in dummy-coding: 0 for the reference allele (Lo152), 1 for the non-reference allele. Accordingly, β_{SNP} is a scalar fixed effect when switching from reference allele to non-reference allele.

$\boldsymbol{Q}_{STRUCTURE}\boldsymbol{\beta}_{STRUCTURE}$

Design matrix $\boldsymbol{Q}$ ($n\times(k-1)$), containing the first $(k-1)$ membership fractions, which were obtained from the `STRUCTURE` software. The k-th fraction is not used, as it is a linear combination of the others due to the sum-to-one constraint. Fixed effect coefficients vector $\boldsymbol{\beta}$ with dimension $(k-1)\times 1$.

$\boldsymbol{X}_{PLATFORM}\boldsymbol{\beta}_{PLATFORM}$

Platform specific design matrix $\boldsymbol{X}$ ($n \times p$) for fixed effects vector $\boldsymbol{\beta}$ ($p \times 1$).

$\boldsymbol{Z}_{PLATFORM}\boldsymbol{\gamma}_{PLATFORM}$

Platform specific design matrix $\boldsymbol{Z}$ ($n \times m$) for random effects vector $\boldsymbol{\gamma}$ ($m \times 1$). Random effects are assumed to follow a multivariate normal distribution, $\boldsymbol{\gamma}_{PLATFORM} \sim \mathrm{N}(\mathbf{0}, \boldsymbol{D})$, with covariance matrix $\boldsymbol{D}$.

$\boldsymbol{Z}_{GENOTYPE}\boldsymbol{\gamma}_{GENOTYPE}$

Design matrix $\boldsymbol{Z}$ ($n \times l$) for the random genotype effects and random effects vector $\boldsymbol{\gamma}$ ($l \times 1$). For the genotype effects the distributional assumption is

$$\tilde{\gamma} \sim N(\mathbf{0}, \sigma_g^2 \boldsymbol{K}),$$

where $\boldsymbol{K}$ is the kinship matrix and σ_g^2 is the genotypic variation to be estimated. The peculiarity of $\tilde{\gamma}$ is its correlation structure given through the matrix $\boldsymbol{K}$. The software we used for model fitting only allowed some limited types of covariance matrices, correlated random intercepts were not directly supported. That is, user input of a

correlation matrix was not possible. However, uncorrelated random intercepts, which were supported, are equivalent to the use of an identity matrix instead of $\boldsymbol{K}$. In order to still account for kinship in the estimation of genotype effects the correlation structure was shifted in the design matrix $\boldsymbol{Z}$, which was constructed as follows: The incidence matrix $\widetilde{\boldsymbol{Z}}$, which links each observation to its genotype effect, was post-multiplied by the transpose of the Cholesky-root of $\boldsymbol{K}$, denoted by $\boldsymbol{K}^{T/2}$. The Cholesky-root is well-defined for symmetric, positive semi-definite matrices, a property which is guaranteed using the allele-similarity method from Hayes and Goddard (2008). That is,

$$\boldsymbol{K} = \boldsymbol{K}^{T/2}\boldsymbol{K}^{1/2},$$

with $\boldsymbol{K}^{1/2}$ being the right Cholesky-root, which is an upper-triangular-matrix, and $\boldsymbol{K}^{T/2}$ the transpose of it, which is a lower-triangular-matrix. From $\tilde{\boldsymbol{\gamma}} \sim \mathrm{N}(\boldsymbol{0}, \sigma_g^2\boldsymbol{I})$, it holds that

$$\boldsymbol{Z}\tilde{\boldsymbol{\gamma}} \sim N(\boldsymbol{0}, \sigma_g^2\boldsymbol{Z}\boldsymbol{I}\boldsymbol{Z}').$$

From $\boldsymbol{Z} = \widetilde{\boldsymbol{Z}}\boldsymbol{K}^{T/2}$, it holds that

$$\sigma_g^2\boldsymbol{Z}\boldsymbol{I}\boldsymbol{Z}' = \sigma_g^2\widetilde{\boldsymbol{Z}}\boldsymbol{K}\widetilde{\boldsymbol{Z}}',$$

which is the desired variance for $\boldsymbol{Z}_{GENOTYPE}\boldsymbol{\gamma}_{GENOTYPE}$:

$$\mathbb{V}(\boldsymbol{Z}_{GENOTYPE}\boldsymbol{\gamma}_{GENOTYPE}) = \sigma_g^2\widetilde{\boldsymbol{Z}}\boldsymbol{K}\widetilde{\boldsymbol{Z}}'.$$

Therefore $\boldsymbol{Z}_{GENOTYPE}$ was set to $\widetilde{\boldsymbol{Z}}\boldsymbol{K}^{T/2}$ in the mixed model and $\boldsymbol{\gamma} \sim \mathrm{N}(\boldsymbol{0}, \sigma_g^2\boldsymbol{I})$.

$\boldsymbol{\varepsilon}$ Residual error $\boldsymbol{\varepsilon}$ ($n \times 1$), assumed to comprise independent and identically distributed random normal errors with mean zero and variance σ^2: $\boldsymbol{\varepsilon} \sim N(\boldsymbol{0}, \boldsymbol{I}\sigma^2)$.

2.2.5 Phenotypic variation

To test phenotypic variation between genotypes, the same platform-specific models as described for the SNP-FT association analyses were fitted for each platform omitting the SNP and population structure fixed effects. Within the controlled platform, separate models were fitted for each combination of temperature and year; for the semi-controlled platform, separate models were fitted for each month of each year; and for the field platform, separate models were fitted for each geographic location—altogether 15 subgroups in all three platforms. Within this grouping, mean outcomes per genotype were calculated. That is, the replicates of each genotype were averaged and summarized in boxplots.

Genetic variation was reported as the variance component corresponding to the random genotype effect in each model, with a p-value computed using the likelihood ratio test (LRT),

	Marker 1	Marker 2	Marker 3	Marker 4
Genotype 1	A	A	A	A
Genotype 2	A	B	B	B
Genotype 3	A	C	A	B

Table 2.1: Example markers for kinship estimation.

a conservative estimate since the true asymptotic distribution of the LRT statistic is a mixture of chi-square distributions (Fitzmaurice et al., 2004). This analysis aims to give an overview of the measured variability in the trials and is therefore reported first in the results section.

2.2.6 About the kinship matrix

The kinship matrix is supposed to express genetic similarity between different individuals or genotypes. Regarding the kinship matrix as an empirical correlation matrix might be misleading as it is not clear what the theoretical counterpart (the true underlying parameter) is. However, in the mixed model it is used as a correlation or covariance matrix in the prior distribution of the random genotype effects. The documentation of the `kin()` function in the `synbreed` R-package (Wimmer et al., 2012) is a good starting point for further reading about the different types of kinship estimation and their interpretation. The scale of the kinship matrix, in terms of a scalar factor multiplied with the matrix $\boldsymbol{K}$, is arbitrary for the fit of the linear mixed model and also the inference is unaffected when the variance parameter associated with $\boldsymbol{K}$, σ_g^2, is estimated (and not fixed). Clearly, quantities such as heritability, $h^2 = \frac{\sigma_g^2}{\sigma_g^2+\sigma^2}$, highly depend on how the kinship matrix is derived. Balding (2013) shows recent developments.

Below are some examples of how the entries of the kinship matrix $\boldsymbol{K}$ influence the estimation in a linear mixed model. Suppose there are SSR markers from three homozygous inbred lines at four loci, demonstrated in the following table: The simple matching coefficient of Reif et al. (2005) in the standardized version of Hayes and Goddard (2008) is calculated as

$$\tilde{S}_{xy} = (S_{xy} - S_{min})/(1 - S_{min}),$$

for genotype x and genotype y, with S_{xy} the proportion of loci with identical alleles, and S_{min} the minimum S between all genotypes. As Genotype 1 and Gentoype 3 have two identical alleles out of four, their coefficient is 2/4. The minimum between all three genotypes is 1/4, leading to a similarity coefficient between Genotype 1 and Genotype 3 of

$$\tilde{S}_{\text{Genotpye 1,Genotype 3}} = \tilde{S}_{13} = \frac{\frac{2}{4} - \frac{1}{4}}{1 - \frac{1}{4}} = 1/3.$$

The coefficients for all pairs of the three genotypes in this example are stored in the kinship

matrix

$$\boldsymbol{K} = \begin{bmatrix} 1 & 0 & 1/3 \\ 0 & 1 & 1/3 \\ 1/3 & 1/3 & 1 \end{bmatrix},$$

where the rows and columns are ordered accordingly to Genotype 1, 2, and 3.

To illustrate how such a kind of correlation matrix affects the estimation of the random effects $\boldsymbol{\gamma}$, we consider the fixed artificial outcome vector $\boldsymbol{y}$ of six plants from three genotypes and three different scenarios of kinship matrices. The data are coded as:

y	Genotype
1	1
1	1
1	2
4	2
2	3
3	3

and $\boldsymbol{Z} = \begin{bmatrix} 1 & 0 & 0 \\ 1 & 0 & 0 \\ 0 & 1 & 0 \\ 0 & 1 & 0 \\ 0 & 0 & 1 \\ 0 & 0 & 1 \end{bmatrix}$.

For the mixed model

$$\boldsymbol{y} = \mathbf{1}\beta_0 + \boldsymbol{Z}\boldsymbol{\gamma} + \boldsymbol{\varepsilon}, \quad \boldsymbol{\gamma} \sim \mathrm{N}(\mathbf{0}, \sigma_g^2 \boldsymbol{K}), \quad \boldsymbol{\varepsilon} \sim \mathrm{N}(\mathbf{0}, \sigma^2 \boldsymbol{I}),$$

with given variance parameters $\sigma_g^2 = \sigma^2 = 1$, the variance of $\boldsymbol{y}$ is

$$\mathbb{V}(\boldsymbol{y}) = \boldsymbol{I} + \boldsymbol{Z}\boldsymbol{K}\boldsymbol{Z}' = \boldsymbol{V}.$$

The estimates of the fixed effect β_0 and the random effects $\boldsymbol{\gamma}$ are

$$\hat{\beta}_0 = \underbrace{(\mathbf{1}'\boldsymbol{V}^{-1}\mathbf{1})^{-1}\mathbf{1}'\boldsymbol{V}^{-1}}_{\boldsymbol{H}_{\text{fix}}}\boldsymbol{y}$$

and

$$\hat{\boldsymbol{\gamma}} = \underbrace{\boldsymbol{K}\boldsymbol{Z}'\boldsymbol{V}^{-1}}_{\boldsymbol{H}}\underbrace{(\boldsymbol{y} - \mathbf{1}\hat{\beta}_0)}_{\tilde{\boldsymbol{y}}}.$$

We present three matrices $\boldsymbol{K}$, representing different grades of correlation between random

effects of genotypes:

$$\boldsymbol{K}_1 = \begin{bmatrix} 1 & 0 & 0 \\ 0 & 1 & 0 \\ 0 & 0 & 1 \end{bmatrix} \text{(no correlation)},$$

$$\boldsymbol{K}_2 = \begin{bmatrix} 1 & 0.35 & 0.05 \\ 0.35 & 1 & 0.21 \\ 0.05 & 0.21 & 1 \end{bmatrix} \text{(moderate correlation)},$$

$$\boldsymbol{K}_3 = \begin{bmatrix} 1 & 0.9 & 0.1 \\ 0.9 & 1 & 0.5 \\ 0.1 & 0.5 & 1 \end{bmatrix} \text{(strong correlation)}.$$

No correlation ($\boldsymbol{K}_1$) Choosing $\boldsymbol{K}_1$ corresponds to assuming no correlation between the random effects coefficients of the genotypes and, with no further covariates as in this example, the intercept coefficient $\hat{\beta}_0$ equals the sample mean of $\boldsymbol{y}$,

$$\hat{\beta}_0 = \sum_{i=1}^{6} y_i = (1 + 1 + 1 + 4 + 2 + 3)/6 = 2,$$

assigning the same weight to all observations. The hat-matrix $\boldsymbol{H}$ gives information on how the intercept-centered outcome values $\tilde{\boldsymbol{y}}$ contribute to the estimation of the random effects $\boldsymbol{\gamma}$. With $\boldsymbol{K}_1$ we obtain

$$\boldsymbol{H}_1 = \begin{bmatrix} 0.33 & 0.33 & 0 & 0 & 0 & 0 \\ 0 & 0 & 0.33 & 0.33 & 0 & 0 \\ 0 & 0 & 0 & 0 & 0.33 & 0.33 \end{bmatrix},$$

which means that $\hat{\gamma}_1$, the random effect for Genotype 1, is $0.33 \cdot \tilde{y}_1 + 0.33 \cdot \tilde{y}_2$. Only the two measurements of plants with Genotype 1 affect the estimation—it is independent of the others. The shrinkage effect impinging on the coefficients is reflected in the row-wise sums, which are all smaller than 1.

Moderate correlation ($\boldsymbol{K}_2$) With $\boldsymbol{K}_2$ we assume a correlation between the effect of Genotype 1 and Genotype 2 of 0.35, between Genotype 1 and 3 of 0.05, and between Genotype 2 and 3 of 0.21. The intercept $\hat{\beta}_0$ is now a weighted mean of $\boldsymbol{y}$, with the weights $(0.17, 0.17, 0.14, 0.14, 0.18, 0.18)$ calculated from $\boldsymbol{H}_{\text{fix}}$. The greatest weight (0.18) is assigned to the two observations of Genotype 3, because this genotype contributes the greatest amount of independent data relative to the others, implied by the assumption that its coefficient has the lowest correlations with the others. In other words, $\hat{\beta}_0$ leans closer towards the observations of Genotype 3 relative to the observations of Genotype 1 and Genotype 2. The

(rounded) hat-matrix $\boldsymbol{H}$ for the random effects is

$$\boldsymbol{H}_2 = \begin{bmatrix} 0.32 & 0.32 & 0.04 & 0.04 & 0.00 & 0.00 \\ 0.04 & 0.04 & 0.32 & 0.32 & 0.02 & 0.02 \\ 0.00 & 0.00 & 0.02 & 0.02 & 0.33 & 0.33 \end{bmatrix},$$

reflecting that observations from all genotypes are involved in the estimation of all three random genotype effects. (The values 0.00 are not exactly zero, but occur due to rounding).

Strong correlation ($\boldsymbol{K}_3$) With $\boldsymbol{K}_3$ we specified a correlation matrix with a very high correlation between Genotype 1 and Genotype 2 (0.9), together with a relatively low but still considerable correlation between Genotype 1 and Genotype 3 (0.5). $\boldsymbol{K}_3$ is still positive-definite, but the smallest of its three eigenvalues 2.07, 0.92, and 0.01 is barely larger than zero. This circumstance can lead to negative entries of the hat-matrix for the random effects:

$$\boldsymbol{H}_3 = \begin{bmatrix} 0.23 & 0.23 & 0.18 & 0.18 & -0.04 & -0.04 \\ 0.18 & 0.18 & 0.2 & 0.2 & 0.09 & 0.09 \\ -0.04 & -0.04 & 0.09 & 0.09 & 0.31 & 0.31 \end{bmatrix}.$$

Random effects estimates for Genotype 1 are pushed away from the observations of Genotype 3, relative to the intercept-centered observations $\tilde{\boldsymbol{y}}$ (and vice-versa). As Genotype 2 is assumed to contribute the smallest amount of independent information reflected by the highest row-sum in $\boldsymbol{K}_3$, it is assigned the lowest weight in the estimation of β_0. The fixed effects hat-matrix is

$$\boldsymbol{H}_{\text{fix}} = \begin{bmatrix} 0.21 & 0.21 & 0.06 & 0.06 & 0.23 & 0.23 \end{bmatrix}.$$

The non-zero entries in $\boldsymbol{K}_2$ and $\boldsymbol{K}_3$ result in $\hat{\beta}_0$ not longer being interpretable as overall mean, not even in the considered balanced linear mixed model. However, the balance is still present in a consideration given in Table 2.2, where the estimates of all three scenarios are presented.

Scenario	$\hat{\beta}_0$	$\hat{\gamma}_1$	$\hat{\gamma}_2$	$\hat{\gamma}_3$	$\bar{\hat{\gamma}} = \frac{\hat{\gamma}_1+\hat{\gamma}_2+\hat{\gamma}_3}{3}$	$\hat{\beta}_0 + \bar{\hat{\gamma}}$
No correlation	2	-0.67	0.33	0.33	0	2
Moderate correlation	1.99	-0.60	0.27	0.36	0.01	2
Strong correlation	1.86	-0.23	-0.06	0.57	0.14	2

Table 2.2: Fixed effect estimates and random effect predictions according to the three scenarios of kinship matrices. Non-integers are rounded to two decimal places.

2.2.7 Platform-specific model details

In this section we provide details of the association models, which differed in the three platforms and were not covered in Section 2.2.4.

Controlled platform analyses The outcome vector $\boldsymbol{y}$ was a recovery score, which contained observations of $n = 3360$ test units, and the platform specific effect, $\boldsymbol{\beta}_{PLATFORM}$ included the two years of measurement 2008 and 2009 and two temperatures, -19 °C and -21 °C. A common platform-specific random effect controlling for the seven chambers across the two years 2008 and 2009 was included in the model, $\boldsymbol{\gamma}_{PLATFORM} \sim N(\boldsymbol{0}, \boldsymbol{I}\sigma^2_{chamber})$, as it provided a more parsimonious model with the same goodness-of-fit compared to a nested random effect for chamber within year. No additional explicit generation adjustment for S_1 versus $S_{1:2}$ families was included in the statistical model, as these effects were confounded with the fixed effect adjustment for year and the random chamber effects. In other words, the generation effect was assumed implicitly adjusted for by other year effects in the model. Within fixed effects coded by

$$\underbrace{\boldsymbol{X}_{controlled}}_{n\times 2} = [\boldsymbol{x}_1, \boldsymbol{x}_2], \quad \boldsymbol{\beta}_{controlled} = (\beta_1, \beta_2),$$

where the individual elements of $\boldsymbol{x}_1$ were 0 or 1 indicating whether an observation belongs to the year 2008 or 2009, and $\boldsymbol{x}_2$ for temperature equal to -21 °C versus -19 °C. For the random chamber effect, the design matrix $\boldsymbol{Z}_{controlled}\,(n \times 7)$ mapped each observation to one of the seven chambers (three in 2008 and four in 2009) and thus to the random effects $\boldsymbol{\gamma}_{controlled}\,(7 \times 1)$. According to the notation in Section 2.2.4, $\boldsymbol{D}$ was an identity matrix of dimension seven.

Semi-controlled platform analyses The outcome vector $\boldsymbol{y}$ was % plants with undamaged leaves measured repeatedly over three months (January, February, and April) in 2008 and two months (February, March) in 2009. The platform-specific fixed effects vector, $\boldsymbol{\beta}_{PLATFORM}$, included three terms: a year effect, an overall linear trend in time for the three months in 2008 and two months in 2009, and an interaction of year and linear trend in time, coded by

$$\underbrace{\boldsymbol{X}_{semi}}_{n\times 3} = [\boldsymbol{x}_1, \boldsymbol{x}_2, \boldsymbol{x}_3], \quad \boldsymbol{\beta}_{semi} = (\beta_1, \beta_2, \beta_3),$$

where elements of $\boldsymbol{x}_1$ were indicators for year 2009, the elements of $\boldsymbol{x}_2$ numeric representations of the month (0,1, or 2 for observations from 2008, and 0 or 1 for observations from 2009), and the elements of $\boldsymbol{x_3}$ were interactions of the years and months (1 for observations from the second month (March) in 2009, and zero otherwise). This design permitted interpretation of β_1 as the change in % plants with undamaged leaves from 2008 to 2009, β_2, the change by month during 2008, and $\beta_2 + \beta_3$, the change by month during 2009.

The platform-specific random effects (vector $\boldsymbol{\gamma}_{PLATFORM}$) consisted of three parts: 1.

replication, which was modeled as a blocking-factor (three replications in each of the two years, leading to six blocks). 2. a random intercept and 3. a random trend according to month for each plant group (the set of 25 plants where the outcome was determined). In principle we had 1,020 of these plant groups originating from the 139 S_1 families in 2008 and 201 $S_{1:2}$ families in 2009, with three replications leading to $3 \times (139 + 201) = 1,020$ outcomes. For the analysis only 200 families in 2009 could be used, leading to 1,017 plant groups. The replication random effect was assumed independent from the random intercept and trend, and for the latter two random effects a correlation coefficient was estimated. Combining the 1,251 observations from 2008 and 1,206 from 2009 led to $n = 1,251 + 1,206 = 2,457$ observations in sum, and the design matrix $\boldsymbol{Z}_{semi}$ and random effects $\boldsymbol{\gamma}_{semi}$ were constructed as follows:

$$\underbrace{\boldsymbol{Z}_{semi}}_{n\times 2040} = \left[\underset{n\times 6}{\boldsymbol{Z}_1}, \underset{n\times 1017}{\boldsymbol{Z}_2}, \underset{n\times 1017}{\boldsymbol{Z}_3}\right],$$

where $\boldsymbol{Z}_1$ was an incidence matrix mapping the outcomes to one of the six replications, $\boldsymbol{Z}_2$ was an incidence matrix mapping each observation to a plant group, and $\boldsymbol{Z}_3$ had the same non-zero entries as $\boldsymbol{Z}_2$, but contained the numeric representation of the corresponding month instead of an entry of 1 (same as $\boldsymbol{x}_2$ in the fixed effects design above). With $\boldsymbol{\gamma}_{semi}$ we denote the stacked vector of random effects,

$$\underset{1\times 2040}{\boldsymbol{\gamma}_{semi}} = (\boldsymbol{\gamma}_1, \boldsymbol{\gamma}_2, \boldsymbol{\gamma}_3),$$

where $\boldsymbol{\gamma}_1$ was a vector with six elements $(\gamma_{11}, \ldots, \gamma_{16}) = \{\gamma_{1i}\}_{i=1,\ldots,6}$, and both $\boldsymbol{\gamma}_2$ and $\boldsymbol{\gamma}_3$ were vectors with 1,017 elements each. The 2×1 vector $(\gamma_{2j}, \gamma_{3j})$ contained j-th element of each $\boldsymbol{\gamma}_2$ and $\boldsymbol{\gamma}_3$, which allows to define the distributional assumption as

$$\begin{aligned} \gamma_{1i} &\sim \mathrm{N}(0, \sigma^2_{rep}), \quad i = 1, \ldots, 6, \\ (\gamma_{2j}, \gamma_{3j}) &\sim \mathrm{N}(\boldsymbol{0}, \boldsymbol{D}), \quad j = 1, \ldots, 1017, \end{aligned}$$

where $\boldsymbol{D}$ is a 2×2 unstructured covariance matrix to be estimated. There were thus four variance parameters to estimate.

Field platform analyses The outcome vector $\boldsymbol{y}$ was % survival and the platform-specific fixed effect $\boldsymbol{\beta}_{PLATFORM}$ included indicator variables for the six environments, five environments in 2009 and one in 2010. In total $n = 3,216$ outcomes could be considered in the model. Platform-specific random effects included a block effect nested within environments arising from the lattice design. That is, the fixed effects design matrix $\boldsymbol{X}_{field}\,(n \times 5) = [\boldsymbol{x}_1, \boldsymbol{x}_2, \boldsymbol{x}_3, \boldsymbol{x}_4, \boldsymbol{x}_5]$ maps the observations to the environments (location in year), where Minsk 2009 is the reference category. From the lattice design there were 198 blocks (nested within environments), modeled by a random intercept per block: $\boldsymbol{Z}_{field}\,(n \times 198)$, with random effects vector $\boldsymbol{\gamma}_{field}$, which was assumed to be normally distributed, with individual elements

$\gamma_j \sim \mathrm{N}(0, \sigma^2_{block})$, independent for $j = 1, \ldots, 198$.

2.2.8 Haplotype-FT association model and gene×gene interaction

In addition to the effect of single SNPs in the association models, the effects of haplotypes were estimated as well. A haplotype bundles the information of several markers from adjacent locations and allows a categorization. From a statistical perspective they are categorical variables defined by the interaction of other categorical variables. For example, if there is information on three SNPs available, with two levels each, there are $2^3 = 8$ haplotype phases possible, with usually not each of these phases actually observed.

Here, haplotype phase was determined by subtracting the common parent Lo152 alleles and haplotypes were defined within each candidate gene using DnaSP v5.10 (Rozas et al., 2003). Haplotype-FT associations were performed using candidate gene haplotypes with MAF $> 5\%$. The same platform-specific statistical models controlling for population structure, kinship, and platform-specific effects were used to test associations between haplotypes of the respective candidate genes and FT. For these analyses $\boldsymbol{\beta}_{hap}$ replaced β_{SNP} as a measure of the haplotype effect of the non-reference, compared to the reference haplotype Lo152. First, significant differences between haplotypes of one gene were assessed using the LRT. If the overall statistic was significant, individual haplotype effects were tested against the reference haplotype Lo152 via t-tests. Based on haplotype information gene×gene interactions (= haplotype×haplotype intercations) were assessed using the likelihood ratio test, comparing the full model with main effects plus interaction to the reduced model with main effects only.

2.2.9 Obtaining model-based results

Analyses of marker-FT associations were conducted using the `lme4` package (Bates and Mächler, 2010), implemented in R (R Core Team, 2012). The LRTs were performed as follows. For a single term in the model (SNP or haplotype) and platform the available data were determined, as missing values were different for every SNP and MAF-rule. Two mixed models were fitted, a full model, which contained the marker effect of interest ($\boldsymbol{x}_{SNP}\beta_{SNP}$, $\boldsymbol{x}_{hap}\boldsymbol{\beta}_{hap}$, or $\boldsymbol{x}_{hap\times hap}\boldsymbol{\beta}_{hap\times hap}$), and a reduced model not containing that term. The reduced model to test the gene×gene interaction was a model containing both genes in an additive way. The test statistic was then calculated as $D = 2\,l_{full} - 2\,l_0$, where l_{full} and l_0 were the log-likelihood values of the full and reduced models, respectively. Under the null hypothesis of no effect (or interaction), the test statistic asymptotically follows a χ^2-distribution, $D \overset{a}{\sim} \chi^2(df)$, with the degrees of freedom df being the difference in numbers of parameters of the two models, which comes down to a 1 in a SNP-test, for example. The p-values were reported as the probability mass above the observed test statistic: p-value $= \mathbf{P}(X > D)$, with $X \sim \chi^2(df)$. Significance of individual haplotype effects $\hat{\beta}$ was assessed via the t-statistic performed at the two-sided $\alpha = 0.05$ level. The t-statistic was derived using the elements of the estimated

variance-/covariance matrix available in the model output, t-value $= \hat{\beta}/\widehat{\mathbb{V}}(\hat{\beta})$, and P-values as p-value $= 2\,\mathbf{P}(X > |t\text{-value}|)$, with $X \sim t(df)$. For the degrees of freedom we used the number of observations minus the number of fixed effects in the model. A multiple testing problem arises, which inflates the false positive rate of the study. A simple and common way to handle this problem is the Bonferroni correction where the significance level is divided by the number of tests. However, the Bonferroni correction is too conservative and only suitable for independent tests, an assumption violated in this study due to a high LD between some of the SNPs as previously shown (Li et al., 2011). Therefore, the less stringent significance level of $\alpha = 0.05$ was used in order to retain candidates for further validation in upcoming experiments. The exact p-values are available in Supplementary file 3 of Li et al. (2011) and can be adjusted for multiple testing. Empirical correlations between the 170 SNP-FT associations reported among the three phenotyping platforms were performed using Pearson's correlation, based on the t-values from the corresponding association tests. The genetic variation explained by an individual SNP or haplotype was calculated as

$$100 \times ((\hat{\sigma}_g^2 - \hat{\sigma}_{gSNP}^2)/\hat{\sigma}_g^2),$$

where $\hat{\sigma}^2$ are the estimates of the respective genetic variances, in the reduced model without an individual SNP (σ_g^2), and in the model including an individual SNP, σ_{gSNP}^2) (Mathews et al., 2008). This ad-hoc measure can result in negative estimates since variance components of genetic effects do not automatically decrease with more adjustment in a model. Negative estimates were truncated to zero.

2.3 Results

2.3.1 Phenotypic data analyses

Phenotypic assessments of FT were carried out in 12 environments from three different phenotyping platforms. Phenotypic data was analyzed separately in each environment (Figure 2.1). Genotypic variation for FT was significant at both temperatures for both years in the controlled platform ($p < 0.001$). Recovery scores ranged from a median near 2.5 (between intensive and moderate damage) at -19 °C in 2008 to a median near 1.0 (little sign of life) at -21 °C in 2009. As expected, recovery scores were higher at -19 °C than at -21 °C in the same year but were lower in 2009 than in 2008, probably due to different generations of rye material (S_1 vs $S_{1:2}$ families). The high variability at -2 °C in 2008 might have been induced by substantial variation between chambers (there was significant variation due to chamber ($p < 0.01$)). In the semi-controlled platform, genotypic variation for FT was significant during all months for both years ($p < 0.01$). Linear decreasing trends were observed during each year, which was expected since that was longitudinal data and thus the damaged portions of plants increased during the progression of winter. In the field

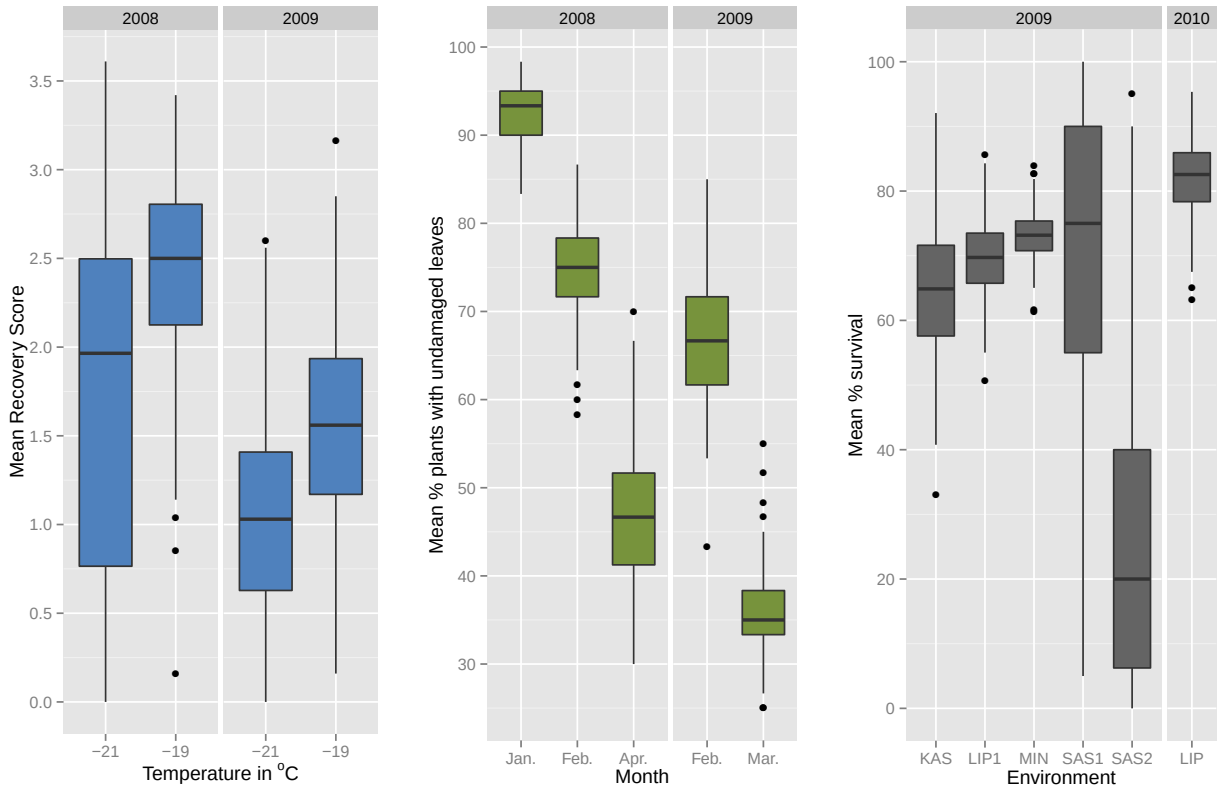

Figure 2.1: Phenotypic variation in three phenotyping platforms: controlled platform (left), semi-controlled platform (center), and field platform (right). The boxplots are based on the average phenotypic values of replicates for each genotype. Boxes indicate the interquartile range of the data, with a horizontal line representing the median and the vertical lines beyond the boxes indicating the variability outside the upper and lower quartiles. Outliers are indicated by circles. Figure recreated from Li et al. (2011).

platform, genotypic variation for FT was significant in four (LIP1, LIP2, SAS1, and SAS2) of the six environments ($p < 0.05$). Compared to other environments, SAS1 and SAS2 showed a better differentiation for FT among genotypes, ranging from 5% to 100% with a median 75% survival rate, and 0% to 95% with a median 20% survival rate, respectively. The large difference of survival rates between SAS1 and SAS2 was probably due to different altitudes and consequently varying severity of frost stress.

Phenotypic variation To test phenotypic variation between genotypes, the same platform-specific models as described for the SNP-FT association analyses were fitted for each platform omitting the SNP and population structure fixed effects. Within the controlled platform, separate models were fitted for each temperature and year combination; for the semi-controlled platform, separate models were fitted for each month of each year; and for the field platform, separate models were fitted for each geographic location—altogether 15 subgroups in all three platforms. Within this grouping, mean outcomes per genotype were calculated. That is, the replicates of each genotype were averaged and summarized in boxplots.

The genetic variation was reported as the variance component corresponding to the random genotype effect in each model, with a p-value computed using LRT, a conservative estimate since the true asymptotic distribution of the LRT is a mixture of chi-square distributions (Fitzmaurice et al., 2004).

2.3.2 Population structure and kinship

Based on the analysis of population structure using SSR markers, $k = 3$ was the most probable number of groups. Populations PR2733 (Belarus) and Petkus (Germany) formed two distinct groups, while populations EKOAGRO, SMH2502, and ROM103 (all from Poland) were admixed in the third group with shared membership fractions with population PR2733 (Figure 2.2). This could likely be attributed to seed exchange between the populations from Belarus and Poland. The relatedness among the 201 genotypes estimated from the allele-similarity kinship matrix ranged from 0.11 to 1.00 with a mean of 0.37. Compared to the Eastern European populations, genotypes from Petkus showed a higher relatedness among each other with a mean of 0.53.

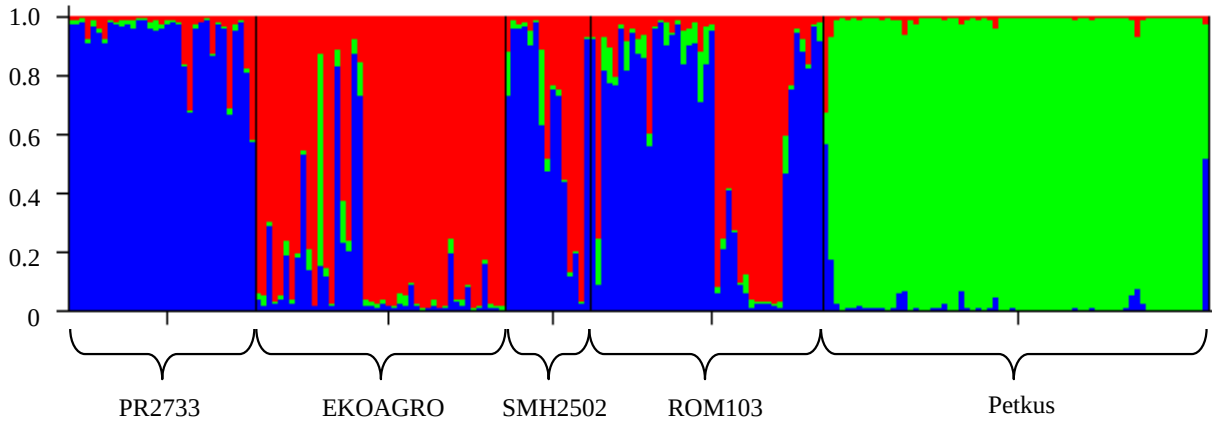

Figure 2.2: Population structure based on genotyping data of 37 SSR markers. Each genotype is represented by a thin vertical line, which is partitioned into $k = 3$ colored segments that represent the genotype's estimated membership fractions shown on the y-axis in k clusters. Genotypes were sorted according to populations along the x-axis and information on population origin is given. Figure reproduced from Li et al. (2011).

2.3.3 Association analyses

SNP-FT associations were performed using 170 SNPs from twelve candidate genes. In the controlled platform, 69 statistically significant SNPs were identified among nine genes: *ScCbf2*, *ScCbf9b*, *ScCbf11*, *ScCbf12*, *ScCbf15*, *ScDhn1*, *ScDhn3*, *ScDreb2*, and *ScIce2* (all $p < 0.05$; Figure 2.3). In the semi-controlled platform, 22 statistically significant ($p < 0.05$) SNPs were identified among five genes: *ScCbf2*, *ScCbf11*, *ScCbf12*, *ScCbf15*, and

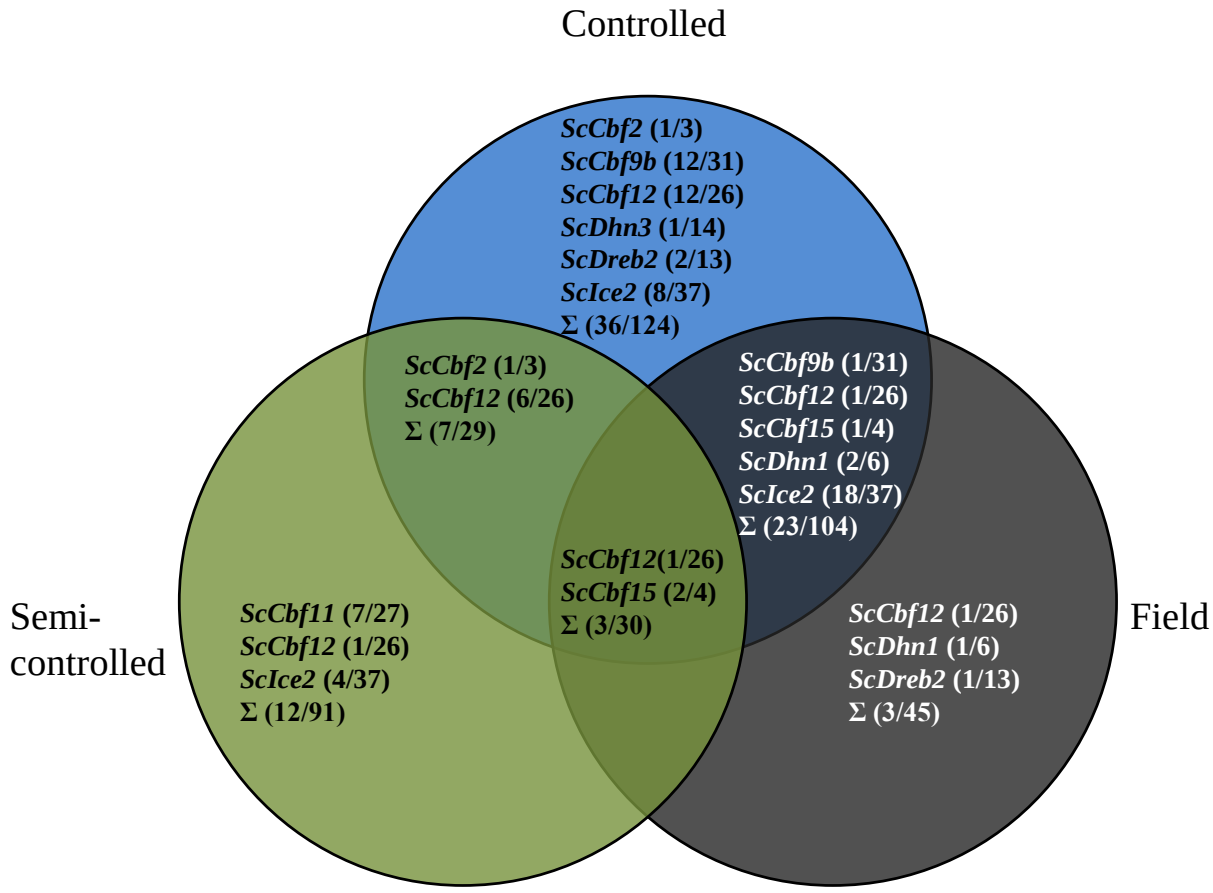

Figure 2.3: Venn diagram of SNPs from candidate genes significantly ($p < 0.05$) associated with frost tolerance in three phenotyping platforms. The first and second numbers in each bracket are the number of significant SNPs and total number of SNPs in each candidate gene. Figure reproduced from Li et al. (2011).

*ScIce*2. In the field platform, 29 statistically significant ($p < 0.05$) SNPs were identified among six genes: *ScCbf*9*b*, *ScCbf*12, *ScCbf*15, *ScDhn*1, *ScDreb*2, and *ScIce*2. Eighty-four SNPs from nine genes were significantly associated with FT in at least one of the three platforms, and 33 SNPs from six genes were significantly associated with FT in at least two of the three platforms. Across all three phenotyping platforms, two SNPs in *ScCbf*15 and one SNP in *ScCbf*12 were significantly associated with FT; all of these three SNPs are non-synonymous, causing amino acid replacements. No SNP-FT associations were found for SNPs in *ScCbf*6, *ScCbf*14, or *ScVrn*1. Full information on SNP-FT associations for all platforms can be found in Supplementary file 3 of Li et al. (2011). Allelic effects (β_{SNP}) of the 170 SNPs studied were relatively low, ranging from -0.43 to 0.32 for recovery scores in the controlled platform, -2.17% to 2.44% for % plants with undamaged leaves in the semi-controlled platform, and -3.66% to 4.30% for % survival in the field platform (Figure 2.4). 45.5% of all significant SNPs found in at least one platform had positive allelic effects, indicating the non-reference allele conveyed superior FT to the reference allele. The largest positive β_{SNP} among the 170 SNPs in the field platform was observed for SNP 7 in *ScIce*2

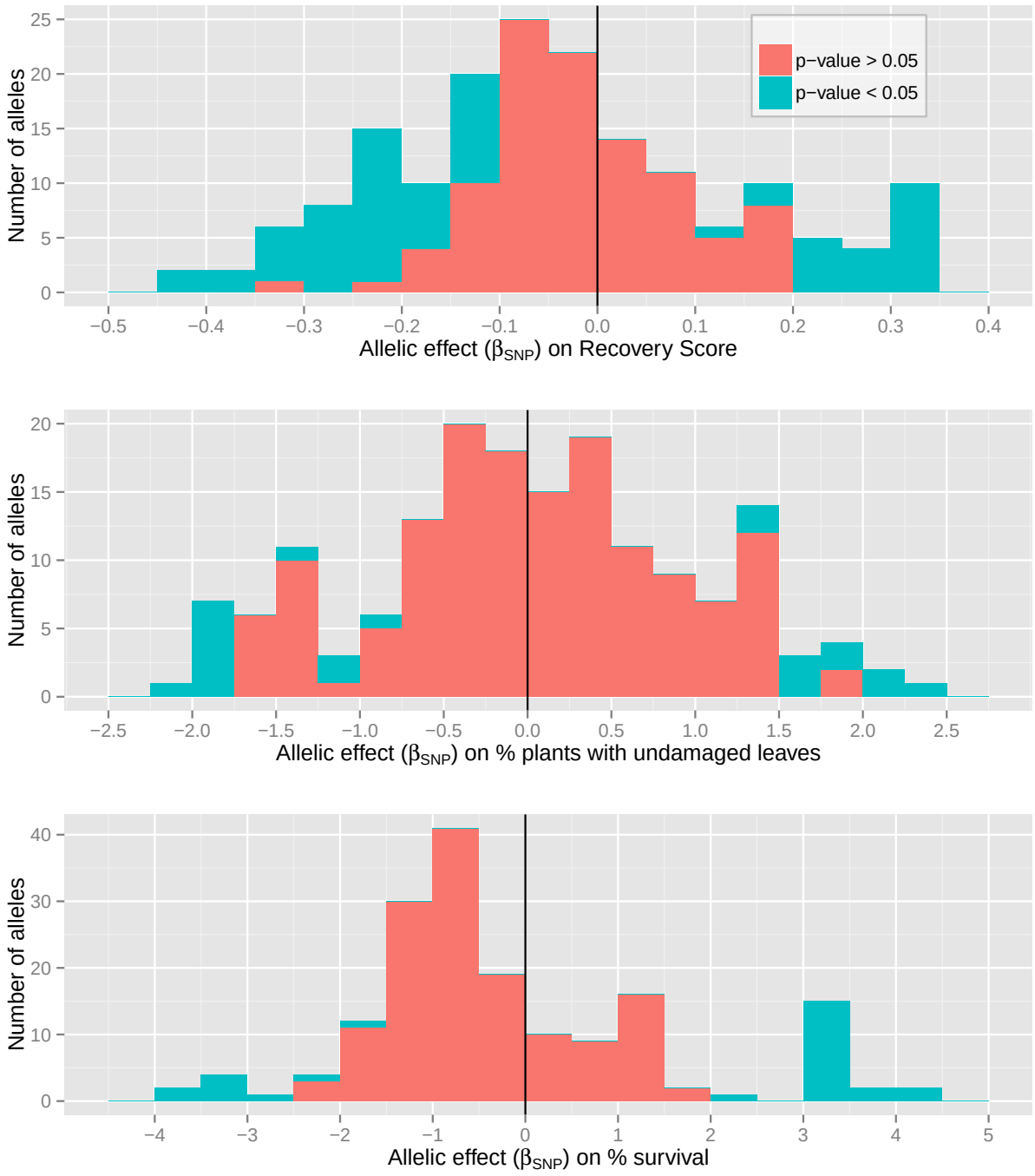

Figure 2.4: Distribution of allelic effects (β_{SNP}) from FT association models in controlled (top), semi-controlled (middle), and field platforms (bottom). The significance threshold ($p < 0.05$) for each platform is indicated by different colors. Figure recreated from Li et al. (2011).

($\beta_{SNP} = 4.30$). This favorable allele was present predominantly in the PR2733 population (55.2%), and occurred at much lower frequency in the other four populations (EKOAGRO: 4.7%, Petkus: 0%, ROM103: 7.1% and SMH2502: 6.7%). The proportion of genetic variation explained by individual SNPs ranged from 0% to 27.9% with a median of 0.4% in the controlled platform, from 0% to 25.6% with a median of 1.2% in the semi-controlled platform,

and from 0% to 28.9% with a median of 2.0% in the field platform (Figure 2.5). These distributions were highly concentrated near zero.

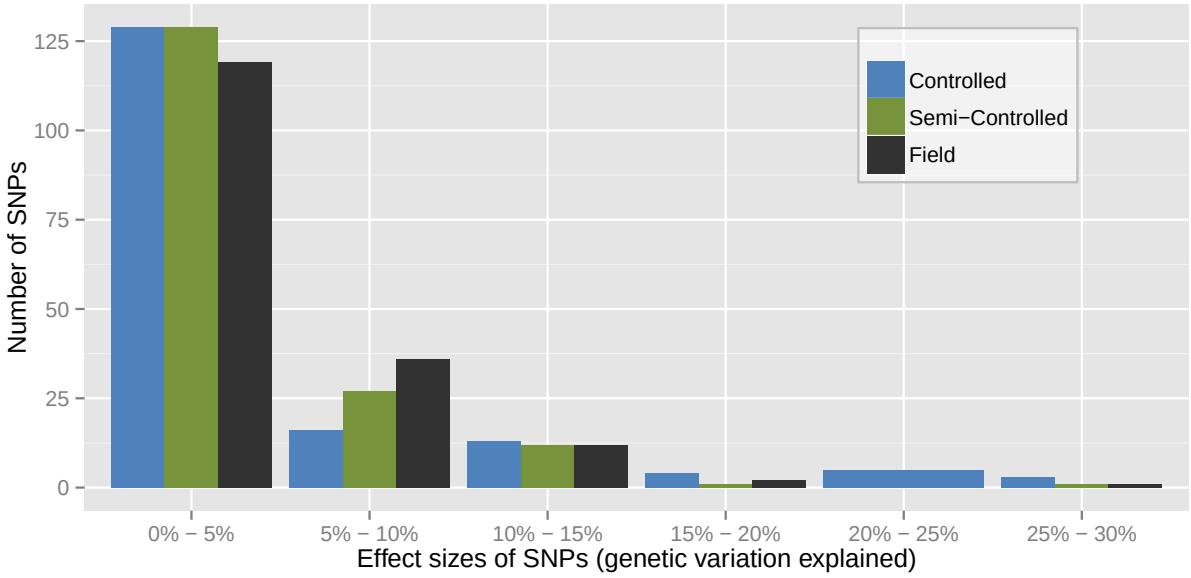

Figure 2.5: Distributions of effect sizes of SNPs in three phenotyping platforms. Effect sizes are displayed as genetic variation explained by individual SNPs. Figure recreated from Li et al. (2011).

Empirical correlations of the SNP-FT association results, in terms of t values, between the three phenotyping platforms were moderate to low. The highest correlation coefficient was observed between the controlled and semi-controlled platform with $r = 0.56$, followed by correlations between the controlled and field platform with $r = 0.54$, and the semi-controlled and field platform with $r = 0.18$. When correlations were restricted to the significant SNPs, slightly higher correlation coefficients were observed with $r = 0.64$ between the controlled and semi-controlled platform, $r = 0.66$ between the controlled and field platform, and $r = 0.34$ between the semi-controlled and field platform.

Haplotype-FT associations were performed using 30 haplotypes (MAF $> 5\%$) in eleven candidate genes. Because only one haplotype in $ScDhn1$ had a MAF $> 5\%$, $ScDhn1$ was excluded from further analysis. Large numbers of rare haplotypes (MAF $< 5\%$) were found in $ScCbf9b$ ($N = 62$) and $ScCbf12$ ($N = 22$), resulting in large numbers of missing genotypes (87.9% and 61.3%) for the association analysis. Haplotypes 2, 3, and 4 in $ScCbf2$ were significantly ($p < 0.05$) associated with FT in the controlled platform. For haplotypes 1 and 2 in $ScCbf15$ and haplotype 1 in $ScIce2$, significant associations ($p < 0.05$) were found across two and three platforms, respectively (Table 2.3). Haplotype effects ($\boldsymbol{\beta}_{Hap}$) were relatively low and comparable to the allelic effects (β_{SNP}) ranging from -0.31 to 0.49 (recovery score), -1.71% to 2.74% (% plants with undamaged leaves), and -3.32% to 3.47% (% survival) in the controlled, semi-controlled and field platforms, respectively. The highest positive effect on survival rate was observed for haplotype 1 of $ScIce2$ in the field platform, implicating

this haplotype as the best candidate with superior FT. This favorable haplotype was present mainly in the PR2733 population (35.7%), occurring in much lower frequencies in the other four populations (0.0% in EKOAGRO, 0.0% in Petkus, 5.3% in ROM103, and 6.7% in SMH2503). The proportion of genetic variation explained by the haplotypes ranged from 0% to 25.7% with a median of 1.6% in the controlled platform, from 0% to 17.6% with a median of 1.4% in the semi-controlled platform, and from 0% to 9.3% with a median of 4.8% in the field platform.

Out of all possible gene×gene interactions tested on the basis of haplotypes, eleven, six, and one were significantly ($p < 0.05$) associated with FT in the controlled, semi-controlled and field platforms, respectively. $ScCbf15 \times ScCbf6$, $ScCbf15 \times ScVrn1$, $ScDhn3 \times ScDreb2$, and $ScDhn3 \times ScVrn1$ were significantly associated with FT across two platforms, and none was significantly associated with FT across all three platforms (Figure 2.6).

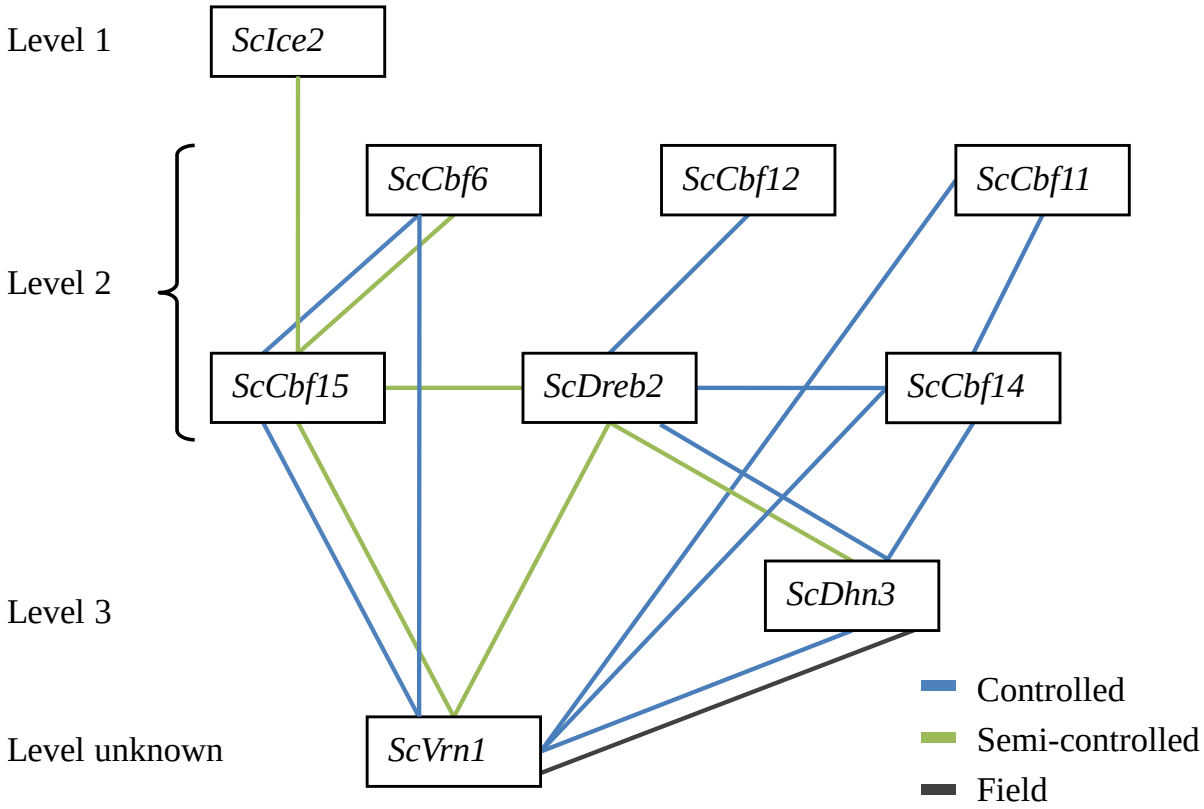

Figure 2.6: Significant ($p < 0.05$) gene×gene interactions for frost tolerance in three phenotyping platforms. Candidate genes are sorted into three levels according to the frost responsive cascade (Yamaguchi-Shinozaki and Shinozaki, 2006). The level where $ScVrn1$ belongs to is still unknown. Figure reproduced from Li et al. (2011).

Candidate gene	Name of haplotype[a]	Controlled (recovery score 0-5)[b]			Semi-controlled (% plants with undamaged leaves)			Field (% survival)		
		p-value[c]	β_{Hap}	% genetic variation explained	p-value	β_{Hap}	% genetic variation explained	p-value	β_{Hap}	% genetic variation explained
ScCbf2	Overall[d]	**<0.001**	-	25.7	0.21	-	16.3	0.40	-	5.0
	2	**0.04**	-0.11	-	0.51	-0.51	-	0.73	-0.51	-
	3	**<0.001**	0.49	-	0.19	1.36	-	0.12	3.32	-
	4	**<0.001**	-0.39	-	0.21	-1.43	-	0.74	0.57	-
ScCbf15	Overall	**<0.01**	-	0.6	0.09	-	17.6	0.09	-	4.4
	1	**<0.01**	-0.22	-	**0.04**	-1.69	-	0.06	-3.32	-
	2	**<0.01**	-0.21	-	0.13	-0.92	-	**0.04**	-2.59	-
ScIce2	Overall	**0.04**	-	4.8	**0.02**	-	13.3	0.13	-	8.1
	1	**<0.01**	0.29	-	**<0.01**	2.74	-	**0.02**	3.47	-

[a] Haplotypes with minor allele frequency (MAF) > 5%

[b] 0: completely dead. 1: little sign of life. 2: intensive damage. 3: moderate damage. 4: small damage. 5: no damage

[c] p-values < 0.05 are printed in bold

[d] All haplotypes (MAF > 5%) within a candidate gene

Table 2.3: Summary of haplotypes significantly associated with frost tolerance in at least one platform, their haplotype effects, and percentage of genetic variation explained by the haplotypes.

2.4 Discussion

FT is a complex trait with polygenic inheritance. While the genetic basis of FT has been widely studied in cereals by bi-parental linkage mapping and expression profiling, exploitation of the allelic and phenotypic variation of FT in rye by association studies has lagged behind (Francia et al., 2007; Baga et al., 2007; Campoli et al., 2009). This study reports the first candidate gene-based association study in rye examining the genetic basis of FT.

Statistically significant SNP-FT associations were identified in nine candidate genes hypothesized to be involved in the frost responsive network among which the transcription factor *Ice*2 is one of the key factors. Others are the *Cbf* gene family, the *Dreb*2 gene and dehydrin gene family (*Dhn*). For a biological discussion of their role in the frost responsive network and connections to findings in other studies, we refer to Li et al. (2011).

Effect sizes of markers, commonly expressed as percentage of the genetic variance explained by markers, are of primary interest in association studies since they are the main factors that determine the effectiveness of subsequent marker assisted-selection processes. Two hypotheses for the distribution of effect sizes in quantitative traits have been proposed: Mather's "infinitesimal" model and Robertson's model (Mackay, 2001). The former assumes an effectively infinitesimal number of loci with very small and nearly equal effect sizes; the latter, an exponential trend of the distribution of effects, whereby a few loci have relatively large effects and the rest only small effects. Findings in this study support the latter, with distributions of SNP effect sizes (percentage of the genetic variance explained by individual SNPs) highly concentrated near zero and few SNPs having large effects (maximum 28.8% explained genetic variation). A similar distribution of haplotype effect sizes was observed. A recent review summarizing association studies in 15 different plant species also implicated Robertson's model and further suggested that phenotypic traits, species, and types of variants may impact distributions of effect sizes (Ingvarsson and Street, 2010).

Epistasis, generally defined as the interaction between genes, has been recognized for over a century (Bateson, 1902), and recently it has been suggested that it should be explicitly modeled in association studies in order to detect "missing heritabilities" (Phillips, 2008; Wu et al., 2010). In this study, eleven, six, and one significant ($p < 0.05$) gene×gene interaction effects were found in the controlled, semi-controlled and field platforms, respectively, suggesting that epistasis may play a role in the frost responsive network. From the frost responsive network, one might hypothesize that transcription factors interact with their downstream target genes, for example, that *ScIce*2 interacts with the *ScCbf* gene family and the latter interacts with COR genes, such as the dehydrin (*Dhn*) gene family. Indeed, significant interactions were observed in $ScIce2 \times ScCbf15$, $ScCbf14 \times ScDhn3$, and $ScDreb2 \times ScDhn3$. Some candidate genes in the same cascade level also interact with each other, such as members of the *ScCbf* gene family, $ScCbf6 \times ScCbf15$ and $ScCbf11 \times ScCbf14$.

Similar interactions within the *Cbf* gene family were also observed in *Arabidopsis* where

AtCbf2 was indicated as a negative regulator of *AtCbf1* and *AtCbf3* (Novillo et al., 2004). In this study, *ScVrn1* was not significantly associated with FT but had significant interaction effects with six other candidate genes, underlining the important role of *ScVrn1* in the frost responsive network. It is worth to point out that the power of detecting gene×gene interaction might be low due to the relatively small sample size.

Low to moderate empirical correlations of SNP-FT associations were observed across the three platforms reflecting the complexity of FT and thus the need for different platforms in order to more accurately characterize FT. There are at least two reasons possibly explaining the relatively low to medium empirical correlations of SNP-FT associations: 1) the different duration and intensity of freezing temperature and 2) the different levels of confounding effects from environmental factors, other than frost stress, per se. In the controlled platform, plants were cold-hardened and then exposed to freezing temperatures (−19 °C or −21 °C) in a short period of six days using defined temperature profiles. Recovery score in the controlled platform represents the most pure and controlled measurement of FT among the three platforms, since the effect of environmental factors other than frost stress is minimized.

In the semi-controlled platform, plants were exposed to much longer freezing periods with fluctuating temperatures and repeated frost-thaw processes. In addition, a more complex situation occurred in this platform, requiring plants to cope with other variable climatic factors such as changing photoperiod, natural light intensity, wind, and limited water supply. Thus, the measurement % plants with undamaged leaves in the semi-controlled platform reflects the combined effect of various environmental influences and stresses on the vitality of leaf tissue but does not mirror survival of the crown tissue as an indicator for frost tolerance. In the field platform, winter temperatures were generally lower than in the semi-controlled platform due to the strong continental climate in Eastern Europe and Canada.

The measurement % survival in the field is further confounded by environmental effects, such as snow-coverage, soil uniformity, topography, and other unmeasured factors. The different experimental platforms permit the identification of different sets of genes associated with FT, which might impact the correlations of SNP-FT associations across platforms. It is worth pointing out that the correlation between the controlled and semi-controlled platform was higher than between the semi-controlled and field platform. One possible explanation is that plant growth in boxes in both controlled and semi-controlled platforms results in a rather similar environment where roots are more exposed to freezing than in the field. Several studies have suggested that different genes might be induced under different frost stress treatments. A large number of blueberry genes induced in growth chambers were not induced under field conditions (Dhanaraj et al., 2007).

In rye, Campoli et al. (2009) drew the conclusion that expression patterns of different members of the *Cbf* gene family were affected by different acclimation temperatures and sampling times. Most prior studies on FT have been conducted in controlled environments. However, the relatively low to medium correlation among platforms in this study suggest

that future studies should consider various scenarios in order to obtain a more complete picture of the genetic basis of FT in rye.

Chapter 3

Phenology

This chapter emphasizes and extends the statistical methods used in the article "First flowering of wind-pollinated species with the greatest phenological advances in Europe" (C. Ziello, A. Böck, N. Estrella, D. P. Ankerst, and A. Menzel, 2012), while shortening the biological background and subject matter interpretations. The author of this thesis was second author and primary statistician of the forenamed article and performed all statistical analyses.

3.1 Introduction

Phenology is the science of naturally recurring events in nature, such as leaf unfolding and flowering of plants in spring, fruit ripening, as well as the arrival and departure of migrating birds and the timing of animal breeding (Koch et al., 2009). It offers quantitative evidence of climate change impacts on ecosystems, indicating an increasing advancement of flowering phases in recent decades (Rosenzweig et al., 2007). A stronger tendency for winter and spring phenological phases to advance, relative to summer phases, has been reported in the literature (Lu et al., 2006; Menzel et al., 2006). Only few studies have assessed the influence of plant traits on the response to global warming. A recent study in this direction reported a greater temporal advancement among entomophilous (insect-pollinated) plants compared to anemophilous (wind-pollinated) species (Fitter and Fitter, 2002).

Changes in the pollen season, particularly related to its timing, duration, and intensity, are one of the most likely consequences of climate change (Huynen et al., 2003). A threat of these changes to human health is the expected further increase of the worldwide burden of pollen-related respiratory diseases (Beggs, 2004; D'Amato et al., 2007; D'Amato and Cecchi, 2008). Most research in this area has been addressed to observing and forecasting the phenological behavior of single species characterized by a high allergenic effect, such as birch or ragweed (Laaidi, 2001; Rasmussen, 2002; Rogers et al., 2006; Wayne et al., 2002). We expand the research on climate change effects on phenology and present a statistical meta-analysis based on a massive data set, permitting the quantification of differences in phenological tem-

poral trends due to pollination mode and woodiness, as well as yearly patterns of trends. Ultimately, this leads to the identification of groups which are more likely to show changes in their phenology and, hence, more likely to increase harm to humans.

3.2 Data structure

The analyzed phenological data consist of flowering records based on an abundant data set, which covers dates of diverse phenological phases, and comprises more than 35,000 series of flowering in Central Europe (Menzel et al., 2006). Most of these data are available at the COST (European COoperation in the field of Scientific and Technical research) database, collected within the in the meantime concluded COST Action 725 (Koch et al., 2009). We selected series with a length of more than 15 years between 1971 and 2000, which were available in aggregated form as a linear regression of the flowering time (coded as day of year, *doy*) on calendar year (*cy*) for each series. The common linear regression was assumed:

$$doy = \beta_0 + \beta_1\, cy + \varepsilon,$$

with $\varepsilon \sim \mathrm{N}(0, \sigma^2)$, the Normal distribution with mean 0 and variance σ^2. For our statistical analysis, we used the estimates $\hat{\beta}_{1i}$, $se(\hat{\beta}_{1i})$, and $\overline{doy}_i$ of the $i = 1, \ldots, 5971$ selected series of flowering:

$\hat{\beta}_{1i}$ Estimated regression slope of the ith series, interpreted as the average trend or time shift of flowering time in days per year for an increase of one calendar year.

$se(\hat{\beta}_{1i})$ Standard error of $\hat{\beta}_{1i}$, a measure of how precisely the average trend was captured by the linear regression model.

$\overline{doy}_i$ Average flowering time across all years of study in series i, which carries equivalent information as the estimated intercept $\hat{\beta}_{0i}$, when used along with $\hat{\beta}_{1i}$, because $\hat{\beta}_0 = \overline{doy} - \hat{\beta}_1\, \overline{cy}$.

The 5,971 analyzed series were measured in 983 phenological stations spread over 13 countries in Europe (list of countries by decreasing number of stations: Germany, Switzerland, Russia, Austria, Czech Republic, Slovenia, Latvia, Norway, United Kingdom, Croatia, Finland, Estonia, and Slovakia) (Figure 3.1). The spatial information about the phenological stations was recorded as geographic latitude and longitude, and the altitude above sea level.

Phenological aspects The study contains records on 28 different species, all angiosperms. They are listed in Fig. 3.2 ordered by mean flowering dates. The disparity in the number of anemophilous (wind-pollinated) and entomophilous (insect-pollinated) species (7 versus 21) results from the low percentage ($\approx 10\%$) of wind-pollinated species among the angiosperms. Note that all considered wind-pollinated species are allergenic, that is they

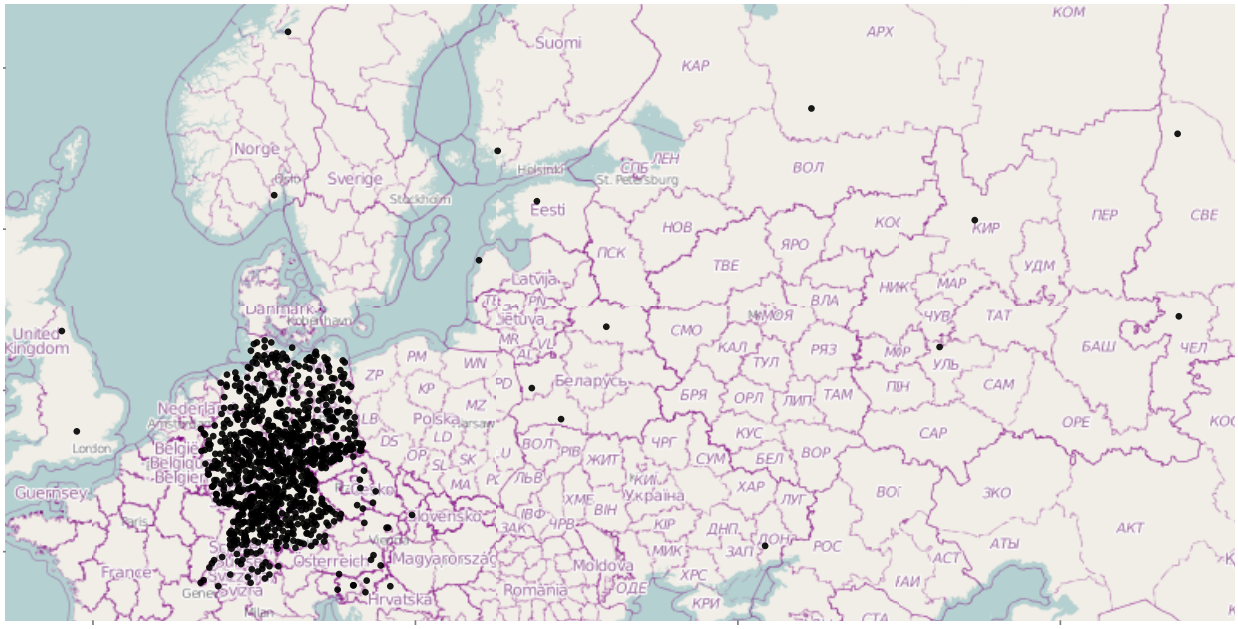

Figure 3.1: Locations of the phenological stations. Background map from OpenStreetMap.

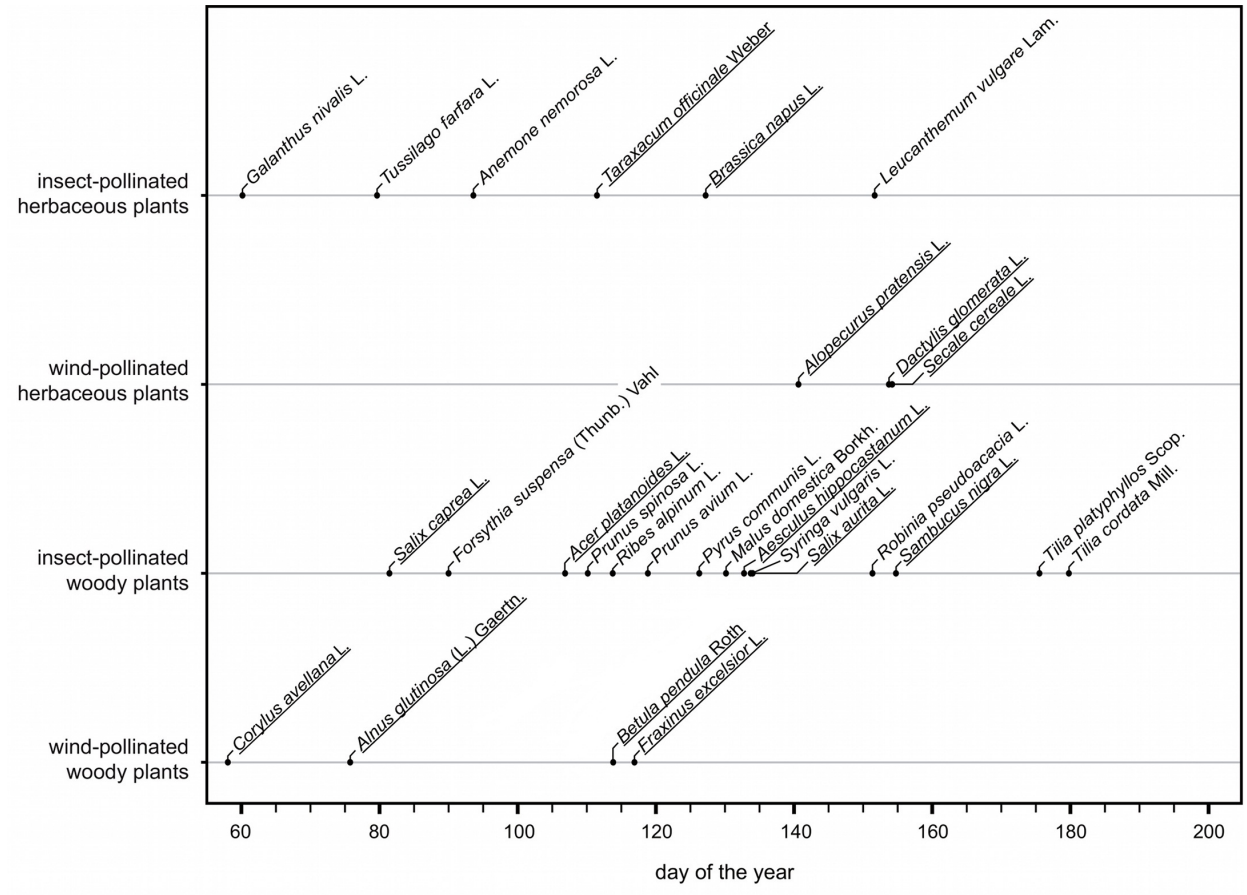

Figure 3.2: Flowering chronology of the studied species, according to pollination mode and woodiness. Allergenic plants are underlined. Figure reproduced from Ziello et al. (2012).

can cause a malfunction of the immune system, which leads to overproduction of antibodies. Allergenicity is a characteristic also present among insect-pollinated species, but the pollen of anemophilous plants is considerably higher in amount and aggressiveness, at least for angiosperms. This aspect allows consideration of wind-pollinated species as representatives of allergenic species, so that the results of their monitoring can be used to reasonably estimate the consequences of climate change on allergic human subjects.

The classification of allergenic plants follows the information available at the website of the EAN (European Aeroallergen Network). Flowering phenophases available are *first flower opens* and *full flowering* (50% of flowers open). Woodiness, which classifies plants in those having a persistent woody stem or being a herb, is another trait linked to allergenicity. As most sensitized subjects are allergic to grass pollen (i.e. pollen of non-woody plants) (Esch, 2004; Jaeger, 2008), these allergens together with the pollen of the plant genus Ambrosia (McLauchlan et al., 2011; Ziska et al., 2011) are the most studied allergens in the literature. Of similar importance is the allergenic effect of some tree species, such as birch (D'Amato et al., 2007), whose pollen cause severe reactions in humans, particularly at northern latitudes where it is predominant.

3.3 Statistical methods

3.3.1 Overview

In this section we provide an overview on the statistical methods used to analyze the phenology data, with details in the next section. The influence of pollination mode and woodiness on flowering trends (first flowering and full flowering) was assessed using weighted linear mixed models, with weights chosen as the precision, i.e. the inverse of the variance of the data regressions that were provided (Becker and Wu, 2007). Statistical significance of results was assessed using 1,000 bootstrap samples (Efron and Tibshirani, 1994), and goodness of fit was calculated by means of an R^2 measure for mixed models based on the likelihood (Xu, 2003). Bootstrap samples were also presented in graphs to reflect uncertainty. Fixed effects considered were woodiness, pollination mode, and mean phenodate for each series, which was also provided along with the estimated regression coefficient. A random effect for stations was included, which implies correlation between observations from the same station, and data from different stations were modelled independently. More advanced spatial structures, such as the exponential correlation structure (Pinheiro and Bates, 2000, p. 230) that uses the coordinate information of stations, were also considered, but did not show any impact on the estimates of interest and were therefore rejected. Altitude above sea level of stations was excluded as a fixed effect since it neither showed significance, nor affected other estimates when included in the model, as similarly found in previous work (Ziello et al., 2009).

A series of model-based analyses was performed in duplicate for first flowering trends and full flowering trends. In detail, the estimates $\hat{\beta}_1$ (subscript i suppressed) obtained from the linear regressions of flowering time (first flowering and full flowering, respectively) for the 5,971 flowering series served as observations of the response variable "flowering trends" in unit days per year (d/yr). First, univariate regressions of the effects of woodiness and pollination on flowering trends were performed. Then, the linear effect of mean date ($\overline{doy}_i$) on trends was assessed separately by pollination mode and woodiness, and by combinations of pollination mode and woodiness in an overall model for both phenological phases. Finally, the linearity constraint of the mean date effect was relaxed via a spline approach to evaluate the robustness of the general conclusions drawn under assumption of a linear effect. Frayed ends of spline curves arise mainly from arbitrary extrapolation of the spline when bootstrap samples do not cover the whole time range, and should be used as natural limits for interpretation.

3.3.2 Details

Heterogeneity The outcome of interest, trend in flowering time, is not directly measured but results rather from an aggregation of observations by the pre-manufactured linear regressions. We therefore conducted a meta-analysis, with procedures adjusted to the specific situations. For example, comparison of the means of two groups with a t-test assumes that observations within samples are identically distributed, which is not fulfilled by the flowering trends. Every single trend, being an estimated coefficient, has its own variance and follows asymptotically the large sample normal distribution: $\hat{\beta}_1 \overset{a}{\sim} \mathrm{N}(\beta_1, se(\hat{\beta}_1)^2)$, with $\hat{\beta}_1$ the estimator of the trend and $se(.)$ its standard error. As outlined in Becker and Wu (2007), we used weights defined by the squared standard error, $1/se(\hat{\beta}_1)^2$, in our calculations to account for different variances of the trend estimators. In practice, a pooled t-test adjusted with such defined weights can be performed in a linear regression framework with heteroscedastic errors, and fitted by weighted least squares. For ease of notation, let $\boldsymbol{y}$ be the combined vector of outcomes, $\boldsymbol{x}$ a 0/1 vector indicating the membership to the two samples, and $\boldsymbol{w}$ the vector of weights. All three vectors are of same length $n = n_1 + n_2$, with n_1 the number of observations in sample 1 and n_2 the number of observations in sample 2. The two-sample pooled t-test for equal means in both groups,

$$H_0 : \mu_1 = \mu_2 \text{ versus } H_A : \mu_1 \neq \mu_2,$$

is identical to the test of

$$H_0 : \beta_1 = 0 \text{ versus } H_A : \beta_1 \neq 0,$$

in the linear regression model

$$y_i = \beta_0 + \beta_1 x_i + \varepsilon_i, \quad \varepsilon_i \sim \mathrm{N}(0, \sigma^2),\ i = 1, \ldots, n.$$

The coefficients vector $\boldsymbol{\beta} = (\beta_0, \beta_1)$ is estimated by

$$\hat{\boldsymbol{\beta}} = (\boldsymbol{X}'\boldsymbol{X})^{-1}\boldsymbol{X}'\boldsymbol{y}, \text{ with } \boldsymbol{X} = \begin{bmatrix} 1 & x_1 \\ \vdots & \vdots \\ 1 & x_n \end{bmatrix},$$

and the associated variance/covariance matrix by

$$\widehat{\mathbb{V}}(\hat{\boldsymbol{\beta}}) = \hat{\sigma}^2(\boldsymbol{X}'\boldsymbol{X})^{-1}, \quad \hat{\sigma}^2 = \frac{1}{n-2}(\boldsymbol{y} - \boldsymbol{X}\hat{\boldsymbol{\beta}})'(\boldsymbol{y} - \boldsymbol{X}\hat{\boldsymbol{\beta}}).$$

In our analysis we used the weighted least square estimates of $\boldsymbol{\beta}$, which account for heteroscedastic errors via weigths $\boldsymbol{w}$:

$$\hat{\boldsymbol{\beta}} = (\boldsymbol{X}'\boldsymbol{W}\boldsymbol{X})^{-1}\boldsymbol{X}'\boldsymbol{W}\boldsymbol{y},$$

with diagonal matrix $\boldsymbol{W} = diag(\boldsymbol{w})$, and variance/covariance matrix

$$\widehat{\mathbb{V}}(\hat{\boldsymbol{\beta}}) = \hat{\sigma}^2(\boldsymbol{X}'\boldsymbol{W}\boldsymbol{X})^{-1}, \quad \hat{\sigma}^2 = \frac{1}{n-2}(\boldsymbol{y} - \boldsymbol{X}\hat{\boldsymbol{\beta}})'\boldsymbol{W}(\boldsymbol{y} - \boldsymbol{X}\hat{\boldsymbol{\beta}}).$$

The t-statistic for the test of equal means is then

$$t = \frac{\hat{\beta}_1}{\sqrt{\widehat{\mathbb{V}}(\hat{\boldsymbol{\beta}})_{2,2}}},$$

where $\widehat{\mathbb{V}}(\hat{\boldsymbol{\beta}})_{2,2}$ denotes the second entry on the diagonal of $\widehat{\mathbb{V}}(\hat{\boldsymbol{\beta}})$

Spatial correlation We assessed the potential spatial correlation between observations on nearby locations by means of a gaussian random field $\gamma(s)$, with $s \in \mathbb{R}^2$ being the pair of coordinates. The model was specified by the mean function $\mu(s) = \mathbb{E}(\gamma(s))$, variance function $\tau^2(s) = \mathbb{V}(\gamma(s))$, and correlation function $\rho(s, s')$. Specifically, we assumed constant mean $\mu(s) \equiv \mu$ and constant variance $\tau^2(s) \equiv \tau^2$, and a correlation function $\rho(s, s') = \rho(h)$ solely depending on the (great-circle) distance h of two locations. In contrast to the euclidean distance, the great-circle distance accounts for the spherical shape of the earth. Pinheiro and Bates (2000, p. 230) give an overview of spatial correlation structures; of these, we applied the spherical correlation function $\rho(h; \phi)$ with distance h and range ϕ, which controls the maximum distance of locations having a non-zero correlation. The model is written as

$$y(s) = \boldsymbol{x'}\boldsymbol{\beta} + \gamma(s) + \varepsilon(s),$$

with $y(s)$ the estimated trends at location s, $\boldsymbol{x'}\boldsymbol{\beta}$ the fixed effects, $\gamma(s)$ the random field defined above, and $\varepsilon(s)$ the usual error term, $\varepsilon(s) \sim \mathrm{N}(0, \sigma^2)$ independent of $\gamma(s)$. This

model implies that the correlation between the observations $y(s)$ and $y(s')$ is given by

$$\text{Corr}(y(s), y(s')) = \rho(h; \phi).$$

The same model can be expressed as a linear mixed model (see Fahrmeir et al., 2007, p. 327 ff),

$$\boldsymbol{y} = \boldsymbol{X\beta} + \boldsymbol{Z\gamma} + \boldsymbol{\varepsilon},$$

with the following components:

$\boldsymbol{y}$ Vector of temporal flowering trends.

$\boldsymbol{X\beta}$ Fixed effect design matrix and effects, specifics provided later.

$\boldsymbol{Z}$ Design matrix for the random effects; an incidence matrix (entries of zero and one) mapping each single observation to its phenological station.

$\boldsymbol{R}$ Correlation matrix derived from the correlation function $\rho(h; \phi)$ and the distance matrix $\boldsymbol{H}$, which contains the distance between every pair of phenological stations,

$$\boldsymbol{R}[i, j] = \rho(\boldsymbol{H}[i, j]; \phi),$$

with $\rho(.)$ given by

$$\rho(h; \phi) = \begin{cases} 1 - \frac{3}{2}|h/\phi| + \frac{1}{2}|h/\phi|^3 & 0 \leq h \leq \phi, \\ 0 & h > \phi. \end{cases}$$

$\boldsymbol{\gamma}$ Vector of multivariate normally distributed random station effects $\boldsymbol{\gamma} \sim \text{N}(\boldsymbol{0}, \tau^2 \boldsymbol{R})$.

$\boldsymbol{\varepsilon}$ Vector of independent but heteroscedastic errors,

$$\boldsymbol{\varepsilon} \sim \text{N}(\boldsymbol{0}, \sigma^2 \boldsymbol{W}^{-1}),$$

where the weight matrix is specified as a diagonal matrix $\boldsymbol{W} = \text{diag}(\boldsymbol{w})$, with $\boldsymbol{w}$ the inverse squared standard errors of the trend estimators. The strict diagonal structure of $\boldsymbol{W}$ reflects the assumption of independent observations within a station given the random station effect γ.

The impact of spatial correlation is to pull estimates of station effects towards their neighbors, referred to as spatial smoothing. The amount of smoothing is controlled by the variance parameter τ^2, estimated from the data during the model-fitting. For an illustration of the involved matrices, we give an example on observations from four different stations in Germany using a range parameter of $\phi = 50$ (km):

Station	Latitude	Longitude	y	$se(y)$
1	51.7833	6.0167	-0.16196	0.28756
2	51.6333	6.1833	-0.04226	0.26424
3	51.0500	6.2333	-0.28621	0.27743
4	51.5833	6.2500	0.03426	0.29378

$$\boldsymbol{H} = \begin{bmatrix} 0 & 20.27 & 82.91 & 27.48 \\ 20.27 & 0 & 64.95 & 7.23 \\ 82.91 & 64.95 & 0 & 59.31 \\ 27.48 & 7.23 & 59.31 & 0 \end{bmatrix}, \quad \boldsymbol{R} = \begin{bmatrix} 1 & 0.43 & 0 & 0.26 \\ 0.43 & 1 & 0 & 0.78 \\ 0 & 0 & 1 & 0 \\ 0.26 & 0.78 & 0 & 1 \end{bmatrix},$$

$$\boldsymbol{Z} = \begin{bmatrix} 1 & 0 & 0 & 0 \\ 0 & 1 & 0 & 0 \\ 0 & 0 & 1 & 0 \\ 0 & 0 & 0 & 1 \end{bmatrix}, \quad \boldsymbol{W} = \begin{bmatrix} 12.09 & 0 & 0 & 0 \\ 0 & 14.32 & 0 & 0 \\ 0 & 0 & 12.99 & 0 \\ 0 & 0 & 0 & 11.59 \end{bmatrix}.$$

The assumption of no spatial correlation between effects of different stations is expressed by an identity matrix $\boldsymbol{R}$. However, since this approach still induces correlation within observations of the same station due to the shared random effect, it is denoted as unstructured spatial correlation.

Inference The aim of this study was to compare the temporal trends between the different types of pollination and woodiness, as well as to asses how the trends differ with respect to average flowering time in year, $\overline{doy}$. As stated previously, we entered the categorical variables pollination (wind versus insect) and woodiness (woody versus non-woody) as factor variables in the model matrix $\boldsymbol{X}$. We estimated the different phenological phases (first flowering and full flowering) in separate models, i.e. we applied the same model structure to the two data subsets containing only first- and full flowering data, respectively. Subsequently, we combined both phases in an overall model, using the complete dataset and an additional covariate, indicating the phenological phase. In an exploratory analysis we assessed the effects of woodiness and pollination type in main effects models, while ignoring other effects. This technically violates the principle of marginality (Nelder, 1977). We therefore used a more complex model for inference, which simultaneously incorporated all variables. Initially, the effect of average flowering time in year (variable $\overline{doy}$) on the temporal trend was estimated

linearly. More specifically, the generic form of $\boldsymbol{X\beta}$ contained the following terms,

$$\begin{aligned}\boldsymbol{X\beta} =& \mathbf{1}\beta_0 + \beta_{woody} I(\boldsymbol{x}_1 = woody) + \beta_{wind} I(\boldsymbol{x}_2 = wind) + \\ & \beta_{woody,wind} I(\boldsymbol{x}_1 = woody) I(\boldsymbol{x}_2 = wind) + \\ & \beta_{\overline{doy}} \overline{doy} + \beta_{\overline{doy},woody} \overline{doy} I(\boldsymbol{x}_1 = woody) + \\ & \beta_{\overline{doy},wind} \overline{doy} I(\boldsymbol{x}_2 = wind) + \\ & \beta_{\overline{doy},woody,wind} \overline{doy} I(\boldsymbol{x}_1 = woody) I(\boldsymbol{x}_2 = wind),\end{aligned}$$

where the indicator function $I(\boldsymbol{x})$ of a vector is meant to act element-wise on $\boldsymbol{x}$ and returns the evaluations as vector again. It evaluates to 1 if the x belongs to the specified category, and to 0 otherwise. In other words this is a two-way interaction model. Again, we provide an example:

Woodiness (x_1)	Pollination mode (x_2)	Average flowering time ($\overline{doy}$)
woody	wind	125.414
woody	insect	113.414
non-woody	wind	113.700
non-woody	insect	114.034

results in the design matrix,

$$\boldsymbol{X} = \begin{bmatrix} 1 & 1 & 1 & 1 & 125.414 & 125.414 & 125.414 & 125.414 \\ 1 & 1 & 0 & 0 & 113.414 & 113.414 & 0 & 0 \\ 1 & 0 & 1 & 0 & 113.700 & 0 & 125.414 & 0 \\ 1 & 0 & 0 & 0 & 114.034 & 0 & 0 & 0 \end{bmatrix},$$

and the associated vector of fixed effects,

$$\boldsymbol{\beta}' = (\beta_0, \beta_{woody}, \beta_{wind}, \beta_{woody,wind}, \beta_{\overline{doy}}, \beta_{woody,\overline{doy}}, \beta_{wind,\overline{doy}}, \beta_{\overline{doy},woody,wind}).$$

Later, to verify the linearity assumption, the constraint was relaxed, allowing a more flexible relationship by means of a spline function. We applied polynomial splines on a B-spline basis, as outlined in Section 1.3.3. We also assessed the effect of altitude above sea level using a spline of that form.

Hypotheses tests Based on the coefficients $\boldsymbol{\beta}$ we formulated the hypotheses of interest. The significance of the linear relationship between $\overline{doy}$ and flowering time for non-woody & insect-pollinated plants (1), woody & insect-pollinated plants (2), non-woody & wind-pollinated plants (3), and woody & wind-pollinated plants (4) can be assessed by tests of

the hypotheses

$$
\begin{aligned}
H_1 &: \beta_{\overline{doy}} = 0 \\
H_2 &: \beta_{\overline{doy}} + \beta_{woody,\overline{doy}} = 0 \\
H_3 &: \beta_{\overline{doy}} + \beta_{wind,\overline{doy}} = 0 \\
H_4 &: \beta_{\overline{doy}} + \beta_{woody,\overline{doy}} + \beta_{wind,\overline{doy}} + \beta_{\overline{doy},woody,wind} = 0,
\end{aligned}
$$

which can be expressed as tests of linear combinations $\boldsymbol{c}_j'\boldsymbol{\beta}, j = 1, \ldots, 4$ of the coefficient vector with $\boldsymbol{C} = (\boldsymbol{c}_1', \ldots, \boldsymbol{c}_4')'$ specified as

$$
\boldsymbol{C} = \begin{bmatrix}
0 & 0 & 0 & 1 & 0 & 0 & 0 & 0 \\
0 & 0 & 0 & 1 & 0 & 1 & 0 & 0 \\
0 & 0 & 0 & 1 & 0 & 0 & 1 & 0 \\
0 & 0 & 0 & 1 & 0 & 1 & 1 & 1
\end{bmatrix}.
$$

For mixed models with unbalanced designs, as present here, the exact distribution of $\boldsymbol{C}\hat{\boldsymbol{\beta}}$ under the null hypotheses is unknown. Approximations can be held using t-distributions (Pinheiro and Bates, 2000, p. 90), with the degrees of freedom to be specified. As an alternative, we applied a nonparametric bootstrap to asses the statistical significance of the hypothesis tests. We drew $B = 1,000$ bootstrap samples of the dataset, and fitted the model for each sample leading to estimates $\hat{\boldsymbol{\beta}}(b)$, $b = 1, \ldots, B$. We estimated $\mathbb{V}(\boldsymbol{c}_j'\hat{\boldsymbol{\beta}})$ by its empirical counterpart, the sample variance of $(\boldsymbol{c}_j'\hat{\boldsymbol{\beta}}(1), \ldots, \boldsymbol{c}_j'\hat{\boldsymbol{\beta}}(B))$, denoted as $s_B^2(\boldsymbol{c}_j'\hat{\boldsymbol{\beta}})$, for $j = 1, \ldots, 4$. p-values for the tests of the hypothesis

$$
H_{0,j} : \boldsymbol{c}_j'\boldsymbol{\beta} = 0 \text{ vs. } H_{A,j} : \boldsymbol{c}_j'\boldsymbol{\beta} \neq 0
$$

are obtained as

$$
p\text{-value} = 2 \cdot (1 - \Phi(|z_j|)),
$$

with $\Phi(.)$ the standard normal distribution, and

$$
z_j = \frac{\boldsymbol{c}_j'\hat{\boldsymbol{\beta}}}{\sqrt{s_B^2(\boldsymbol{c}_j'\hat{\boldsymbol{\beta}})}}.
$$

Multiple tests on the same data require an adjustment to in order to control the overall level of false-positive findings. Therefore, we calculated the p-values based on quantiles of the joint (asymptotic) multivariate normal distribution of the vector of test statistics z_j (Bretz et al., 2011, chap. 3). We applied the multiple comparison adjustment for 17 hypotheses tests, which are based on parameter estimates of the overall model. We tested for equal slope parameters of the covariate $\overline{doy}$ for different categories of pollination and woodiness

and assessed whether the flowering trends y were the same between these categories. For the latter comparison we set the average flowering date to $\overline{doy} = 100$. Therefore, the results are to be interpreted for plants which flower on average at the 100th day of the year.

Additionally, we visualized the uncertainty of the estimates by plotting all bootstrap samples using transparent colors, simultaneously showing the data on the original scale along with model-based predictions of the flowering trends. Predictions are limited to regions of the covariate-space in the data that were involved in the particular estimation. We recommend to limit interpretation to these areas and not to extrapolate. The pseudo R^2 for linear mixed models discussed by Xu (2003) is based on the maximized log-likelihood of the full model, $l(\hat{\boldsymbol{\beta}})$, containing all covariates, and the maximized log-likelihood of the null model, $l(\hat{\beta}_0)$, including only an intercept coefficient as fixed effect, with the same random effects structure in both models. It is calculated as

$$R^2 = 1 - \exp\left(-\frac{2}{n}(l(\hat{\boldsymbol{\beta}}) - l(\hat{\beta}_0))\right),$$

with n the number of observations, and can roughly be interpreted as the proportion of variance explained by the considered fixed effects.

Computational aspects We performed all analyses and graphs within the R environment (R Core Team, 2012). An implementation for the calculation of great-circle distances is readily available in the `sp` package (Bivand et al., 2008), returning distances in kilometers. For mixed models with a simple random effects structure, such as uncorrelated random intercepts, we used the `lme4` package (Bates and Mächler, 2010) and and extensions thereof in the `gamm4` package, allowing for inclusion of splines (Wood, 2012). Models with structured spatial correlations required specification of the design- and correlation matrices, which was performed using `mgcv` (Wood, 2006) and `regress` (Clifford and McCullagh, 2012) packages. For model-fitting the restricted log-likelihood was optimized and used for tests and parameter estimates. Calculation of the pseudo R^2 was done using maximum likelihood. Programs for bootstrapping were taken from `boot` package (Canty and Ripley, 2010), for multiple testing adjustment from the `multcomp` package (Hothorn et al., 2008).

3.4 Results

Model structure By using different values of the range parameter for the spherical correlation function, $\phi = 50, 70, 100, 150\ km$, we observed no practical impact of the structured spatial correlation on the fixed effects in the model. A random intercept for station specified by an identity matrix $\boldsymbol{R}$ was kept in the model. Altitude above sea level did not affect other estimated effects when included in the model and neither a linear relationship nor a spline function for altitude was statistically significantly different from zero. These results confirm findings by Ziello et al. (2009) observed in a related application.

We present the statistical results in three stages. In the first exploratory stage, we report an overview of the flowering dates, dealing with different variables of interest (pollination mode, woodiness, and average flowering time during year) one at a time. The results are model-based by using individual regression models to account for the spatial design and the required weighting. The estimated effects can roughly be interpreted as averages over variables not included, and are highly dependent on the balance of the groups and variables in the dataset. We did not do any adjustment of the p-values at this stage. The results in the second stage are based on a single, more complex model (overall model with interaction terms included). The p-values in this stage were adjusted for the number of comparisons, allowing to control the overall level of false positive findings. In the third stage we assessed the implication of linearity using a non-linear model as a diagnostic tool. As in stage one we report only raw p-values.

3.4.1 Exploratory results

Average trends for first and full flowering over all species and stations were throughout significantly negative when assessed for wind-pollinated and insect-pollinated plants as well as for woody and non-woody plants (Trend column in Table 3.1, p-values for trends equal to zero all < 0.001, not shown in table). This indicates an earlier start of first and full flowering phases, ranging between 0.489 days per year for wind-pollinated plants and 0.279 days per year for woody plants in the first flowering phase during the period 1971–2001. Full flowering phases of both pollination modes advanced approximately 0.3 d/yr. First flower opening phases of non-woody plants advanced 0.417 ($\pm$ 0.003) d/yr compared to 0.279 ($\pm$ 0.006) d/yr in woody plants. When comparing mean trends of first and full flowering for all plant groups except woody, the first flowering trend is larger than the respective full flowering one, leading to a longer flowering period, here defined as time between first and full flowering. Comparing the strength of advancement, we observed significantly earlier first

Phenological phase	Plant group	Trend (d/yr)	p-value
First flower opens	wind-pollinated	-0.489 $\pm$ 0.019	< 0.001
	insect-pollinated	-0.377 $\pm$ 0.003	
	non-woody	-0.417 $\pm$ 0.003	< 0.001
	woody	-0.279 $\pm$ 0.006	
Full flowering	wind-pollinated	-0.312 $\pm$ 0.009	0.11
	insect-pollinated	-0.337 $\pm$ 0.010	
	non-woody	-0.317 $\pm$ 0.009	0.27
	woody	-0.332 $\pm$ 0.011	

Table 3.1: Average temporal trends for first flower opening and full flowering phases, with significance of differences for pollination mode and woodiness.

flowering for wind-pollinated versus insect-pollinated plants, and woody versus non-woody

plants (p-value < 0.001). For full flowering there was no significant difference (p-value $= 0.11$ and 0.27, respectively; Table 3.1).

The linear effect of average flowering date (day of year) on these time trends is visualized in Fig. 3.3.

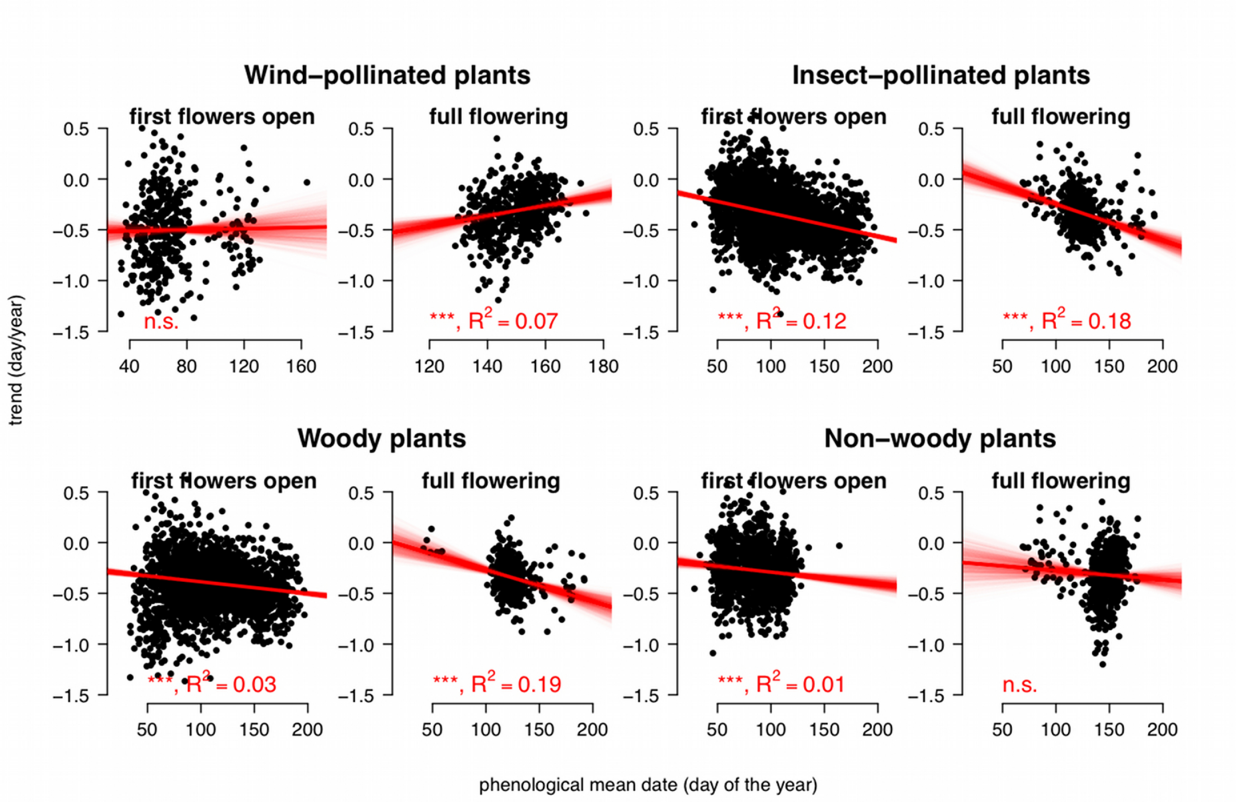

Figure 3.3: Long term time trends of flowering in days per year plotted against mean flowering date, by pollination types (top) and woodiness (bottom), each group in turn separately for phenophase. Red lines indicate the fit from the weighted linear mixed model, with thick and thin lines representing the averaged and single bootstrap samples, respectively, the latter reflecting uncertainty. Significances ($***$ for $p < 0.001$, $**$ for $p < 0.01$, $*$ for $p < 0.05$, n.s. for not significant) of linear mean date effect are indicated, together with the model R^2. Figure reproduced from Ziello et al. (2012).

For first flower opening phases of wind-pollinated plants there was no statistically significant relationship between trends and mean phenodates ($p = 0.81$). Full flowering phases revealed instead the expected pattern, with greater advances in the first part of the year ($p < 0.001$). Surprisingly, trends for insect-pollinated plants had the reverse association with mean phenodates, with larger advances observed later in the year ($p < 0.001$). Woody and non-woody species exhibited the same unexpected pattern, full flowering for non-woody species being the only group with trends non-significantly dependent on mean phenodates ($p = 0.32$).

Null hypothesis	Phenological phase	Plant group	Adjusted p-value[1]
$\beta = 0$	First flowering	insect, non-woody	0.008
		wind, woody	1.0
		insect, woody	< 0.001
$\beta = 0$	Full flowering	wind, non-woody	< 0.001
		insect, non-woody	< 0.001
		insect, woody	< 0.001
$\beta_{first} = \beta_{full}$	-	insect, non-woody	0.006
	-	insect, woody	0.36
$\beta_{woody,wind} = \beta_{non-woody,insect}$	First flowering	-	1.0
$\beta_{woody} = \beta_{non-woody}$		insect	0.14
$\beta_{wind} = \beta_{insect}$		woody	0.61
$\beta_{wind} = \beta_{insect}$	Full flowering	non-woody	< 0.001
$\beta_{insect,woody} = \beta_{wind,non-woody}$		-	< 0.001
$\beta_{woody} = \beta_{non-woody}$		insect	0.85

β denotes the slope for the linear dependence of the flowering trend on the average flowering time in year of a flower.
[1] Adjusted over the 17 multiple comparisons.

Table 3.2: Results of tests on slope parameters for the effect of phenological mean date on trends.

3.4.2 Overall model

All trends were significantly dependent (adjusted p-values < 0.05) on the average flowering dates except for the first flowering of wind-pollinated woody species (Table 3.2). The strength of the dependence on mean flowering time did not differ from each other for the first flowering phase. For the full flowering phase non-woody insect-pollinated plants advanced more with increasing average flowering date than their wind-pollinated counterpart (directions in Figure 3.4, p-values in Table 3.2). For first flowering, at average flowering date equal to day of year 100, woody plants showed a stronger advancement compared to non-woody plants for insect-pollinated plants in the subgroup of insect-pollinated plants ($p < 0.001$, Table 3.3). The insect-pollinated species consistently advanced more for flowering times later in the year (negative slope) for both phases, only wind-pollinated non-woody species showed the opposite pattern and advanced less ($p = 0.001$) for plants flowering later in the year (positive slope). A comparison of the strength of advancement (slope coefficients) between first flowering and full flowering was possible for insect-pollinated non-woody plants and insect-pollinated woody plants. The latter did not show a difference between first and full flowering ($p = 0.36$); non-woody did, they advanced more in full flowering ($p = 0.006$). The results can be assessed most conveniently by Figure 3.4, which combines information

Null hypothesis	Plant group	Adjusted p-value[1]
$\mathbb{E}(y_{woody,wind}) = \mathbb{E}(y_{non-woody,insect})$	-	< 0.001
$\mathbb{E}(y_{woody}) = \mathbb{E}(y_{non-woody})$	insect	< 0.001
$\mathbb{E}(y_{wind}) = \mathbb{E}(y_{insect})$	woody	< 0.001

[1] Adjusted over the 17 multiple comparisons.

Table 3.3: Results of tests on differences in the expected value of long term trends (y) between plant groups in the first flowering phase, with an average flowering day of year = 100 ($\overline{doy}$).

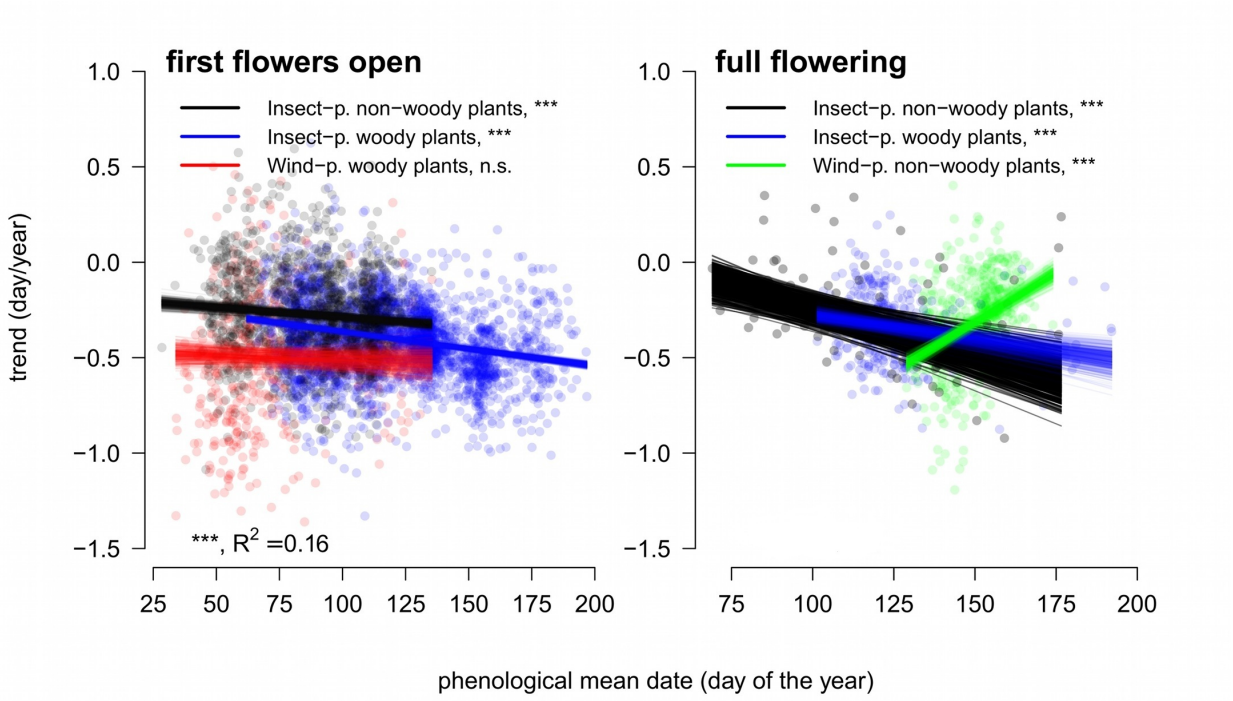

Figure 3.4: Long term time trends of flowering in days per year plotted against mean flowering date according to woodiness and pollination. Lines show bootstrap estimates, which reflect uncertainty. For sake of visibility, first flowering and full flowering are shown in separate figures. Figure reproduced from Ziello et al. (2012).

about direction, absolute level, and significance of effects.

3.4.3 Diagnostics

Results of the regression with non-linear effects generally confirmed those for the linear models, and are shown in Figure 3.5. For first flower opening, modelled curves of wind-pollinated woody species showed that they exhibited more advances than for insect-pollinated woody species, which did not vary with phenodates ($p = 0.12$): the non-significant influence of phenological mean date on trends found in the previous analysis was hence not induced by overly-restrictive linearity assumptions. For the two remaining groups, a significant advancement of mean flowering dates was evidenced, where the size of advancement statistically significantly depended on phenological mean dates ($p < 0.05$). For full flowering, wind-

pollinated non-woody species exhibited less advancement, depending on the phenological mean date ($p < 0.001$), than insect-pollinated woody and non-woody plants, whose trends were in both cases depending on the phenological mean date as well ($p < 0.001$).

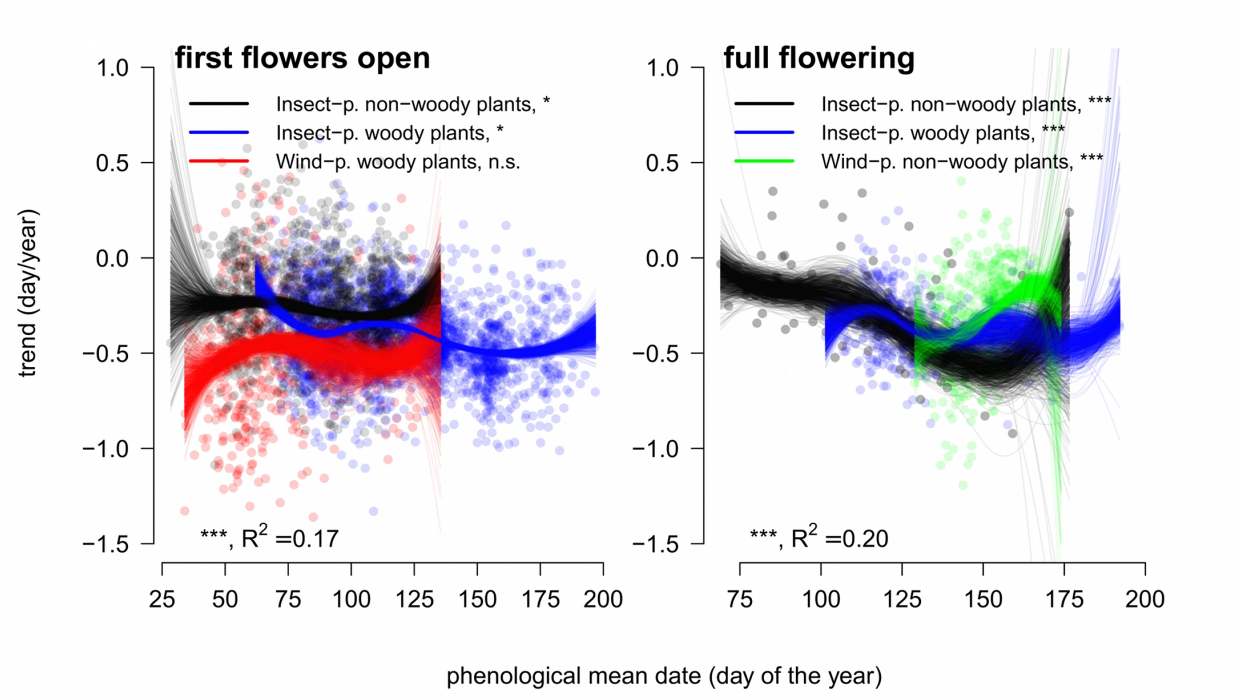

Figure 3.5: Long term time trends, modeled by flexible splines, of flowering in days per year plotted against mean flowering date according to woodiness and pollination. Individual lines show bootstrap estimates, which reflect uncertainty. Figure reproduced from Ziello et al. (2012).

3.5 Discussion

Observed changes in flowering The present study confirmed earlier reports of advancing trends in flowering dates (Menzel et al., 2006; Rosenzweig et al., 2007), independent of pollination mode and woodiness. However, from previous literature we expected a seasonal pattern with stronger advances of early-occurring phases (Lu et al., 2006; Menzel et al., 2006; Rosenzweig et al., 2007). We found this behavior only in the full flowering phases in insect-pollinated non-woody species. Instead, for the majority of groups, our results did not match the patterns previously reported, and indicated a decreasing advancement for species flowering later in the year.

Since onset of flowering phases are advancing more than later occurring full flowering phases, the flowering period of all the combined species is therefore lengthening. Such a prolongation of flowering has only rarely been inferred from phenological ground observations, since typically only single phenophases such as the start of flowering are studied. In this sense, the present study represents a step forward since first and full flowering dates of numerous

species have been analyzed and a prolongation of this flowering period has been inferred, which is of paramount importance for those allergic individuals that could likely experience a prolongation of their main suffering period. Due to the substantial lack of phenological data for the end of flowering, changes in the dates of this phase, which could directly assess the lengthening of the complete flowering period, can only be hypothesized. However, studies of direct pollen measurements have also reported longer pollen seasons (Rosenzweig et al., 2007), confirming the occurrence of longer flowering periods.

Differentiation of trends by pollination mode Phases related to the onset of flowering of wind-pollinated species exhibited the greatest advances, providing evidence that the phenology of anemophilous species may be more strongly affected by climate change, even if showing the weakest changes by year among the analyzed groups (Figure 3.4, Table 3.2). Compared to insect-pollinated species, wind-pollinated ones exhibited a larger prolongation of the flowering period, as inferred from the stronger advance of first flower opening phases compared to full flowering phases. It could hence also be inferred that the combined flowering period of all the species analyzed lengthened more for wind-pollinated than for insect-pollinated plants, which is a finding of high importance for pollen-associated allergic diseases.

Several studies have reported on differences in phenology and ecology between pollination modes (Bolmgren et al., 2003; Rabinowitz et al., 1981). In contrast to the findings of this study, Fitter and Fitter (2002) reported that in a recent context of general and fast phenological changes in Great Britain, insect-pollinated species were more likely to flower early than wind-pollinated species. In addition to a different geographical area, this discrepancy could be due to different criteria for the selection of phenological series: they used records longer than 23 years in the periods 1954-2000, requiring at least 4 years in the decade 1991-2000. In the current study, we selected series covering a shorter period (1971-2000) and were exhaustive as at least 29 out of 30 years were analyzed. Hence, in this study the years 1991-2000 are much more represented and results may better mirror the effects of the pronounced warming of such a decade. We identify this in the magnitudes of changes: the median advances found by Fitter and Fitter (2002) are three to six days for five decades, equivalent to a trend of -0.1 and -0.12 days per year (d/yr). In the present study, the mean trends are all stronger than -0.3 d/yr, reaching almost -0.5 d/yr. Another difference to Fitter and Fitter (2002) is in contrast to our findings. We found trends of insect-pollinated species to be stronger later in the season, they reported that insect-pollinated species that flowered early were much more sensitive to warming than those that flowered later. We return to this later in the discussion.

Hypothesized reasons for stronger flowering responses of wind-pollinated species Wind-pollination is a functional trait that can be preferentially found in specific geographical conditions, such as high altitudes and latitudes, in open vegetation structures such as Savannah, in habitats presenting seasonal loss of leaves such as northern temperate deciduous forests, or in island floras (Ackerman, 2000; Regal, 1982; Whitehead, 1969). Among

the widespread angiosperms (≈ 230,000 plant species), around 18% of families are abiotically pollinated, and at least 10% of species are wind-pollinated (Ackerman, 2000; Friedman and Barrett, 2009). All of the strongest allergenic species included in this study (e.g. birch, grasses) belong to this group.

We observed a stronger advance in first flowering dates for wind-pollinated compared to insect-pollinated species, and hypothesized that in addition to their pollination syndrome (a set of characteristics that co-occur among plants using the same pollination agent) anemophilous angiosperms have inherited a more rapid adaptedness, in other words a major plasticity. Angiosperms in general show higher evolutionary rates since their first evolutionary stages than gymnosperms, having probably originated in an environment that favored rapid reproduction (Regal, 1982). Fertilization periods, temporal gaps between pollination and consequent fertilization, are in fact known to be shorter in angiosperms than in gymnosperms (Williams, 2008). The key to the huge success of angiosperms may be due to this rapidity, even if the reasons for their fast and wide-step radiation are still not completely understood. Within angiosperms, wind-pollinated species may have changed their pollination mode as a reaction to unfavorable environmental conditions, enabling more capability for responding to the variability of climate. This aptitude would make anemophilous angiosperms particularly sensitive to environmental changes, and thus a group of strong responders to global warming.

This enhanced sensitivity to warming is made more credible due to the absence of limiting factors, such as the availability of pollinators. Entomophilous plants could be less free to react to temperature variations because their pollinator strategies would not match those changes. Hence, they would be less likely to change their ecological internal clock.

The effect of woodiness and time of the year As Table 3.1 might suggest, the onset of flowering of non-woody species advanced more than that of woody species for the first flowering phase. This effect needs to be relativized when looking at the significance tests in Table 3.2, where pollination mode is considered. In addition, for full flowering the pollination mode makes a difference for the effect of woodiness. However, when considering the seasonal variation, the predominant effect of pollination mode over the trait of woodiness is clear. In fact, advancements for woody and non-woody insect-pollinated species were quite similar in both flowering phases. In light of the results of this study, the dependence of the observed first flowering trends on the season seems to be more complex than previously reported. For entomophilous species the former finding of smaller advances of phases occurring early in the year is in contrast with the current study (Fitter and Fitter, 2002). This difference in intra-annual patterns of changes could be due to differences in number of locations monitored, as for example, only one station from Great Britain was available and 983 in continental Europe.

3.6 Limitations and future directions

The current study was based on aggregated data as the observations on station level were not available on a yearly basis. Additionally, the records on the long terms trends were not complete for all the four flowering phases on some species-station combinations. Both circumstances prohibited direct assessment of developments in the length of flowering periods and consideration of interdependencies between dates flowering phases within a year. Consider the mechanism of how the records were obtained for an individual plant or could be obtained in the future, sketched in Figure 3.6.

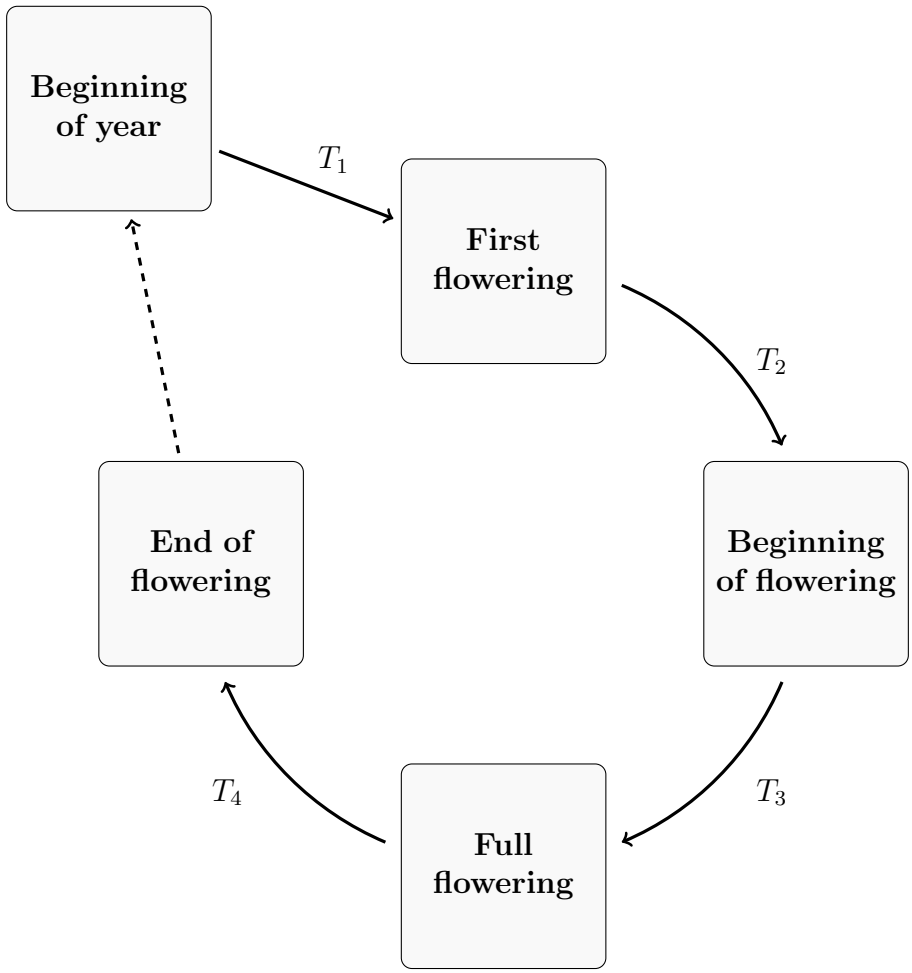

Figure 3.6: Phenological flowering phases with in-between-times $T_1, \ldots, T_4$ regarded as random variables. Time is counted in days.

Recording each of the flowering stages on a single plant or species bases yields a dataset as shown in Figure 3.4. To assess a change in the length of the flowering season over the years a univariate linear model with outcome variable

$$y_i = t_{2i} + t_{3i} + t_{4i}, \quad i = 1, \ldots, n,$$

can be used and extended to allow for non-linear effects of calender year, random effects

	Sojourn in flowering phase[1]				further covariates such as
Plant/species	$T_1 = t_1$	$T_2 = t_2$	$T_3 = t_3$	$T_4 = t_4$	calendar year and location
$i = 1$	t_{11}	t_{21}	t_{31}	t_{41}	$\boldsymbol{x}_1$
$\vdots$	$\vdots$	$\vdots$	$\vdots$	$\vdots$	$\vdots$
$i = n$	t_{1n}	t_{2n}	t_{3n}	t_{4n}	$\boldsymbol{x}_n$

[1]According to Figure 3.6 phases are: No flowering (beginning of year), first flowering, beginning of flowering, full flowering, end of flowering.

Table 3.4: Observations of phenological phases on individual plant level.

for species, and spatial effects for station. A more sophisticated approach is the estimation of a multivariate model, which explicitly accounts for (or models the) correlations between observations of a plant within a calendar year. The vector-valued outcome variable,

$$\boldsymbol{y}_i = (t_{1i}, t_{2i}, t_{3i}, t_{4i}), \quad i = 1, \ldots, n,$$

is accordingly modeled as a function of the covariate vector $\boldsymbol{x}_i$, and again extensions for random and spatial effects are possible (Timm, 2002, chap. 6).

However, the suggested models all assume normally distributed outcome variables $T_1, \ldots, T_4$. A natural alternative are time-to-event-models, motivated by the characteristic of time spans to be non-negative. In detail, a multi-state model is appropriate, where the states (flowering phases) occur progressively in time. The transitions between flowering phases are described by hazard rates $\lambda(t)$, a function of time t (see Section 1.3.3), and several ways to account for the flowering history of a plant are possible. Completely ignoring the differences in flowering phases and the flowering history leads to a common hazard rate for every kind of event (phase). This results in a two-state survival model assuming all $T_1, \ldots, T_4$ to be identically distributed within a plant. In other words we expect the time to first flowering to be same as the time between first flowering and beginning of flowering and so on. More realistic seems a hazard rate which depends on the current state of plant and time. These models are so-called Markovian if only depending on the current state and time without incorporating previous states. Additional information, such as the sojourn time in the previous state or the end of flowering in the previous year can be included as covariates. This implies some rearrangement of the data set, outcome variables of earlier phases serve as covariates for the current phase. Survival models extended for random effects so-called frailty models account for heterogeneity between species or location (Hanagal, 2011, chap. 12).

Chapter 4

Prostate cancer

This chapter emphasizes the statistical methods used in the articles "Evaluating the PCPT risk calculator in ten international biopsy cohorts: results from the prostate biopsy collaborative group" (D.P. Ankerst, A. Boeck et al., 2012a) and "Evaluating the prostate cancer prevention trial high grade prostate cancer risk calculator in 10 international biopsy cohorts: results from the prostate biopsy collaborative group" (D.P. Ankerst, A. Boeck et al, 2012b). The author of this thesis was second author of the forenamed articles, responsible for all statistical analyses and produced all figures and tables appearing in the articles and this thesis.

4.1 Introduction

The Prostate Cancer Prevention Trial (PCPT) was a North American phase III randomized, double-blind, placebo-controlled study of the chemoprevention effects of finasteride versus placebo on prostate cancer development. Study participation was limited to men older than 54 years of age, who have a prostate-specific antigen (PSA) level less than or equal to 3.0 ng/mL and have a normal digital rectal exam (DRE) result. They were annually screened and referred to interim biopsy (six-core) whenever their PSA exceeded 4.0 ng/mL or their DRE was abnormal. Follow-up time was seven years. At the end of this follow-up time, all men were requested to undergo a prostate biopsy regardless of their current PSA value and DRE result, or whether they had previously undergone a prostate biopsy that was negative for prostate cancer. Data of 5,519 participants from the placebo arm of the PCPT were used to develop a risk calculator for prostate cancer (PCPTRC) and a calculator for predicting high-grade (Gleason grade ≥ 7) prostate cancer (PCPTHG). The PCPTRC and PCPTHG were posted online on the websites of the Health Science Center in San Antonio, a part of the University of Texas, in 2006. Since then it is used by patients and clinicians worldwide as a counseling aid for the decision to undergo prostate biopsy.

In this work we present a study on the external validity of the PCPTRC (Ankerst et al., 2012) and the PCPTHG (Ankerst et al., 2012) on multiple cohorts in order to identify

potential populations where it may or may not be applicable. To that end, we highlight the characteristics of the study populations used to build the calculators in comparison to those used for the validation. Statistical measures which are suitable to quantify the performance of the calculators as a prediction tool are discussed.

4.2 Methods

4.2.1 PCPT data and risk models

All participants of the PCPT had a normal DRE and PSA level less than or equal to 3.0 ng/mL at the beginning of the trial. PSA and DRE tests were performed annually. If any DRE result was abnormal or if a participant's PSA value exceeded 4.0 ng/mL, they were recommended to undergo a prostate biopsy. At the end of the seven years on study, all participants who had not been diagnosed for prostate cancer were asked to undergo an end-of-study prostate biopsy. Based on the placebo arm of the PCPT a subset of 5,519 individuals were used to build the PCPTRC and PCPTHG calculator. This subset included all participants who underwent a prostate biopsy after any of the six annual visits or at the seventh year visit, when an end-of-study biopsy was recommended. Further inclusion criteria were a PSA test and DRE within one year of the biopsy as well as an additional PSA measurement during the three years before the biopsy to compute PSA velocity. For participants with multiple biopsies, the most recent study biopsy was used to assess the effect of a prior negative biopsy on prostate cancer risk (Thompson et al., 2006).

Characteristics of the patients, which are relevant for the risk prediction models are: the results of the prostate-specific antigen screening, the digital rectal examination, the age of the participant, the prostate cancer history of the participant's family, and if the participant already underwent a biopsy. Descriptions and exact definitions of those characteristics are given in Table 4.1. For purposes of prostate cancer risk modeling, the covariates in the following multivariable logistic regression models were coded as numerical values, also outlined in Table 4.1. Model selection based on BIC and out-of-sample AUCs yielded the following formulas to predict the risk of prostate cancer and high-grade prostate cancer, respectively:

Risk of prostate cancer, $\mathbf{P}(PCA)$,

$$\begin{aligned} PCA\text{-score} = &-1.7968 + 0.8488 \cdot \log PSA + 0.2693 \cdot FamHist + \\ &0.9054 \cdot DRE - 0.4483 \cdot PriorBiop, \\ \mathbf{P}(PCA) = &\frac{1}{1+\exp(-PCA\text{-score})}. \end{aligned} \tag{4.1}$$

Risk of high-grade prostate cancer, $\mathbf{P}(HG)$,

$$\begin{aligned} HG\text{-score} = &-6.2461 + 1.2927 \cdot \log PSA + 0.0306 \cdot age + \\ &1.0008 \cdot DRE + 0.9604 \cdot AA - 0.3634 \cdot PriorBiop, \\ \mathbf{P}(HG) = &\frac{1}{1+\exp(-HG\text{-score})}. \end{aligned} \tag{4.2}$$

Characteristic	Definition	Coding in model (variable acronym)
Prostate cancer	Status (yes/no) if the biopsy of a participant led to a cancer diagnosis.	Outcome variable in PCPTRC, with 0 = no, 1 = yes (PCA).
Gleason Score	Cancerous tissue from the biopsy is examined under the microscope to quantify the aggressiveness of the cancer. Ranges from 2 (low aggressiveness) to 10 (high aggressiveness).	Not directly used.
High-grade cancer	Status (yes/no) if a high-grade disease prostate cancer was detected, which was defined as the presence of a Gleason Score of 7 or higher.	Outcome variable in PCPTHG, with 0 = no, 1 = yes (HG).
PSA level	Prostate-specific antigen.	Logarithm of PSA in ng/mL used as metric covariate ($\log PSA$).
Age	Participant's age at the prostate biopsy.	Metric covariate (age).
DRE	Status (yes/no) if there was an abnormal result of digital rectal examination performed during the year before the biopsy.	Indicator variable with no = 0, yes = 1 (DRE).
Family history	Status (yes/no) if a participant's relative of first degree was diagnosed with prostate cancer.	Indicator variable with no = 0, yes = 1 ($FamHist$).
Prior biopsy	Status (yes/no) if the participant already underwent a biopsy, which in this case must have been negative due to inclusion criteria of the study.	Indicator variable with no = 0, yes = 1 ($PriorBiop$).
Race	Classification of the participant's race in African-American and not African-American.	Indicator variable with not African-American = 0, African-American = 1 (AA).

Table 4.1: Definitions of variables and risk factors used for risk prediction of prostate cancer or high-grade prostate cancer.

4.2.2 Validation cohorts

Data were included from ten European and US cohorts belonging to the Prostate Biopsy Collaborative Group (PBCG), where criteria for biopsy referral and sampling schemes are summarized in (Vickers et al., 2010). These included five screening cohorts from the European Randomized Study of screening for Prostate Cancer (ERSPC), three additional screening cohorts, San Antonio Biomarkers Of Risk of prostate cancer study (SABOR), Texas, US, ProtecT, United Kingdom, and Tyrol, Austria, and two US clinical cohorts, from Cleveland Clinic, Ohio, and Durham VA, North Carolina. All cohorts except for ERSPC Goeteborg and Rotterdam Rounds 1 included some patients who had been previously screened. All biopsies after a positive biopsy for prostate cancer were excluded from the analysis.

Validation of both risk calculators (PCPTRC and PCPTHG) are based on these cohorts. Due to the differing set of predictor variables for the calculators as well as the occurrence of missing values, the data which was used for validation do not match exactly. The validation results are presented separately for each calculator. Clinical characteristics of each cohort were summarized in terms of median and range (age and PSA) and by numbers (percent) in each category (DRE, family history, race, prior biopsy, prostate cancer, and Gleason grade) for the PCPTRC validation. For the PCPTHG validation clinical characteristics were summarized similarly in terms of descriptive statistics, including median, ranges and percentages. An iterative multiple imputation procedure was used to impute missing values of any of the risk factors when the percentage of missing data for a risk factor in a cohort was less than 100% (Janssen et al., 2010). For details on the procedure we refer to van Buuren (2007). The number of iterations was set to 20, and PCPTRC/PCPTHG risks were gauged as the average of five imputations of the missing risk factor. For cohorts where the race or DRE was not recorded for any participants, single imputation of "not of African origin" or "negative DRE", respectively, was implemented.

For each biopsy in the data set, the PCPTRC (or PCPTHG) risk of a positive biopsy (or high-grade cancer) was computed, requiring PSA, DRE, family history, and prior biopsy (or PSA, DRE, prior biopsy, and race), given by the formulas 4.1 and 4.2.

4.2.3 Validation measures

Several validation measures were calculated to assess the performance of the risk prediction and were displayed in graphs. In what follows we use the notation corresponding to previous chapters, that is,

$$\hat{y}_i \text{ for a single risk prediction of person } i \text{ and}$$
$$\hat{\boldsymbol{y}} \text{ for a vector of predictions for several persons,}$$

which range in the interval $(0; 1)$ resulting from the formulas for $\mathbf{P}(PCA)$ and $\mathbf{P}(HG)$. With $y_i \in \{0; 1\}$ and $\boldsymbol{y}$, respectively, we denote the true cancer (PCA) or high-grade (HG) status

of a person.

ROC and AUC Discrimination was calculated via receiver operating characteristic curves (ROC). Areas underneath the ROC curve (AUC) were calculated for predicted risks and compared to those with PSA alone for each cohort. As already previously described in Section 1.2.3, the AUC is applicable to assess the discrimination ability of both a metric covariate, like PSA, and of risk predictions $\hat{\boldsymbol{y}}$. For the interpretation we refer to the aforementioned section, where also calculation formulas are given. The rank-based Wilcoxon test was used to infer the differences in AUCs of the $\hat{\boldsymbol{y}}$ and PSA values in terms of statistical significance.

Hosmer-Lemeshow test As a measure of calibration, the Hosmer-Lemeshow (HL) goodness-of-fit test was used (Hosmer and Lemeshow, 2000, p. 147). A risk prediction model shows good calibration if there is a strong similarity between observed outcomes $\boldsymbol{y}$ and predicted risks $\hat{\boldsymbol{y}}$, which is described in more detail in Section 1.3.6. The test statistic of the HL-test sums the squared differences of predictions and true outcomes over $G = 10$ groups. The pair of vectors $(\hat{\boldsymbol{y}}, \boldsymbol{y})$ is gathered in groups by deciles of the predicted risks $\hat{\boldsymbol{y}}$, that is, the 10% smallest $\hat{y}_i$ define a group, the next largest 10% define the second group, and so on. This results in nearly equally-sized groups with $n/10$ pairs of $(\hat{y}_i, y_i)$, where n is the total sample size. With n_g we denote the particular sample size in group g, $g = 1, \ldots, 10$. The χ^2-type test statistic is thus

$$HL = \sum_{g=1}^{G} \frac{\left(O_g - n_g \bar{\hat{y}}_g\right)^2}{n_g \bar{\hat{y}}_g (1 - \bar{\hat{y}}_g)},$$

with O_g being the sum of observed cancers in group g,

$$O_g = \sum_{i=1}^{n_g} y_i,$$

and $\bar{\hat{y}}_g$ being the average prediction risk in group g,

$$\bar{\hat{y}}_g = \frac{1}{n_g} \sum_{i=1}^{n_g} \hat{y}_i.$$

Applied on data from an external validation, under the null-hypothesis HL asymptotically follows a χ^2-distribution with nine degrees of freedom:

$$\begin{aligned} &H_0 : \text{No difference between observed outcome and model-predicted risk,} \\ &H_A : \text{Observed outcome differs from prediction, and} \\ &HL \overset{a}{\sim} \chi^2(df = 9). \end{aligned}$$

Thus, for this test a p-value of $p < 0.05$ indicates a poor agreement between predicted

PCPTRC/PCPTHG risks and actual observed risk. However, it must be brought to attention that the null hypothesis is of good calibration, which will result in low power to detect miscalibration for small sample sizes, and we would only reject the null hypothesis if it was very severe. Furthermore, even in a situation with a quite perfectly calibrated model, we would reject the null hypothesis in a sufficiently large study (Steyerberg, 2009, p. 274 ff).

Calibration plot A visualization of the HL test and its decile-based categorization is the calibration plot. In the graph, the ten average predicted risks $\bar{\hat{y}}_g$ are laid out against the actual observed risks $\bar{y}_g = O_g/n_g$ of these categories. For an easier visual assessment, the occurring points are connected by lines in order of the predicted risks (x-axis). Vertical lines indicate Bonferroni adjusted 95% confidence intervals (CI) of the observed risks, based on their standard errors,

$$se(\bar{y}_g) = \sqrt{\frac{\bar{y}_g(1-\bar{y}_g)}{n_g}}),$$

$$CI_g = \bar{y}_g \pm 2.08\, se(\bar{y}_g).$$

The factor 2.08 in the above formula reflects the Bonferroni adjustment over $G = 10$ decile groups to reach an overall confidence level of 95% ($\alpha = 0.05$), and is the $(1 - \frac{\alpha/2}{10}) = 0.9975$-quantile of the standard normal distribution needed for a two-sided CI. Good calibration is indicated when the line chart is close to the graph of an identity function, which corresponds to a 45 ° line if both axis scales are isometric. The identity function graphs are drawn as ledger lines. At least the confidence intervals should overlap that line for acceptable calibration. Additionally, good discrimination of the model is indicated when the line chart is spread out over the range of the x-axis, that is the risk predictions $\hat{y}_i$ cover the whole interval of possible values between 0 and 1.

For the PCPTHG a modified version of the calibration plot is shown, although it has the same interpretation. It was not based on a hard grouping of the data by deciles, but using a smoothing technique to soften the dependency on the arbitrarily chosen number of $G = 10$ groups. Steyerberg (2009) suggested the loess smoother as described in Cleveland et al. (1992), but practically identical results were achieved using a smoothing-spline approach a binomial GLM (see Section 1.3.3), with the advantage that 95% pointwise CIs were readily available. In short, the observed outcomes $\boldsymbol{y}$ are modeled as a non-linear function of the predicted risks $\hat{\boldsymbol{y}}$. Opposite to the decile-based calibration plot, the distribution, or spread, of the predicted risks cannot be assessed immediately; a rug plot displaying the shape of the distribution, similar to a histogram, is overlaid at the bottom of the graph to overcome this.

Net benefit The clinical net benefit (Vickers and Elkin, 2006; Rousson and Zumbrunn, 2011) aims to account for the consequences of a decision suggested by the prediction model. Usually, decision-theoretic approaches attach utilities U to every possible option and seek for optimal decision rules. However, for a concrete application some knowledge outside the data at hand have to be present, which allow these utilities to be quantified. The idea of providing

clinical net benefit makes a compromise between both: It does not require any additional information, but leaves it to the end-user to provide the missing piece of information based on his particular circumstances. Imagine the situation where a decision has to be made if a patient undergoes a treatment or not, where the true, but unknown, probability for disease is denoted with p, and each of the four possible scenarios has attached its utility $(U_1, \ldots, U_4)$, as sketched in the Figure 4.1:

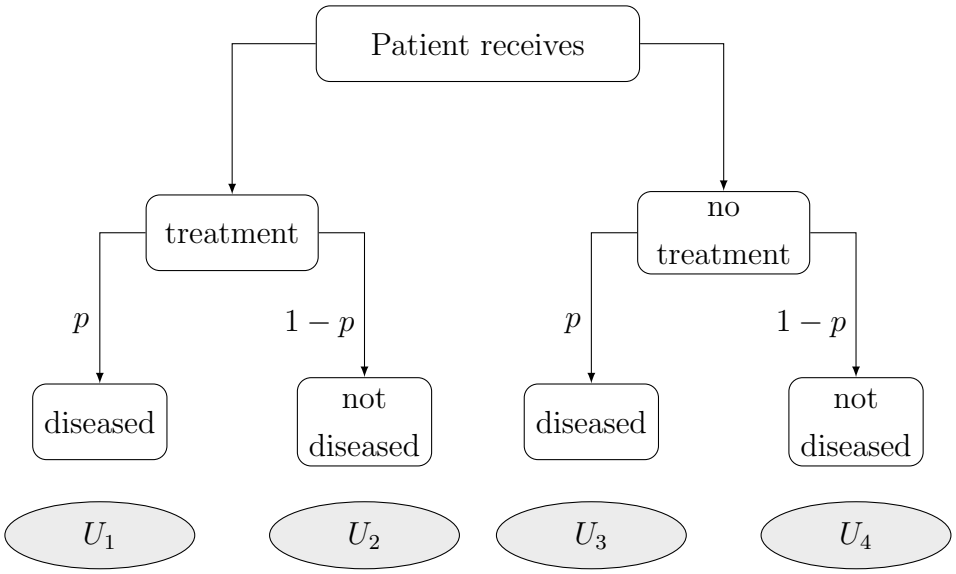

Figure 4.1: Decision tree on clinical net benefit.

In their definition of net benefit, Vickers and Elkin (2006) focus on the left arm of the tree, the treatment arm. The rationale is to treat an individual only if the expected utility in the disease case is bigger than the expected utility in the non-diseased case,

$$p\,U_1 > (1-p)\,U_2\,.$$

With fixed utilities, this depends only on the probability p, where p_t is the threshold probability when both expected utilities are equal,

$$\begin{aligned} p_t\,U_1 &\stackrel{!}{=} (1-p_t)\,U_2 \\ \Rightarrow p_t &= \frac{U_2}{U_1+U_2}\,. \end{aligned}$$

This signifies, that the decision is based on the utilities attached to a true postive (U_1) and a false positive (U_2) result, which is transformed to a probability threshold p_t. Thus, setting

$U_1 = 1$, which is just a standardization of the utilities, we can express U_2 as a function of p_t,

$$\begin{aligned} p_t &\overset{U_1=1}{=} \frac{U_2}{1+U_2} \\ \Rightarrow U_2 &= \frac{p_t}{1-p_t}\,. \end{aligned}$$

The net benefit for a prediction model is defined as the sum of all benefits minus the sum of all costs. A benefit arises when a diseased person is treated, and is quantified with $U_1 = 1$. Costs arise when a non-diseased person is treated and is quantified with $U_2 = \frac{p_t}{1-p_t}$. The expected net benefit as a function of p_t (and therefore of U_1 and U_2) thus is

$$\mathbb{E}\left(netben(p_t)\right) = \underbrace{p \cdot 1}_{\text{benefit}} - \underbrace{(1-p) \cdot \left(\frac{p_t}{1-p_t}\right)}_{\text{costs}}.$$

Replacing the unknown p by its empirical counterpart, the fraction of true positives, leads to the estimated net benefit

$$netben(p_t) = \frac{\text{true positve count}}{n} - \frac{\text{false positive count}}{n}\left(\frac{p_t}{1-p_t}\right),$$

where n is the number of all observations in the validation set. In the notation used throughout this thesis, with $\hat{y}_i$ as a individual risk prediction and y_i as a true outcome, the formula for the net benefit is

$$netben_{\text{model}}(p_t) = \frac{1}{n}\sum_{i=1}^{n} I(\hat{y}_i > p_t) I(y_i = 1) - \frac{1}{n}\sum_{i=1}^{n} I(\hat{y}_i > p_t) I(y_i = 0)\left(\frac{p_t}{1-p_t}\right). \quad (4.3)$$

Besides the model-based strategy, the net benefit is calculated for two additional decision strategies, which are rather extreme. They consist of not treating anyone and treating everyone, regardless of their individual threshold probability. The net benefit for treating nobody is constant zero,

$$netben_{\text{treat none}}(p_t) = 0, \quad (4.4)$$

while for treating everyone it is

$$netben_{\text{treat all}}(p_t) = \underbrace{\frac{1}{n}\sum_{i=1}^{n} I(y_i = 1)}_{\text{prevalence}} - \underbrace{\frac{1}{n}\sum_{i=1}^{n} I(y_i = 0)}_{1-\text{ prevalence}}\left(\frac{p_t}{1-p_t}\right), \quad (4.5)$$

which is a decreasing function of p_t, ranging from prevalence down to negative infinity. Finally, the net benefit graphs of the three functions 4.3, 4.4, and 4.5, are shown for a reasonable

range of threshold probabilities, which reflect the different individual circumstances of an individual.

In the context of this validation study, "treatment" corresponds to the decision whether a person undergoes a prostate biopsy. The graph shows for which areas of personal probability thresholds p_t the prediction model is useful for the patients, or in other words, shows where the benefit is higher compared to the other two strategies. The threshold serves a proxy how the patient weighs the harms of a unnecessary biopsy compared to a delayed diagnosis of prostate cancer. The scale of the net benefit has the following interpretation: A prediction model with a net benefit of 0.12 (at a specific p_t) is equivalent to a strategy that identifies 12 cancers in 100 patients with no unnecessary biopsies (Vickers, 2008).

4.3 Results

As mentioned above, patients within the cohorts used for the evaluation of the overall cancer calculator and the high-grade cancer calculator differed slightly due to the different set of missing values in the predictor variables. The tables and graphs are presented separately for each of the evaluations.

4.3.1 Cohort characteristics

Among the PBCG cohorts used to evaluate the PCPTRC, age was fairly consistent with a median in the early sixties (Table 4.2). Median PSA values ranged from 3.4 ng/ml in the SABOR cohort to 5.2 ng/ml in the Durham VA cohort, and rates of abnormal DRE, from a low of 10% in the Goeteborg Rounds 2–6 and Tyrol cohorts to a high of 31% in the Tarn cohort. Family history of prostate cancer was only reported in half of the cohorts and those reported all fell at or below 11% except for SABOR at 29%. This was an artifact of selection bias for the SABOR cohort since its protocol included a family history substudy that offered biopsies to men with PSA less than 4.0 ng/ml and a positive family history. African origin was not reported in the European cohorts but could be presumed to be negligible. The Durham VA cohort provided a contrast, with 45% of the individuals being of African origin. This cohort also had the highest cancer rate of 47% exceeding all nine other cohorts where the rates ranged from 26 to 39%. The Distribution of biopsy Gleason grades indicated a majority of low-grade cancers (Gleason 6 or less) in the ERSPC and SABOR screening cohorts, but only approximately half or less low-grade cancers were observed in the Tarn section of the ERSPC and the more clinical cohorts, Cleveland Clinic and Durham VA cohorts.

High-grade prostate cancer rates ranged from 4% in Goeteberg Rounds 2–6 to 22% in the Durham VA cohort, which was characterized by the highest percentage of men with African origin (45%), one of the risk factors included in the PCPTHG (Table 4.3).

	Goeteborg Round 1	Goeteborg Rounds 2–6	Rotterdam Round 1	Rotterdam Rounds 2–3	Tarn	SABOR	Cleveland Clinic	ProtecT	Tyrol	Durham VA
Number of patients	740	1,241	2,895	1,494	298	392	2,631	7,324	4,199	1,856
Number of biopsies	740	1,241	2,895	1,494	298	392	3,286	7,324	5,644	2,419
Age										
median (range)	61 (51, 70)	63 (53, 71)	66 (55, 75)	67 (59, 75)	64 (55, 71)	63 (50, 75)	64 (50, 75)	63 (50, 72)	63 (50, 75)	64 (50, 75)
PSA median	4.7	3.6	5.0	3.5	4.5	3.4	5.8	4.4	4.2	5.2
(range)	(0.5, 226.0)	(2.0, 88.8)	(0.0, 245.0)	(0.4, 99.5)	(1.6, 131.0)	(0.2, 919.2)	(0.2, 491.7)	(3.0, 847.0)	(0.1, 3,210.0)	(0.1, 1,355.6)
<3.0ng/ml	33 (4%)	205 (17%)	147 (5%)	417 (28%)	26 (9%)	166 (42%)	337 (10%)	0 (0%)	1,614 (29%)	309 (13%)
$\geq$ 3.0ng/ml	707 (96%)	1,036 (83%)	2,748 (95%)	1,077 (72%)	272 (91%)	226 (58%)	2,949 (90%)	7,324 (100%)	4,030 (71%)	2,110 (87%)
DRE result										
Normal	614 (83%)	1,117 (90%)	2,137 (74%)	1,182 (79%)	179 (60%)	280 (71%)	3,083 (94%)	0	5,076 (90%)	887 (37%)
Abnormal	126 (17%)	124 (10%)	758 (26%)	312 (21%)	92 (31%)	112 (29%)	203 (6%)	0	568 (10%)	265 (11%)
Unknown	0	0	0	0	27 (9%)	0	0	7,324 (100%)	0	1,267 (52%)
Family history										
No	0	0	1,708 (59%)	875 (59%)	0	280 (71%)	1,690 (51%)	5,736 (78%)	0	0
Yes	0	0	328 (11%)	160 (11%)	0	112 (29%)	373 (11%)	454 (6%)	0	0
Unknown	740 (100%)	1,241 (100%)	859 (30%)	459 (31%)	298 (100%)	0	1,223 (37%)	1,134 (15%)	5,644 (100%)	2,419 (100%)
African origin										
No	0	0	0	0	0	349 (89%)	2,818 (86%)	6,933 (95%)	0	1,218 (50%)
Yes	0	0	0	0	0	43 (11%)	422 (13%)	34 (0%)	0	1,079 (45%)
Unknown	740 (100%)	1,241 (100%)	2,895 (100%)	1,494 (100%)	298 (100%)	0	46 (1%)	357 (5%)	5,644 (100%)	122 (5%)
Prior biopsy										
Yes	0	0	0	0	0	96 (24%)	1,091 (33%)	0	1,555 (28%)	568 (23%)
No	740 (100%)	1,241 (100%)	2,895 (100%)	1,494 (100%)	298 (100%)	296 (76%)	2,195 (67%)	7,324 (100%)	4,089 (72%)	1,851 (77%)
Cancer	192 (26%)	322 (26%)	800 (28%)	388 (26%)	96 (32%)	133 (34%)	1,292 (39%)	2,570 (35%)	1,562 (28%)	1,148 (47%)
Biopsy Gleason grade*										
$\leq$ 6	152 (79%)	269 (84%)	508 (64%)	297 (77%)	42 (44%)	95 (71%)	669 (52%)	1,703 (66%)	911 (58%)	606 (53%)
7	33 (17%)	45 (14%)	234 (29%)	78 (20%)	37 (39%)	28 (21%)	478 (37%)	729 (28%)	319 (20%)	387 (34%)
$\geq$ 8	7 (4%)	8 (2%)	52 (6%)	13 (3%)	14 (15%)	7 (5%)	145 (11%)	138 (5%)	137 (9%)	141 (12%)
Unknown	0	0	6 (1%)	0	3 (3%)	3 (2%)	0	0	195 (12%)	14 (1%)

* Biopsy gleason grade reports percent of cancers

Table 4.2: Clinical characteristics of each cohort used in the PCPTRC evaluation: age and PSA report median (range), all others report number n (%).

Cohort (screening vs. clinical, primary number of cores)	ERSPC cohorts									
	Goeteborg Round 1 (screening, 6 cores)	Goeteborg Rounds 2-6 (screening, 6 cores)	Rotterdam Round 1 (screening, 6 cores)	Rotterdam Rounds 23 (screening, 6 cores)	Tarn (screening, 10-12 cores)	SABOR (screening, 10 cores)	Cleveland clinic (clinical, 10-14 cores)	ProtecT (screening, 10 cores)	Tyrol (screening, 10 cores)	Durham VA (clinical, 10-14 cores)
Number of patients	740	1,241	2,889	1,494	295	389	2,631	7,324	4,029	1,846
Number of biopsies	740	1,241	2,889	1,494	295	389	3,286	7,324	5,449	2,405
Age										
median (range)	61 (51, 70)	63 (53, 71)	66 (55, 75)	67 (59, 75)	64 (55, 71)	63 (50, 75)	64 (50, 75)	63 (50, 72)	62 (50, 75)	64 (50, 75)
PSA median (range)	4.7 (0.5, 226.0)	3.6 (2.0, 88.8)	5.0 (0.0, 245.0)	3.5 (0.4, 99.5)	4.4 (1.6, 131.0)	3.4 (0.2, 919.2)	5.8 (0.2, 491.7)	4.4 (3.0, 847.0)	4.1 (0.1, 3,210.0)	5.2 (0.1, 1,250.3)
DRE result										
Normal	614 (83%)	1,117 (90%)	2,135 (74%)	1,182 (79%)	177 (60%)	279 (72%)	3,083 (94%)	0	4,958 (91%)	887 (37%)
Abnormal	126 (17%)	124 (10%)	754 (26%)	312 (21%)	91 (31%)	110 (28%)	203 (6%)	0	491 (9%)	265 (11%)
Unknown	0	0	0	0	27 (9%)	0	0	7,324 (100%)	0	1,253 (52%)
African origin										
No	0	0	0	0	0	346 (89%)	2,818 (86%)	6,933 (95%)	0	1,212 (50%)
Yes	0	0	0	0	0	43 (11%)	422 (13%)	34 (0%)	0	1,071 (45%)
Unknown	740 (100%)	1,241 (100%)	2,889 (100%)	1,494 (100%)	295 (100%)	0	46 (1%)	357 (5%)	5,449 (100%)	122 (5%)
Prior biopsy										
Yes	0	0	0	0	0	95 (24%)	1,091 (33%)	0	1,524 (28%)	565 (23%)
No	740 (100%)	1,241 (100%)	2,889 (100%)	1,494 (100%)	295 (100%)	294 (76%)	2,195 (67%)	7,324 (100%)	3,925 (72%)	1,840 (77%)
Cancer	192 (26%)	322 (26%)	794 (27%)	388 (26%)	93 (32%)	130 (33%)	1,292 (39%)	2,570 (35%)	1,367 (25%)	1,134 (47%)
High-grade cancer (% biopsies)	40 (5%)	53 (4%)	286 (10%)	91 (6%)	51 (17%)	35 (9%)	623 (19%)	867 (12%)	456 (8%)	528 (22%)
AUC of PCPTHG in % (AUC PSA, p-value to PSA)	87.6 (82.4, 0.01)	72.0 (59.6, <0.001)	82.2 (77.5, <0.001)	74.1 (69.8, 0.046)	76.7 (64.1, <0.001)	69.5 (68.0, 0.60)	63.9 (59.3, <0.001)	75.4 (75.1, 0.35)	73.2 (69.2, <0.001)	73.9 (69.6, <0.001)
Number of unnecessary biopsies for thresholds 5, 10, 20% (percent of negative biopsies)	632, 275, 123 (90.3, 39.3, 17.6)	1,054, 222, 35 (88.7, 18.7, 2.9)	2,512, 1,575, 646 (96.5, 60.5, 24.8)	1,246, 448, 111 (88.8, 31.9, 7.9)	233, 134, 38 (95.5, 54.9, 15.6)	219, 116, 34 (61.9, 32.8, 9.6)	2,334, 1,517, 579 (87.6, 57.0, 21.7)	5,849, 2,083, 448 (90.6, 32.3, 6.9)	3,197, 1,705, 649 (64.0, 34.1, 13.0)	1,691, 1,306, 699 (90.1, 69.6, 37.2)
Number of missed high-grade cancers for thresholds 5, 10, 20% (percent of positive biopsies)	0, 3, 8 (0, 7.5, 20.0)	2, 25, 41 (3.8, 47.2, 77.4)	0, 26, 72 (0, 9.1, 25.2)	5, 28, 55 (5.5, 30.8, 60.4)	0, 4, 29 (0, 7.8, 56.9)	5, 14, 25 (14.3, 40.0, 71.4)	39, 162, 377 (6.3, 26.0, 60.5)	27, 266, 526 (3.1, 30.7, 60.7)	56, 154, 266 (12.3, 33.8, 58.3)	7, 45, 162 (1.3, 8.5, 30.7)

Table 4.3: Clinical characteristics of each cohort used in the PCPTHG evaluation: age and PSA report median (range), all others report number n (%).

4.3.2 Evaluating the prostate cancer risk calculator

Table 4.4 gives the external validation report for the PCPTRC in terms of discrimination, calibration, and clinical net benefit. AUCs of the PCPTRC ranged from a low of 56.2% in the Goeteborg Rounds 2–6 cohort to a high of 72.0% in the Goeteborg Round 1 cohort. While the AUC of the PCPTRC exceeded the AUC of PSA in all cohorts, it failed to be statistically significantly greater in 4 of the 10 cohorts: Rotterdam Rounds 2–3, Tarn, SABOR, and ProtecT, all screening rather than clinical cohorts.

Cohort (n)	**Discrimination** AUC PCPTRC (%) (P-value for comparison to the AUC of PSA)	**Calibration** Risk range where PCPTRC primarily overpredicts Goodness-of-fit P-value	**Net benefit** Range of PCPTRC risks of positive biopsy showing improved net benefit over the rules of biopsying everyone or no one (%)
ERSPC Goeteborg Round 1 (n=740)	72.0 (< 0.0001)	Entire range $P < 0.0001$	None
ERSPC Goeteborg Rounds 2–6 (n=1,241)	56.2 (< 0.0001)	Entire range $P < 0.0001$	None
ERSPC Rotterdam Round 1 (n=2,895)	70.0 (< 0.0001)	Entire range $P < 0.0001$	None
ERSPC Rotterdam Rounds 2–3 (n=1,494)	61.0 (0.15)	Entire range $P < 0.0001$	None
ERSPC Tarn (n=298)	66.7 (0.07)	No overprediction $P < 0.0001$	27–35
SABOR, US (n=392)	65.4 (0.20)	No overprediction $P = 0.24$	15–45
Cleveland Clinic, US (n=3,286)	58.8 (< 0.0001)	50% and higher $P < 0.0001$	35–45
ProtecT, UK (n=7,324)	63.9 (0.14)	50% and lower $P < 0.0001$	30-85
Tyrol, Austria (n=5,644)	66.7 (< 0.0001)	Entire range $P < 0.0001$	18–41
Durham VA, US (n=2,419)	71.5 (< 0.0001)	No overprediction $P = 0.0008$	25–100

Table 4.4: Discrimination, calibration, and net benefit metrics of risk predictions obtained form the PCPTRC.

Calibration plots of Figure 4.2 indicate that the PCPTRC overestimated the risk of prostate cancer for men of low, medium and high risks for all of the ERSPC cohorts except for the Tarn section, where 95% confidence intervals of the observed risks overlapped with predicted PCPTRC risks. The latter, however, could be attributed to the small sample size of the Tarn section (n = 298), which results in wider confidence bands and a greater chance of overlapping. For similar reasons, the PCPTRC appeared calibrated for the SABOR cohort (n

= 392). The PCPTRC also overpredicted in risk ranges of practical relevance (below 50%) for the large Cleveland Clinic, ProtecT and Tyrol cohorts (Table 4.4). However, for the Durham cohort (n = 2,419), which had the highest cancer prevalence (47%), the PCPTRC was calibrated across all risk areas. The Hosmer-Lemeshow test rejected goodness-of-fit for all cohorts except for the SABOR cohort, but this test has the undesirable quality of being more likely to reject the null hypothesis of goodness of fit as the sample size increases so is not as objective a benchmark for calibration as the calibration plots.

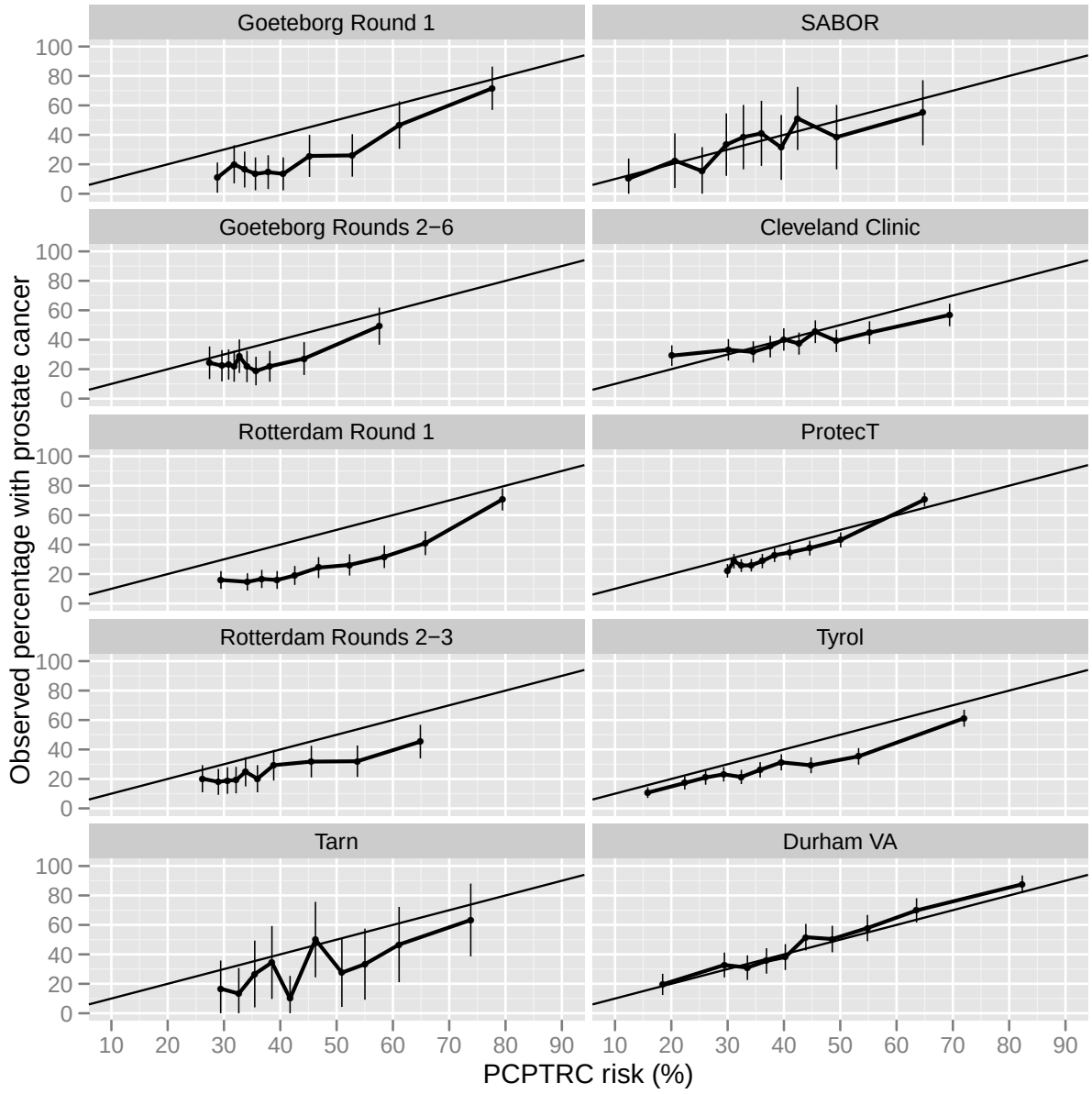

Figure 4.2: Calibration plots for the PCPTRC showing average PCPTRC risks for men grouped by their PCPTRC risk value (x-axis) compared to the actual percentage of diagnosed prostate cancer in these groups (y-axis). Perfect calibration would fall on the black diagonal line where predicted risks equal observed rates of prostate cancer. Figure reproduced from Ankerst et al. (2012).

The last column of Table 4.4 shows the range of risk thresholds for which the PCPTRC had higher clinical net benefit than the alternative strategies of biopsying all or none of the men. A risk threshold is the minimum risk at which a patient and clinician would opt for biopsy and varies between individuals due to personal preference. One reasonable threshold is 20%, suggesting that it would be worth conducting no more than five biopsies to find one cancer; a reasonable range of thresholds might be 15–30%. There was limited (ERSPC Tarn, Cleveland Clinic, ProtecT) to no clinical benefit at all (other four ERSPC cohorts) to using the PCPTRC to determine a subgroup of men to be biopsied compared to biopsying all of those meeting cohort-specific criteria for biopsy. For the remaining three cohorts, SABOR, Tyrol, and Austria, clinical benefit was observed at reasonable risk ranges: 15–45%, 18–41%, and 25–100%, respectively (Table 4.4).

4.3.3 Evaluating the High Grade prostate cancer risk calculator

Across the 25,512 biopsies from the ten cohorts combined, the AUC of the PCPTHG was 74.6 %, a modest three percentage points increase over the AUC for PSA (71.5 %, $p < 0.0001$). Use of PCPTHG risk thresholds of 5, 10 and 20 % as definitions of a positive test for referral to biopsy would have resulted in 84.4, 41.7, and 15.0 %, respectively, of all high-grade negative biopsies testing positive (percent unnecessary biopsies), and 4.7, 24.0 and 51.5 % missed high-grade prostate cancer cases, respectively. According to the individual cohorts, these statistics are shown in Table 4.3.

Evaluation of the PCPTHG for ten- and higher-core biopsy schemes–comparison with six-core The last six cohorts of Table 4.3 and Figures 4.3 and 4.4 implemented ten- and higher-core schemes. The median AUC of the PCPTHG for high-grade disease detection in the ten- and higher-core cohorts was 73.5 % (range 63.9 % - 76.7 %). Both the median and range were lower than those for the four ERSPC cohorts that had six-core biopsy schemes (median 78.1 %; range 72.0 % - 87.6 %). In two of the six ten- and higher-core cohorts, the PCPTHG did not reach statistically significant improvement in direct comparison to PSA for high-grade cancer discrimination (p-values > 0.05); in all four six-core cohorts, the PCPTHG performed statistically significantly better than PSA (p value < 0.05) (Table 4.3). Of all cohorts included in the analysis, only the 10-core Cleveland Clinic cohort showed clear evidence of underprediction, and this was restricted to risk ranges of less than 15 % (Figure 4.3). The PCPTHG primarily overpredicted high-grade prostate cancer in all six-core ERSPC screening studies. Clinical net benefit was not lower for the six higher-core biopsy scheme cohorts compared with the six-core biopsy cohorts; in fact, it was often higher (Figure 4.4). In three of the four six-core ESRPSC screening cohorts, there was no clinical benefit to using the PCPTHG across all risk thresholds.

Comparison of the PCPTHG in healthy/screening versus clinically referred populations Restricting attention to cohorts with ten- and higher-core biopsy schemes, the four screening cohorts had PCPTHG AUCs of 76.7 % (Tarn), 69.5 % (SABOR), 75.4 % (ProtecT) and 73.2 % (Tyrol), respectively, which overlapped with the AUCs observed in the clinical cohorts, 63.9 % (Cleveland Clinic) and 73.9 % (Durham VA, USA). Of note is the large 10-point difference between the Cleveland Clinic and Durham VA AUCs (Table 4.3). There were no obvious differences between calibrations or in clinical net benefits in the higher-core screening cohorts compared with the higher-core clinical cohorts (Figs. 4.3, 4.4).

Comparison of the PCPTHG of US versus European populations Restricting attention to cohorts with ten- and higher-core biopsy schemes, this comparison involves the three US cohorts – SABOR (AUC = 69.5 %), Cleveland Clinic (63.9 %) and Durham VA (73.9 %)–versus the three European cohorts–Tarn (76.7 %), ProtecT (75.4 %) and Tyrol (73.2 %) (Table 4.3). The range of AUCs for the European cohorts is in fact shifted higher than that for the US cohorts. The sample size of Tarn cohort is too low to make inference

concerning calibration. For low levels of high-grade risk (<10 %) the PCPTHG appears as good or better calibrated in the two remaining European higher-core cohorts (ProtecT and Tyrol) compared with the US cohorts (Figure 4.3). The higher-core European screening cohorts, Tarn, ProtecT and Tyrol, show comparable clinical net benefit to the US higher-core cohorts, with the exception of the US Cleveland Clinic cohort, where the PCPTHG had

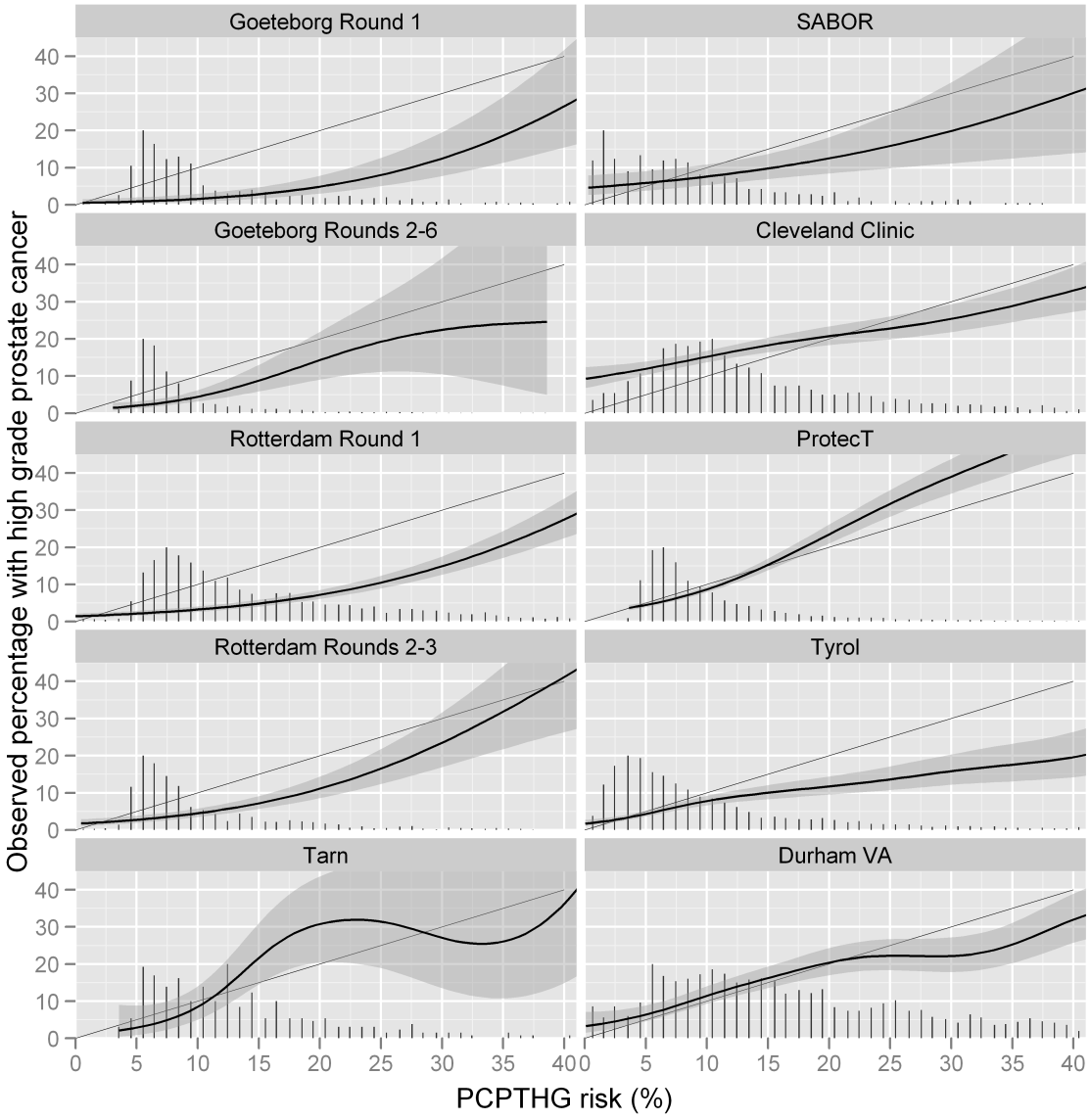

Figure 4.3: Calibration plots for the PCPTHG showing average PCPTHG risks for men grouped by their PCPTHG risk value (x-axis) compared with the actual percentage with a diagnose of high-grade prostate cancer (y-axis). Shaded areas represent approximate 95 % confidence intervals. Perfect calibration would fall on the diagonal line where predicted risks equal observed rates of high-grade prostate cancer, and adequate calibration is indicated where shaded regions overlap the diagonal lines. Vertical bars at the bottom are scaled histograms depicting relative frequencies of participants obtaining specified PCPTHG risks. Figure reproduced from Ankerst et al. (2012).

lower clinical net benefit (Figure 4.4).

4.4 Discussion

Since its publication in 2006 and being posted online for external validation, several single institutions or study reports of successful or failed validation of the PCPTRC have appeared, leading to confusion as to whether the tool can be recommended in practice (Cavadas et al., 2010; Eyre et al., 2009; Hernandez et al., 2009; Nguyen et al., 2010; Oliveira et al., 2011; Parekh et al., 2006; van den Bergh et al., 2008). By examining the spectrum of answers ob-

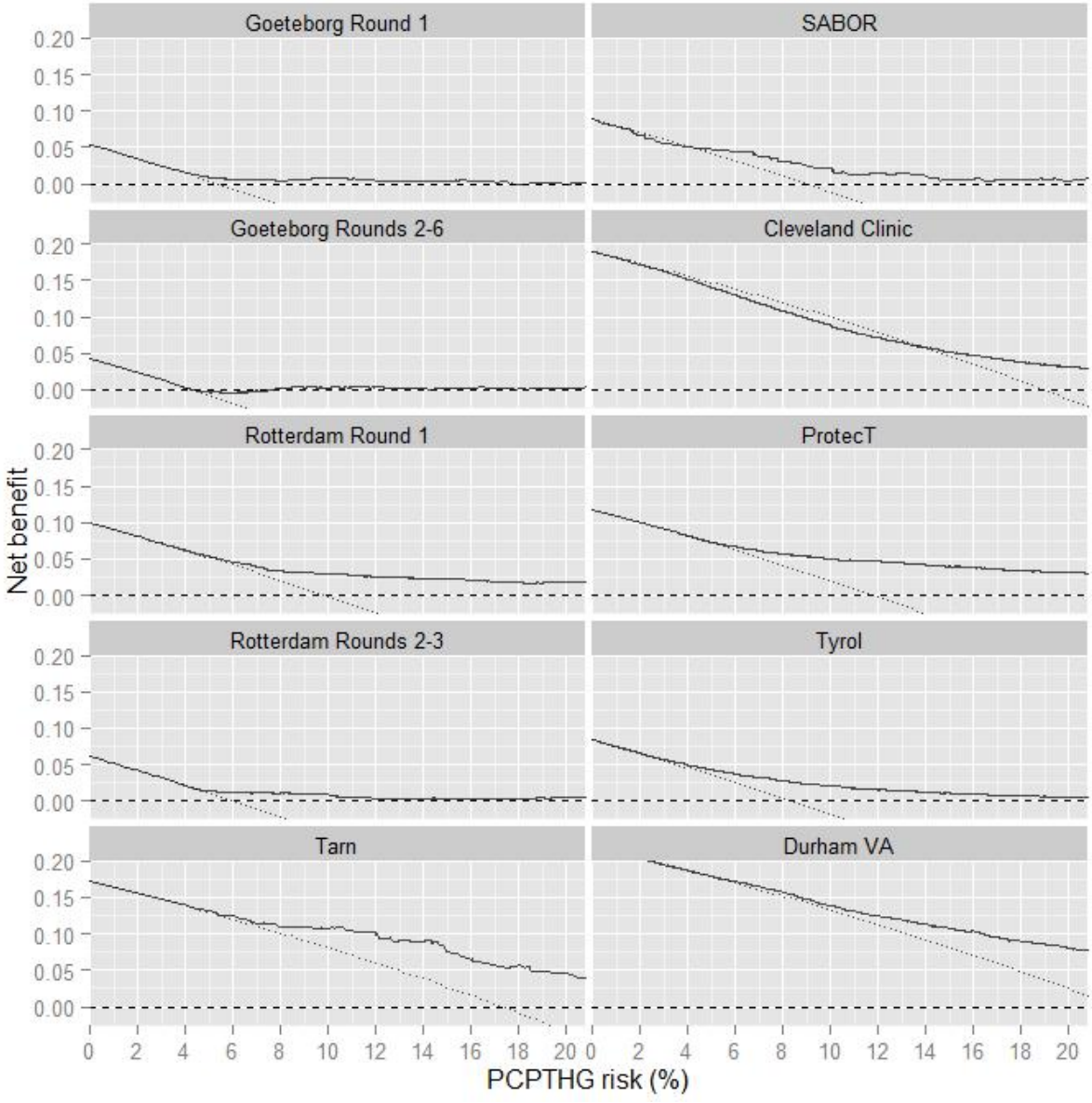

Figure 4.4: Net benefit curves for the PCPTHG (solid black line) versus the rules of biopsying all men (dashed line) and no men (dotted horizontal line at 0). A risk tool has clinical net benefit for a specific risk threshold (x-axis) used for referral to biopsy when its net benefit curve is higher than the curves corresponding to biopsying all men or no men. Figure reproduced from Ankerst et al. (2012).

tained in a wide variety of cohorts using three complementary validation metrics, this report illuminates the inherent variability of results of external validation by cohort and chosen metric. This variation is not unique to the PCPTRC, but would rather extend to validation studies of all risk-prediction tools and the rapidly increasing numbers of investigations of new markers for enhancing prostate cancer, including the urine/blood markers PCA3, AMACR, MMP-2, and GSTP1/RASSF1A methylation status (Ankerst et al., 2008; Prior et al., 2010). Indeed, these results are a convincing demonstration that properties such as "calibration [are] best seen not as a property of a prediction model, but of a joint property of a model and the particular cohort to which it is applied" (Vickers and Cronin, 2010).

The AUC appears to be the most ubiquitous criterion implemented for validation in urologic research, but even in the absence of a calculator, the AUC for PSA itself evaluated across the ten cohorts of this study varied from no utility at all (AUC = 50.9%, Goeteborg Rounds 2–6) to fairly decent performance (AUC = 67.0%, Goeteborg Round 1) (data provided by Kattan). The AUC suffers an additional disadvantage because it is influenced by the selection of patients for inclusion based on PSA: Including only patients with PSA exceeding 3.0 ng/ml downwardly influences the AUC compared to an AUC based on a sample without such a restriction. The PCPTRC amounts to a weighted average of PSA along with the dichotomous (yes versus no) risk factors of DRE, family history and prior biopsy, and therefore its AUC typically tracks the one of PSA in the same cohort. Accordingly, the AUC of the PCPTRC was also lowest in Goeteborg Rounds 2–6 (AUC = 56.2%) and highest in Goeteborg Round 1 (AUC = 72.0%). In these two cohorts along with four others, the AUC of the PCPTRC was statistically significantly higher than that of PSA. As noted by Kattan (2011), the key for unbiased inference of markers or calculators is head-to-head comparisons within cohorts and not across cohorts, as it is hard to control for unmeasurable cohort differences.

Calibration plots confirmed an earlier PBCG observation that for most cohorts, the PCPTRC tends to give prostate cancer risk predictions that are too high, overestimating actual risks both in the PSA <4.0 ng/ml range, the range on which the PCPTRC was largely developed, and grossly overestimating outside this range (Vickers et al., 2010). The calibration plots revealed that the PCPTRC was better calibrated for cohorts with larger prevalences of cancer, in particular the Durham VA clinical cohort. A limitation of all results is that single imputation had to be performed for missing risk factors in several cohorts, and this would affect calibration. For example, family history was not recorded in five of the ten cohorts, therefore for these cohorts, the optimal value "no family history" was used for all participants. Unfortunately even with the assumption of "no family history" the PCPTRC still overestimated the risk and would have been worse if the actual values of family history were available. Additionally, because the lowest PCPTRC risks observed in many of the cohorts fell near 30%, the current study provides no assessment of calibration of PCPTRC for lower risks that might be of greatest interest for decision-making concerning a biopsy.

Clinical net benefit is a more recently proposed validation metric that seeks to quantify the net benefit to a patient for using a particular decision rule to opt for a prostate biopsy, specifically, by choosing a threshold risk and deciding to undergo biopsy only if risk predicted by the decision rule exceeds this value. For each possible threshold, the net benefit of using the PCPTRC along with this threshold for referral to biopsy is assessed relative to just the rule of referring everyone in the cohort for biopsy. However, this application of the net benefit requires the underlying risk predictions to be well calibrated, which is property that is not naturally given in external predictions. The five ERSPC cohorts had per protocol referral of men for biopsy for PSA exceeding 3.0 ng/ml (4.0 ng/ml in some sections at some years), and there was no observed benefit to using the PCPTRC for these men with primarily high risks to begin with. In contrast, net benefit of using the PCPTRC at thresholds 15–45% was observed in the SABOR cohort, a cohort with lower PSA values, and most similar in nature to the PCPT cohort as described above. Among the remaining cohorts, there was only limited net benefit at limited ranges of PCTPRC thresholds.

In sum, this study has shown that the PCPTRC may not be universally applicable, that in the population of men with elevated PSA (above 3.0 ng/ml) who would most seriously consider prostate biopsy; the PCTPRC may overestimate the risk of finding prostate cancer. This result could be due to that the PCPTRC was fit on a different population of men, primarily healthy men with PSA less than 3.0 ng/ml. The accuracy of the PCPTRC on such a healthy population of men is not ruled out by the current validation study, since no cohorts of this type were included.

The evaluation of the PCPTHG did not show decreased performance for contemporary cohorts that use a higher number of cores compared to cohorts that had implemented six-core biopsy schemes (used in the PCPT), in cohorts comprising clinical patients rather than healthy patients undergoing screening, or in European versus US cohorts. Two primary advantages of the PCPTHG are that it requires only easily obtainable patient parameters that are part of a routine clinical exam (not including prostate volume) and that it is available on the internet. On some populations and judged by some criteria, the PCPTHG was no better than other screening methodologies; for example, in SABOR and ProtecT, the AUC of the PCPTHG did not differ statistically significantly from PSA (Table 4.3). These two cohorts implemented contemporary ten- and higher-core biopsy schemes. Extended core sampling has been shown to increase both prostate cancer and high-grade disease detection (Takenaka et al., 2006; O'Connell et al., 2004; Eskicorapci et al., 2004). Nevertheless, on no population and according to no scale, was the PCPTHG worse than simpler screening measures such as PSA, and this combined with the PCPTHG's simplicity and availability implies that it can be implemented as a complementary aid to the physician and patient in their decision to go forward or not with prostate biopsy, without the expectation that it could cause harm to the patient.

There are several limitations to the current study on risk calculation of high grade

prostate cancer. The primary limitation is that comparison of cohorts that evolved under different protocols as a means of assessing whether specific factors, such as 6- versus higher-core biopsy schemes, affects performance characteristics of a risk tool is no substitution for a single protocol analysis where individual factors, such as actual number of biopsy cores taken, are recorded for each patient. Cohorts were classified according to the primary number of cores used. Nevertheless, given this limitation, we believe a multiple external validation of a risk tool gives a more balanced assessment of the operating characteristics of a risk tool than a single evaluation study and can be more informative as to when and where the risk tool works in practice.

Another limitation is that all men underwent prostate biopsy and thus had one or more risk factors for prostate cancer. It was not possible to account for subtle differences in biopsy technique that might have had significant impact on high-grade cancer detection rates, such as choice of specific location to obtain cores independent of the number of cores. Furthermore, a central pathology review was not achievable, so it is possible that variation in aggressiveness in declaring biopsy specimens to have high-grade cancer might have occurred. The PCPTHG was designed to predict high-grade disease defined as Gleason score of seven and higher, but contemporary risk prediction typically focuses on clinically significant cancer, which may not include a Gleason score of seven. The information on ethnicity needed for the race covariate, a key risk factor in the PCPTHG, was entirely missing for 6 of the cohorts. Since these cohorts were all European, it could be assumed that their African origin proportion was negligible. DRE was not recorded for the ProtecT cohort and so assumed to be normal for all participants in that cohort. This can alternatively be considered a bonus evaluation of the robustness of the online PCPTHG, since it now allows use without DRE performed and then defaults to normal. This feature followed a prior study on SABOR that revealed DRE to be highly unstable, reverting to normal the year after an abnormal result in nearly 75 % of incidences (Ankerst et al., 2009).

There are currently many online nomograms and risk calculators available for prostate cancer, and it can be confusing figuring which calculator is optimal (Vickers and Cronin, 2010). Though novel biomarkers, such as %freePSA, and additional parameters, such as prostate volume, could improve upon existing calculators, the cost of including a more-difficult-to-obtain risk factor has to be weighed against a more widely applicable risk calculator. The rate of complications from prostate biopsy ranges from 2 to 4 %, and individual patients and doctors will vary in their assessment of how high a risk of high-grade disease needs to be to prompt them to biopsy (Thompson and Ankerst, 2012). Therefore, we recommend that PCPTHG risks in the range of 5-20 % be used depending on how much the individual weights the harm of a missed high-grade cancer to the harm of an unnecessary biopsy.

Findings of this study have implications for other risk-prediction tools beyond the PCPTRC and PCPTHG. It is typical in urologic research to declare definitive success or failure

of a tool based on a single validation measure evaluated on data from a single institution. However, if validation is a function of both the model and the cohort being studied, there are two consequences. First, those proposing models must explore the properties of the model in different cohorts, and investigate the aspects of a cohort that affect model performance. Second, clinicians should be cautious in using a model unless it has been shown to provide added value, such as benefit, in a very similar population to the one in which it is being used clinically.

Conclusion

In this thesis, we presented the development and implementation of statistical models in four different fields of recent research within the life sciences. The underlying data structures included the monitoring of tree stands over several decades, strictly planned growing trials of rye, aggregated flowering trends from huge databases, and patient data from several international clinical cohorts. Although the study aims varied, the flexible framework of regression analysis could be employed as appropriate concept for most of the demands. Still the common linear regression model is the workhorse of applied statistics and basis for generalizations in all fields of research, with a long list of applications described in the literature.

The generalizations we presented and need for future work include the use of random effects structures (Chapters 1–3), multivariate analysis of correlated outcomes, and a move towards integrated modeling of external information and outcome (Chapters 2–4), and splines for flexible modeling of covariate effects (Chapters 1, 3).

Models for random effects In this thesis random effects were mainly used to account for dependence within the outcomes originating from hierarchical structures or shared characteristics. While the random spatial effects in the phenology application were motivated by geographical locations, the random genotype effects in the rye study reflected the genetic similarity of plants to each other. Both approaches define a measure of distance between two sample units with larger distance inducing declining correlations. Consequently, the same thoughts given on the kinship matrix also apply to the spatial aspects of the flowering dates: In both cases sample units closer in terms of the distance measure provide less independent information than distant ones for inference on flowering trends and SNPs, respectively, based on the fixed effects of the model. For all of the above applications the distribution of random effects was assumed to be normal. The estimation of the parameters of a normal distribution is known to be sensitive to outliers, which could in turn also lead to biased estimates of the fixed effects in the model. A robustification to that end is the use of t-distributions (Lange et al., 1989). They have a higher mass on their tails compared to the normal distribution allowing the estimate of the central tendency to be less influenced by single extreme observations. With the extension to skew-t distributions it is further possible to catch existing skewness in the distribution of random effects (Ho and Lin, 2010). If the assumptions on the random effects density $p(.)$ should allow characteristics such as multimodality or non-

standard skewness, mixture distributions offer a sustainable way. The density of a mixture distribution $m(.)$ is a convex combination of K densities $f_k(.)$

$$m(x;\boldsymbol{\theta}) = \sum_{k=1}^{K} w_k \, f_k(x;\boldsymbol{\theta_k}), \quad \sum_{k=1}^{K} w_k = 1,$$

where $\boldsymbol{\theta}$ is the parameter vector of the mixture distribution comprising the parameters $\boldsymbol{\theta_k}$ of each mixture component and the non-negative weights w_k: $\boldsymbol{\theta} = (\boldsymbol{\theta}_k, w_k, \ldots, \boldsymbol{\theta}_K, w_K)$. However, the estimation now also includes the number K of mixture components in addition to the parameters in $\boldsymbol{\theta}$, which is much more demanding than estimation of a fixed number parameters in the first place. This kind of model belongs to the class of variable dimension models (Marin and Robert, 2007, p. 170). Standard optimization routines such as gradient methods often fail on the non-trivial likelihood surface and need problem specific extensions. From a Bayesian perspective, reversible jump Markov chain techniques (Green, 1995) allow to infer the number of components simultaneously with the other parameters. Ideally, the use of mixture models reveals interpretable clusters in the data. Although parametric, mixture models can be seen as a step towards nonparametric density estimation (in our case for the random effects) making very little assumptions on the shape of underlying distribution.

In a strictly nonparametric Bayesian approach $p(.)$ is assumed to be a random unknown quantity and a prior is needed over the infinite space of density or distribution functions. Such random probability measures can be specified using Dirichlet processes (DP)(Ferguson, 1973). To obtain priors for continuous densities extensions to Dirichlet process mixtures (DPM) (Antoniak, 1974) can be used (we refer to the references for a formal definition; here, only a sketch is given). The distribution of the random effects vector $\boldsymbol{b}_i$ for the ith out of N groups is characterized hierarchically as

$$\begin{aligned}
\boldsymbol{b}_i|\boldsymbol{\theta}_i &\overset{*}{\sim} f(\boldsymbol{b}_i|\boldsymbol{\theta}_i) \,(^*\text{distibuted not identically but independently, i.e. exchangeable}),\\
\boldsymbol{\theta}_i|G &\overset{\text{iid}}{\sim} G, \quad i = 1, \ldots, N,\\
G &\sim DP(\alpha, G_0),
\end{aligned}$$

with $\boldsymbol{\theta}_i$ the parameter vector of an arbitrary continuous density and G a random probability measure defined through a DP with concentration parameter α and base measure G_0, which is also a distribution on the desired support of $\boldsymbol{b}_i$. Due to the cluster property of the involved DP (MacEachern, 1994) the N $\boldsymbol{\theta}_i$s are partitioned into k sets of clusters, with $0 < k \leq N$. Since these random effects are defined for a group of observations, a single cluster comprises of one or more of those groups. All observations in a cluster share an identical value of $\boldsymbol{\theta}_i$ but the random effects $\boldsymbol{b}_i$ within a cluster are different because of the continuity of $f(.)$. In summary, this concept enables a very accurate prediction of the random effects, that is close to the data, and clusters can still be identified by the parameters $\boldsymbol{\theta}_i$. Applications of DPM as

priors for random effects within generalized linear mixed models can be found in Kleinman and Ibrahim (1998a), an implementation in R is provided by Jara et al. (2011).

Multivariate analysis of correlated outcome It is common to refer to a multivariate (or multiple) outcome when for a single sample unit more than one random feature is observed. A simple example is the collection of the height and weight of 100 individuals leading to a bivariate outcome for each of the 100 individuals. Also the monitoring of the same outcome over multiple time points leads to multivariate outcomes, such as the longitudinal observations of the percentage of damaged leaves in the growing trials (Section 2.2.1).

In principle, multivariate analyses are to be preferred over separate univariate analyses since it carries several advantages: the correlation between the different outcomes is explicitly modeled and can be inferred, hypotheses of interest can be globally tested, that is the aggregation of separate results is circumvented, and multiple testing which requires adjustment can be avoided. Furthermore, an efficiency gain may be expected in the situation of missing values and a more realistic assessment of the overall impact with respect to the study aim is possible (McCulloch, 2008).

Whenever the multiple outcomes are commensurate, that is all outcomes share the same scale, multivariate extensions of univariate GLMs can be applied. For m normally distributed outcomes the multivariate linear model (MLM) is given by

$$\underset{n\times m}{\boldsymbol{Y}} = \underset{n\times p}{\boldsymbol{X}}\,\underset{p\times m}{\boldsymbol{B}} + \underset{n\times m}{\boldsymbol{E}},$$

where $\boldsymbol{Y}$ is matrix with n oberservations (rows) on m outcomes (columns), $\boldsymbol{X}$ is the design matrix derived from the predictor variables, $\boldsymbol{B}$ the matrix of coefficients, and $\boldsymbol{E}$ the matrix of errors. In standard cases, the observations on different sample units are assumed to be independent and a potential non-zero covariance is specified between the m outcomes within a sample: $\boldsymbol{\varepsilon}_i' \overset{\text{iid}}{\sim} \mathrm{N}_m(\mathbf{0}, \boldsymbol{\Sigma})$, with $\boldsymbol{\varepsilon}_i'$ the ith row of $\boldsymbol{E}$ and $\mathrm{N}_m(\mathbf{0}, \boldsymbol{\Sigma})$ the m-dimensional normal distribution with mean vector zero and covariance matrix $\boldsymbol{\Sigma}$. There are m variance and $m(m-1)/2$ covariance parameters in $\boldsymbol{\Sigma}$ in this setup. However, a model definition equal to the above equation can be obtained by specifying a formally univariate model. Therefore, the rows of the matrices $\boldsymbol{Y}$ and $\boldsymbol{B}$ are stacked into vectors $\boldsymbol{y}$ and $\boldsymbol{\beta}$, and the design matrix $\boldsymbol{X}$ is inflated to dimension $n \cdot m \times m \cdot p$ (see Izenman, 2008, p.162).

The model equation is then

$$\underset{nm\times 1}{\boldsymbol{y}} = \underset{nm\times mp}{\boldsymbol{X}}\ \underset{mp\times 1}{\boldsymbol{\beta}} + \underset{nm\times 1}{\boldsymbol{\varepsilon}},$$

where $\boldsymbol{\varepsilon}$ is normally distributed with mean vector zero and a block-diagonal covariance matrix

$$\mathrm{Cov}(\boldsymbol{\varepsilon}) = \begin{bmatrix} \underset{m\times m}{\boldsymbol{\Sigma}} & \mathbf{0} & \cdots & \mathbf{0} \\ \mathbf{0} & \underset{m\times m}{\boldsymbol{\Sigma}} & \cdots & \mathbf{0} \\ \vdots & & \ddots & \vdots \\ \mathbf{0} & \cdots & \mathbf{0} & \underset{m\times m}{\boldsymbol{\Sigma}} \end{bmatrix}.$$

This point on the equivalence is made for three reasons; a) the term "multivariate" cannot be directly tied to the pure dimension of the statistical model but rather to the underlying assumptions in the structure of the error term; b) the MLM is not bound to this rectangle scheme. Not all entries in $\boldsymbol{Y}$ and $\boldsymbol{X}$ must be available, i.e. it is not mandatory to have observations of all m outcomes on all n units to specify a multivariate model; the stacking is still possible, and the regressors x need not to be equal for each of the outcomes; c) a connection to mixed models is made, exemplary for a the random intercept model. For the latter, more restrictive assumptions on the outcome variables/error terms are made: Conditional on the regressors, the same variation in all m types of outcomes is assumed, i.e. homoscedastic errors, and in addition the correlation between the outcomes is assumed to be positive and constant between all $m(m-1)/2$ pairs of outcomes. These are plausible considerations for a model on repeated measures in longitudinal studies. Technically, the covariance matrix $\boldsymbol{\Sigma}$ is therefore parametrized with two parameters, a variance σ^2 on the diagonal and a common covariance $\rho\sigma^2$ on the off-diagonals ($\rho \geq 0$). Thus, when i indicates the observation and j the outcome it holds that

$$\begin{aligned} &\mathrm{Cov}(y_{ij}, y_{i'j'}) = \sigma^2 \text{ for all } i = i' \text{ and } j = j' \ (= \mathbb{V}(y_{ij})), \\ &\mathrm{Cov}(y_{ij}, y_{i'j'}) = \rho\sigma^2 \text{ for all } i = i' \text{ and } j \neq j', \\ &\mathrm{Cov}(y_{ij}, y_{i'j'}) = 0 \text{ for all } i \neq i'. \end{aligned}$$

This however is equivalent to the marginal distribution of $\boldsymbol{y}$ in a linear mixed model with random intercept

$$\begin{aligned} &y_{ij} = \boldsymbol{x}_{ij}'\boldsymbol{\beta} + \gamma_i + \varepsilon_{ij}, \quad i = 1, \ldots, n, \quad j = 1, \ldots, n_i, \\ &\varepsilon_{ij} \overset{\text{iid}}{\sim} \mathrm{N}(0, \tilde{\sigma}^2), \\ &\gamma_i \overset{\text{iid}}{\sim} \mathrm{N}(0, \sigma_\gamma^2), \quad \gamma_i, \varepsilon_{ij} \text{ independent}, \end{aligned}$$

where $\mathbb{V}(y_{ij}) = \tilde{\sigma}^2 + \sigma_\gamma^2$ corresponds to σ^2 from the MLM and the covariance σ_γ^2 of observations sharing a random effect corresponds to $\rho\sigma^2$. Note that this restricted MLM and the

random intercept model are only equivalent in their marginal presentation. The conditional specification of the random intercept model is more explicit. It makes specific additive assumptions on the composition of the variance. As a consequence marginal inference in both models is expected to provide similar but not identical results.

In conclusion, the mixed models extensively used throughout this thesis already represent forms of multivariate and simultaneous inference. Further directions towards this goal of analysis of the sojourn in flowering stages in the phenology chapter are indicated in Section 3.6. The situation of the growing trials of Chapter 2 is somewhat different and discussed in the following paragraphs.

For the situation of multiple commensurate outcomes obtained on the same sample unit the considerations of the previous section apply. However, the growing trials of Chapter 2 were run in three independent platforms (controlled, semi-controlled, open field) with different outcomes (mean recovery score, % leaf damage, % survival). The analysis was conducted in separate models with platform specific adjustments and in a second step the results on SNP effects were bundled over the platforms using their p-values (Figure 2.3). Understanding the genotypes as central entity with multiple outcomes nested in platforms, trials, locations, years, blocks etc. one could construct a huge common multivariate model for all observations at hand. In a first attempt on could build a model with interaction terms of a platform indicator being created and the terms present in the three individual models. All these interactions are needed as the outcomes—although all metric—are on different scales and effect sizes (i.e. both fixed and random effects coefficients) depend on that scale. With that overall model at hand it would be possible to formally test composite null hypotheses such as "SNP1 has a positive effect on frost tolerance" by

$$\begin{aligned} H_0: &\quad \beta_{\text{SNP1, platform } i} \leq 0 \; \forall \, i = 1, 2, 3, \qquad \text{vs.} \\ H_A: &\quad \beta_{\text{SNP1, platform } i} > 0 \;\; \text{for at least one } i, \end{aligned}$$

within one single model. The conclusion however would coincide with those obtained by separate models. Technically, this is due to the independence (zero covariance) of the observations between different platforms. The observations are uncoupled by the interaction terms and the per-platform variances. Hence, the formal unified analysis as sketched above does not provide advantages over separate analyses. To overcome this problem arising with non-commensurate outcomes one would need to make more restrictive assumptions with respect to the scales involved or the cross-outcome direction of the effects (omitting interaction terms), or less restrictive assumptions with respect to the assumed dependence for elimination of structural zeros in the covariance matrix. One approach towards that end exists in extending the random intercept model from above, which is presented conceptually here and is described in more detail in McCulloch (2008).

For ease of notation only two non-commensurate outcomes y_1, y_2 are considered, but ideas

apply for multiple outcomes as well. Again, non-commensurate outcomes denote variables measured on different scales including count data, binary data, or as in case of the growing trials metric outcomes on different ranges. Both outcomes must measure an underlying quantity such as frost tolerance in the same direction, say, y_1 on metric scale, y_2 on binary scale. They can be sampled under completely different circumstances, but their individual observations can be classified coherently (such as by genotype). The class membership is indicated by a random intercept γ_i in a conditional model for both outcomes

$$\begin{aligned}
\log\left(\frac{\mathbf{P}(y_{1ij}|\gamma_i)}{1-\mathbf{P}(y_{1ij}|\gamma_i)}\right) &= \boldsymbol{x}'_{1ij}\,\boldsymbol{\beta_1} + \gamma_i, && \text{(logistic regression for } y_1\text{)},\\
y_{2ij}|\gamma_i &= \boldsymbol{x}'_{2ij}\,\boldsymbol{\beta_2} + \lambda\,\gamma_i + \varepsilon_{1ij}, && \text{(linear regression for } y_2\text{)},\\
\gamma_i &\overset{\text{iid}}{\sim} G && \text{(distribution } G \text{ to be specified)},
\end{aligned}$$

where $\boldsymbol{x}_{1ij}$ and $\boldsymbol{x}_{2ij}$ are outcome-specific covariate vectors and $\varepsilon_{1ij} \overset{\text{iid}}{\sim} \mathrm{N}(0, \sigma^2)$. Due to the shared random effect γ_i the observation of the same class i are marginally correlated across outcomes. The difference in scale is taken into account by the parameter λ, which, however, assumes the random effects to act in the same direction in all settings (outcomes). McCulloch (2008) discusses consequences with distributions where the variance is a functional of the mean such as Bernoulli distributions used with binary data. Since the outcomes of the growing trials presented in this thesis are on metric scale this would not be an issue. To account also for the dependence between genotypes induced by the kinship the iid-assumption of γ_i must be relaxed by specifying a suitable multivariate prior G for the vector $\boldsymbol{\gamma}$ comprising all single random genotype effects γ_i. In these models with shared random effect across outcomes, the hypothesis of interest specified above could be tested simultaneously for all platforms in a model based way. An alternative approach focusing on the marginal distribution is suggested in Roy et al. (2003). Models for multivariate outcomes on different scales using copulas are described in Joe (1997).

Flexible modeling of covariate effects Revealing the true functional form of the association between outcome and covariates is a fundamental objective in statistical models. Probably too ambitious, at least good approximations which fulfill the specific purpose of the model are needed. The standard configuration of linear effects is a plausible choice when a rather rough quantification of direction and strength of a suspected global trend is desired. However, in situations where the association is more complex the linear approximation cannot detect small scale deviations and can lead to biased estimates. Regression models can be straightforwardly generalized by adding transforms of covariates to the predictor and allowing interaction effects. The problem of variable selection rapidly becomes cumbersome when several covariates are involved. The use of penalized splines as described in Section 1.3.3 is suitable to flexible model smooth relationships and is also able to capture small scale effects if the knot-setup is chosen accordingly. The concept of penalization helps to prevent

overfitting due to wiggly function profiles.

In turn, the stochastic correspondent of the penalization approach fits perfectly in the concept of random effects models whose merits have been broadly discussed. The underlying constructive formulation of splines via basis functions can be extended in more dimensions for the estimation of interaction surfaces and spatial effects. The equivalence of Kriging and the use of radial basis functions should be noted here (Dubrule, 1984). Being linear in their coefficients spline approximations can be represented as linear models allowing the use of established numerical routines and also subject matter considerations on the functional shape such as monotonicity can be embedded in the design matrices of the regression model (Wood, 1994).

Even though statistical models can provide good approximations to unknown dependency structures the final decision cannot be objective but rests with the researcher. Not least because often a set of candidate models performs equally well. We experienced that in real world examples the profitably complexity is relatively low compared to what is offered from more theoretical research activities. Although simpler models are known to generalize better on external data and in new situations it is challenging to set definitive limits of complexity before an analysis. In particular, the analysis of designed experiments, which are less subject to undesired ambient conditions, can demonstrate the limits of predictability of complex (biological) systems—or provide fresh impetus.

List of performance measures

This appendix provides an overview of measures useful for assessing model performance. The list contains both visual and numerical approaches. The notation used is $\hat{\boldsymbol{y}}$ for the vector of predictions/risks from a model, and $\boldsymbol{y}$ for the true status (0 or 1). The main goal is to quantify the relationship between observed outcomes $\boldsymbol{y}$ and the corresponding estimation $\hat{\boldsymbol{y}}$. Some of the measures require a cut-off value or grouping of $\hat{\boldsymbol{y}}$, which will be denoted by *cut* (Tom, 2006).

relevant/concordant/discordant pairs The following terms describe the agreement of observation-prediction pairs: $((y_i, \hat{y}_i), (y_j, \hat{y}_j))$ (Tutz, 2000, p. 111ff).

N denotes the number of relevant pairs with different outcomes,

$$\begin{aligned} N &= \sum_{i,j} I(y_i \neq y_j) \\ &= 2\left(\sum_i I(y_i = 1) \sum_i I(y_i = 0)\right). \end{aligned}$$

N_c the number of concordant pairs,

$$N_c = \sum_{i,j} (I(y_i < y_j) I(\hat{y}_i < \hat{y}_j)) + \sum_{i,j} (I(y_i > y_j) I(\hat{y}_i \geq \hat{y}_j)),$$

and N_d the number of discordant pairs,

$$N_d = \sum_{i,j} I(y_i < y_j) I(\hat{y}_i > \hat{y}_j) + \sum_{i,j} I(y_i > y_j) I(\hat{y}_i < \hat{y}_j).$$

Kendall's τ

$$\tau = \frac{N_c - N_d}{n(n-1)/2}.$$

Goodman and Kruskal's γ

$$\gamma = \frac{N_c - N_d}{N_c + N_c}.$$

Somer's D

$$D = \frac{N_c - N_d}{N}.$$

TPF True Positive Fraction, also called *recall*. Based on *cut* the $\hat{\boldsymbol{y}}$ are classified as 0 or 1 (alive or dead, control or case). TPF is the fraction of all $\boldsymbol{y} = 1$ which had a $\hat{\boldsymbol{y}}$ higher than *cut*

$$TPF_{cut} = \frac{\sum I(\hat{y}_i > cut) I(y_i = 1)}{\sum I(y_i = 1)}.$$

FPF False Positive Fraction. Based on *cut* the $\hat{\boldsymbol{y}}$ are classified as 0 or 1 (alive or dead, control or case). FPF is the fraction of all $\boldsymbol{y} = 0$ which had a $\hat{\boldsymbol{y}}$ higher than *cut*,

$$FPF_{cut} = \frac{\sum I(\hat{y}_i > cut) I(y_i = 0)}{\sum I(y_i = 0)}.$$

Sensitivity same as TPF, also called the true positive rate.

Specificity same as $1 - FPF$, also called the true negative rate.

PPV Positive Predictive Value is the fraction of true positives to all positives (either true or false):

$$PPV_{cut} = \frac{\sum I(\hat{y}_i > cut) I(y_i = 1)}{\sum I(\hat{y}_i > cut)}.$$

NPV Negative Predictive Value:

$$NPV_{cut} = \frac{\sum I(\hat{y}_i < cut) I(y_i = 0)}{\sum I(\hat{y}_i < cut)}.$$

F-measure Harmonic mean of PPV and TPF:

$$F = 2 \cdot \frac{TPF \cdot NPV}{TPF + TPF}.$$

ROC The Receiver Operating Characteristic (ROC) curve shows the graph of TPF_{cut} (y-axis) and FPF_{cut} (x-axis) for all possible *cut*.

AUC Area Under the ROC-curve. Measures the discrimination power of $\hat{\boldsymbol{y}}$ independent of a specific *cut*. A useless predictor has an AUC of 0.5, a perfect one an AUC of 1. Besides other possibilities the AUC can be calculated as the number of concordant pairs divided by the number of relevant pairs (Agresti, 2007, p.159):

$$AUC = \frac{N_c}{N}.$$

Pseudo R^2 (Veall and Zimmermann, 1996). For logistic regression, Nagelkerke (1991) standardized the binomial likelihood-based R^2_{Lik} with the theoretically maximal reachable R^2, which depends on the proportion of success ($y_i = 1$) in the data set to ensure the value of 1 for a perfect fit, analogous to linear regression. Log likelihoods of intercept-only and risk factor-based prediction models are given by

$$l_0 = \sum_i \left(y_i \log \bar{y} + (y_i - 1) \log(1 - \bar{y})\right),$$

$$l_{pred} = \sum_i \left(y_i \log \hat{y}_i + (y_i - 1) \log(1 - \hat{y}_i)\right),$$

respectively, yielding

$$R^2_{Lik} = 1 - \exp\{(l_0 - l_{pred})(2/n)\},$$

and Nagelkerke's R^2_{Nag}

$$R^2_{Nag} = \frac{R^2_{Lik}}{1 - \exp\{l_0(2/n))\}}.$$

Correlation Pearson correlation $r_{Pearson}$ between $\hat{\boldsymbol{y}}$ and $\boldsymbol{y}$,

$$r_{Pearson}(\hat{\boldsymbol{y}}, \boldsymbol{y}) = \frac{\sum(\hat{y}_i - \bar{\hat{y}})(y_i - \bar{y})}{\sqrt{\sum(\hat{y}_i - \bar{\hat{y}})^2}\sqrt{\sum(y_i - \bar{y})^2}},$$

is analogous to linear regression's multiple correlation coefficient R. Its absolute value has limited interpretation, nevertheless, $r_{Pearson}$ is useful for comparing different predictions for the same outcome (Agresti, 2007, p.144).
Spearman correlation is a nonparametric alternative, which measures how good an arbitrary monotone function can capture the relationship between the two variables. The values $\hat{y}_i$ and y_i are replaced by their ranks $rg(\hat{y}_i)$ and $rg(y_i)$ and the Pearson correlation is calculated,

$$r_{Spearman}(\hat{\boldsymbol{y}}, \boldsymbol{y}) = r_{Pearson}(rg(\hat{\boldsymbol{y}}), rg(\boldsymbol{y})).$$

Ties are assigned the average of the ranks associated with the tied observations (van Belle and Fisher, 2004, p. 327).

Wilcoxon statistic W The Wilcoxon rank-sum test and the Mann-Whitney-U test refer to equivalent tests, in the literature the term Wilcoxon-Mann-Whitney test is also used (Bergmann et al., 2000). The test statistic is based on the sum of ranks, $rg(\hat{\boldsymbol{y}})$, for either $y_i = 1$ or $y_i = 0$ observations, with the ranks derived from the entire $\hat{\boldsymbol{y}}$ vector. Let n_0 be the number of $\hat{y}_i = 0$, and n_1 the number of $y_i = 1$, (it holds $n_0 + n_1 = n$),

then

$$W = \sum_{i=1}^{n} rg(\hat{y}_i) I(y_i = 0) - \frac{n_0(n_0+1)}{2},$$

or

$$W = \sum_{i=1}^{n} rg(\hat{y}_i) I(y_i = 1) - \frac{n_1(n_1+1)}{2},$$

which will be different in general, but lead to the same conclusions when used for statistical testing. W is equivalent to the AUC (Hanley and McNeil, 1982),

$$AUC = \frac{W}{n_0 n_1}.$$

Again, ties are assigned the average of the ranks associated with the tied observations.

Hosmer-Lemeshow The Hosmer-Lemeshow-Test (Lemeshow and Hosmer Jr, 1982; Hosmer and Lemeshow, 1980, 2000, p.147) groups the observations by deciles (if $G = 10$) of risks ($\hat{\boldsymbol{y}}$) and calculates a χ^2 measure.

$$HL = \sum_{g=1}^{G} \frac{\left(O_g - n_g \bar{\hat{y}}_g\right)^2}{n_g \bar{\hat{y}}_g (1 - \bar{\hat{y}}_g)},$$

with O_g being the sum of observed $y_i = 1$ in group g,

$$O_g = \sum_{i=1}^{n_g} y_i,$$

and $\bar{\hat{y}}_g$ is the average prediction risk in group g,

$$\bar{\hat{y}}_g = \frac{1}{n_g} \sum_{i=1}^{n_g} \hat{y}_i.$$

H_0 : No difference between observed outcome and model-predicted risk,

H_A : Observed outcome differs from prediction,

$HL \overset{a}{\sim} \chi^2(df = G-1)$ when applied to an external validation dataset and

$HL \overset{a}{\sim} \chi^2(df = G-2)$ for internal validation.

Brier Score or mean predicted squared error:

$$Brier = \frac{1}{n} \sum_{i} (y_i - \hat{y}_i)^2.$$

A perfect prediction has a score of 0. The score of a non-informative model depends on the proportion of sucesses ($y_i = 1$) in the data set. As with Nagelkerke's R^2 it can be scaled with its maximum $Brier_{max}$ for a given proportion,

$$Brier_{sc} = 1 - \frac{Brier}{Brier_{max}},$$

with

$$Brier_{max} = \bar{\hat{y}}(1 - \bar{\hat{y}})^2 + (1 - \bar{\hat{y}})\bar{\hat{y}}^2 = \bar{\hat{y}}\,(1 - \bar{\hat{y}}),$$

and $\bar{\hat{y}}$ being the arithmetic mean of $\hat{\boldsymbol{y}}$ (Steyerberg, 2009, p.257). $Brier_{sc}$ ranges between zero and one. In opposite to R^2_{Nag} the scaling depends on the predictions $\hat{\boldsymbol{y}}$ and not only on the actual outcome $\boldsymbol{y}$. This limits the use of the scaled version to assess different models on external data.

Deviance residuals depend on assumed distribution. (McCullagh and Nelder, 1989, p.34, p.39). For Bernoulli distributions, deviance residuals are given by

$$rD_i = sign(y_i - \hat{y}_i)\sqrt{2\left(y_i \log\left(\frac{y_i}{\hat{y}_i}\right) + (1 - y_i)\log\left(\frac{1 - y_i}{1 - \hat{y}_i}\right)\right)}.$$

An overall measure of goodness-of-fit is the sum of squared deviance residuals $\sum(rD_i)^2$.

Pearson residuals also depend on the assumed distribution of $\boldsymbol{y}$. They standardize the difference between y_i and $\hat{y}_i$ by its standard deviation. In case of assuming a Bernoulli distribution they are given by

$$rP_i = \frac{y_i - \hat{y}_i}{\sqrt{\hat{y}_i(1 - \hat{y}_i)}}.$$

As overall measure of goodness-of-fit the squared sum is used: $\sum rP_i^2$. Further standardized Pearson residuals exist, which use the leverage of observations and claim to have unit variance (Hosmer and Lemeshow, 2000, p.173).

Discrimination slope denotes the absolute difference in average predictions between successes and failures (Steyerberg, 2009, p.264),

$$|\bar{\hat{\boldsymbol{y}}}_{y=0} - \bar{\hat{\boldsymbol{y}}}_{y=1}|,$$

or in more computational notation,

$$\left|\frac{1}{n_0}\sum_{i=1}^{n}\hat{y}_i I(y_i = 0) - \frac{1}{n_1}\sum_{i=1}^{n}\hat{y}_i I(y_i = 1)\right|,$$

where n_0 is the number of $y_i = 0$ and n_1 the number of $y_i = 1$. Better models have a larger discrimination slope.

t-statistic (for discrimination) Similar to the discrimination slope the test statistic of the two sample t-test can be used to assess separation ability. The two samples are formed on the outcome variable $y_i = 0$ versus $y_i = 1$. Again, larger values of the test statistic imply better predictions.

Calibration-in-the-large compares the average predictions and the average outcome:

$$\bar{y} - \bar{\hat{y}},$$

with $\bar{\hat{y}} = \frac{1}{n}\sum \hat{y}_i$. Larger deviations from zero imply worse predictions, with negative sign corresponding to over-prediction (too high risks) and positive sign to under-prediction.

t-statistic (for calibration) Similar to calibration-in-the-large the test statistic of the paired t-test can be utilized, to assess the differences between predictions and outcome,

$$t = \frac{\bar{y}_D}{sd(\boldsymbol{y}_D)},$$

with $\boldsymbol{y}_D$ being the vector of differences $\boldsymbol{y} - \hat{\boldsymbol{y}}$, $\bar{y}_D$ its arithmetic mean and $sd()$ the empirical standard deviation.

Calibration slope CS is the estimated slope coefficient, $\hat{\beta}$, in a logistic regression model of true outcomes y_i on the predicted risks $\hat{y}_i$, i=1, ..., n,

$$\log\left(\frac{P(y_i = 1)}{1 - P(y_i = 1)}\right) = \alpha + \beta \log\left(\frac{\hat{y}_i}{1 - \hat{y}_i}\right),$$

$$CS \equiv \hat{\beta},$$

that is, the model predictions $\hat{y}_i$ are transformed and used as the regressor variable in the logistic model. A calibration slope for a perfectly calibrated model is 1, while coefficients lower than 1 indicate that the predictions are too extreme. Too extreme means that the observed mortality is higher than predicted for low-risk observations and lower than predicted for high-risk observations (Steyerberg et al., 2001). The calibration slope is also linked to discrimination, higher slopes imply better discrimination (Steyerberg, 2009, p.264).

Bibliography

Abbott, R. D. (1985). Logistic regresson in survival analysis. *American Journal of Epidemiology 121*(3), 465–471.

Ackerman, J. D. (2000). Abiotic pollen and pollination: Ecological, functional, and evolutionary perspectives. *Plant Systematics and Evolution 222*(1), 167–185.

Adame, P., M. d. Río, and I. Cañellas (2010). Modeling individual-tree mortality in Pyrenean oak (Quercus pyrenaica Willd.) stands. *Annals of Forest Science 67*(8), 10.

Agresti, A. (2007). *An introduction to categorical data analysis* (2nd ed.). Hoboken NJ: John Wiley & Sons.

Akaike, H. (1974). A new look at the statistical model identification. *IEEE Transactions on Automatic Control 19*(6), 716–723.

Ankerst, D. P., A. Böck, S. J. Freedland, J. Stephen Jones, A. M. Cronin, M. J. Roobol, J. Hugosson, M. W. Kattan, E. A. Klein, F. Hamdy, D. Neal, J. Donovan, D. J. Parekh, H. Klocker, W. Horninger, A. Benchikh, G. Salama, A. Villers, D. M. Moreira, F. H. Schröder, H. Lilja, A. J. Vickers, and I. M. Thompson (2012). Evaluating the prostate cancer prevention trial high grade prostate cancer risk calculator in 10 international biopsy cohorts: results from the prostate biopsy collaborative group. *World Journal of Urology*. Accepted on 22.04.2012.

Ankerst, D. P., A. Böck, S. J. Freedland, I. M. Thompson, A. M. Cronin, M. J. Roobol, J. Hugosson, J. Stephen Jones, M. W. Kattan, E. A. Klein, F. Hamdy, D. Neal, J. Donovan, D. J. Parekh, H. Klocker, W. Horninger, A. Benchikh, G. Salama, A. Villers, D. M. Moreira, F. H. Schröder, H. Lilja, and A. J. Vickers (2012). Evaluating the PCPT risk calculator in ten international biopsy cohorts: results from the prostate biopsy collaborative group. *World Journal of Urology 30*(2), 181–187.

Ankerst, D. P., J. Groskopf, J. R. Day, A. Blase, H. Rittenhouse, B. H. Pollock, C. Tangen, D. Parekh, R. J. Leach, and I. Thompson (2008). Predicting prostate cancer risk through incorporation of prostate cancer gene 3. *The Journal of Urology 180*(4), 1303–1308; discussion 1308.

Ankerst, D. P., R. Miyamoto, P. V. Nair, B. H. Pollock, I. M. Thompson, and D. J. Parekh (2009). Yearly prostate specific antigen and digital rectal examination fluctuations in a screened population. *The Journal of Urology 181*(5), 2071–2075; discussion 2076.

Antoniak, C. E. (1974). Mixtures of Dirichlet processes with applications to Bayesian nonparametric problems. *The Annals of Statistics*, 1152–1174.

Aranzana, M. J., S. Kim, K. Y. Zhao, E. Bakker, M. Horton, K. Jakob, C. Lister, J. Molitor, C. Shindo, and C. L. Tang (2005). Genome-wide association mapping in Arabidopsis identifies previously known flowering time and pathogen resistance genes. *PLOS Genetics 1*(5), e60.

Assmann, E. (1961). *Waldertragskunde: Organische Produktion, Struktur, Zuwachs und Ertrag von Waldbeständen*. München: BLV Verlagsgesellschaft.

Badawi, M., Y. V. Reddy, Z. Agharbaoui, Y. Tominaga, J. Danyluk, F. Sarhan, and M. Houde (2008). Structure and functional analysis of wheat ICE (inducer of CBF expression) genes. *Plant Cell Physiology 49*(8), 1237–1249.

Baga, M., S. V. Chodaparambil, A. E. Limin, M. Pecar, D. B. Fowler, and R. N. Chibbar (2007). Identification of quantitative trait loci and associated candidate genes for low-temperature tolerance in cold-hardy winter wheat. *Functional and Integrative Genomics 7*(1), 53–68.

Balding, D. (2013). Kinship and heritability: some recent developments. *Presentation at the 5th Paris Workshop on Genomic Epidemiology*. `http://innovationcenter.netne.net/paris_workshop/downloads/presentations/BaldingDavid_Paris2013.pdf`. Accessed on 30.07.2013.

Bates, D. and M. Mächler (2010). *lme4: Linear mixed-effects models using S4 classes*. R package version 0.999375-37.

Bateson, W. (1902). *Mendel's principles of heredity*. University Press.

Becker, B. J. and M.-J. Wu (2007). The synthesis of regression slopes in meta-analysis. *Statistical Science 22*(3), 414–429.

Beggs, P. J. (2004). Impacts of climate change on aeroallergens: past and future. *Clinical and Experimental Allergy 34*(10), 1507–1513.

Bergmann, R., J. Ludbrook, and W. P. J. M. Spooren (2000). Different outcomes of the Wilcoxon-Mann-Whitney test from different statistics packages. *The American Statistician 54*(1), 72–77.

Bigler, C. and H. Bugmann (2003). Growth-dependent tree mortality models based on tree rings. *Canadian Journal of Forest Research 33*(2), 210–221.

Bivand, R., E. J. Pebesma, and V. G. Rubio (2008). *Applied spatial data: analysis with R*. New York: Springer.

Böck, A., J. Dieler, P. Biber, H. Pretzsch, and D. P. Ankerst (2013). Predicting tree mortality for european beech in southern germany using spatially explicit competition indices. *Forest Science*. Accepted.

Bolmgren, K., O. Eriksson, and H. P. Linder (2003). Contrasting flowering phenology and species richness in abiotically and biotically pollinated angiosperms. *Evolution 57*(9), 2001–2011.

Bravo-Oviedo, A., H. Sterba, M. del Río, and F. Bravo (2006). Competition-induced mortality for Mediterranean Pinus pinaster Ait. and P. sylvestris L. *Forest Ecology and Management 222*(1-3), 88–98.

Breslow, N. E., N. E. Day, et al. (1980). *Statistical methods in cancer research. Vol. 1. The analysis of case-control studies.* Distributed for IARC by WHO.

Bretz, F., T. Hothorn, and P. Westfall (2011). *Multiple Comparisons Using R*. New York: CRC Press.

Brown, H. and R. Prescott (2006). *Applied mixed models in medicine*. Hoboken NJ: John Wiley & Sons.

Brunner, E. and U. Munzel (2000). The nonparametric Behrens-Fisher problem: Asymptotic theory and a small-sample approximation. *Biometrical Journal 42*(1), 17–25.

Buchman, R. G., S. P. Pederson, and N. R. Walters (1983). A tree survival model with application to species of the great lakes region. *Canadian Journal of Forest Research 13*, 601–608.

Burgman, M., W. Incoll, P. Ades, I. Ferguson, T. Fletcher, and A. Wohlers (1994). Mortality models for mountain and alpine ash. *Forest Ecology and Management 67*(1-3), 319–327.

Campoli, C., M. A. Matus-Cadiz, C. J. Pozniak, L. Cattivelli, and D. B. Fowler (2009). Comparative expression of Cbf genes in the Triticeae under different acclimation induction temperatures. *Molecular Genetetics and Genomics 282*(2), 141–152.

Canty, A. and B. Ripley (2010). *boot: Bootstrap R (S-Plus) functions*. R package version 1.2-43.

Carstensen, B. (2005). Demography and epidemiology: Practical use of the lexis diagram in the computer age. or: Who needs the cox-model anyway? *Annual meeting of Finnish Statistical Society*. `http://publichealth.ku.dk/sections/biostatistics/reports/2006/`.

Cavadas, V., L. Osório, F. Sabell, F. Teves, F. Branco, and M. Silva-Ramos (2010). Prostate cancer prevention trial and European randomized study of screening for prostate cancer risk calculators: a performance comparison in a contemporary screened cohort. *European Urology 58*(4), 551–558.

Chinnusamy, V., J. Zhu, and J. K. Zhu (2007). Cold stress regulation of gene expression in plants. *Trends in Plant Science 12*(10), 444–451.

Choi, D. W., B. Zhu, and T. J. Close (1999). The barley (Hordeum vulgare L.) dehydrin multigene family: Sequences, allele types, chromosome assignments, and expression characteristics of 11 Dhn genes of cv Dicktoo. *Theoretical and Applied Genetics 98*(8), 1234–1247.

Cleveland, W. S., E. Grosse, and W. M. Shyu (1992). Local regression models. In J. M. Chambers and T. Hastie (Eds.), *Statistical models in S*, pp. 309–376. New York: Chapman and Hall/CRC.

Clifford, D. and P. McCullagh (2012). *regress: The regress package*. R package version 1.3-8.

Cox, D. R. (1972). Regression models and life-tables. *Journal of the Royal Statistical Society. Series B (Statistical Methodology) 34*(2), 187–220.

Cupples, L. A., R. B. D'Agostino, K. Anderson, and W. B. Kannel (1988). Comparison of baseline and repeated measure covariate techniques in the Framingham Heart Study. *Statistics in Medicine 7*(1-2), 205–222.

D'Agostino, R. B., M. L. Lee, A. J. Belanger, L. A. Cupples, K. Anderson, and W. B. Kannel (1990). Relation of pooled logistic regression to time dependent Cox regression analysis: the Framingham Heart Study. *Statistics in Medicine 9*(12), 1501–1515.

D'Amato, G. and L. Cecchi (2008). Effects of climate change on environmental factors in respiratory allergic diseases. *Clinical and Experimental Allergy 38*(8), 1264–1274.

D'Amato, G., L. Cecchi, S. Bonini, C. Nunes, I. Annesi-Maesano, H. Behrendt, G. Liccardi, T. Popov, and P. Van Cauwenberge (2007). Allergenic pollen and pollen allergy in Europe. *Allergy 62*(9), 976–990.

Das, A., J. Battles, P. J. van Mantgem, and N. L. Stephenson (2008). Spatial elements of mortality risk in old-growth forests. *Ecology 89*(6), 1744–1756.

Das, A. J., J. J. Battles, N. L. Stephenson, and P. J. van Mantgem (2007). The relationship between tree growth patterns and likelihood of mortality: a study of two tree species in the sierra nevada. *Canadian Journal of Forest Research 37*, 580–597.

Devlin, B. and K. Roeder (1999). Genomic control for association studies. *Biometrics 55*, 997–1004.

Dhanaraj, A. L., N. W. Alkharouf, H. S. Beard, I. B. Chouikha, B. F. Matthews, H. Wei, R. Arora, and L. J. Rowland (2007). Major differences observed in transcript profiles of blueberry during cold acclimation under field and cold room conditions. *Planta 225*(3), 735–751.

Dobbertin, M. and G. S. Biging (1998). Using the non-parametric classifier CART to model forest tree mortality. *Forest Science 44*(4), 507–516.

Dorffling, K., S. Schulenburg, G. Lesselich, and H. Dorffling (1990). Abscisic acid and proline levels in cold hardened winter wheat leaves in relation to variety-specific differences in freezing resistance. *Journal of Agronomy and Crop Science 165*(4), 230–239.

Dubrule, O. (1984). Comparing splines and Kriging. *Computers & Geosciences 10*(2), 327–338.

Duchateau, L., P. Janssen, and J. Rowlands (1998). *Linear mixed models. An introduction with applications in veterinary research*. ILRI (International Livestock Research Institute).

Efron, B. and R. Tibshirani (1994). *An Introduction to the Bootstrap*. New York: Chapman and Hall/CRC.

Eid, T. and E. Tuhus (2001). Models for individual tree mortality in norway. *Forest Ecology and Management 154*(1-2), 69–84.

Eilers, P. and B. Marx (1996). Flexible smoothing with B-splines and penalties. *Statistical Science 11*(2), 89–121.

Esch, R. (2004). Grass pollen allergens. In R. Lockey, S. Bukantz, and J. Bousquet (Eds.), *Allergens and Allergen Immunotherapy*, pp. 185–206. New York: Marcel Dekker.

Eskicorapci, S. Y., D. E. Baydar, C. Akbal, M. Sofikerim, M. Günay, S. Ekici, and H. Ozen (2004). An extended 10-core transrectal ultrasonography guided prostate biopsy protocol improves the detection of prostate cancer. *European Urology 45*(4), 444–449.

European Randomized study of Screening for Prostate Cancer (2013). Background to Study. `http://http://www.erspc-media.org/erspc-background/`. Accessed on 10.10.2013.

Eyre, S. J., D. P. Ankerst, J. T. Wei, P. V. Nair, M. M. Regan, G. Bueti, J. Tang, M. A. Rubin, M. Kearney, I. M. Thompson, and M. G. Sanda (2009). Validation in a multiple urology practice cohort of the Prostate Cancer Prevention Trial calculator for predicting prostate cancer detection. *The Journal of Urology 182*(6), 2653–2658.

Fahrmeir, L., T. Kneib, and S. Lang (2007). *Regression: Modelle, Methoden und Anwendungen*. Berlin; Heidelberg: Springer.

Fahrmeir, L., R. Künstler, I. Pigeot, and G. Tutz (2003). *Statistik. Der Weg zur Datenanalyse* (4 ed.). Berlin: Springer.

Fan, Z., J. M. Kabrick, and S. R. Shifley (2006). Classification and regression tree based survival analysis in oak-dominated forests of Missouri's Ozark highlands. *Canadian Journal of Forest Research 36*, 1740–1748.

Ferguson, T. S. (1973). A Bayesian analysis of some nonparametric problems. *The Annals of Statistics*, 209–230.

Fitter, A. H. and R. S. R. Fitter (2002). Rapid changes in flowering time in british plants. *Science (New York, N.Y.) 296*(5573), 1689–1691.

Fitzmaurice, G. M., N. M. Laird, and J. H. Ware (2004). *Applied Longitudinal Analysis*. Wiley Series in Probability and Statistics. Hoboken NJ: John Wiley & Sons.

Fortin, M., S. Bédard, J. DeBlois, and S. Meunier (2008). Predicting individual tree mortality in northern hardwood stands under uneven-aged management in southern Québec, Canada. *Annals of Forest Science 65*(2), 205–205.

Fowler, D. B., L. V. Gusta, and N. J. Tyler (1981). Selection for winterhardiness in wheat. III. screening methods. *Crop Science 21*(6), 896–901.

Fowler, D. B. and A. E. Limin (1987). Exploitable genetic variability for cold tolerance in commercially grown cereals. *Canadian Journal of Plant Science 67*(1), 278–278.

Francia, E., D. Barabaschi, A. Tondelli, G. Laido, F. Rizza, A. M. Stanca, M. Busconi, C. Fogher, E. J. Stockinger, and N. Pecchioni (2007). Fine mapping of a HvCBF gene cluster at the frost resistance locus Fr-H2 in barley. *Theoretical and Applied Genetics 115*(8), 1083–1091.

Fridman, J. and G. Stahl (2001). A three-step approach for modelling tree mortality in swedish forests. *Scandinavian Journal of Forest Research 16*(5), 455–466.

Friedman, J. and S. C. H. Barrett (2009). Wind of change: new insights on the ecology and evolution of pollination and mating in wind-pollinated plants. *Annals of Botany 103*(9), 1515–1527.

Galiba, G., S. A. Quarrie, J. Sutka, A. Morgounov, and J. W. Snape (1995). RFLP mapping of the vernalization (Vrn1) and frost resistance (Fr1) genes on chromosome 5A of wheat. *Theoretical and Applied Genetics 90*(7-8), 1174–1179.

Gbur, E. E., W. Stroup, K. McCarter, S. Durham, L. Young, M. Christman, M. West, and M. Kramer (2012). *Analysis of generalized linear mixed models in the agricultural and natural resources sciences*. Madison: American Society of Agronomy.

Gneiting, T. and A. E. Raftery (2007). Strictly proper scoring rules, prediction, and estimation. *Journal of the American Statistical Association 102*(477), 359–378.

Green, P. J. (1995). Reversible jump Markov chain Monte Carlo computation and Bayesian model determination. *Biometrika 82*(4), 711–732.

Gusta, L. V., R. Willen, P. Fu, A. J. Robertson, and G. H. Wu (1997). Genetic and environmental control of winter survival of winter cereals. *Acta Agronomica Academiae Scientiarum Hungaricae 45*(3), 231–240.

Hackauf, B. and P. Wehling (2002). Identification of microsatellite polymorphisms in an expressed portion of the rye genome. *Plant Breeding 121*(1), 17–25.

Hamilton, D. A. (1986). A logistic model of mortality in thinned and unthinned mixed conifer stands of Northern Idaho. *Forest Science 32*(4), 989–1000.

Hanagal, D. D. (2011). *Modeling Survival Data Using Frailty Models*. New York: Chapman & Hall/CRC.

Hanley, J. A. and B. J. McNeil (1982). The meaning and use of the area under a receiver operating characteristic (ROC) curve. *Radiology 143*(1), 29–36.

Harjes, C. E., T. R. Rocheford, L. Bai, T. P. Brutnell, C. B. Kandianis, S. G. Sowinski, A. E. Stapleton, R. Vallabhaneni, M. Williams, and E. T. Wurtzel (2008). Natural genetic variation in lycopene epsilon cyclase tapped for maize biofortification. *Science 319*(5861), 330–333.

Harrell, F., K. Lee, and D. Mark (1996). Tutorial in biostatistics multivariable prognostic models: issues in developing models, evaluating assumptions and adequacy, and measuring and reducing errors. *Statistics in Medicine 15*, 361–387.

Hasenauer, H., D. Merkl, and M. Weingartner (2001). Estimating tree mortality of Norway spruce stands with neural networks. *Advances in Environmental Research 5*(4), 405–414.

Hastie, T. and R. Tibshirani (1990). *Generalized additive models*. New York: Chapman and Hall/CRC.

Hayes, B. J. and M. E. Goddard (2008). Technical note: prediction of breeding values using marker-derived relationship matrices. *Journal of Animal Science 86*(9), 2089–2092.

Hernandez, D. J., M. Han, E. B. Humphreys, L. A. Mangold, S. S. Taneja, S. J. Childs, G. Bartsch, and A. W. Partin (2009). Predicting the outcome of prostate biopsy: comparison of a novel logistic regression-based model, the prostate cancer risk calculator, and prostate-specific antigen level alone. *BJU International 103*(5), 609–614.

Ho, H. J. and T.-I. Lin (2010). Robust linear mixed models using the skew t distribution with application to schizophrenia data. *Biometrical Journal 52*(4), 449–469.

Hommo, L. M. (1994). Hardening of some winter wheat (Triticum aestivum L.), rye (Secale cereals L.), triticale (Triticosecale Wittmack) and winter barley (Hordeum vulgare L.) cultivars during autumn and the final winter survival in Finland. *Plant Breeding 112*(4), 285–293.

Hosmer, D. and S. Lemeshow (1980). Goodness of fit tests for the multiple logistic regression model. *Communications in Statistics – Theory and Methods 9*(10), 1043–1069.

Hosmer, D. and S. Lemeshow (2000). *Applied logistic regression*. Hoboken NJ: John Wiley & Sons.

Hothorn, T., F. Bretz, and P. Westfall (2008). Simultaneous inference in general parametric models. *Biometrical Journal 50*(3), 346—363.

Houde, M., R. S. Dhindsa, and F. Sarhan (1992). A molecular marker to select for freezing tolerance in Gramineae. *Molecular Genetics and Genomics 234*(1), 43–48.

Huynen, M., B. Menne, H. Behrendt, R. Bertollini, S. Bonini, R. Brandao, et al. (2003). Phenology and human health: allergic disorders. *Report of a WHO meeting, Rome, Italy 16*, 17.

Ingvarsson, P. K. and N. R. Street (2010). Association genetics of complex traits in plants. *New Phytologist 189*(4), 909–922.

Izenman, A. J. (2008). *Modern multivariate statistical techniques: regression, classification, and manifold learning*. New York: Springer.

Jaeger, S. (2008). Exposure to grass pollen in europe. *Clinical and Experimental Allergy Reviews 8*(1), 2–6.

Janssen, K. J. M., A. R. T. Donders, J. Harrell, Frank E, Y. Vergouwe, Q. Chen, D. E. Grobbee, and K. G. M. Moons (2010). Missing covariate data in medical research: to impute is better than to ignore. *Journal of Clinical Epidemiology 63*(7), 721–727.

Jara, A., T. E. Hanson, F. A. Quintana, P. Müller, and G. L. Rosner (2011). Dppackage: Bayesian non-and semi-parametric modelling in R. *Journal of Statistical Software 40*(5), 1–30.

Joe, H. (1997). *Multivariate models and dependence concepts*, Volume 73.

Kalbfleisch, J. D. and R. L. Prentice (2002). *The Statistical Analysis of Failure Time Data* (2 ed.). Hoboken NJ: John Wiley & Sons.

Kattan, M. W. (2011). Factors affecting the accuracy of prediction models limit the comparison of rival prediction models when applied to separate data sets. *European Urology 59*(4), 566–567.

Khlestkina, E. K., H. M. T. Ma, E. G. Pestsova, M. S. Roder, S. V. Malyshev, V. Korzun, and A. Borner (2004). Mapping of 99 new microsatellite-derived loci in rye (Secale cereale L.) including 39 expressed sequence tags. *Theoretical and Applied Genetics 109*(4), 725–732.

Kiernan, D., E. Bevilacqua, R. Nyland, and L. Zhang (2009). Modeling tree mortality in low-to medium-density uneven-aged hardwood stands under a selection system using generalized estimating equations. *Forest Science 55*(4), 343–351.

King, G. and L. Zeng (2001). Logistic regression in rare events data. *Political Analysis 9*(2), 137–163.

Kleinman, K. P. and J. G. Ibrahim (1998a). A semi-parametric Bayesian approach to generalized linear mixed models. *Statistics in Medicine 17*(22), 2579–2596.

Kleinman, K. P. and J. G. Ibrahim (1998b). A semiparametric Bayesian approach to the random effects model. *Biometrics 54*(3), 921.

Kneib, T. (2006). Mixed model-based inference in geoadditive hazard regression for interval-censored survival times. *Computational Statistics and Data Analysis 51*(2), 777–792.

Kneib, T. and L. Fahrmeir (2004). A mixed model approach for structured hazard regression. *SFB 386 Discussion Paper 400, University of Munich*.

Koch, E., A. Donelly, W. Lipa, A. Menzel, and J. Nekovář (Eds.) (2009). *Final Scientific Report of COST 725: Establishing a European Dataplatform for Climatological Applications*. European Cooperation in the field of Scientific and Technical Research.

Laaidi, M. (2001). Regional variations in the pollen season of Betula in Burgundy: two models for predicting the start of the pollination. *Aerobiologia 17*(3), 247–254.

Landwehr, J. M., D. Pregibon, and A. C. Shoemaker (1984). Graphical methods for assessing logistic regression models. *Journal of the American Statistical Association 79*(385), 61–71.

Lange, K. L., R. J. Little, and J. M. Taylor (1989). Robust statistical modeling using the t distribution. *Journal of the American Statistical Association 84*(408), 881–896.

Lemeshow, S. and D. Hosmer Jr (1982). A review of goodness of fit statistics for use in the development of logistic regression models. *American Journal of Epidemiology 115*(1), 92–106.

Li, Y., A. Böck, G. Haseneyer, V. Korzun, P. Wilde, C.-C. Schön, D. P. Ankerst, and E. Bauer (2011). Association analysis of frost tolerance in rye using candidate genes and phenotypic data from controlled, semi-controlled, and field phenotyping platforms. *BMC Plant Biology 11*, 146.

Li, Y. L., G. Haseneyer, C.-C. Schön, D. P. Ankerst, V. Korzun, P. Wilde, and E. Bauer (2011). High levels of nucleotide diversity and fast decline of linkage disequilibrium in rye (Secale cereale L.) genes involved in frost response. *BMC Plant Biology 11*, 6.

Lu, P., Q. Yu, J. Liu, and X. Lee (2006). Advance of tree-flowering dates in response to urban climate change. *Agricultural and Forest Meteorology 138*(1–4), 120–131.

MacEachern, S. N. (1994). Estimating normal means with a conjugate style Dirichlet process prior. *Communications in Statistics–Simulation and Computation 23*(3), 727–741.

Mackay, T. F. C. (2001). The genetic architecture of quantitative traits. *Annual Review of Genetics 35*, 303–339.

Malosetti, M., C. G. van der Linden, B. Vosman, and F. A. van Eeuwijk (2007). A mixed-model approach to association mapping using pedigree information with an illustration of resistance to phytophthora infestans in potato. *Genetics 175*(2), 879–889.

Marin, J.-M. and C. P. Robert (2007). *Bayesian core: a practical approach to computational Bayesian statistics*. New York: Springer.

Mathews, K. L., M. Malosetti, S. Chapman, L. McIntyre, M. Reynolds, R. Shorter, and F. Eeuwijk (2008). Multi-environment QTL mixed models for drought stress adaptation in wheat. *Theoretical and Applied Genetics 117*(7), 1077–1091.

McCullagh, P. and J. A. Nelder (1989). *Generalized Linear Models* (2 ed.). New York: Chapman and Hall/CRC.

McCulloch, C. (2008). Joint modelling of mixed outcome types using latent variables. *Statistical Methods in Medical Research 17*(1), 53–73.

McCulloch, C. E. and S. R. Searle (2001). *Generalized, Linear and Mixed Models* (1 ed.). Hoboken NJ: Wiley & Sons.

McIntosh, M. W. and M. S. Pepe (2002). Combining several screening tests: Optimality of the risk score. *Biometrics 58*(3), 657–664.

McLauchlan, K., C. Barnes, and J. Craine (2011). Interannual variability of pollen productivity and transport in mid-North America from 1997 to 2009. *Aerobiologia 27*(3), 181–189.

Menzel, A., T. H. Sparks, N. Estrella, E. Koch, A. Aasa, R. Ahas, K. Alm-Kübler, P. Bissolli, O. Braslavská, A. Briede, F. M. Chmielewski, Z. Crepinsek, Y. Curnel, Å. Dahl, C. Defila, A. Donnelly, Y. Filella, K. Jatczak, F. Måge, A. Mestre, Ø. Nordli, J. Peñuelas, P. Pirinen, V. Remišová, H. Scheifinger, M. Striz, A. Susnik, A. J. H. Van Vliet, F.-E. Wielgolaski, S. Zach, and A. Zust (2006). European phenological response to climate change matches the warming pattern. *Global Change Biology 12*(10), 1969–1976.

Monserud, R. A. (1976). Simulation of forest tree mortality. *Forest Science 22*(4), 438–444.

Monserud, R. A. and H. Sterba (1999). Modeling individual tree mortality for Austrian forest species. *Forest Ecology and Management 113*(2-3), 109–123.

Montgomery, D. C. (2001). *Design and analysis of experiments* (5 ed.). Hoboken NJ: John Wiley & Sons.

Mood, C. (2010). Logistic regression: Why we cannot do what we think we can do, and what we can do about it. *European Sociological Review 26*(1), 67–82.

Mrode, R. and R. Thompson (2005). *Linear models for the prediction of animal breeding values*. Wallingford: CABI.

Nagelkerke, N. (1991). A note on a general definition of the coefficient of determination. *Biometrika 78*(3), 691–692.

Nelder, J. A. (1977). A Reformulation of Linear Models. *Journal of the Royal Statistical Society. Series A (Statistics in Society) 140*(1), 48–77.

Nguyen, C. T., C. Yu, A. Moussa, M. W. Kattan, and J. S. Jones (2010). Performance of prostate cancer prevention trial risk calculator in a contemporary cohort screened for prostate cancer and diagnosed by extended prostate biopsy. *The Journal of Urology 183*(2), 529–533.

Novillo, F., J. M. Alonso, J. R. Ecker, and J. Salinas (2004). CBF2/DREB1C is a negative regulator of CBF1/DREB1B and CBF3/DREB1A expression and plays a central role in stress tolerance in Arabidopsis. *Proceedings of the National Academy of Sciences of the United States of America 101*(11), 3985–3990.

O'Connell, M. J., C. S. Smith, P. E. Fitzpatrick, C. O. Keane, J. M. Fitzpatrick, M. Behan, H. F. Fenlon, and J. G. Murray (2004). Transrectal ultrasound-guided biopsy of the prostate gland: value of 12 versus 6 cores. *Abdominal Imaging 29*(1), 132–136.

Oliveira, M., V. Marques, A. P. Carvalho, and A. Santos (2011). Head-to-head comparison of two online nomograms for prostate biopsy outcome prediction. *BJU International 107*(11), 1780–1783.

Palahi, M., T. Pukkala, J. Miina, and G. Montero (2003). Individual-tree growth and mortality models for Scots pine (Pinus sylvestris L.) in north-east Spain. *Annals of Forest Science 60*(1), 1–10.

Parekh, D. J., D. P. Ankerst, B. A. Higgins, J. Hernandez, E. Canby-Hagino, T. Brand, D. A. Troyer, R. J. Leach, and I. M. Thompson (2006). External validation of the prostate cancer prevention trial risk calculator in a screened population. *Urology 68*(6), 1152–1155.

Phillips, P. C. (2008). Epistasis – the essential role of gene interactions in the structure and evolution of genetic systems. *Nature Reviews Genetics 9*(11), 855–867.

Pinheiro, J. C. and D. M. Bates (2000). *Mixed Effects Models in S and S-Plus*. Statistics and Computing. New York: Springer.

Pregibon, D. (1981). Logistic regression diagnostics. *The Annals of Statistics*, 705–724.

Pretzsch, H. (1992). Modellierung der Kronenkonkurrenz von Fichte und Buche in Rein- und Mischbeständen. *Allgemeine Forst- und Jagdzeitung 163*(11/12), 203–213.

Pretzsch, H. (2001). *Modellierung des Waldwachstums*. Blackwell Wissenschafts-Verlag.

Pretzsch, H., P. Biber, and J. Dursky (2002). The single tree-based stand simulator SILVA: construction, application and evaluation. *Forest Ecology and Management 162*(1), 3–21.

Prior, C., F. Guillen-Grima, J. E. Robles, D. Rosell, J. M. Fernandez-Montero, X. Agirre, R. Catena, and A. Calvo (2010). Use of a combination of biomarkers in serum and urine to improve detection of prostate cancer. *World Journal of Urology 28*(6), 681–686.

Pritchard, J. K., M. Stephens, N. A. Rosenberg, and P. Donnelly (2000). Association mapping in structured populations. *American Journal of Human Genetics 67*(1), 170–181.

R Core Team (2012). *R: A Language and Environment for Statistical Computing*. Vienna, Austria: R Foundation for Statistical Computing.

Rabinowitz, D., J. K. Rapp, V. L. Sork, B. J. Rathcke, G. A. Reese, and J. C. Weaver (1981). Phenological properties of wind- and insect-pollinated prairie plants. *Ecology 62*(1), 49–56.

Rafalski, A. (2002). Applications of single nucleotide polymorphisms in crop genetics. *Current Opinion in Plant Biology 5*(2), 94–100.

Rasmussen, A. (2002). The effects of climate change on the birch pollen season in Denmark. *Aerobiologia 18*(3), 253–265.

Rathbun, L. C., V. LeMay, and N. Smith (2010). Modeling mortality in mixed-species stands of coastal British Columbia. *Canadian Journal of Forest Research 40*, 1517–1528.

Regal, P. J. (1982). Pollination by wind and animals: Ecology of geographic patterns. *Annual Review of Ecology and Systematics 13*, 497–524.

Reif, J. C., A. E. Melchinger, and M. Frisch (2005). Genetical and mathematical properties of similarity and dissimilarity coefficients applied in plant breeding and seed bank management. *Crop Science 45*(1), 1–7.

Rogers, C. A., P. M. Wayne, E. A. Macklin, M. L. Muilenberg, C. J. Wagner, P. R. Epstein, and F. A. Bazzaz (2006). Interaction of the onset of spring and elevated atmospheric CO2 on ragweed (Ambrosia artemisiifolia L.) pollen production. *Environmental health perspectives 114*(6), 865–869.

Rogowsky, P. M., F. L. Y. Guidet, P. Langridge, K. W. Shepherd, and R. M. D. Koebner (1991). Isolation and characterisation of wheat-rye recombinants involving chromosome arm 1DS of wheat. *Theoretical and Applied Genetics 82*(5), 537–544.

Rose, C. E., D. B. Hall, B. D. Shiver, M. L. Clutter, and B. Borders (2006). A multilevel approach to individual tree survival prediction. *Forest Science 52*(1), 31–43.

Rosenzweig, C., G. Casassa, D. J. Karoly, A. Imeson, C. Liu, A. Menzel, S. Rawlins, T. L. Root, B. Seguin, P. Tryjanowski, et al. (2007). Assessment of observed changes and responses in natural and managed systems. In M. L. Parry (Ed.), *Climate Change 2007: Impacts, Adaptation and Vulnerability: Working Group II Contribution to the Fourth Assessment Report of the IPCC Intergovernmental Panel on Climate Change.*, pp. 79–131. Cambridge University Press.

Rousson, V. and T. Zumbrunn (2011). Decision curve analysis revisited: overall net benefit, relationships to ROC curve analysis, and application to case-control studies. *BMC Medical Informatics and Decision Making 11*(1), 45.

Roy, J., X. Lin, and L. M. Ryan (2003). Scaled marginal models for multiple continuous outcomes. *Biostatistics 4*(3), 371–383.

Rozas, J., J. C. Sanchez-DelBarrio, X. Messeguer, and R. Rozas (2003). DnaSP, DNA polymorphism analyses by the coalescent and other methods. *Bioinformatics 19*(18), 2496–2497.

Saulescu, N. N. and H. J. Braun (2001). Cold tolerance. In M. P. Reynolds, J. Ortiz-Monasterio, and A. McNab (Eds.), *Application of Physiology in Wheat Breeding*, pp. 111–123.

Schober, R. (1967). Buchen-Ertragstafel für mäßige und starke Durchforstung. In *Die Rotbuche 1971*, Volume 43/44 of *Schriften der Forstlichen Fakultät Göttingen und der Niedersächsischen Forstlichen Versuchsanstalt*, pp. 333. Frankfurt am Main: JD Sauerländer's Verlag.

Schwarz, G. (1978). Estimating the dimension of a model. *The Annals of Statistics 6*(2), 461–464.

SILVA website (2013). Chair for Forest Growth and Yield, Technische Universiät München. `http://www.wwk.forst.tu-muenchen.de/research/methods/modelling/silva/`. Accessed on 28.02.2013.

Skrondal, A. and S. Rabe-Hesketh (2009). Prediction in multilevel generalized linear models. *Journal of the Royal Statistical Society. Series A (Statistics in Society) 172*(3), 659–687.

Steyerberg, E. W. (2009). *Clinical prediction models: a practical approach to development, validation, and updating*. New York: Springer.

Steyerberg, E. W., F. E. Harrell Jr, G. J. Borsboom, M. Eijkemans, Y. Vergouwe, and J. F. Habbema (2001). Internal validation of predictive models: Efficiency of some procedures for logistic regression analysis. *Journal of Clinical Epidemiology 54*(8), 774–781.

Steyerberg, E. W., A. J. Vickers, N. R. Cook, T. Gerds, M. Gonen, N. Obuchowski, M. J. Pencina, and M. W. Kattan (2010). Assessing the performance of prediction models. *Epidemiology 21*(1), 128–138.

Stich, B., J. Mohring, H. P. Piepho, M. Heckenberger, E. S. Buckler, and A. E. Melchinger (2008). Comparison of mixed-model approaches for association mapping. *Genetics 178*(3), 1745–1754.

Szumilas, M. (2010). Explaining odds ratios. *Journal of the Canadian Academy of Child and Adolescent Psychiatry 19*(3), 227–229.

Takenaka, A., R. Hara, Y. Hyodo, T. Ishimura, Y. Sakai, H. Fujioka, T. Fujii, Y. Jo, and M. Fujisawa (2006). Transperineal extended biopsy improves the clinically significant prostate cancer detection rate: a comparative study of 6 and 12 biopsy cores. *International Journal of Urology 13*(1), 10–14.

Tester, M. and P. Langridge (2010). Breeding technologies to increase crop production in a changing world. *Science 327*(5967), 818–822.

Thomashow, M. F. (1999). Plant cold acclimation: Freezing tolerance genes and regulatory mechanisms. *Annual Review of Plant Physiology 50*, 571–599.

Thompson, I. M. and D. P. Ankerst (2012). The benefits of risk assessment tools for prostate cancer. *European Urology 61*(4), 662–663.

Thompson, I. M., D. P. Ankerst, C. Chi, P. J. Goodman, C. M. Tangen, M. S. Lucia, Z. Feng, H. L. Parnes, and J. Coltman, Charles A (2006). Assessing prostate cancer risk: results from the prostate cancer prevention trial. *Journal of the National Cancer Institute 98*(8), 529–534.

Thornsberry, J. M., M. M. Goodman, J. Doebley, S. Kresovich, D. Nielsen, and E. S. Buckler (2001). Dwarf8 polymorphisms associate with variation in flowering time. *Nature Genetics 28*(3), 286–289.

Timm, N. H. (2002). *Applied Multivariate Analysis*. New York: Springer.

Tom, F. (2006). An introduction to ROC analysis. *Pattern Recognition Letters 27*, 861–874.

Tutz, G. (2000). *Die Analyse kategorialer Daten*. München, Wien, Oldenbourg: Oldenbourg Wissenschaftsverlag.

Vagujfalvi, A., G. Galiba, L. Cattivelli, and J. Dubcovsky (2003). The cold-regulated transcriptional activator Cbf3 is linked to the frost-tolerance locus Fr-A2 on wheat chromosome 5A. *Molecular Genetics and Genomics 269*(1), 60–67.

van Belle, G. and L. Fisher (2004). *Biostatistics: a methodology for the health sciences*. Hoboken NJ: John Wiley & Sons.

van Buuren, S. (2007). Multiple imputation of discrete and continuous data by fully conditional specification. *Statistical Methods in Medical Research 16*(3), 219–242.

van den Bergh, R. C. N., M. J. Roobol, T. Wolters, P. J. van Leeuwen, and F. H. Schröder (2008). The prostate cancer prevention trial and European randomized study of screening for prostate cancer risk calculators indicating a positive prostate biopsy: a comparison. *BJU International 102*(9), 1068–1073.

Veall, M. and K. Zimmermann (1996). Pseudo-r2 measures for some common limited dependent variable models. *Journal of Economic Surveys 10*(3), 241–259.

Venables, W. N. and B. D. Ripley (1999). *Modern applied statistics with S-PLUS*. New York: Springer.

Vickers, A. J. (2008). Decision curve analysis. *Presentation at the International Symposium: Measuring the Accuracy of Prediction Models*. `http://www.lerner.ccf.org/qhs/outcomes/documents/vickers.pdf`. Accessed on 30.09.2013.

Vickers, A. J. and A. M. Cronin (2010). Everything you always wanted to know about evaluating prediction models (but were too afraid to ask). *Urology 76*(6), 1298–1301.

Vickers, A. J., A. M. Cronin, M. J. Roobol, J. Hugosson, J. S. Jones, M. W. Kattan, E. Klein, F. Hamdy, D. Neal, J. Donovan, D. J. Parekh, D. P. Ankerst, G. Bartsch, H. Klocker, W. Horninger, A. Benchikh, G. Salama, A. Villers, S. J. Freedland, D. M. Moreira, F. H. Schröder, and H. Lilja (2010). The relationship between prostate-specific antigen and prostate cancer risk: the prostate biopsy collaborative group. *Clinical Cancer Research 16*(17), 4374–4381.

Vickers, A. J. and E. B. Elkin (2006). Decision curve analysis: A novel method for evaluating prediction models. *Medical Decision Making 26*(6), 565–574.

Wang, J. (2010). A nonparametric approach using Dirichlet process for hierarchical generalized linear mixed models. *Journal of Data Science 8*, 43–59.

Wayne, P., S. Foster, J. Connolly, F. Bazzaz, and P. Epstein (2002). Production of allergenic pollen by ragweed (Ambrosia artemisiifolia L.) is increased in CO2-enriched atmospheres. *Annals of allergy, asthma and immunology: official publication of the American College of Allergy, Asthma, & Immunology 88*(3), 279–282.

Whitehead, D. R. (1969). Wind pollination in the angiosperms: Evolutionary and environmental considerations. *Evolution 23*(1), 28–35.

Williams, J. H. (2008). Novelties of the flowering plant pollen tube underlie diversification of a key life history stage. *Proceedings of the National Academy of Sciences of the United States of America 105*(32), 11259–11263.

Wimmer, V., T. Albrecht, H.-J. Auinger, and C.-C. Schoen (2012). synbreed: a framework for the analysis of genomic prediction data using R. *Bioinformatics 28*(15), 2086–2087.

Wood, S. (1994). Monotonic smoothing splines fitted by cross validation. *SIAM Journal on Scientific Computing 15*(5), 1126–1133.

Wood, S. (2012). *gamm4: Generalized additive mixed models using mgcv and lme4*. R package version 0.1-6.

Wood, S. N. (2006). *Generalized Additive Models: An Introduction with R*. New York: Chapman & Hall.

World Health Organization (2013). Definitions of emergencies. `http://www.who.int/hac/about/definitions/en/index.html`. Accessed on 28.02.2013.

Wu, X. S., H. Dong, L. Luo, Y. Zhu, G. Peng, J. D. Reveille, and M. M. Xiong (2010). A novel statistic for genome-wide interaction analysis. *PLOS Genetics 6*(9), e1001131.

Wunder, J., B. Reineking, J. F. Matter, C. Bigler, and H. Bugmann (2007). Predicting tree death for fagus sylvatica and abies alba using permanent plot data. *Journal of Vegetation Science 18*(4), 525–534.

Xu, R. (2003). Measuring explained variation in linear mixed effects models. *Statistics in Medicine 22*(22), 3527–3541.

Yamaguchi-Shinozaki, K. and K. Shinozaki (2006). Transcriptional regulatory networks in cellular responses and tolerance to dehydration and cold stresses. *Annual Review of Plant Biology 57*, 781–803.

Yang, Y., S. J. Titus, and S. Huang (2003). Modeling individual tree mortality for white spruce in Alberta. *Ecological Modelling 163*(3), 209–222.

Yao, X., S. J. Titus, and S. E. MacDonald (2001). A generalized logistic model of individual tree mortality for aspen, white spruce, and lodgepole pine in Alberta mixedwood forests. *Canadian Journal of Forest Research 31*, 283–291.

Youden, W. (1950). Index for rating diagnostic tests. *Cancer 3*(1), 32–35.

Yu, J. M., G. Pressoir, W. H. Briggs, I. V. Bi, M. Yamasaki, J. F. Doebley, M. D. McMullen, B. S. Gaut, D. M. Nielsen, and J. B. Holland (2006). A unified mixed-model method for association mapping that accounts for multiple levels of relatedness. *Nature Genetics 38*(2), 203–208.

Zhao, D., B. Borders, and M. Wilson (2004). Individual-tree diameter growth and mortality models for bottomland mixed-species hardwood stands in the lower Mississippi alluvial valley. *Forest Ecology and Management 199*(2-3), 307–322.

Zhao, K., M. Aranzana, S. Kim, C. Lister, C. Shindo, C. Tang, C. Toomajian, H. Zheng, C. Dean, and P. Marjoram (2007). An Arabidopsis example of association mapping in structured samples. *PLOS Genetics 3*, e4.

Ziello, C., A. Böck, N. Estrella, D. P. Ankerst, and A. Menzel (2012). First flowering of wind-pollinated species with the greatest phenological advances in Europe. *Ecography 35*(11), 1017–1023.

Ziello, C., N. Estrella, M. Kostova, E. Koch, and A. Menzel (2009). Influence of altitude on phenology of selected plant species in the Alpine region (1971–2000). *Climate Research 39*, 227–234.

Ziska, L., K. Knowlton, C. Rogers, D. Dalan, N. Tierney, M. A. Elder, W. Filley, J. Shropshire, L. B. Ford, C. Hedberg, P. Fleetwood, K. T. Hovanky, T. Kavanaugh, G. Fulford, R. F. Vrtis, J. A. Patz, J. Portnoy, F. Coates, L. Bielory, and D. Frenz (2011). Recent warming by latitude associated with increased length of ragweed pollen season in central north america. *Proceedings of the National Academy of Sciences 108*(10), 4248–4251.

Zou, K. H. and S.-L. T. Normand (2001). On determination of sample size in hierarchical binomial models. *Statistics in Medicine 20*(14), 2163–2182.

Zuur, A. F. (2009). *Mixed effects models and extensions in ecology with R*. New York: Springer.